

SUBMERSIBLE WALKING DREDGER/ MINER

SRITAMA SARKAR



SUBMERSIBLE WALKING DREDGER/ MINER

BY

© SRITAMA SARKAR

**A thesis submitted to the School of Graduate Studies in partial
fulfillment of the requirements for the degree of
Doctor of Philosophy**

Faculty of Engineering and Applied Science

Memorial University of Newfoundland

April, 2007

St. John's

Newfoundland, Canada



Library and
Archives Canada

Bibliothèque et
Archives Canada

Published Heritage
Branch

Direction du
Patrimoine de l'édition

395 Wellington Street
Ottawa ON K1A 0N4
Canada

395, rue Wellington
Ottawa ON K1A 0N4
Canada

Your file *Votre référence*
ISBN: 978-0-494-31329-9
Our file *Notre référence*
ISBN: 978-0-494-31329-9

NOTICE:

The author has granted a non-exclusive license allowing Library and Archives Canada to reproduce, publish, archive, preserve, conserve, communicate to the public by telecommunication or on the Internet, loan, distribute and sell theses worldwide, for commercial or non-commercial purposes, in microform, paper, electronic and/or any other formats.

The author retains copyright ownership and moral rights in this thesis. Neither the thesis nor substantial extracts from it may be printed or otherwise reproduced without the author's permission.

AVIS:

L'auteur a accordé une licence non exclusive permettant à la Bibliothèque et Archives Canada de reproduire, publier, archiver, sauvegarder, conserver, transmettre au public par télécommunication ou par l'Internet, prêter, distribuer et vendre des thèses partout dans le monde, à des fins commerciales ou autres, sur support microforme, papier, électronique et/ou autres formats.

L'auteur conserve la propriété du droit d'auteur et des droits moraux qui protègent cette thèse. Ni la thèse ni des extraits substantiels de celle-ci ne doivent être imprimés ou autrement reproduits sans son autorisation.

In compliance with the Canadian Privacy Act some supporting forms may have been removed from this thesis.

Conformément à la loi canadienne sur la protection de la vie privée, quelques formulaires secondaires ont été enlevés de cette thèse.

While these forms may be included in the document page count, their removal does not represent any loss of content from the thesis.

Bien que ces formulaires aient inclus dans la pagination, il n'y aura aucun contenu manquant.


Canada

**To
Sri Aurobindo**

And

The Mother

Summary

The use of surface floating dredgers in deep inland reservoirs and continental shelves, either for dredging or mining purposes, is restricted by several operational limitations. Use of smaller surface floating dredgers in deep inland reservoirs is constrained by the ladder (a long truss like structure 'arm' that supports the excavation tool) length. Bigger dredgers have operational restrictions and mobilization problems. In shelf areas, the dredging operation is less precise due to currents, winds and waves. The floating pipelines, floats and winch wires are obstacles to navigational paths for other surface vessels. High investment costs are involved in the construction of bigger high capacity dredgers. It is difficult to modify such systems once they are constructed. The limitation of the existing technology served as the main motivation to design an active legged submersible dredger/ miner, which is described in this thesis. The designed vehicle is named the 'Golden Tortoise' because it simulates the belly crawling motion of a tortoise or turtle. A full scale prototype vehicle was manufactured by Excavation & Equipment Manufacturing (P) Ltd., (EEM (P) Ltd.) India. The prototype vehicle is suitable for operation in deep inland reservoirs up to a depth of 50 m and is designed to excavate sand, silt or clay mixtures in various proportions.

Parametric performance models were developed to evaluate the locomotion, excavation and transportation processes of the designed vehicle. Periodic gait plans were developed for straight line and curvilinear locomotion on natural terrain. Experimental validation of the theoretical gait plans was performed, which showed that the average slip was about 20 % at the foot/ soil interface in medium to relatively fine sands. Parametric models were developed for the evaluation of the locomotion cycle time of the designed vehicle. The locomotion cycle time was also measured from the gait plan tests and was found to be an average of 30 seconds. The static

load incident at each foot as a function of the vehicle weight and the leg joint parameters was predicted by developing a two-dimensional model based on simple beam theory. Prototype tests were performed to measure the static load incident at each foot as a function of the leg swing angle. The maximum static load measured due to weight of the vehicle was approximately 13 kN. The subsequent soil settlement and failure were estimated based on the theories of elasticity and plastic equilibrium as well as the shallow foundation theories. The dynamic load as a function of the leg actuating hydraulic cylinders was also considered for predicting the soil response. Comparisons between the different performance parameters of tracked vehicles and the designed legged vehicle were made. The shear stress–shear displacement relationship for different types of terrain was considered to predict the traction available for each foot during locomotion under different slip conditions. It was observed that the foot with grousers (lugs or teeth underneath the foot) provided more tractive effort compared to a tracked vehicle of similar dimensions and weight in cohesive soils.

Parametric performance models for the designed excavation system were developed based on the theories of earth moving machinery and their dynamics. The performance of the designed excavation system was evaluated based on the excavation production, spillage generated and the excavation power required under varying operational and soil conditions.

Parametric models were developed for evaluation of the designed pump-pipeline system by integrating the two-phase flow theories developed by various previous researchers. The models predict the total head loss in the pipeline system and hence the required pump power and also the limiting settling velocity condition and thereby the chances of pipeline blockage. In the present design this means that the suitable pipeline diameter is between 0.15 to 0.3 m to achieve a production of $61 \text{ m}^3/\text{hr}$ with a maximum volumetric concentration of 18 %. The mean mixture

velocity in the pipeline should vary between 2 to 5 m/sec to achieve the desired production and avoid pipeline blockage. A conceptual model was developed showing the complex interrelationships existing between the dredging and locomotion processes.

The results from this thesis can now be used to design the requisite controllers for the automatic operation of the 'Golden Tortoise'.

Acknowledgement

I would like to express my sincere gratitude to my supervisor Dr. Neil Bose, Canada Research Chair in Offshore and Underwater Vehicles Design, for his constant help and guidance during the entire course of this research work. His valuable scientific suggestions and advice during the work are gratefully acknowledged. I am also thankful to my supervisory committee members, Dr. Raymond Gosine, Dean of Engineering, Memorial University of Newfoundland and Dr. Dan Walker, President, Oceanic Consulting Corporation, Newfoundland, Canada for their valuable suggestions and comments during the execution of the research work.

I would also like to thank Excavation & Equipment Manufacturing (EEM) (P) Ltd., India for their knowledge exchange, manufacturing and testing the full scale prototype vehicle in their workshop premises. My special thanks go to the EEM workshop team members who were involved with the manufacture and testing of the prototype vehicle. I would like to express my sincere thanks to Mr. Mridul Kumar Sarkar, Managing director, EEM (P) Ltd., who is one of the collaborators in this project, for his constant suggestions and active participation during the manufacture and testing phases of the prototype vehicle. His practical experience in designing and manufacturing of inland dredgers and operational management of dredging jobs was very beneficial to this thesis work.

I am also thankful to Mr. Tony van der Steen, has been a renowned submersible dredging engineer from The Netherlands for his valuable suggestions and comments on the present thesis work. Mr. Van der Steen is a consultant of EEM (P) Ltd. since 1989. I am also grateful to Prof. Ir. W.J. Vlasblom and Dr. Ir. S.A. Miedema, Dredging Technology, Delft University of Technology, The Netherlands. They gave me lots of information regarding dredgers and the process of dredging, which were extremely important and useful to carry out the work. My sincere thanks to

Dr. M.A. Atmanand and Mr. Binu Balakrishnan, National Institute of Ocean Technology, India for their help with the instrumentation and data acquisition system which was used for the execution of the prototype tests. I am also thankful to Dr. R. Ravindran, then Director of National Institute of Ocean Technology, India for granting me the permission to go and see their underwater crawler in the year 2003. This visit and the technical discussions with the underwater crawler team from National Institute of Ocean Technology, India was highly beneficial. I am also thankful to Ing. Enno Schulte, Institut für Konstruktions, Siegen, Germany for providing me with lots of useful references for subsea trafficability, subsea soils and soil behavior. Thanks are also due to the technicians in the Fluids, Electronics and Electrical and Structural Laboratories and also to the Technical Services of the Memorial University of Newfoundland for their valuable suggestions on the instrumentation and strain gage installation techniques.

I acknowledge the financial support from the Atlantic Innovation Fund Project, Subsea Engineering - Underwater operations, robotics and intelligent systems, under the Pan-Atlantic Petroleum Systems Consortium and Memorial University for a graduate fellowship to me for carrying out this research project. I am also thankful to EEM (P) Ltd., India for their full financial support in the construction and testing of the prototype vehicle.

Lastly, I want to express my gratitude and respect to my parents for their inspiration and love which helped me to carry out this research work.

CONTENTS

SUMMARY.....	I
ACKNOWLEDGEMENT	IV
CONTENTS	VI
LIST OF FIGURES.....	X
LIST OF TABLES.....	XV
LIST OF ABBREVIATIONS.....	XVII
LIST OF SYMBOLS.....	XVIII
LIST OF SUBSCRIPTS.....	XXXII
CHAPTER 1	1
INTRODUCTION	1
1.1 INTRODUCTION	1
1.2 MOTIVATION FOR THE RESEARCH.....	2
1.3 STATE OF THE ART OF TECHNOLOGIES.....	9
1.3.1 <i>Surface Floating Dredgers</i>	9
1.3.2 <i>Submersible Dredgers/ Miners</i>	10
1.3.3 <i>Subsea Trenchers</i>	11
1.3.4 <i>Other Deep Dredging or Mining Technology</i>	12
1.3.5 <i>Robotic Vehicles in Hazardous and/ or Unstructured Environments</i>	12
1.3.6 <i>Comparisons between Available Technologies</i>	13
1.4 STATEMENT OF THE ISSUES	14
1.4.1 <i>Locomotion System and Process</i>	15
1.4.2 <i>Excavation System and Process</i>	17
1.4.3 <i>Transportation System and Process</i>	19
1.5 METHODOLOGY AND OUTLINE	21
CHAPTER 2	27
DESIGN	27
2.1 INTRODUCTION	27
2.2 GENERAL ARRANGEMENT.....	27
2.3 SYSTEM HULL.....	30
2.3.1 <i>Hydrodynamic Performance</i>	30
2.3.2 <i>Hull Types for Submersible Vehicles</i>	36
2.3.3 <i>Hull Construction Material</i>	37
2.3.4 <i>Design of the Pressure Hull</i>	38
2.4 DESIGN OF THE HULL.....	42
2.5 SYSTEM EXCAVATION.....	46
2.5.1 <i>Design of the Cutter and the Ladder Assembly</i>	46
2.5.2 <i>Functionality Tests for the Excavation System</i>	48
2.6 SYSTEM TRANSPORT	52
2.7 SYSTEM LOCOMOTION	53
2.7.1 <i>Terrain of Locomotion</i>	53
2.7.2 <i>Leg Linkage Design</i>	54
2.7.3 <i>Mode of Locomotion</i>	56
2.7.4 <i>Method of Locomotion</i>	58
2.7.5 <i>Task Planning</i>	60
2.7.6 <i>Functionality Tests for the Locomotion System</i>	61
2.8 DESIGN POWER	63

2.9	COMPARISON BETWEEN TRACKED AND DESIGNED LEGGED VEHICLE	69
2.10	CONCLUDING REMARKS	71
CHAPTER 3		72
PERFORMANCE EVALUATION MODELS FOR LOCOMOTION		72
3.1	INTRODUCTION	72
3.2	GAIT PLAN FOR STRAIGHT LINE LOCOMOTION	72
3.2.1	Step Generator.....	73
3.2.2	Experimental and Predicted Results for Straight Line Locomotion	76
3.3	GAIT PLAN FOR CURVILINEAR LOCOMOTION ON LEVEL TERRAIN.....	91
3.3.1	Principle of Curvilinear Motion.....	91
3.3.2	Kinematics of Skid Steering for the Legged Vehicle.....	93
3.3.3	Experimental and Predicted Results for Curvilinear Locomotion.....	98
3.4	LOCOMOTION CYCLE TIME	116
3.4.1	Experimental Results for Locomotion Cycle Time.....	117
3.5	SOIL PRESSURE AND STABILITY	121
3.5.1	Soil Response Models	121
3.5.2	Static and Dynamic Load at Foot/ Soil Interface	124
3.5.3	Static Load.....	125
3.5.4	Dynamic Load	133
3.5.5	Total Load	136
3.5.6	Allowable Load.....	136
3.5.7	Results and Discussions for Soil Response.....	138
3.6	TRACTIVE FORCE GENERATED BY THE DESIGNED LEGGED VEHICLE	144
3.6.1	Tractive Force at the Grousers.....	145
3.6.2	Tractive Force and Slip of Foot.....	149
3.6.3	Tractive Force and Slip of Vehicle Belly.....	151
3.6.4	Tractive Effort and Slip of a Track.....	151
3.6.5	Results and Discussions for Tractive Force and Slip.....	152
3.7	CONCLUDING REMARKS	157
CHAPTER 4		158
PERFORMANCE EVALUATION MODELS FOR EXCAVATION		158
4.1	INTRODUCTION	158
4.2	LOOSENING PRODUCTION	158
4.2.1	Assumptions for Loosening Production.....	159
4.2.2	Working Principle during Dredging.....	159
4.2.3	Volume of Soil Excavated.....	160
4.2.4	Results and Discussions for Loosening Production.....	165
4.3	GATHERING PRODUCTION.....	173
4.3.1	Assumptions made for Gathering Production	174
4.3.2	Forces Acting on the Soil Lump/ Particle.....	175
Gravitational and Buoyancy Forces	178	
Frictional Force.....	178	
Drag and Current Force	178	
Equations of Motion.....	179	
4.3.3	Suction Influence Zone	179
4.3.4	Spillage.....	183
4.3.5	Results and Discussion for Gathering Production	183
4.4	SPECIFIC ENERGY	190
4.5	CONCLUDING REMARKS	196
CHAPTER 5		197
PERFORMANCE EVALUATION MODELS FOR TRANSPORTATION		197

5.1	INTRODUCTION	197
5.2	WORKING PRINCIPLE OF CENTRIFUGAL DREDGE PUMP-PIPELINE SYSTEM.....	199
5.3	DELIVERED SOLID RATE	202
5.4	PIPELINE BLOCKAGE.....	205
5.5	MAJOR FRICTIONAL LOSS IN HORIZONTAL PIPELINE	208
5.6	MAJOR FRICTIONAL LOSS IN INCLINED PIPELINE	212
5.7	STATIC HEAD LOSS	214
5.8	MINOR HEAD LOSS	214
5.9	ENTRY AND EXIT LOSSES.....	215
5.10	PREDICTED RESULTS	216
5.11	CONCLUDING REMARKS	224
CHAPTER 6		226
SYNCHRONIZATION OF LOCOMOTION AND DREDGING PROCESSES		226
6.1	INTRODUCTION	226
6.2	PARAMETERS INFLUENCING DREDGING AND LOCOMOTION PROCESSES	226
6.3	CONCEPTUAL MODEL FOR PERFORMANCE EVALUATION.....	227
6.4	CONCLUDING REMARKS	231
CHAPTER 7		232
CONCLUSIONS AND RECOMMENDATIONS		232
7.1	CONCLUSIONS AND RECOMMENDATIONS.....	232
7.2	DESIGN	234
7.3	LOCOMOTION MODELS	237
7.4	EXCAVATION MODELS.....	244
7.5	TRANSPORTATION MODEL.....	246
7.6	INTEGRATION OF LOCOMOTION AND DREDGING PROCESSES	246
REFERENCE LIST		248
APPENDIX 1		257
SOIL BEHAVIOR - BASIC SOIL PARAMETERS DETERMINING PRODUCTION AND MOBILITY IN GRANULAR AND COHESIVE MATERIAL.....		257
1.0	INTRODUCTION	257
2.0	VEHICLE STABILITY DUE TO SOIL BEARING PRESSURES	257
3.0	SHEAR STRESS-SHEAR DISPLACEMENT RELATIONSHIPS.....	260
4.0	SOIL PARAMETERS DETERMINING EXCAVATION PERFORMANCE.....	263
5.0	SOIL BEHAVIOR DURING EXCAVATION	264
5.1	<i>Phenomena during Excavation of Granular Material.....</i>	265
5.2	<i>Cohesive Material</i>	266
6.0	SOIL CLASSIFICATION BASED ON GRAIN SIZE.....	267
7.0	SHEAR STRENGTH OF GRANULAR AND COHESIVE SOILS	268
8.0	CONCLUDING REMARKS	270
APPENDIX 2		271
DRAG CALCULATIONS		271
1.0	DRAG CALCULATIONS FOR THE LEG	271
2.0	DRAG CALCULATIONS FOR THE CUTTER MODULE.....	273
APPENDIX 3		275
PRESSURE VESSELS CALCULATIONS.....		275
APPENDIX 4		278
DATA USED FOR COMPARISONS BETWEEN CATERPILLAR TRACKED VEHICLES AND DESIGNED LEGGED VEHICLE		278

APPENDIX 5	279
EXPERIMENTAL SET UP, MEASURING TECHNIQUES AND MEASURING INSTRUMENTS FOR THE PROTOTYPE TESTS.....	279
1.0 VEHICLE OPERATION	279
2.0 MEASURED PARAMETERS AND MEASURING TECHNIQUES	279
2.1 <i>Hydraulic Oil Pressure</i>	279
2.2 <i>Time for Cylinder Operation</i>	280
2.3 <i>Leg and Ladder Angles</i>	280
2.4 <i>Step Sizes of the Vehicle</i>	281
2.5 <i>Load Incident at each Leg</i>	282
APPENDIX 6	285
TEST MATRICES, EXPERIMENTAL AND PREDICTED DATA FOR STRAIGHT LINE LOCOMOTION	285
APPENDIX 7	293
TEST MATRICES, EXPERIMENTAL AND PREDICTED DATA FOR CURVILINEAR LOCOMOTION	293
APPENDIX 8	299
LOCOMOTION CYCLE TIME	299
1.0 PARAMETRIC MODEL FOR ESTIMATION OF LOCOMOTION CYCLE TIME	299
1.1 <i>Preparatory Cycle</i>	299
1.2 <i>Motion Cycle</i>	304
1.3 <i>Idle Cycle</i>	305
1.4 <i>Finishing Cycle</i>	307
2.0 UNCERTAINTY ANALYSES FOR GAIT PLANNING TESTS.....	311
APPENDIX 9	318
STATIC LOAD INCIDENT AT LEG	318
APPENDIX 10	320
POSITION ANALYSIS OF LEG LINKAGE AND DYNAMIC LOAD INCIDENT AT LEG.....	320
1.0 POSITION ANALYSIS OF LEG LINKAGE	320
APPENDIX 11	335
TRACTIVE FORCE FOR DESIGNED VEHICLE AND TRACKED VEHICLE	335
APPENDIX 12	337
RELATIONSHIP BETWEEN SWING VELOCITY OF CUTTER AND TRANSLATORY VELOCITY OF HYDRAULIC CYLINDER.....	337
APPENDIX 13	343
RELEVANT DATA FOR ESTIMATION OF HEAD LOSS OF DESIGNED PIPELINE SYSTEM.....	343

List of Figures

Figure number	Figure description	Page number
Figure 1.1	Small and big surface floating dredgers	3
Figure 1.2	Remotely operated grab	5
Figure 1.3	Sub sea crawler	5
Figure 1.4	Principle of operation of passive legged vehicle	7
Figure 1.5	Futuba -2	8
Figure 1.6	Tripod	8
Figure 1.7	Different types of surface floating dredgers	9
Figure 1.8	Subsea tractors and ploughs with skids	11
Figure 1.9	Punaise system	12
Figure 1.10	Different types of mechanical cutters	18
Figure 1.11	Schematic of the 'Golden Tortoise'	26
Figure 2.1	Schematic of 'Golden Tortoise' (Not to scale)	27
Figure 2.2	Prototype vehicle of 'Golden Tortoise'	29
Figure 2.3	Total drag of the four legs vs. linear velocity of the leg	33
Figure 2.4	Total drag of the two cutters vs. swing velocity of the ladder assembly (WSA Wetted surface area)	34
Figure 2.5	Total drag of the two pressure hulls of the cutter module vs. swing velocity of the ladder assembly (FA Frontal area)	34
Figure 2.6	Total drag of the ladder assembly vs. swing velocity of the ladder assembly (using a fixed value of the drag co-efficient based on frontal area)	35
Figure 2.7	Total drag of ladder assembly vs. swing velocity of the ladder assembly (using Hoerner's expressions)	36
Figure 2.8	Main body frame	42
Figure 2.9	Main body frame definition	43
Figure 2.10	Optimum camber angle for the main body frame	44
Figure 2.11	Cutter module using two drum cutters	46
Figure 2.12	Hydraulic drive for cutter	47
Figure 2.13	Overcutting and Undercutting	48
Figure 2.14	Ladder lifting/ lowering and swinging trials	49
Figure 2.15	Arrangements for ladder lift/ lower cylinder connections	49
Figure 2.16	Ladder swing angle (Plan view)	51
Figure 2.17	Cutter rotation trials	52
Figure 2.18	Eductor and Dredge pumps	53
Figure 2.19	Turtle performing belly crawling motion on very soft muddy terrain	53
Figure 2.20	Conceptual design of the leg linkage of 'Golden Tortoise'	54
Figure 2.21	Foot construction (Left Inner construction of the foot, Right Leg with foot)	55
Figure 2.22	Designed leg of the prototype vehicle of 'Golden Tortoise'	56
Figure 2.23	Belly sliding with the swinging of ladder assembly	57
Figure 2.24	Method of locomotion	58

Figure 2.25	Locomotion pattern in a given workspace	61
Figure 2.26	Trials for prototype vehicle supported on its four legs	62
Figure 2.27	Schematic of the power supply for the prototype vehicle	63
Figure 2.28	Power supply for operation of the Directional Control Valves (12 V DC)	64
Figure 2.29	Hydraulic circuits designed	65
Figure 2.30	Hydraulic oil tanks	68
Figure 2.31	Power vs. Ground contact area for 'Caterpillar' tracked vehicles and the designed legged vehicle	69
Figure 2.32	Power vs. Weight for 'Caterpillar' tracked vehicles and the designed legged vehicle	70
Figure 2.33	Power vs. Length/ Width ratio for 'Caterpillar' tracked vehicles and the designed legged vehicle	70
Figure 3.1	Step generator	73
Figure 3.2	Step generator with level difference or submergence	74
Figure 3.3	Step generator due to slip	75
Figure 3.4	Experimental step size and predicted step size without slip for PS_AFT leg during forward straight line locomotion	77
Figure 3.5	Deviation between predicted and experimental step sizes for PS_AFT leg during forward straight line locomotion	77
Figure 3.6	Experimental step size and predicted step size without slip for PS_FWD leg during forward straight line locomotion	77
Figure 3.7	Deviation between predicted and experimental step sizes for PS_FWD leg during forward straight line locomotion	78
Figure 3.8	Experimental step size and predicted step size without slip for SBS_AFT leg during forward straight line locomotion	78
Figure 3.9	Deviation between predicted and experimental step sizes for SBS_AFT leg during forward straight line locomotion	79
Figure 3.10	Experimental step size and predicted step size without slip for SBS_FWD leg during forward straight line locomotion	79
Figure 3.11	Deviation between predicted and experimental step sizes for SBS_FWD leg during forward straight line locomotion	80
Figure 3.12	Experimental and predicted step sizes with different slip percentages during	82
Figure 3.13	Experimental step size and predicted step size without slip for PS_AFT leg during backward straight line locomotion	83
Figure 3.14	Deviation between predicted and experimental step sizes for PS_AFT leg during backward straight line locomotion	83
Figure 3.15	Experimental step size and predicted step size without slip for PS_FWD leg during backward straight line locomotion	84
Figure 3.16	Deviation between predicted and experimental step sizes for PS_FWD leg during backward straight line locomotion	84
Figure 3.17	Experimental step size and predicted step size without slip for SBS_AFT leg during backward straight line locomotion	84
Figure 3.18	Deviation between predicted and experimental step sizes for	85

	SBS_AFT leg during backward straight line locomotion	
Figure 3.19	Experimental step size and predicted step size without slip for SBS_FWD leg during backward straight line locomotion	85
Figure 3.20	Deviation between predicted and experimental step sizes for SBS_FWD leg during backward straight line locomotion	85
Figure 3.21	Experimental and predicted step sizes with different slip percentages for backward straight line locomotion	87
Figure 3.22	Vehicle trajectory and deviation from proposed path during straight line locomotion	89
Figure 3.23	Ratio between swing angles of AFT and FWD legs for different submergences of the FWD legs and zero submergence of AFT legs	90
Figure 3.24	Principle of curvilinear motion	92
Figure 3.25	Principle of skid steering for the legged vehicle	93
Figure 3.26	Step sizes for inner and outer legs for curvilinear locomotion	94
Figure 3.27	Definitions of slip and skid	97
Figure 3.28	Vehicle trajectory for curvilinear locomotion on flat terrain with unequal swing angles of outer and inner legs	99
Figure 3.29	Experimental and predicted step size vs. turning angle of vehicle for curvilinear locomotion with unequal angles (AFT legs)	100
Figure 3.30	Deviation between predicted and experimental step size value for curvilinear locomotion with unequal angles (PS_AFT leg)	100
Figure 3.31	Deviation between predicted and experimental step size value for curvilinear locomotion with unequal angles (SBS_AFT leg)	101
Figure 3.32	Experimental and predicted step size of the vehicle centre of gravity vs. turning radius of vehicle for curvilinear locomotion with unequal angles	102
Figure 3.33	Deviation between predicted and experimental step size of the vehicle centre of gravity for curvilinear locomotion with unequal angles	102
Figure 3.34	Experimental turning radius and predicted turning radius without slip/ skid at the foot/ soil interface	105
Figure 3.35	Experimental turning angle and predicted turning angle without slip/ skid at the foot/ soil interface	105
Figure 3.36	Experimental and predicted values of turning radii and turning angles with slip (slip of outer legs is > slip of inner legs)	107
Figure 3.37	Experimental and predicted values of turning radii and turning angles with slip (slip of inner legs > slip of outer legs)	108
Figure 3.38	Vehicle trajectory for curvilinear locomotion on flat terrain with inner legs fixed	109
Figure 3.39	Experimental step sizes for curvilinear locomotion with inner legs fixed	110
Figure 3.40	Predicted turning behavior under no slip condition	111
Figure 3.41	Predicted turning angle under no slip condition vs. ratio between step sizes of outer and inner legs	112
Figure 3.42	Predicted turning angle under no slip condition vs. ratio between angular velocities of outer and inner legs	113

Figure 3.43	Predicted turning behavior of the designed vehicle with slip	114
Figure 3.44	Locomotion cycle time for forward straight line locomotion	118
Figure 3.45	Locomotion cycle time for backward straight line locomotion	119
Figure 3.46	Locomotion cycle time for curvilinear locomotion with inner legs fixed	120
Figure 3.47	Locomotion cycle time for curvilinear locomotion with unequal angles	121
Figure 3.48	Soil response force system during locomotion	122
Figure 3.49	Total and differential settlement	123
Figure 3.50	Failure pattern under the foot	124
Figure 3.51	Static load due to weight at the foot/ soil interface	126
Figure 3.52	Predicted and experimental vertical load at foot/ soil interface	129
Figure 3.53	Predicted and experimental values of ratios between vertical force of FWD and AFT legs	132
Figure 3.54	Dynamic force transfer at the foot/ soil interface	134
Figure 3.55	Inclined loading on foot	136
Figure 3.56	Vertical dynamic force at foot/ soil interface	139
Figure 3.57	Horizontal dynamic force at the foot/ soil interface	140
Figure 3.58	Total force at the foot/ soil interface	141
Figure 3.59	Bearing capacity in granular soil for different foot shape	142
Figure 3.60	Bearing capacity in cohesive soil for different foot shape	143
Figure 3.61	Comparisons between required soil strength for cohesive soil for tracked and designed legged vehicle	144
Figure 3.62	Tractive force without soil failure	146
Figure 3.63	Tractive force generated vs. slip for 'Caterpillar' tracked vehicle D3B in granular soil	153
Figure 3.64	Tractive forces generated by four feet of the designed legged vehicle under different slip percentages in granular soil (without grouser)	154
Figure 3.65	Tractive force generated vs. slip for 'Caterpillar' tracked vehicle D3B in cohesive soil	155
Figure 3.66	Tractive forces generated by the designed legged vehicle under different slip percentages in cohesive soil (with grousers)	156
Figure 3.67	Tractive force generated during belly sliding	156
Figure 4.1	Working principle during excavation	160
Figure 4.2	Lacing of blades on cutter drum	161
Figure 4.3	Path of two successive cutter blades during 'overcutting'	162
Figure 4.4	Feed and depth of cut	164
Figure 4.5	Swing velocity of cutter and the angle between ladder boom and horizontal (Swing velocity of the ladder = 0.18 m/sec)	166
Figure 4.6	Swing velocity of cutter and the angle between ladder boom and horizontal (Swing velocity of the ladder = 0.035 m/sec)	167
Figure 4.7	Cutter blade trajectories during 'overcutting'	170
Figure 4.8	Cutter blade trajectories during 'undercutting'	171
Figure 4.9	Cutter blade trajectories during 'undercutting'	172
Figure 4.10	Forces acting on a soil lump/ particle	176

Figure 4.11	Soil particle position with respect to suction mouth (Top Plan view, Bottom Front view)	180
Figure 4.12	Suction influence zone[Based on Apgar, 1973]	182
Figure 4.13	Soil lump/particle trajectory and velocity with diameter of soil lump/particle = 2 mm in the Z direction	184
Figure 4.14	Soil lump/ particle trajectory and velocity with diameter of soil lump/ particle = 20 mm in the Z direction	185
Figure 4.15	Soil lump/ particle trajectory and velocity with diameter of soil lump/ particle = 2 mm in the Y direction	186
Figure 4.16	Soil lump/ particle trajectory and velocity with diameter of soil lump/ particle = 20 mm in the Y direction	187
Figure 4.17	Position of centers of suction mouth, leading and trailing cutters	188
Figure 4.18	Suction influence zone in front of the suction mouth of rectangular cross section	189
Figure 4.19	Similarity between crown cutter pick points and the virtual blades of drum cutter (Left Crown cutter, Right Drum cutter)	191
Figure 4.20	Specific energy and cutter power for non-cohesive granular material under non-cavitating condition	194
Figure 4.21	Specific energy and cutter power in granular and non-cohesive material under cavitating condition	195
Figure 4.22	Specific energy and cutter power for cohesive soils	196
Figure 5.1	Transport system	198
Figure 5.2	Working point and working range of a pump-pipeline system	200
Figure 5.3	Total head loss for designed pipeline configuration ($C_{vd} = 0.18$, $Q_s = 61 \text{ m}^3/\text{hr}$, $h_d = 50 \text{ m}$, Length of horizontal pipeline section = 200 m)	218
Figure 5.4	Required mixture velocities for horizontal pipeline section	220
Figure 5.5	Deposition limit velocity for inclined pipeline section	221
Figure 5.6	Suitable transport velocity and mean mixture velocity for inclined pipeline section with different angles of inclination	222
Figure 5.7	Required pump power	223
Figure 6.1	Conceptual model showing the interrelationships between dredging and locomotion processes (E Excavation, L Locomotion, T Transportation)	230
Figure 7.1	Prototype vehicle of 'Golden Tortoise'	232

List of Tables

Table number	Table description	Page number
Table 1.1	Comparison between surface floating and submersible dredgers/miners	13
Table 1.2	Comparison between submersible crawlers, vehicles with skids and legged vehicles	14
Table 1.3	Comparison between airlift and submersible centrifugal dredge pumps	14
Table 1.4	Suitability of excavation tools in various types of materials [Based on Chaziteodorou, 1977; Herbich, 2000; Vlasblom, 1999]	18
Table 1.5	Possible combinations of excavation and transportation systems [Based on Chaziteodorou, 1977; Herbich, 2000; Vlasblom, 1999]	21
Table 2.1	Design data about the prototype of 'Golden Tortoise'	30
Table 2.2	Estimated critical pressures and corresponding operating depths for ballast tanks (Thickness of pressure hull = 3 mm)	41
Table 2.3	Estimated critical pressures and corresponding operating depths for hydraulic and electric-electronics modules (Thickness of pressure hull = 2 mm)	41
Table 2.4	Weight and buoyancy of the prototype vehicle 'Golden Tortoise'	45
Table 2.5	Locomotion vs. Terrain	57
Table 2.6	Electrical circuits	64
Table 3.1	Average deviation percentage for forward straight line locomotion	81
Table 3.2	Average deviation percentage for backward straight line locomotion	86
Table 3.3	Longitudinal tilt of vehicle for different level differences between AFT and FWD legs	91
Table 3.4	Transverse tilt of vehicle for different level differences between PS and SBS legs	91
Table 3.5	Representative values of step size and deviation for curvilinear locomotion with unequal angles	103
Table 3.6	Different series of Figure 3.36 and Figure 3.37	106
Table 3.7	Total locomotion cycle time during the entire locomotion test for straight line locomotion	120
Table 3.8	Design properties of different components of the vehicle	127
Table 3.9	Moment arm and moment for the different components of the vehicle	127
Table 3.10	Deviations for vertical force at foot/ soil interface	130
Table 3.11	Weight of vehicle calculated from experimental results	132
Table 3.12	Rupture distance for grousers in granular soil	147
Table 3.13	Rupture distance for grousers in cohesive soil	147
Table 4.1	Variations in translatory velocity of cutter	167
Table 4.2	Parameters for cutter blade trajectories during overcutting	168
Table 4.3	Parameters for cutter blade trajectories during undercutting	171
Table 4.4	Loosening production calculated by the method of area integration	173
Table 4.5	Loosening production calculated by the method of feed of cutter	173

Table 4.6	Spillage percent as a function of cutter rpm	190
Table 5.1	Operational, environmental and soil data for prediction of nominal transport velocity	204
Table 5.2	Diameter of pipeline, mean mixture velocity and mixture flow rate	222
Table 6.1	Geometrical, operational and environmental parameters affecting the dredging and locomotion processes	227

List of Abbreviations

AFT	After
AROV	Autonomous remotely operated vehicle
ASTM	American Society for Testing and Materials
AUV	Autonomous underwater vehicle
BS	British Standard
DC valve	Directional control valve
EEM (P) Ltd.	Excavation & Equipment Manufacturing Private Limited
FRP	Fibre reinforced plastics
FWD	Forward
GPS	Global positioning system
GRP	Glass reinforced plastics
IKS, Siegen, Germany	Institut für Konstruktions, Siegen, Germany
NIOT, India	National Institute for Ocean Technology (India)
PS	Port side
ROV	Remotely operated vehicle
<i>rpm</i>	Revolutions per minute
SBS	Starboard side
SWAD	Submersible walking auto dredger
TID, The Netherlands	Training Institute for Dredging, The Netherlands
MCB	Molded circuit breaker

List of Symbols

A_{belly}	Contact area of the vehicle belly with soil [m ²]
$A_{contact}$	Contact area of any load bearing structure with the soil [m ²]
A_{fa}	Projected frontal area of any submerged body [m ²]
A_{foot}	Contact area of the foot with soil [m ²]
A_{hc}	Cross-sectional area of the hydraulic cylinder bore [m ²]
A_{hc_rod}	Cross-sectional area of the hydraulic cylinder rod [m ²]
A_{pipe}	Cross sectional area of the pipe [m ²]
$A_{soilwedge}$	Cross sectional area of the soil wedge dislodged by two successive cutter blades [m ²]
A_{sp}	Projected frontal area of a sphere [m ²]
A_{track}	Contact area of a track [m ²]
A_{wsa}	Wetted surface area of any submerged body [m ²]
a	Adhesion of the soil [kPa]
a_{hc}	Loss factor of the hydraulic cylinder [-]
a_{rcrc_cutter}	Recirculation factor, due to the extra energy required for recirculation of the excavated material within a drum cutter or around a rotavator cutter [-]
a_{serv_cutter}	Service factor for cutter power estimation [-]
a_{soil_cutter}	Soil factor for cutter power estimation [-]
a_{sm}	Suction mouth entry factor, dependent on the grating, surface finish etc. [-]
a_{so_pump}	System operation factor for pump [-]
B	Smaller dimension of a contact patch with soil i.e. width of a rectangular contact area or radius of a circular contact area [m]

B_{belly}	Width of the vehicle belly in contact with the soil [m]
B_{blade}	Width of the cutter blade [m]
B_{cut}	Maximum width of cut during excavation [m]
B_{foot}	Width of the foot [m]
$B_{grouser}$	Width of the grouser attached to the foot [m]
B_{sm}	Width of the suction mouth [m]
B_{strip}	Width of strip foundation [m]
$B_{vehicle}$	Width of the vehicle [m]
C_d	Drag co-efficient [-]
C_{d_fa}	Drag co-efficient based on projected frontal area [-]
C_{d_wsa}	Drag co-efficient based on wetted surface area [-]
C_f	Resistance co-efficient for estimation of the drag co-efficient [-]
C_v	Volumetric concentration [%]
C_{vd}	Delivered volumetric concentration [%]
C_{vdsi}	In-situ delivered volumetric concentration [%]
C_{vdsi_calc}	Calculated in-situ delivered volumetric concentration, [%]
C_{vdsi_del}	Delivered in-situ delivered volumetric concentration, [%]
c	Soil cohesion [kPa]
D_{cutter}	Diameter of the cutter [m]
D_{pipe}	Diameter of the pipeline [m]
D_{pipe_suc}	Diameter of the suction pipe [m]

D_{pipe_del}	Diameter of the delivery pipe [m]
D_{sb}	Diameter of any submerged body [m]
D_{eq_sm}	Equivalent pipe diameter for the suction mouth [m]
d_{10}	Grain size of soil at 10 % passing [mm]
d_{50}	Grain size of soil at 50 % passing / Mass-median diameter [mm]
d_{85}	Grain size of soil at 85 % passing [mm]
d_{mf}	Decisive soil particle diameter [mm]
d_n	Respective percentile and gives the particles' diameter for which n percent of (by mass) the particles in a soil sample are finer [mm]
ΔD	Durand deposition parameter in inclined pipelines [-]
E_s	Specific energy for soil excavation [kJ/m ³]
E_{s_coh}	Specific energy for excavation of cohesive soil [kJ/ m ³]
$E_{s_gran_c}$	Specific energy required to excavate non-cohesive granular soil under cavitating condition [kJ/ m ³]
$E_{s_gran_nc}$	Specific energy required to excavate non-cohesive granular soil under non-cavitating condition [kJ/ m ³]
e	Actual pore volume of the soil in the field [%]
e_{max}	Pore volume of the soil in the loosest state [%]
e_{min}	Pore volume of the soil in the densest state [%]
F_b	Buoyancy force [kN]
F_{cur}	Current force [kN]
F_d_fa	Drag force based on projected frontal area [kN]
$F_d_soillump$	Drag force on the soil lump/ particle [kN]

F_d_wsa	Drag force based on wetted surface area [kN]
$F_f_soil_cutter$	Frictional force between soil lump/ particle and cutter blade [kN]
F_g	Gravitational force [kN]
F_e	Force generated by leg-swing hydraulic cylinder during expansion [kN]
$F_{shc_leg_e1}$	Force acting along the leg generated by the leg-swing hydraulic cylinder during expansion [kN]
$F_{shc_leg_e2}$	Turning force acting normal to the leg generated by the leg-swing hydraulic cylinder during expansion [kN]
F_r	Force generated by the leg-swing hydraulic cylinder during retraction [kN]
F_p_foot	Tractive force available at the foot/ soil interface [kN]
$F_p_foot_max$	Maximum tractive force available at the foot/ soil interface [kN]
$F_p_foot_in$	Tractive force available at the inner foot/ soil interface [kN]
$F_p_foot_out$	Tractive force available at the outer foot/ soil interface [kN]
$F_p_grouser$	Tractive force generated per unit width of the grouser attached to the foot [kN]
F_p_track	Tractive effort of the track [kN]
$F_{prp_vert_leg}$	Proportional vertical static load transferred to a particular leg swing pin [kN]
$F_{prp_vert_leg_hor}$	Horizontal component of $F_{prp_vert_leg}$ acting at the foot hinge pin [kN]
$F_{prp_vert_leg_vert}$	Vertical component of $F_{prp_vert_leg}$ acting at the foot hinge pin [kN]
$F_{total_hor_foot}$	Total (static and dynamic) horizontal load at the foot hinge pin due to leg swing [kN]

$F_{total_vert_foot}$	Total (static and dynamic) vertical load at the foot hinge pin due to leg swing [kN]
F_{res}	Resisting force due to turning of the vehicle [kN]
F_W	Normal load due to weight of the vehicle [kN]
f_c	Ratio between pump efficiencies for pumping mixture to pumping water [-]
g	Acceleration due to gravity [m/sec ²]
H_{entry_m}	Entry head loss due to mixture flow at the suction mouth [m]
H_{exit_m}	Exit head loss due to mixture flow at the delivery point [m]
$H_{major_hor_m}$	Major head loss in the horizontal pipeline section due to mixture flow [m]
$H_{major_inc_m}$	Major head loss in the inclined pipeline section due to mixture flow [m]
H_{man}	Manometric head of pump [m]
H_{minor_m}	Minor head loss in the pipeline due to mixture flow [m]
$H_{st_del_m}$	Static head loss due to mixture flow from water level to delivery point [m]
$H_{st_suc_m}$	Static head loss due to mixture flow from suction mouth to water level [m]
$H_{st_total_m}$	Total static head loss due to mixture flow [m]
h_{camber}	Height of camber of the main body frame [m]
h_{cut}	Depth of cut for dredging [m]
h_{del}	Elevation of discharge from water level during dredging [m]
$h_{grouser}$	Height of grouser [m]
h_{ridge}	Ridge height of the excavated soil [m]
$h_{surcharge}$	Depth of surcharge [m]

h_w	Depth of water/ Depth of operation [m]
Δh_{belly}	Sinkage of the vehicle belly [expressed as a percentage of camber height of the main body frame or in meters]
Δh_{foot}	Submergence of the foot [m]
Δh_{leg}	Level difference between two legs with respect to the ground [m]
Δh_{soil}	Soil sinkage [m]
I_f	Hydraulic gradient for liquid flow [-]
I_m	Hydraulic gradient for mixture flow in horizontal pipeline [-]
$I_{m\omega}$	Hydraulic gradient for mixture flow in inclined pipeline [-]
i	Slip or skid [%]
j	Shear displacement of the soil [cm/m]
K	Shear deformation modulus of soil in shear stress–shear displacement relationship proposed by Janosi and Hanamoto [cm]
K_{leg}	Ratio of the angular velocities of the outer and inner legs [-]
k	Permeability of the soil [m/sec]/ Pipeline roughness in Darcy-Weisbach friction factor [m]
L_{belly}	Length of the vehicle belly in contact with the soil [m]
L_{camber}	Length of the camber of the main body frame [m]
L_e	Effective leg length [m]
L_{e_in}	Effective leg length of the inner leg [m]
L_{e_out}	Effective leg length of the outer leg [m]
L_{foot}	Length of the foot [m]
L_{ladder}	Length of the ladder (as measured from the ladder yoke pin and the tip of last blade of cutter) [m]

L_{l_pc}	Lifting distance of leg during preparatory cycle [m]
L_o	Perpendicular distance between the leg pin centre and the foot pin centre [m]
L_{pipe_hor}	Length of the horizontal pipeline section [m]
L_{pipe_inc}	Length of the inclined pipeline section [m]
L_{sb}	Length of any submerged body [m]
L_{sm}	Length of the suction mouth [m]
L_{track}	Length of the track [m]
$L_{vehicle}$	Length of the vehicle without the ladder assembly [m]
l_s	Rupture distance between two grousers attached to the foot [m]
l_{sp}	Length of shear plane for each grouser [m]
M	Empirical exponent sensitive on particle size distribution in GIW model [-]
M_{res}	Moment of turning resistance exerted on the feet by the ground [kN-m]
m	Exponent in Vesic's Bearing capacity equation [-]
m_L	Exponent in longitudinal direction in Vesic's Bearing capacity equation [-]
$m_{soillump}$	Mass of a spherical soil lump/ particle [kg]
N_{cutter}	Cutter power [kW]
N_{cutter_av}	Average cutting power [kW]
N_c	Bearing capacity factor for a long rectangle due to the soil cohesion [-]
N_{pump}	Pump power [kW]
N_q	Bearing capacity factor for a long rectangle due to the soil surcharge [-]
N_γ	Bearing capacity factor for a long rectangle due to the weight of the soil [-]

N_{ϕ}	Flow value in passive earth pressure estimation [-]
n_{soil}	In-situ pore volume of the soil [-]
O_i	Instantaneous centre of rotation of the vehicle [-]
P	Horizontal component of load in case of inclined loading [kN]
P_{gather}	Gathering production [m ³ /sec]
P_{loose}	Loosening production [m ³ /sec]
P_{max}	Maximum value of horizontal component of load in case of inclined loading [kN]
P_{entry_m}	Pressure drop due to entry losses for mixture flow [kPa]
P_{exit_m}	Pressure drop due to exit losses for mixture flow [kPa]
P_{ho}	Hydraulic oil pressure [kPa]
$P_{major_hor_m}$	Pressure drop in the horizontal pipeline section for mixture flow [kPa]
$P_{major_inc_m}$	Pressure drop in the inclined pipeline section for mixture flow [kPa]
P_{minor_m}	Minor pressure drop for mixture flow [kPa]
P_{soil_normal}	Normal pressure acting on the soil [kPa]
$P_{st_total_m}$	Total pressure drop due to the static head loss for mixture flow [kPa]
P_v	Vapor pressure of water [kPa]
$P_{soil_surcharge}$	Soil surcharge [kPa]
Q	Total inclined load acting on any shallow foundation [kN]
Q_m	Mixture flow rate through the dredging pipeline [m ³ /sec]
Q_o	Vertical load acting on soil [kN]

Q_{pump}	Flow rate of the dredge pump [m ³ /sec]
Q_{shc_ladder}	Hydraulic oil flow in the ladder-swing hydraulic cylinder [m ³ /sec]
Q_{solid}	Delivered solid flow rate [m ³ / sec]
q_0	Bearing capacity of the soil/ Allowable ground pressure [kPa]
R_{cutter}	Radius of the cutter [m]
R_{cutter_edge}	Radius of the circle described by the cutter edge during rotation [m]
Re	Reynolds number [-]
$R_{soillump}$	Radius of the soil lump/ particle [m]
R_{swing_cutter}	Radius of rotation of the cutter tip with respect to the pivot point of the ladder assembly [m]
R_{turn}	Turning radius of the vehicle without slip or skid at the foot/ soil interface [m]
$\overset{\cdot}{R}_{turn}$	Modified turning radius of the vehicle with slip or skid [m]
r	Distance of the soil lump/ particle from the centre of the suction mouth in the horizontal direction [m]
rpm_{cutter}	Cutter rpm [-]
rpm_{pump}	Dredge pump rpm [-]
S	Feed of the cutter [m]
S_u	Undrained shear strength of cohesive soil [kPa]
T	Ambient temperature [degree C]
TF	Transport factor in the dredging pipeline system [-]
t	Time [sec]
t_{swing_leg}	Time required for swinging the leg [sec]

V_{soil_total}	Total volume of the soil dislodged by the cutter per unit of time [m ³ /sec]
v	Linear velocity [m/sec]
v_{cur}	Velocity of the current [m/sec]
v_{cutter}	Tangential velocity of the cutter [m/sec]
v_{dl}	Deposition limit velocity for horizontal pipeline section [m/sec]
$v_{dl\omega}$	Deposition limit velocity for inclined pipeline section [m/sec]
v_{leg_in}	Linear velocity of the inner leg [m/sec]
v_{leg_out}	Linear velocity of the outer leg [m/sec]
$v_{lhc_leg_e}$	Velocity of the leg-lift hydraulic cylinder during expansion [m/sec]
v_j	Speed of slip of the foot in a direction opposite to the direction of vehicle motion [m/sec]
v_m	Mean mixture velocity in the dredging pipeline [m/sec]
v'_m	Transport velocity for mixture flow in horizontal pipeline section [m/sec]
$v_m_pipe_del$	Mean mixture velocity in the delivery pipeline [m/sec]
$v_m_pipe_suc$	Mean mixture velocity in the suction pipeline [m/sec]
$v_{m\omega}$	Transport velocity for mixture flow in inclined pipeline section [m/sec]
v_o	Flow velocity of mixture into the suction mouth [m/sec]
$v_{pipe_suc_entry}$	Suction velocity at the suction pipe entry [m/sec]
v_r	Resultant velocity with which the soil lumps/ particles leaves the cutterhead [m/sec]
$v_{setl_maxsize}$	Settling velocity of the largest diameter of the soil lump/ particle [m/sec]
v_{shc_ladder}	Velocity of the ladder-swing hydraulic cylinder [m/sec]

v_{shc_leg}	Velocity of the leg-swing hydraulic cylinder [m/sec]
v_{sm}	Velocity at the suction mouth [m/sec]
v_{swing_cutter}	Translatory velocity of the cutter [m/sec]
v_{swing_ladder}	Swing velocity of the ladder assembly [m/sec]
$v_{vehicle_theo}$	Theoretical velocity of the vehicle [m/sec]
v_{50}	Value of mean mixture velocity in the pipeline (v_m) at which one half of solids is suspended in a carrier flow [m/sec]
x_j	Distance of the point at which shear displacement is considered from the front of the contact area of a track [m]
x_{step}	Total step size of individual leg [m]
x_{step_fnl}	Step size due to final swing angle of the leg [m]
x'_{step_fnl}	Step size due to final swing angle of the leg after slip [m]
x_{step_in}	Step size of the inner leg [m]
x_{step_intl}	Step size due to initial swing angle of the leg [m]
x_{step_max}	Maximum step size of the leg [m]
x_{step_min}	Minimum step size of the leg [m]
x_{step_out}	Step size of the outer leg [m]
Δx	Slip at the foot/ soil interface [m]
z_{blade}	Number of cutter blades in a row [-]
$z_{grouser}$	Number of grousers attached to the foot [-]
z_{cutter_row}	Number of rows of cutter blades along the length of the cutter [-]
α	Angle between the ladder boom and the horizontal [degree]

α_{cur}	Angle between the current force and the horizontal [degree]
α_{camber}	Camber angle of the main body frame [degree]
α_{swing}	Half -swing angle of the ladder assembly [degree]
β	Angle between the dipper and the horizontal [degree]
γ	Exponent for hydraulic gradient for mixture flow in inclined pipe with Wilson model [-]
γ_{leg}	Swing angle of leg [degree]
γ_{leg_fnl}	Final angle of leg swing [degree]
γ'_{leg_fnl}	Final angle of leg swing due to slip [degree]
γ_{ladder}	Angle between the axis of the ladder swing cylinder and the central axis of the vehicle [degree]
γ_{leg_intl}	Initial angle of leg swing [degree]
$\gamma_{leg_intl_in}$	Initial angle of leg swing for the inner leg during vehicle turning [degree]
$\gamma_{leg_intl_out}$	Initial angle of leg swing for the outer leg during vehicle turning [degree]
γ_{soil}	Specific weight of the soil [kN/m ³]
δ_{soil_foot}	Angle of friction between the soil and the foot [degree]
η_{pump}	Pump efficiency [%]
λ_{cutter}	Ratio between rotary and translatory velocities of the cutter [-]
λ_f	Darcy-Weisbach friction factor [-]
ϕ_{soil}	Angle of internal friction of the soil [degree]
ϕ_{blade}	Angle between two successive cutter blades [radians]
μ_{fT}	Dynamic viscosity of water at T degree C [Pa.s]

μ_{soil_blade}	Coefficient of friction between the soil and the cutter blade [-]
ν	Kinematic viscosity of the surrounding fluid [m^2/sec]
θ_r	Angle which the resultant velocity (v_r) [m/sec] makes with the horizontal [degree]
ρ_f	Density of the surrounding fluid or water [kg/m^3]
ρ_{f0}	Density of the surrounding fluid or water at 0 degree C [kg/m^3]
ρ_{fT}	Density of the surrounding fluid or water at T degree C [kg/m^3]
ρ_m	Density of the mixture [kg/m^3]
ρ_{rel_f}	Relative density of the fluid [-]
ρ_{rel_m}	Relative density of the mixture [-]
ρ_{rel_soil}	Relative density of the soil [-]
ρ_{soil}	Density of the soil [kg/m^3]
ρ_{si}	Density of the in-situ soil [kg/m^3]
σ_p	Passive earth pressure [kPa]
τ	Shear stress of the soil [kPa]
τ_{max}	Maximum shear stress of the soil [kPa]
τ_{res}	Residual shear stress of the soil [kPa]
ω	Pipeline inclination [degree]
Ω_{cutter}	Angular velocity of the cutter [rad/sec]
Ω_{leg}	Angular velocity of the leg [rad/sec]
Ω_{leg_in}	Angular velocity of the inner leg [rad/sec]
Ω_{leg_out}	Angular velocity of the outer leg [rad/sec]

Ω_{shc_e}	Angular velocity of the leg swing cylinder during expansion [rad/sec]
Ω_{shc_r}	Angular velocity of the leg swing cylinder during retraction [rad/sec]
$\Omega_{vehicle}$	Yaw velocity of the vehicle without slip or skid at the foot/ soil interface [rad/sec]
$\Omega'_{vehicle}$	Modified yaw velocity of the vehicle with slip or skid [rad/sec]
ψ	Angle between the tangential velocity of the cutter and the horizontal [degree]
ξ	Minor loss co-efficient in dredging pipelines [-]
ζ_c	Shape factor in soil bearing capacity equation due to the soil cohesion [-]
ζ_q	Shape factor in soil bearing capacity equation due to the soil surcharge [-]
ζ_γ	Shape factor in soil bearing capacity equation due to the soil weight [-]
ζ_{ci}	Inclination factor in soil bearing capacity equation due to the soil cohesion [-]
ζ_{qi}	Inclination factor in soil bearing capacity equation due to the soil surcharge [-]
$\zeta_{\gamma i}$	Inclination factor in soil bearing capacity equation due to the soil weight [-]

List of Subscripts

<i>av</i>	Average
<i>b</i>	Buoyancy
<i>belly</i>	Vehicle belly
<i>blade</i>	Blade of the cutter
<i>boom</i>	Ladder boom of the designed vehicle
<i>c</i>	Cavitating condition during soil excavation
<i>camber</i>	Camber underneath the main body frame of the designed vehicle
<i>coh</i>	Cohesive
<i>cur</i>	Current
<i>cutter</i>	Cutter for excavation
<i>d</i>	Drag
<i>del</i>	Delivery
<i>dipper</i>	Dipper of the ladder assembly
<i>dl</i>	Deposition limit
<i>e</i>	Expansion/ Effective
<i>edge</i>	Cutter blade edge
<i>entry</i>	Entry to the suction mouth of the dredging pump-pipeline system
<i>eq</i>	Equivalent
<i>exit</i>	Exit from the dredging pump-pipeline system at the delivery end
<i>f</i>	Fluid/ Friction
<i>fa</i>	Frontal area
<i>fnl</i>	Final

<i>foot</i>	Foot attached to the leg of the vehicle/ Footing for shallow foundation theories
<i>g</i>	Gravitation
<i>gather</i>	Gathering of soil during excavation
<i>gran</i>	Granular soil
<i>grouser</i>	Lug or teeth attached underneath the foot
<i>hc</i>	Hydraulic cylinder
<i>ho</i>	Hydraulic oil
<i>hor</i>	Horizontal
<i>i</i>	Instantaneous
<i>ic</i>	Idle cycle
<i>in</i>	Inner
<i>inc</i>	Inclined
<i>intl</i>	Initial
<i>l</i>	Lift
<i>ladder</i>	Ladder structure of the designed vehicle
<i>leg</i>	Leg of the designed vehicle used for locomotion
<i>lhc</i>	Lift hydraulic cylinder
<i>lo</i>	Lower
<i>loose</i>	Loosening of soil during excavation
<i>m</i>	Mixture
<i>man</i>	Manometric
<i>max</i>	Maximum
<i>maxsize</i>	Maximum size
<i>mf</i>	Decisive soil particle defined by MTI, Holland

<i>min</i>	Minimum
<i>n</i>	n percentile for soil samples
<i>nc</i>	Non-cavitating condition during soil excavation
<i>p</i>	Tractive force
<i>pc</i>	Preparatory cycle for locomotion
<i>pipe</i>	Pipe
<i>prp</i>	Proportional
<i>pump</i>	Dredge pump
<i>out</i>	Outer
<i>r</i>	Retraction/ Resultant
<i>rcrc</i>	Recirculation
<i>rel</i>	Relative
<i>res</i>	Resisting/ Residual
<i>ridge</i>	Soil ridge formed during excavation
<i>rod</i>	Hydraulic cylinder rod
<i>row</i>	Row of cutter blades
<i>s</i>	Specific
<i>sb</i>	Submerged body
<i>setl</i>	Settling
<i>serv</i>	Service
<i>shc</i>	Swing hydraulic cylinder
<i>si</i>	In-situ
<i>soillump</i>	Soil lump or particle dislodged by cutter
<i>sm</i>	Suction mouth

<i>soilwedge</i>	Soil wedge dislodged by two successive cutter blades
<i>sp</i>	Sphere
<i>st</i>	Static
<i>step</i>	Step size of individual leg
<i>suc</i>	Suction
surcharge	Surcharge of soil
<i>swing</i>	Swinging
<i>so</i>	System operation
<i>T</i>	Temperature
<i>theo</i>	Theoretical
<i>track</i>	Track used for locomotion in any off-road vehicle
<i>turn</i>	Turning
<i>u</i>	Undrained
<i>v</i>	Volumetric/ Vapor pressure
<i>vd</i>	Delivered volumetric
<i>vd_{si}</i>	Delivered volumetric in-situ
<i>vehicle</i>	Vehicle is the designed vehicle named 'Golden Tortoise'
<i>vert</i>	Vertical
<i>w</i>	Water
<i>wsa</i>	Wetted surface area
<i>ω</i>	Inclination of dredging pipeline

CHAPTER 1

INTRODUCTION

1.1 Introduction

Submersible dredgers/ miners are bottom moving remotely operated vehicles. The performance of a submersible dredger/ miner is judged by the ability of the vehicle to perform locomotion on unstructured to partially structured submerged natural terrain, while excavating and transporting the excavated material to the surface, at a desired rate and concentration level, with a given power supplied through an umbilical cable. Suitable positioning and navigational equipment is required for locomotion of the vehicle along the desired path with minimal error. 'Autonomy' to a desired level, is necessary for the effective and efficient working of the vehicle. The vehicle is launched in and recovered from the working environment. Either an onshore support station or a support vessel is indispensable for such operations. A submersible dredger/ miner can thus be divided into the following systems of 1) hull, 2) excavation, 3) transport, 4) locomotion, 5) positioning and navigation, 6) instrumentation, automation and control, 7) power, and 8) auxiliary – launching and recovery.

The basic mobility requirement for a submersible dredger/ miner considers the performance of the vehicle in soft terrain and obstacle negotiation and avoidance. The performance of the excavation system is judged by the excavation production, the spillage generated, and the excavation power required for a particular soil type. The performance of the transportation system is determined by its ability to transport the excavated material at a given rate and solids concentration without pipeline blockage.

The locomotion, excavation and transportation processes of a submersible dredger/ miner are interrelated with each other in a very complex fashion. Identification and modeling of such complex interrelationships is essential for the overall performance evaluation of any submersible dredger/ miner. Adequate knowledge about the locomotion, excavation and transportation processes together with the soil mechanical aspects of these processes for a submersible dredger/ miner is essential prior to the modeling of the interactions between these processes.

A survey of the state of the art about the available technologies including surface floating dredgers, submersible dredgers and trenchers, other deep dredging/ mining techniques and legged robots were performed. The review helped in understanding the limitations of the existing technologies and hence the necessity of development of new technology. A short description of the issues concerning the locomotion, excavation and transportation processes of a submersible dredger/ miner are presented in this chapter. The contents of the thesis are outlined in this chapter as well.

1.2 Motivation for the Research

The worldwide demand of potable and irrigation water and hydro-electric power plants led to the construction of dams and associated reservoirs in the 20 th century, with depths varying between 20 and 120 m. The flushing gate systems of such reservoirs are sometimes not effective in removing the sediments, resulting in cumulative sedimentation effects both around the flushing gates and in the reservoirs. Surface floating cutter suction dredgers are used to clear this sedimentation in shallow reservoirs, while grabs, airlift systems and submersible centrifugal dredge pumps are used for deep reservoirs [Richardson, 2002]. Small surface floating dredgers are constrained by their ladder (a long truss-like structure ‘arm’ that supports the excavation tool) length while big ones are unable to operate in such small confined areas (Figure 1.1). The

absence of good approach roads makes it difficult to transport big dredgers to such sites and some may be just too big to be transported over land. Modification of such big vessels is difficult if not impossible.

Grabs lack accuracy and precision and the average production is very low. In airlift systems, compressed air is introduced in a vertical closed conduit which transports the excavated material to the surface as a three phase flow. The use of airlifts, though well known in dredging and mining operations from great depths, is a very low efficiency system. Van der Steen [1989] suggested the use of submersible dredgers for deep inland reservoirs.

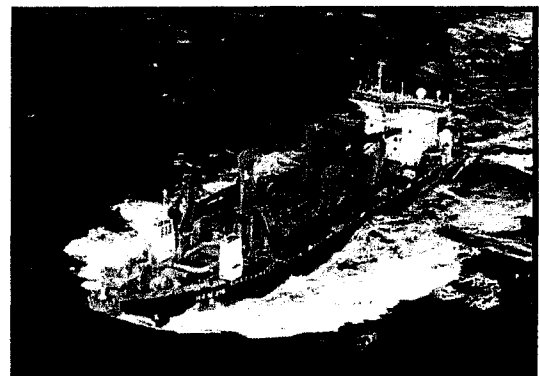
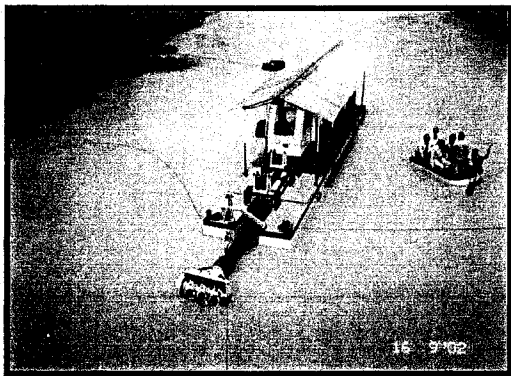


Figure 1.1 Small and big surface floating dredgers (Courtesy EEM, India and IHC, The Netherlands)

In shelf areas dredging is done for maintenance of navigational channels, reclamation works, beach replenishments, new construction and mining purposes. Shallow and deep water dredging and trenching operations are necessary for offshore oil and gas and telecommunications industries. Increasing demand and depletion of land mineral resources is leading the world to consider the ocean as a future source of minerals [Barker et al., 1990; Denovan, 1996; Desa, 1999; Kuo, 1994; Mangkusubroto, 1995; Moon et al., 1997; Scott, 2001]. Surface floating cutter suction and trailing suction hopper dredgers are primarily used for dredging and mining

operations in offshore areas, which have several limitations due to 1) effect of currents, waves and winds, 2) presence of long floating pipelines, anchor and winch wires, and 3) depth of operation.

Currents, waves and wind forces can cause large motions of these dredgers and hence of the dredging tools at the seabed [Herbich, 2000; Nakamaru et al., 1992]. Such motions decrease the production or cause damage to the ladder structure and the excavation tools. Surface floating dredgers commonly operate in moderate sea state having significant wave height from 1.25 to 2.50 m with sea state code number 4 (Tupper, 2000, p 92). Surface floating dredgers may effectively operate up to moderate breeze condition (Beaufort scale 4) having wind speed of 5.5 to 7.9 m/sec (Tupper, 2000, p 86). These values are representative values. Exact values will depend on the design of a particular dredger.

Long floating pipelines, floats, anchors and winch wires cause obstacles to the navigational paths of the other surface vessels. The floating pipeline operation can be disrupted during inclement weather.

The dredging projects of the past decade were carried out at an ever increasing depth and scale [Verheul et al., 2004]. The average depth of the continental shelves is about 70 m and the maximum depth is about 200 m. The dredging depth of the present day surface floating dredgers (excluding grabs) is < 100 m [Vlasblom, 2000, 1999]. 'Vasco da Gama', the world's largest trailing suction hopper dredger has a maximum dredging depth of 155 m [Ports and Dredging, 2003]. Boskalis Offshore BV and Tideway used a remotely operated grab and drag system for excavation of glory holes in the offshore White Rose Oil Fields located approximately 350 km east of St. John's, Newfoundland, Canada [Web page 1.1]. The excavation of the glory holes is

to a depth of 120 m, but this grab and drag system has the capability to reach up to 1000 m (Figure 1.2). This system is very accurate and effective for excavation of glory holes or pipeline related works, where the excavated material is not transported to the surface, but is not a suitable option for transporting large quantities of material to the surface.

It is evident from the above discussion that a submersible dredging/ mining platform is a suitable technology, to be used in deep inland reservoirs, shelf areas and tidal inlets. Such a system has the following advantages 1) less effect of surface currents, waves and winds on a submersible system, 2) large part of the delivery pipeline is under water, 3) no anchor or winch wires are necessary, 4) less disturbance to other surface vessels, and 5) depth of operation can be more than surface floating dredgers.

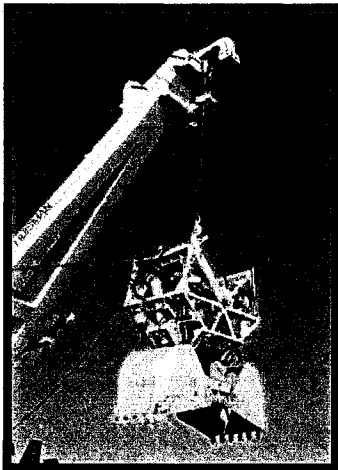


Figure 1. 2 Remotely operated grab
(Courtesy Boskalis Offshore BV and Tideway)

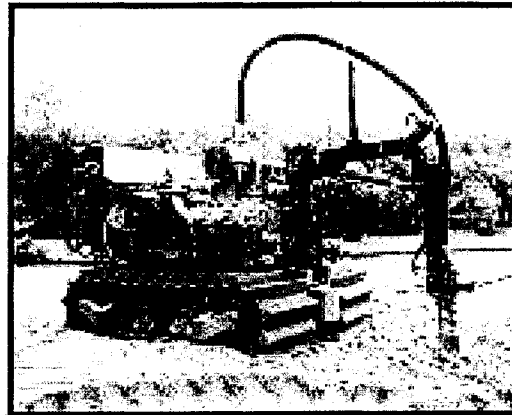


Figure 1. 3 Sub sea crawler
(Courtesy IKS and NIOT)

The submersible dredgers/ miners available in the present day global marketplace are remotely operated vehicles used for harbor dredging or mining activities in the shelf areas [Boezeman et al., 2000; Deepak et al., 2001; Deepak et al., 1999; Handschuh et al., 2001; Jonge et al., 2001; Nakamaru et al., 1992; Van der Steen, 1999-2000; Vlasblom, 2000]. Most of them use tracks for

locomotion (Figure 1.3) A self movable type submersible dredging robot has been developed by Mitsubishi Heavy Industries Ltd. for dredging sands deposited in the storage dams of hydro-electric power stations [Tsuji, 1995]. Tracks are robust, speed effective and easy to control, but require a continuous rolling contact. With varying terrain slopes, tracks are unable to keep the vehicle body horizontal and in extreme cases may be unable to negotiate the slopes. The excavation tool deviates from the desired trajectory if the vehicle body is not horizontal, thus lowering the accuracy of the dredging operation and the average production. Legged locomotion is preferred over unstructured and unprepared natural terrain as it is effective in obstacle avoidance and slope negotiation. Legs are however difficult to control especially with the increase in the design complexity. They also have speed limitations. Speed is not an important criterion for dredging/ mining operations in a given workspace, but is important when the vehicle traverses between widely separated workspaces. The vehicle body can be kept horizontal with individual leg movement, which is preferred for dredging or mining operations.

For most legged vehicles, each leg has two phases 1) 'support phase', where the leg is in contact with the ground and 2) 'transfer phase', where the leg is not in contact with the ground. The gait planning i.e. the pattern of leg placement determines the time for the 'support phase' and the 'transfer phase' of a particular leg. The number of legs in contact with the ground thus determines the normal load incident at each leg [Caurin and Gürman, 1994; Nagy et al., 1992]. The gait planning should be done carefully, particularly for soft terrain, so that the normal pressure distribution at the foot/ soil interface does not produce undesirable settlements and soil failure. Such problems are greatly reduced when the support and transfer phases of all the legs of a legged vehicle are coincident.

The existing legged submersible dredgers perform locomotion by the successive movements of two hydraulically operated frames to which passive legs (legs are actually not responsible for the locomotion, but provide the support only) are attached [Nakamaru et al., 1992; Verheul et al., 2004]. The principle of operation of such passive legged vehicle is shown in Figure 1.4.

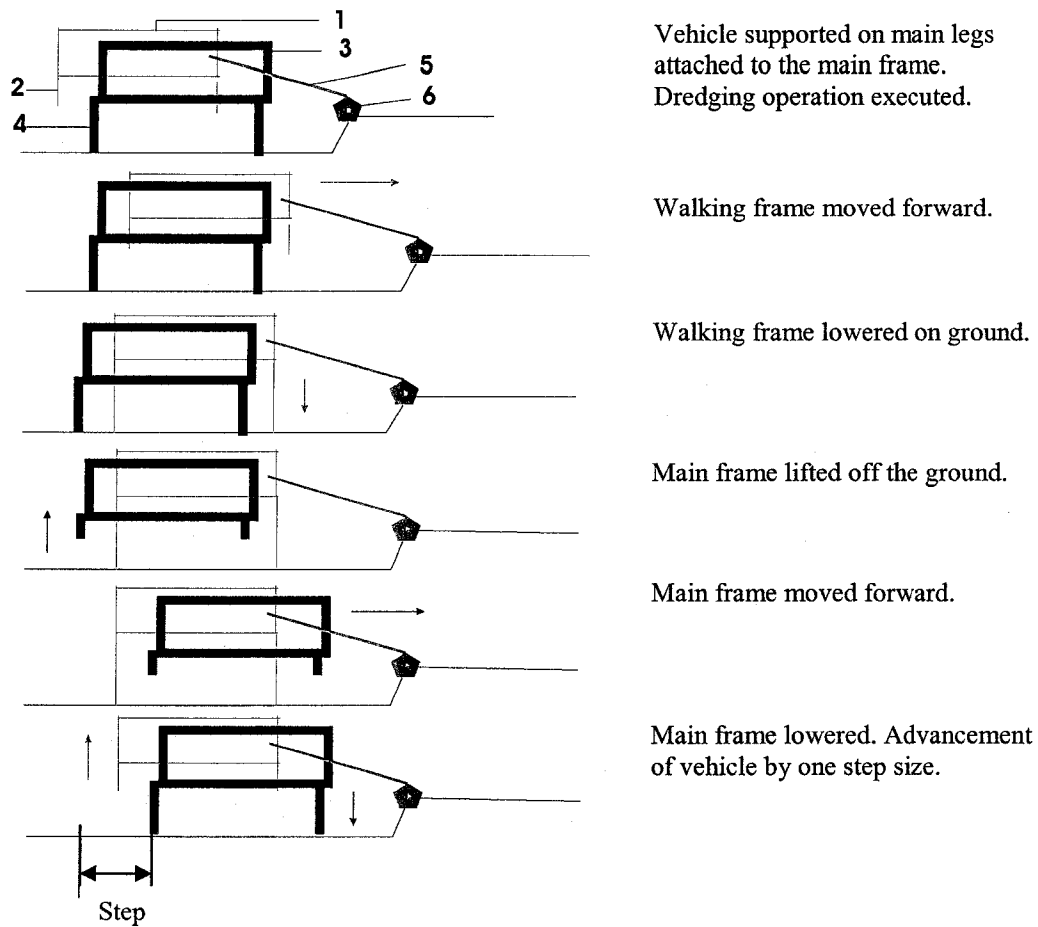


Figure 1.4 Principle of operation of passive legged vehicle (1 Walking frame, 2 Walking leg, 3 Main frame, 4 Main leg, 5 Ladder assembly, 6 Cutter head)

The legs of each frame are in continuous contact with the ground. But it is difficult to operate such vehicles in undulating terrain, where the vehicle body must be kept horizontal for effective dredging or mining operations (Figure 1.5 and Figure 1.6).

The Ship Research Institute, University of Gdansk has designed an unmanned autonomous remotely operated vehicle (AROV), which has three legs for support on the sea bottom [Narewski et al., 2002]. This will be used for deep-sea nodule mining operations [Narewski et al., 2002].

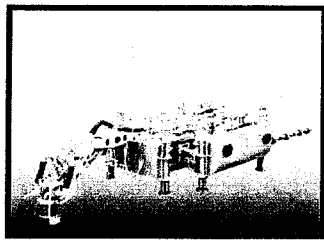


Figure 1.5 Futuba-2

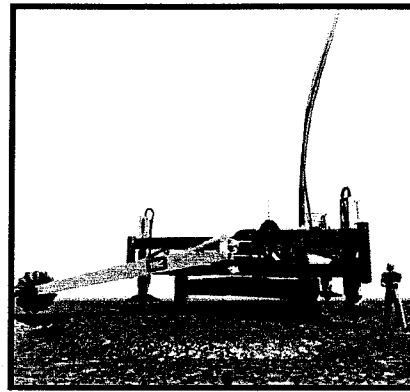


Figure 1.6 Tripod (Verheul et al., 2004)

The limitations of the existing technologies led to the development of the new active legged submersible dredger/ miner described in this thesis. A full scale prototype vehicle was manufactured by Excavation & Equipment Manufacturing (P) Ltd., (EEM (P) Ltd.) India. EEM (P) Ltd. is an inland dredging company from eastern India, which has designed, built and operated small modular surface floating dredgers for the last 26 years. The conceptual and the overall design of the active legged vehicle were developed by the author within the scope of the present research. The basic strength calculations for the different structures, hydraulic and electric power requirements and circuits design, cutter drum and cutter drive design, pressure vessels design and the leg linkage design were done by the author. The centrifugal dredge pump, the eductor pump and the cutter blades were the standard dredger components developed and designed by EEM (P) Ltd., which has been used in the surface floating inland dredgers designed and manufactured by EEM (P) Ltd. for many years. The design of the mechanical load cell and

the hydraulic load cell along with the test set up were performed by the author. During the annual visits to the workshop of EEM (P) Ltd. in India, the author supervised the manufacture of the designed vehicle and also carried out the different prototype tests as described in this thesis.

The designed vehicle is known as the ‘Golden Tortoise’.

1.3 State of the Art of Technologies

1.3.1 Surface Floating Dredgers

The common types of surface floating dredgers used for general dredging works and mining purposes are shown in Figure 1.7.

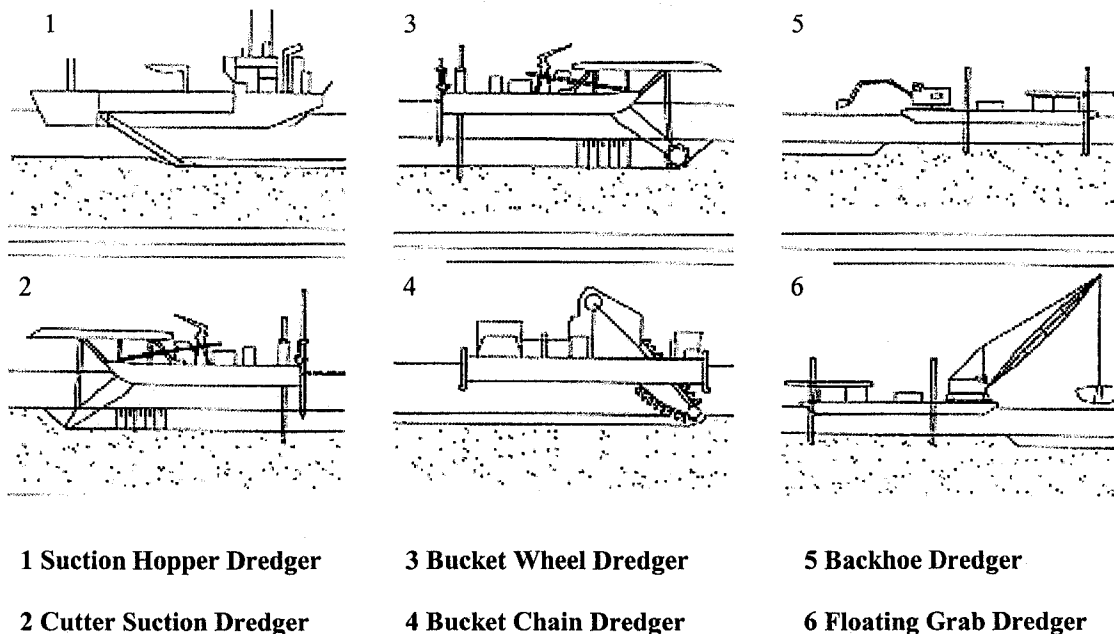


Figure 1.7 Different types of surface floating dredgers

Suction dredgers, cutter suction dredgers and bucket wheel suction dredgers are commonly used for alluvial and offshore mining purposes [Herbich, 2000, 1999]. Suction dredgers are used for mining free flowing material like sand and gravel from depths of 18 to 20 m below water level [Herbich, 2000, 1999]. Cutter suction dredgers are useful in mining alluvial tin, placer gold, sand

and gravels. Bucket wheel suction dredgers are used for marine alluvial or elluvial¹ deposits and are able to cope with various kinds of clays and indurate² sands [Herbich, 2000, 1999]. Simulation studies with a computer model developed by the Centre for Dredging, Texas A & M University, showed the feasibility of using a bucket wheel dredger together with a hydraulic transport system for mining tin ore from the ocean floor at depths greater than 50 m [Albar et al., 2002]. Clam-shell buckets with screening systems can be used for mining underwater sand and gravel from a depth of approximately 50 m.

1.3.2 Submersible Dredgers/ Miners

The world's first submersible dredger was operated by two onboard operators [Bascom, 1970]. This submersible dredger had a dredge ladder with a rotating cutter and a pump. Air and electricity were supplied to the dredge from the shore. The machinery compartment, pump, operator's compartment, ladder and cutter were mounted on a Caterpillar D-9 track type tractor carriage [Bascom, 1970].

The concepts of remotely controlled unmanned submersible dredgers working in seafloor leveling, precision trenching and excavation processes came around the early 1970s [Article in World Dredging & Marine Construction, 1973]. Various types of submersible dredgers including towed, self-propelled, buoyant submersibles and control habitats together with different lifting methods for mining poly-metallic sulphide nodules present at the sea bottom were also evaluated in the early 1970s [Denovan and Norman, 1996]. Most of the designs included some kind of bottom excavation and preparation device together with a segmented steel riser and an airlift system for the transportation of the excavated material [Denovan and Norman, 1996]. Remotely

¹ Weathered material which is still at, or near its point of formation. The term is especially applied to deposits of economic substances.

² Soft sediments hardened due to pressure and cementation.

operated submersible vehicles were also used for subsea sampling and mining placer gold and diamonds [Denovan and Norman, 1996]. The existing submersible tracked and legged vehicles were already discussed in section 1.2.

1.3.3 Subsea Trenchers

The company named SMD Hydrovision from the United Kingdom makes underwater tractors and ploughs for cable and pipeline burial and jetting machines with tracks or skid systems [Webpage 1.2] (Figure 1.8). The trenching machines developed by Dutch Sea Cable BV move either by wheels or skid systems and excavate material using high pressure jets, knives or specially designed chain cutters [Webpage 1.3]. There exists an extensive list of companies and the type of underwater equipment they manufacture [Webpage 1.4]. Underwater vehicles with skids are towed vehicles, which are ideal for cable and pipeline burial work, but are not effective for underwater dredging or mining platforms. For cable and pipeline burial works, the submersible vehicle usually moves along a desired path, whereas for dredging/ mining operations the submersible vehicle has move in a given workspace. Task planning for dredging/ mining operations with the towed vehicle will thus be difficult.

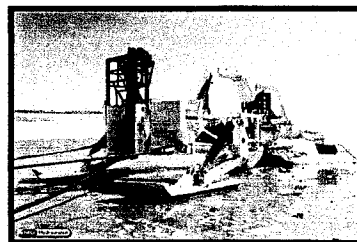
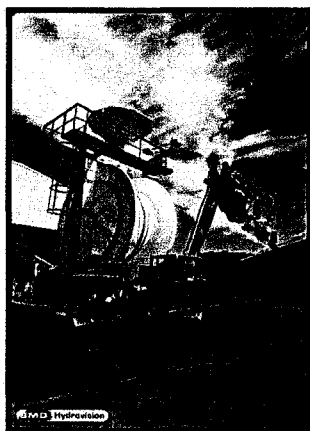


Figure 1.8 Subsea tractors and ploughs with skids (Courtesy SMD Hydrovision, UK)

1.3.4 Other Deep Dredging or Mining Technology

Excavation in deeper water is frequently observed in offshore oil and gas, telecommunications and mining industries, for which different technologies are often used.

Formerly most small-scale deep dredging was performed by diver-operated airlifts [Hill, 1983]. Airlift pumps are being taken into consideration in deep sea mining and transport of manganese nodules from depths down to 5000 m [Weber, 1982]. The offshore diamond mining industries in Namibia and South Africa used airlift systems in the early days which were gradually replaced by remotely operated underwater vehicles [Denovan and Norman, 1996]. Submersible dredge pump systems are also used for dredging operations. The remotely operated water tight submerged pump system known as 'Punaise' can dredge sediments from the sea floor, in large harbors and near the intakes of power stations without affecting navigation or being impacted by storms [Williams, and Visser, 1997] (Figure 1.9).



Figure 1.9 Punaise system (Williams, and Visser, 1997)

1.3.5 Robotic Vehicles in Hazardous and/ or Unstructured Environments

Robotic vehicles are used in nuclear, construction, offshore and chemical industries and in space applications. They are also used for underwater inspection and monitoring, forestry work, military operations, terrestrial mining etc. Considerable information about different types of legged robot is available [Webpages 1.5, 1.6, and 1.7]. Endo et al. [2000], Halme et al. [1999],

and Leppänen et al. [1998] have worked on hybrid land locomotion of wheel-legged robots. Greiner et al. [1996] developed crab-like autonomous legged underwater vehicles for mine hunting in the surf zone. A lobster-like bio-mimetic autonomous underwater vehicle with eight legs has been developed by Northeastern University [Witting et al., 2000]. An aquatic bottom robot developed for measuring sea bottom roughness has six legs, each having two degrees of freedom and a pinned foot [Akizono et al., 1997].

1.3.6 Comparisons between Available Technologies

The comparisons between 1) surface floating dredging or mining vessels and submersible systems, 2) submersible tracked, legged vehicles and vehicles with skids, and 3) airlifts and submerged centrifugal dredge pumps are shown in Tables 1.1, 1.2 and 1.3 respectively.

Table 1.1 Comparison between surface floating and submersible dredgers/ miners

Surface floating dredgers/ miners	Criteria	Submersible dredgers/ miners
Yes	Affected by waves, winds and currents	Less affected
Yes	Navigational restriction to other surface vessels	No
Yes	Dredging depth limitations	Less limitations
Affected by environmental forces	Production output	Less affected by environmental forces
More	Environmental impacts	Less

Table 1.2 Comparison between submersible crawlers, vehicles with skids and legged vehicles

Criteria	Submersible crawlers	Submersible vehicle with skids	Submersible legged vehicles
Self propelled	Yes	No - towed vehicle	Yes
Robust and easy to control	Yes	Not applicable as vehicle is towed	Robustness and control depends upon complexity of leg design
Requires continuous contact with terrain	Yes	Yes	No
Speed effective	Yes	No	No
Effective in slope negotiation on natural terrains	No – once the design limit is exceeded	No	Yes
Obstacle avoidance on natural terrains	No	No	Yes
Vehicle body can be kept horizontal	No	No	Yes

Table 1.3 Comparison between airlift and submersible centrifugal dredge pumps

Airlift	Criteria	Submersible centrifugal pumps
High	Energy consumption	Low
Low	Solids removal	High
No	Constant flow rate	Yes

The comparisons show that a submersible legged platform is effective for dredging or mining operations in deep inland reservoirs and shelf areas. Submersible centrifugal dredge pumps are more effective in transporting solids than airlift systems.

1.4 Statement of the Issues

This section presents a brief review on the locomotion systems commonly used by off-road and submersible vehicles, the excavation tools used for dredging or mining purposes and the transportation techniques used for carrying the excavated material to a desired point. A brief review of the previous works done on the locomotion, excavation and transportation processes is also added. This review helps in the selection of the suitable locomotion, excavation and

transport systems for the designed vehicle and also in the development of the performance evaluation models for such processes.

1.4.1 Locomotion System and Process

The common types of locomotion systems used by different on-land off-road vehicles and bottom crawling submersible vehicles are 1) tracks, 2) wheels, and 3) legs with skids or feet at their ends. The merits and demerits of such systems were already discussed in section 1.3.6.

Extensive work has been done on land locomotion using legs, wheels, tracks and hybrid systems over prepared and unprepared terrains [Amar, 1993; Cubero, 2000; Gee-Clough, 1991; Gerhart et al., 2000; Halme et al., 2000; Lagnemma and Dubowsky, 2002; Leppänen et al., 1998; Sasaki et al., 1991; Wettergreen, 1995; Wong, 1993; Zhaung et al., 1990]. Such works included the kinematics and kinetic modeling of the designed vehicle as well as the prediction of the vehicle performance by considering the mechanical properties of the terrain and its response to vehicular loading i.e. 'terramechanics'. For legged vehicles, gait planning as well as the static and dynamic stability issues are also major research concerns [Dudek and Jenkin, 2000; Halme et al., 2000; Lagnemma and Dubowsky, 2002; Leppänen et al., 1998]. The static and dynamic stability of a vehicle is determined by the position of the centre of gravity of the vehicle in relation to the support polygon created by the legs touching the ground.

The performance evaluations of on-land off-road vehicles were based on three different approaches of 1) application of the theory of elasticity and plastic equilibrium [Bekker, 1956; Wong, 1993], 2) empirical approach [Turnage, 1978; Wong, 1993], and 3) parametric modeling approach [Bekker, 1969; Wong, 1989]. The types of vehicle performance analyses performed by these approaches are discussed in detail by Wong [1993]. The theory of elasticity and plastic

equilibrium produces approximate results for tracked and wheeled vehicles because of the oversimplification of the assumptions used for such analyses. Empirical methods are simple to use and are used for the performance evaluation of vehicles with similar design features or those that have been tested under similar operating conditions but cannot be used for evaluations of new designs. The parametric methods evaluate the vehicle performance based on the measurement of terrain response under loading conditions similar to those exerted by an off-road tracked or wheeled vehicle and on the detailed analyses of the mechanics of the vehicle-terrain interaction [Bekker, 1969; Wong, 1989]. The major design parameters of vehicles, the relevant terrain characteristics including pressure-sinkage and shearing characteristics and the response to repetitive loading are considered for the parametric performance evaluation models of the off-road tracked and wheeled vehicles. Parametric analyses is the most suitable method for evaluation of competing designs, for optimization of the design parameters and for the selection of vehicles for a given mission and environment [Wong, 1993].

The above theories for on-land off-road tracked vehicles were extended or modified by different researchers when applied to subsea tracked vehicles [Choi et al., 2003; Hong and Choi, 2001; Muro, 1988; Nuttall Jr., 1971; Schulte, 2003 a, b and Van der Steen, 1999-2000].

Soil models used for on-land off-road tracked and wheeled vehicles were also used by Caurin [1994] to develop a robot-terrain interaction system for on-land legged vehicles. To the best of the author's knowledge there is no performance evaluation model for legged locomotion on submerged terrain in the published literature.

Because of the advantages of the parametric modeling approach in the evaluation of new designs and evaluation of the vehicle performance under new operating and environmental conditions, it was decided to use the parametric modeling approach in this research.

1.4.2 Excavation System and Process

The common types of excavation tools used by surface floating and submersible dredgers/miners can be subdivided into mechanical and hydraulic excavation tools. The suitability of the various types of mechanical and hydraulic excavation tools for different materials is shown in Table 1.4. The shaded areas are the possible combinations.

Hydraulic excavation tools like jets or agitation systems are suitable only for free flowing material like sand and silt. Crown cutters, drum cutters and dredge wheels are versatile mechanical excavation tools. Sometimes assisting jet systems are used with them. Mechanical cutters can be used for a range of material and hence the literature review was done only on mechanical cutters. Mechanical drum cutter is shown in Figure 1.10. The axis of the drum cutter can be perpendicular to the vehicle longitudinal axis (Figure 1.10) or parallel to the vehicle longitudinal axis.

The excavation system of any submersible dredger/ miner consists of a manipulator arm or ladder assembly to which the mechanical and assisting hydraulic excavation tools are attached [Boezeman et al., 2000; Deepak et al., 1999; Nakamaru et al., 1992; Van der Steen, 1999-2000].

Table 1.4 Suitability of excavation tools in various types of materials [Based on Chaziteodorou, 1977; Herbich, 2000; Vlasblom, 1999]

Excavation tools		Hard packed soil				Loose soil				Rock
		Clay	Silt	Sand	Gravel	Clay	Silt	Sand	Gravel	Limestone/ Coral/ Soft Basalt
M	Backhoe									
	Bucket/dredge wheel									
E	Buc. /dredge Wheel (picks)									
C	Crown - plain									
	Crown- serrated									
H	Crown -offset									
A	Crown- pick pt.									
N	Crown- adapter									
	Drag heads ³									
I	Drum/ rotavator									
C	Dustpan									
	Grab									
A	Mechanical collector									
L	Combination ⁴									
Hydraulic	Jets/ Agitation									

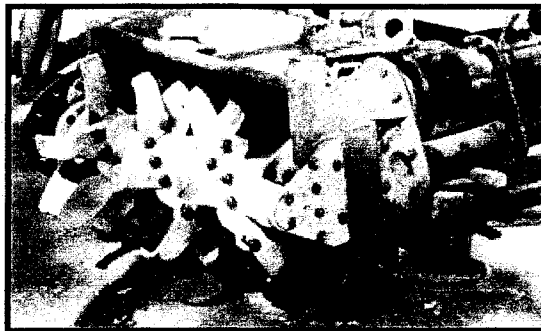


Figure 1.10 Mechanical cutter (Courtesy EEM (P) Ltd., India)

The excavation system of the designed vehicle consists of a twin drum cutter system (cutter axis parallel to the vehicle longitudinal axis, when the ladder assembly is horizontal with zero swing and pitching angles) with the suction mouth situated in between them. The drum cutters and the

³ Assisting jets can be used with drag suction heads in order to facilitate the fluidization of the ocean floor material. Does not work for clayey soil [Herbich, 2000]. Gratings can be used to reduce clogging of pipelines.

⁴ Suitable combination of mechanical excavation tool and jets

suction mouth are attached to a ladder assembly. In this thesis, the performance of the designed excavation system was based on the evaluation of the excavation production, spillage generated and the excavation power required for a particular soil type. Work has been done on the mixture forming processes and prediction of the spillage and hence the excavation production in a crown cutter while excavating hard formations [Burger et al., 1999]. No such work was found in the published literature for a twin drum cutter system with the suction mouth situated in between the two drum cutters.

Evaluation of the cutter power requires adequate knowledge about the two and three dimensional cutting theories for granular soil under non-cavitating and cavitating conditions and for cohesive material [Miedema, 1995, 1994, 1992, 1989 a and b, 1987, 1984; Van Leussen and Van Os, 1987; Van Os, 1977]. In practical works, the concept of specific energy derived from the cutting theories is however easy to apply. Specific energy is defined as the amount of energy required by the cutter to excavate a unit volume of soil. Empirical relationships and specific energy values are available in the literature for crown cutters under cavitating and non-cavitating conditions for granular non-cohesive soils and cohesive soils. Specific energy relations were used for estimating the cutter power for the designed cutter.

1.4.3 Transportation System and Process

The removal and transportation of the excavated material from the submerged ground to the surface is generally carried out by a number of basic evacuation systems 1) centrifugal dredge pumps, 2) eductor pumps, 3) airlift pumps, and 4) positive displacement pumps [Boezeman et al., 2000; Deepak et al., 2003; Deepak et al., 1999; Nakamaru et al., 1992; Van der Steen, 1999-2000]. These systems have in common that their performance depends on the type of material to be removed, such as particle size, specific gravity etc. and they all employ water as the

transportation medium. The rotating impeller of a centrifugal dredge pump imparts energy to the liquid by means of a centrifugal force. The working of the eductor pump is based on the momentum transfer between a high velocity flow and the liquid to be pumped. The functioning of an airlift is based on a density difference between the air-water mixtures within a vertical tube and the surrounding water. Positive displacement pumps operate by forcing a fixed volume of fluid from the inlet pressure section of the pump into the discharging zone of the pump. Positive displacement pumps are not very common in dredging/ mining operations. The construction of eductors and airlifts is relatively simple as they have no moving parts. Their ability to move larger soil particles without blocking is an additional advantage. However the overall efficiency is low, especially when pumping mixtures. The process control for eductors and airlifts is also poor. Centrifugal dredge pumps are far more efficient in dredging/ mining operations. The pipeline or riser system is also included within the transportation system.

The possible combinations of excavation tools and the transportation systems are given in Table 1.5.

Discontinuous or continuous mechanical transportation by ropes and ladders are limited to certain water depths and can be done with great technical effort [Chaziteodorou, 1977]. Continuous hydraulic (centrifugal dredge pump-pipeline system) and hydro-pneumatic (airlift-pipeline or centrifugal dredge pump-airlift-pipeline combination) transportation have been used for a long time for ocean mining activities [Chaziteodorou, 1977]. The eductor and centrifugal dredge pump combination is used in surface floating dredges and for land mining purposes [Bonnington, 1956; EEM Internal Report, 1990].

A centrifugal dredge pump with a supporting eductor pump in series was thus chosen for the designed submersible dredger/ miner. The main function of the supporting eductor pump is to reduce the chances of pipeline blockage.

Table 1.5 Possible combinations of excavation and transportation systems [Based on Chaziteodorou, 1977; Herbich, 2000; Vlasblom, 1999]

Excavation Transport		Drag heads	Cutter	Bucket wheel	Dustpan ⁵	Mech. ⁶ Collector	Backhoe	Jet	Grab	Scrap ⁷	Dragline
Discontinuous	Ropes	Not possible	Not possible	Not possible	Not possible	Not possible	Not possible	Not possible	Not possible	Not possible	Not possible
	Ladders	Not possible	Not possible	Not possible	Not possible	Not possible	Not possible	Not possible	Not possible	Not possible	Not possible
Continuous	Ropes	Not possible	Not possible	Not possible	Not possible	Not possible	Not possible	Not possible	Not possible	Not possible	Not possible
	Ladders	Not possible	Not possible	Not possible	Not possible	Not possible	Not possible	Not possible	Not possible	Not possible	Not possible
	Pipes (centrifugal)	Possible	Possible	Possible	Possible	Possible	Possible	Possible	Possible	Possible	Possible
	Pipes (Airlift)	Possible	Possible	Possible	Possible	Possible	Possible	Possible	Possible	Possible	Possible
	Pipes (hydro jet)	Possible	Possible	Possible	Possible	Possible	Possible	Possible	Possible	Possible	Possible
	Pipes (Containers)	Not possible	Not possible	Not possible	Not possible	Not possible	Not possible	Not possible	Not possible	Not possible	Not possible

-  Combination not possible
-  Combination possible
-  Combination not meaningful

1.5 Methodology and Outline

The review of the state of the art of the existing technologies shows the operational and environmental limitations of such systems in deep inland reservoirs and shelf areas. The review on the locomotion, excavation and transportation processes showed the absence of performance evaluation models for 1) locomotion process of submersible legged vehicles and 2) excavation process using a twin drum cutter system with the suction mouth in between. Work on the

⁵ Defined in Herbich, 2000

⁶ Defined in Herbich, 2000

⁷ Defined in Herbich, 2000

integration of the processes of locomotion, excavation and transportation for a submersible dredger/ miner was also not found in the open literature.

This led to the development of the following new work which is presented in this thesis:

1) Detailed mechanical design of an active legged (legs are actually responsible for the locomotion) submersible dredger/ miner was executed, focusing on the design of the hull, excavation, transportation, locomotion and power systems. Individual feet of the designed vehicle are in continuous contact with the terrain during the change in the position of the centre of gravity of the vehicle. The vehicle body can be kept horizontal by individual movement of the legs. The design thus solves the problems of other active legged vehicles as well as passive legged submersible dredgers.

2) Development of parametric performance evaluation models for the locomotion of the designed submersible legged vehicle by considering the terrain properties and also the response of the terrain to vehicular loading. The bearing capacity of the soil, the normal pressure–sinkage and the shear stress–shear displacement relationships during vehicular loading and the soil response due to repetitive loading are important for the evaluation of the mobility of a submersible legged vehicle.

In case of a legged vehicle, the normal load is applied to the terrain through the foot during the ‘support phase’. Due to the application of the normal load, sinkage can occur. Excessive sinkage can result in difficulty in lifting the foot due to overburden pressure. Also, differential settlement at different feet can result in the change in vehicle attitude and hence disrupt the vehicle operation. The gait planning of a legged vehicle determines whether a particular element of the terrain will be subjected to repetitive loading and also the number of cycles of repetitive loading.

The normal pressure-sinkage and shear stress-shear displacement relationships are altered due to repetitive loading. The normal pressure-sinkage relationships and the effects of repetitive loading were not considered within the scope of the current work. Only the bearing capacity of the soil and the shear stress-shear displacement relationships due to vehicular loading were considered to predict the stability of the designed vehicle and the traction generated by the designed foot and grousers respectively. These models were based on the theories of elasticity and plastic equilibrium as well as shallow foundation theories.

A unique method of locomotion, simulating the belly crawling motion of a tortoise or turtle was developed. Periodic gait plans for straight line and curvilinear locomotion as opposed to non-periodic gait plans commonly observed in natural terrains were developed for the designed vehicle. Parametric models were developed to estimate the locomotion cycle time of the designed vehicle for a given gait plan.

3) Parametric performance evaluation models for the designed excavation system consisting of twin drum cutters with the suction mouth in between were proposed, based on basic theories of earth moving machineries and dynamics. Such models predict the excavation production and also the spillage generated. An analogy between the designed drum cutter and crown cutter with picks was established in order to use the empirical specific energy relations to estimate the required excavation power for the designed cutter in a particular soil type.

4) The transportation of the excavated material to the surface is carried out through very long steeply inclined to vertical pipelines, as opposed to surface floating dredgers where transportation is achieved primarily by very long horizontal pipelines. Parametric performance evaluation models were developed for the transport system by integrating the works of different

researchers to obtain the limiting operating conditions of the centrifugal dredge pump-pipeline system of the designed vehicle. An eductor pump was used in series with the centrifugal dredge pump. The estimation of performance of the eductor pump and its effect on the overall performance of the transport system was kept outside the scope of the present research.

5) Deduction of the complex interrelationships existing between the locomotion, excavation and transportation processes of the designed submersible walking dredger/ miner in order to predict the overall performance under given operating and environmental conditions.

In developing the parametric performance evaluation models, only the soil data were considered. The effect of waves, winds, currents and other environmental factors were kept outside the scope of the present research, since the prototype constructed is suitable for operation in deep inland reservoirs only.

6) Experimental validation of the gait plans, locomotion cycle time and the stability issues due to the soil bearing capacity were performed with the full scale prototype of the designed vehicle. Comparisons between the mobility performance of the designed active legged vehicle and tracked vehicles were done to find the advantages and disadvantages of the designed vehicle over tracked vehicles.

The thesis consists of the following chapters,

Chapter 2 Describes the detailed mechanical design of the active legged submersible dredger/ miner named 'Golden Tortoise'.

Chapter 3 Describes the parametric performance evaluation models developed for locomotion of the designed vehicle. The predicted results as well as the experimental results are

presented in this chapter. Comparisons between the mobility performance of the designed active legged vehicle and tracked vehicles are also given in this chapter.

Chapter 4 Describes the parametric performance evaluation models developed for the excavation of the designed vehicle and also the predicted results.

Chapter 5 Describes the parametric performance evaluation models developed for the transportation process of the excavated material to the surface with the help of a centrifugal dredge pump–pipeline system and also the predicted results.

Chapter 6 The complex interrelationships between the locomotion, excavation and transportation processes for a submersible active legged dredger/ miner are deduced in this chapter using the designed vehicle as an example.

Chapter 7 Draws the conclusions and gives recommendations for further research.

A schematic of the submersible legged dredger/ miner designed and constructed is shown in Figure 1.11.

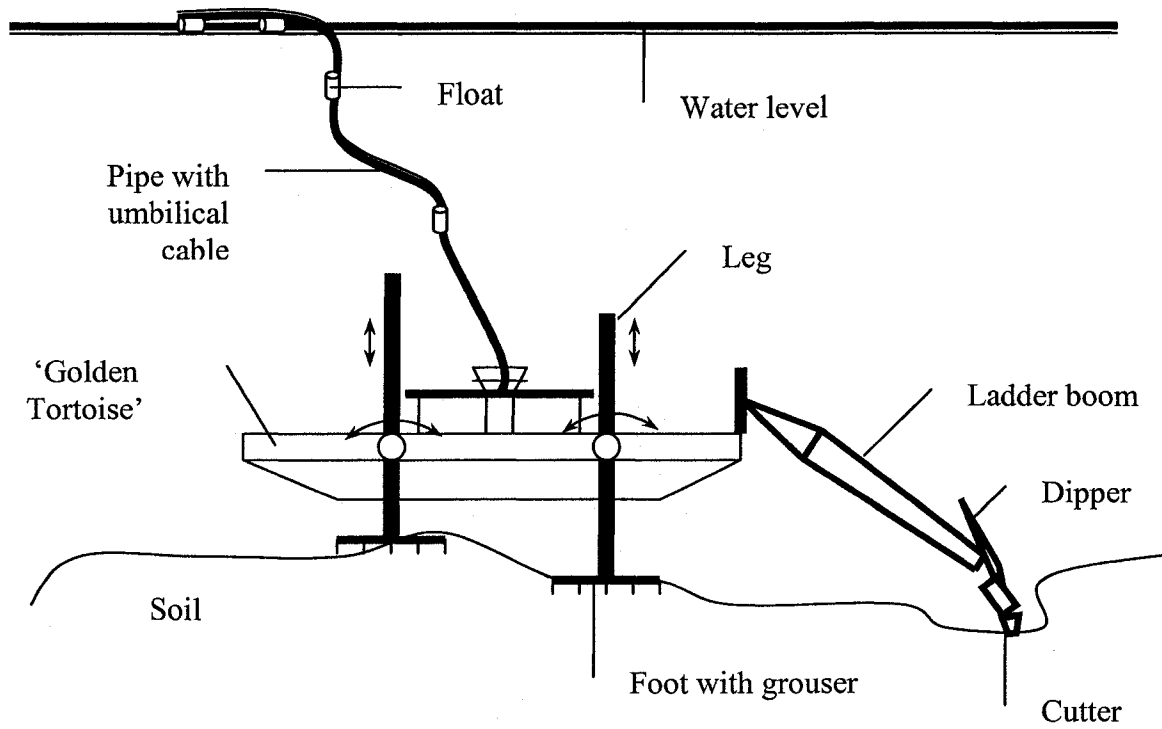


Figure 1.11 Schematic of the 'Golden Tortoise'

CHAPTER 2

DESIGN

2.1 Introduction

This chapter describes the design of the 'Golden Tortoise'. The electro-hydraulically actuated prototype vehicle was remotely operated on land by one person to perform the full-scale prototype tests. The prototype tests, which were performed to evaluate the functionality of the different systems of the designed vehicle, are discussed in this chapter.

2.2 General Arrangement

The general arrangement of the 'Golden Tortoise' is shown in Figure 2.1.

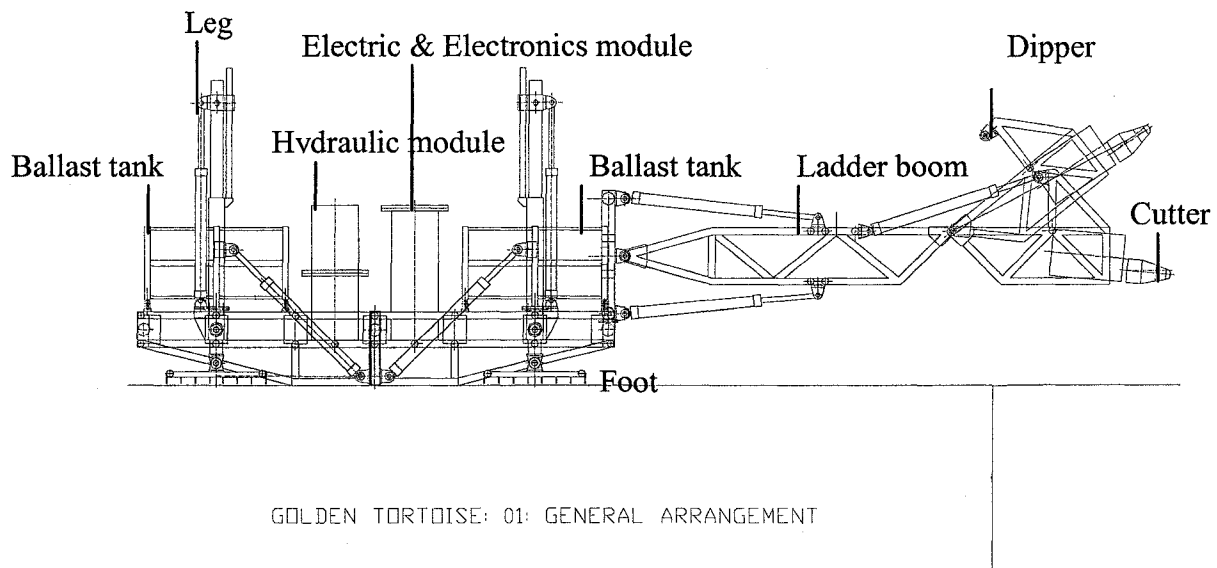


Figure 2.1 Schematic of 'Golden Tortoise' (Not to scale)

The hull consists of the main body frame, where modular dry pressure hulls having either vertical or horizontal orientations are attached. The ballast tanks, the hydraulic modules and the electric-electronics modules are dry pressure hulls. The same arrangement of the ballast tanks, the hydraulic module and the electric-electronics module are repeated on either side of the

designed vehicle. Individual pressure hulls are mounted on resilient material for reducing the vibrations. This also helps in segregation of vibrations of individual pressure hulls.

The designed vehicle has four ballast tanks attached at the four corners of the vehicle. The ballast tanks will help the vehicle to sink and float during launch and recovery operations. The main function of the ballast tanks is to control the bottom load by adjusting the amount of ballast water. Each ballast tank needs to be controlled separately. The load at each leg determines the soil failure criteria and also balances the operational forces thus preventing slippage and overturning of the vehicle during operation. Hydraulics and electric-electronics modules are present on either side of the designed vehicle.

The excavation system includes a ladder assembly and two interchangeable mechanical drum cutters positioned on either side of the suction mouth. The ladder assembly consisting of a boom and a dipper has three degrees of freedom, including a swing motion and a lifting/ lowering motion of the boom and the dipper. The ladder is attached to a rotating yoke, which is fixed to the main body frame.

A centrifugal dredge pump with an assisting annular eductor pump will be used to transport the excavated material to the surface by pipelines attached to the delivery end of the centrifugal dredge pump. Four hydraulically operated legs with pinned feet are used to perform locomotion on natural terrain. Legs are pinned to the main body frame and thus sudden loads from the legs are transferred to the main body frame and not the dry pressure hulls.

The processing and computational tasks for the movement and operation of the submersible legged dredger/ miner will be distributed between onboard and off board components depending upon the complexity and the time critical factors of the desired tasks. Presently a main power

supply line (440 V AC, 50 Hz cycle) is used for the primary power to drive the secondary hydraulic drives. During operation under water, primary electrical power supplied through the umbilical connected to the electrical module of the designed vehicle will drive the secondary hydraulic circuits (Figure 2.1).

The prototype constructed is shown in Figure 2.2. Data about the prototype vehicle is given in Table 2.1. Detailed designs of the different systems of the designed vehicle are discussed in the following sections.

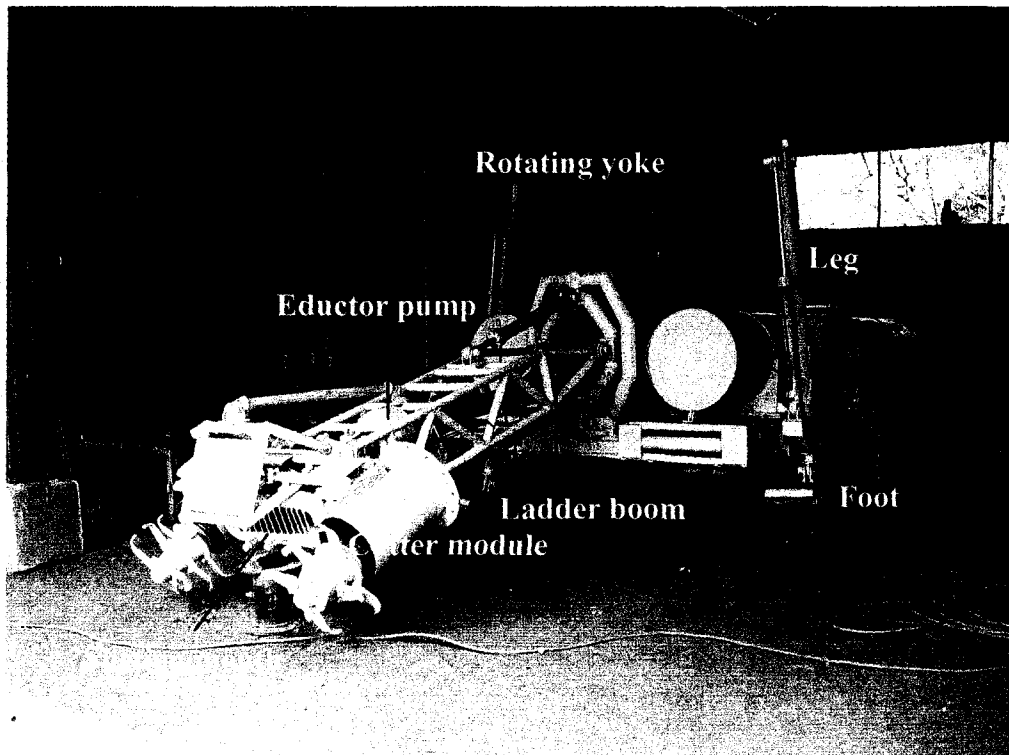


Figure 2.2 Prototype vehicle of 'Golden Tortoise'

Table 2. 1 Design data about the prototype of ‘Golden Tortoise’

Parameter	Specification
1. Overall length of vehicle (without ladder assembly)	3300 mm
2. Overall width of vehicle	2400 mm
3. Overall height of vehicle	1800 mm
4. Ladder length (in fully extended, horizontal position)	2600 mm
5. Overall leg length	1800 mm
6. Maximum swing angle of ladder	30 degree on either side of center line
7. Maximum pitching angle of ladder	45 degree
8. Maximum leg swing angle	30 degree on either side of center line
9. Dredge pump (From EEM (P) Ltd.)	19.5 lit/ s (= 0.019 m ³ / s = 70 m ³ / hr), average assumed concentration 20 % by volume, 1450 rpm Or 70 lit/ s = 0.07 m ³ / s = 252 m ³ / hr
10. Eductor pump (From EEM (P) Ltd.)	15 lit/ s (0.015 m ³ / s)
11. Cutter	Length: 300 mm with 3 equal sections; drum diameter of first section: 165 mm; drum diameter of second section: 100 mm; drum diameter of third section: 70 mm; rpm may vary between 35 to 90
12. Operational depth	50 m
13. Maximum slope of terrain	10 degrees
14. Material to be excavated	Sand, silt, clay or mixture of them in any proportion

2.3 System Hull

The primary design considerations for the hull of any underwater vehicle are the 1) mission of the vehicle, 2) hydrodynamic performance, 3) material availability, 4) design of the pressure hull, 5) ease of manufacture and fabrication, and 6) cost.

2.3.1 Hydrodynamic Performance

The hull form controls the hydrodynamic performance of any submersible vehicle. The hydrodynamic performance is determined by the total drag generated and hence the propulsion energy required. The ‘bare hull drag’ consists of the ‘skin friction drag’ and the ‘form drag’. The friction drag is a function of the speed and the exposed area of the vehicle. Form drag depends on how well a hull shape minimizes the flow separation. Hydrodynamic efficiency is the prime factor considered for designing hull shapes for free swimming submarines and autonomous

underwater vehicles (AUVs) [Allmendinger, 1990]. For low speed submersibles like remotely operated vehicles (ROVs) and submersible dredgers/ miners, hydrodynamic performance is not an important factor. The speed of most ROVs is less than 3 knots [Conway, 1986; Liddle, 1986; Nomoto and Hattori, 1986] and these normally have an open frame type of rectangular hull structure [Nomoto and Hattori, 1986]. The subsea crawler of the Institut für Konstruktions, Siegen, Germany (IKS) and National Institute for Ocean Technology, India (NIOT) has an operational speed of 0.5 m/sec and a maximum speed of 0.75 m/sec [Deepak et al., 2001]. The submersible walking auto dredger (SWAD) has a back and forth walking speed of 0.03 m/ sec and a sideways walking speed of 0.01 m/sec [Nakamaru et al., 1992].

The skin friction drag of the designed submersible legged dredger/ miner was estimated by using the following relationships [Hoerner, 1965],

$$F_{d_fa} = 0.5C_{d_fa}\rho_f v^2 A_{fa} \quad [\text{Equation 2.1}]$$

$$F_{d_wsa} = 0.5C_{d_wsa}\rho_f v^2 A_{wsa} \quad [\text{Equation 2.2}]$$

where, A_{fa} is the projected frontal area [m^2], A_{wsa} is the wetted surface area [m^2], C_{d_fa} is the drag coefficient based on projected frontal area [-], C_{d_wsa} is the drag coefficient based on wetted surface area [-], F_{d_fa} is the drag force based on projected frontal area [kN], F_{d_wsa} is the drag force based on wetted surface area [kN], v is the velocity of the vehicle [m/sec], and ρ_f is the density of surrounding fluid [kg/m^3]. The drag co-efficient can either be chosen from literature or can be estimated by Hoerner's expressions for a bare submerged axisymmetric body [Hoerner, 1965],

$$\text{Re} = \frac{v^* L_{sb}}{\nu} \quad [\text{Equation 2.3}]$$

$$C_f = \frac{0.455}{\log_{10}(\text{Re})^{2.58}} \quad [\text{Schlichting, 1979, p 641}] \quad [\text{Equation 2.4}]$$

$$C_{d_fa} = C_f \left[3 * \frac{L_{sb}}{D_{sb}} + 4.5 * \sqrt{\frac{D_{sb}}{L_{sb}}} + 21 * \left(\frac{D_{sb}}{L_{sb}} \right)^2 \right] \quad [\text{Equation 2.5}]$$

$$C_{d_wsa} = C_f \left[1 + 1.5 * \left(\frac{D_{sb}}{L_{sb}} \right)^{1.5} + 7 * \left(\frac{D_{sb}}{L_{sb}} \right)^3 \right] \quad [\text{Equation 2.6}]$$

where, D_{sb} is the diameter of the submerged body [m], L_{sb} is the length of the submerged body [m], Re is the Reynold's number [-], v is the velocity of the submerged body [m/sec] and ν is the kinematic viscosity of the surrounding fluid [m^2/sec].

The drag force generated by the legs, cutter module and the ladder assembly were estimated. The details of the calculations and the assumptions behind the calculations are presented in Appendix 2. Only the representative graphical results are presented here. The designed velocity of the vehicle was chosen as 0.01 m/sec and the swinging/ pitching velocity of the ladder assembly was assumed to vary from 0.1 to 0.5 m/sec for the drag estimation of the legs, cutter module and ladder assembly. The linear velocity of the leg was estimated from the designed velocity of the vehicle.

The total drag of each leg includes the drag of the leg tube, the drag of the square guide tube and the drag of the hydraulic cylinder used for lifting the leg. The drag co-efficients were estimated by Hoerner's expressions as presented in Equations 2.5 and 2.6. A fixed value of the drag co-efficient for the submerged cylinder based on the projected frontal area ($C_{d_fa}=1.2$) was also selected from literature [Allmendinger, 1990] to estimate the drag of the leg. The total drag force

generated by the four legs in fresh water was plotted against the linear velocity of the leg (Figure 2.3). Similar results were obtained for sea water also.

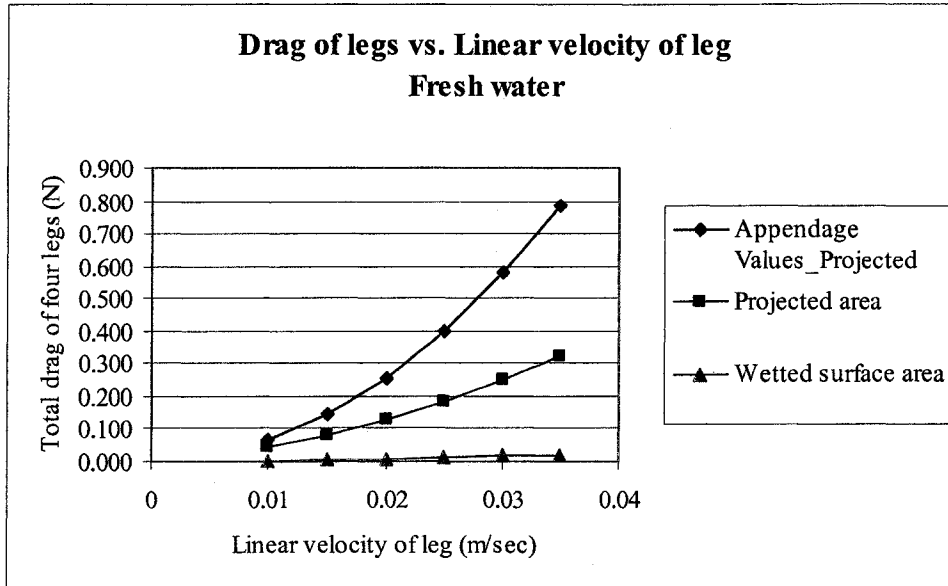


Figure 2.3 Total drag of the four legs vs. linear velocity of the leg

The total drag force of the cutter module includes the drag generated by the cutters and the drag of the pressure hulls housing the cutter drives. The drag co-efficient for the cutter and the pressure hulls were chosen from values in the literature [Allmendinger, 1990]. The drag co-efficient for the cutter was chosen as $C_d(\text{Profile}) = 0.015$ for small domes based on the profile [Allmendinger, 1990]. The drag co-efficient for the pressure hull was chosen as $C_{d_fa} = 1.2$ for cylinders based on the projected area [Allmendinger, 1990]. The drag was calculated for fresh water and sea water conditions. The total drag generated by the two cutters and the two pressure hulls housing the cutter drives, were plotted against the swing velocity of the ladder assembly. These are shown in Figures 2.4 and 2.5.

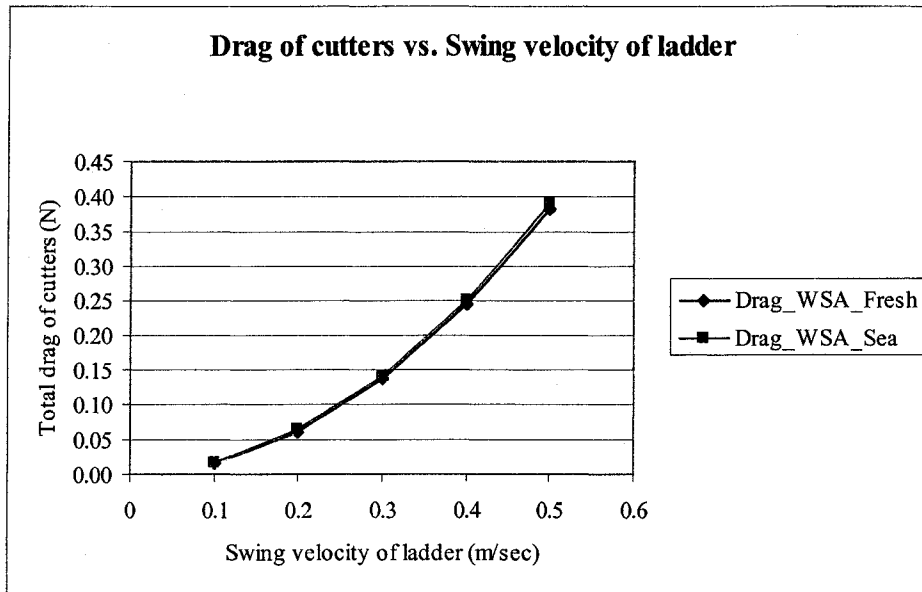


Figure 2. 4 Total drag of the two cutters vs. swing velocity of the ladder assembly (WSA Wetted surface area)

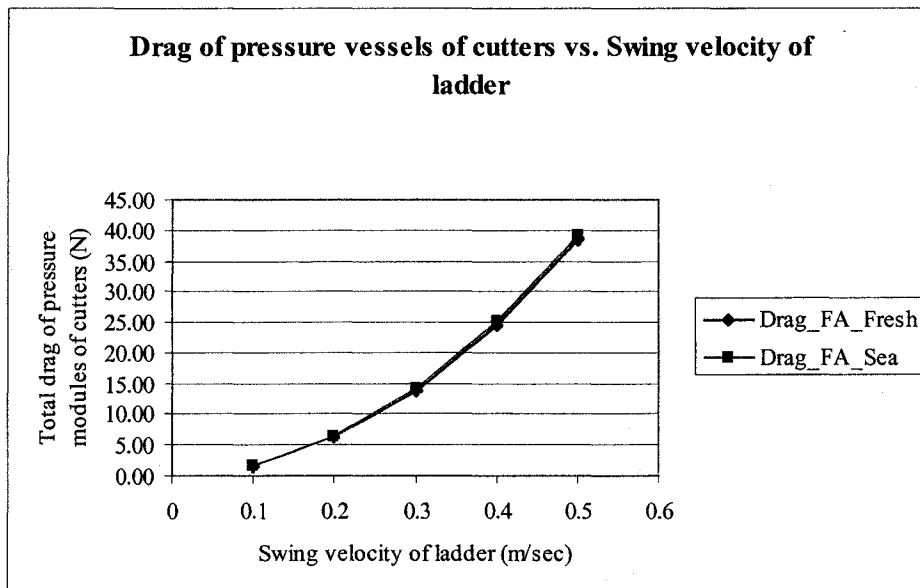


Figure 2. 5 Total drag of the two pressure hulls of the cutter module vs. swing velocity of the ladder assembly (FA Frontal area)

The drag generated by the ladder assembly consists of the drag generated by the boom and the dipper. The projected areas of all the longitudinal and transverse tubular members of the ladder assembly were considered while estimating the drag generated by the ladder assembly for three

scenarios of 1) vehicle performing locomotion while the ladder assembly has zero swing angle and zero pitch angle, 2) ladder assembly has swinging motion from left to right and vice versa, and 3) ladder assembly has pitching motion in a vertical plane. The drag estimated for the ladder assembly is an overestimation because the projected areas of all the tubular members were considered for the three different scenarios. The drag co-efficients were estimated using Hoerner's expressions. A fixed value of drag co-efficient for cylinders based on the projected area ($C_{d_fa} = 1.2$) [Allmendinger, 1990] was also chosen for drag estimation of the ladder assembly. The total drag of the ladder assembly was plotted against the swing velocity of the ladder in fresh water and sea water conditions with a fixed value of the drag co-efficient for cylinders (Figure 2.6).

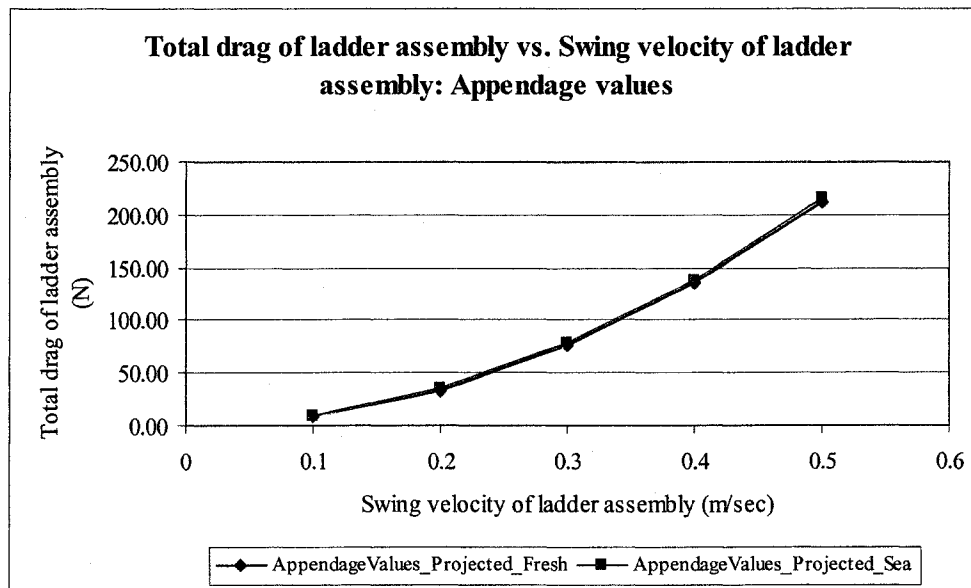


Figure 2. 6 Total drag of the ladder assembly vs. swing velocity of the ladder assembly (using a fixed value of the drag co-efficient based on frontal area)

Figure 2.7 shows the total drag generated by the ladder assembly in fresh water plotted against the swing velocity of the ladder assembly. The drag co-efficients were estimated with the help of Hoerner's expressions.

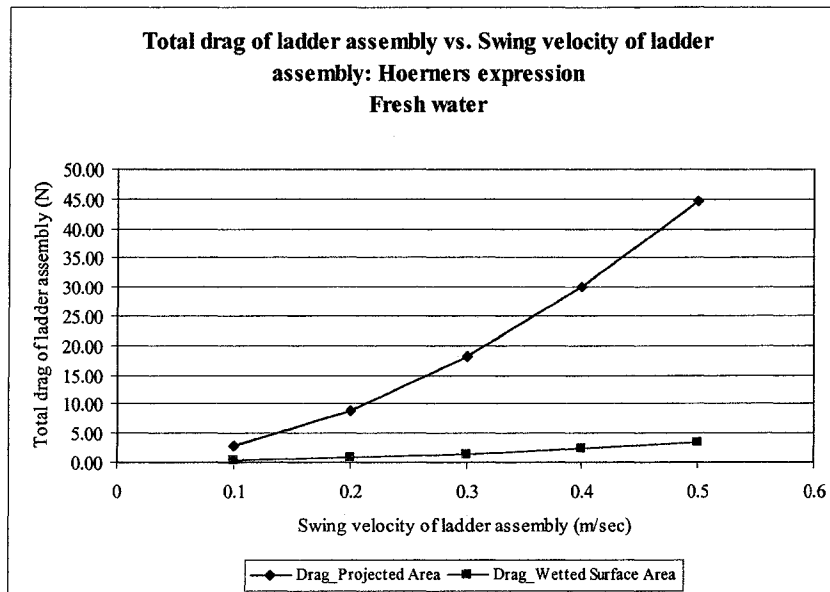


Figure 2. 7 Total drag of ladder assembly vs. swing velocity of the ladder assembly (using Hoerner's expressions)

Typical ocean currents, river flow speeds or tidal currents flowing in opposite direction to the vehicle or vehicle component movements will create much higher drag force than the results presented in this section. The prototype vehicle of the 'Golden Tortoise' is suitable for operations in deep inland reservoirs, where currents and other flows are negligible. Hence these were not included within the analyses.

For free swimming vehicles, the hull form also affects the stability and maneuverability at various operating speeds, which is not a concern for slow submersible bottom moving vehicles.

2.3.2 Hull Types for Submersible Vehicles

Two different types of hulls found for underwater vehicles include wet hulls and dry hulls.

A wet hull allows water inside the outer housing or frame and submerges all the components. Thus water sensitive components are placed in watertight pressure vessels. Watertight connectors are used for connections between different components and propulsion devices. The main

purpose of the hull is to increase the hydrodynamic efficiency and to reduce the weight. These types of designs are especially useful for deep operation as a state of equilibrium is maintained with the surrounding water pressure and the approach reduces the amount of material to be used as well as the cost [Allmendinger, 1990].

A dry hull is completely sealed and does not allow any water to enter. The entire interior is dry and hence this type of hull provides a greater area of flexibility for the layout of moisture sensitive equipment. This also reduces the number of watertight connections needed, but the weight and the pressure differentials across the outer hull are increased compared to a wet hull [Allmendinger, 1990]. A dry hull can be either 1) an ambient pressure dry hull or 2) a pressure hull. The ambient pressure hull regulates the air pressure inside so that it is always in equilibrium with external water pressure creating no pressure difference across the hull. A pressure hull is designated to withstand increasing water pressure up to the 'crush depth'. This is a simpler design without any pressure regulator, but requires a strong hull to withstand higher pressure [Allmendinger, 1990].

For shallow water depth operation, dry pressure hulls are more suitable than wet pressure hulls.

2.3.3 Hull Construction Material

The primary selection criterion for material requirement for pressure hull construction is that the material should withstand the high hydrostatic pressure at the designed depth. Other major factors include 1) resistance to corrosion, 2) high strength to density ratio, 3) capacity to withstand repeated stress cycles without fatigue failure, 4) cost of material, 5) fabrication properties and pressure hull design, 6) susceptibility to temperature, and 7) operating life span of the material [Koblick, 1984; Ross, 1990]. There is no material that satisfies all the particular

requirements and therefore compromises have to be made in less critical areas of the material properties behavior. The most commonly used materials for underwater pressure hulls are [Koblick, 1984; Ross, 1990] 1) high strength metals including high strength steels, aluminum alloys, titanium alloys, and 2) non-metals including glasses, acrylics, glass reinforced plastics (GRPs), fiber-reinforced plastics (FRP), carbon fibers, and ceramics. The pressure hulls of the designed prototype vehicle are not required to dive to great depths and hence mild steel was used as the construction material. It is relatively cheap and easy to weld and fabricate. As the prototype vehicle is expected to be tested in fresh water, so mild steel was used.

2.3.4 Design of the Pressure Hull

In all underwater vehicles some form of pressure hulls should be present to carry the equipment that needs to work in a dry, atmospheric environment. The pressure hull must be weight efficient. Two most common types of pressure hull shapes observed for underwater vehicles are spheres and cylinders. The merits and demerits of the two types are compared from the viewpoints of the major design factors of the pressure hull. The main factors influencing the design of the pressure hull are,

1. Operating depth

With increase in operating depth the external pressure increases. To resist increasing pressure, the pressure hull becomes thicker and heavier. The correct balance between the weight and buoyancy prevents the soil failure due to bearing pressure and slippage for vehicles moving on submerged ground. The buoyancy can be increased by making the pressure hull larger. This will eventually increase the weight in air as also the amount of material required for manufacturing and hence the cost.

2. Space available [Koblic, 1984]

To package a given volume, a sphere requires minimum shell area. To contain this volume against a given pressure (internal or external), a sphere requires the least shell thickness. Hence a sphere requires a minimum volume of shell material and is thus the lightest possible pressure hull shape.

3. Structural efficiency

The structural efficiency is judged by the buoyancy factor, which is defined as the ratio of the pressure hull weight to the displaced water weight. Spherical pressure hulls provide the best structural efficiency [Koblic, 1984].

4. Hydrodynamic form

Cylindrical pressure hulls have a lower buoyancy factor than spherical pressure hulls, but provide good hydrodynamic form.

5. Internal and external arrangements

It is difficult to use the internal volume of a spherical pressure hull efficiently. Cylindrical pressure hulls give better internal arrangements. Off-the-shelf electronics and packages and batteries are rectangular in shape and fit better into cylinders [Ross, 1990]. Additionally, the internal distribution of the various subsystems must leave the vehicle in proper trim, which is easier to do in a cylindrical pressure hull than a spherical one.

6. Cost

Cylindrical pressure hulls are relatively inexpensive to manufacture.

7. Ease of fabrication

Cylindrical pressure hulls are easy to manufacture.

From the above discussion, it was concluded that for shallow water operations (approximately 200 m), cylindrical pressure hulls provide more advantages than spherical ones. Hence cylindrical pressure hulls for the ballast tanks, hydraulic modules, electric-electronics modules, and the pressure hulls housing the cutter drives were selected for the designed vehicle.

Cylindrical pressure hulls with or without stiffeners can have three principle modes of failure [Allmendinger, 1990; Kobic, 1984; Ross, 1990], which are 1) axisymmetric shell yielding, 2) lobar buckling of the shell, and 3) general instability failure. Unstiffened thin-walled circular cylinders are structurally inefficient at withstanding the external pressure, particularly if the pressure hulls are long. To increase the structural efficiency, it is necessary to stiffen them with suitably sized ring-stiffeners, placed at suitable distances apart. Ring stiffeners can be external or internal.

It was necessary to perform the collapse pressure calculations for all the cylindrical dry pressure hulls of the designed vehicle. The critical pressures and the corresponding operating depths for unstiffened circular cylinder as well as for stiffened circular cylinder were carried out. The main aim was to check whether the chosen thickness was safe to operate at the designed depth. Ring stiffeners with rectangular cross section were chosen for the design. The formulas used for the collapse pressure estimation [Allmendinger, 1990] as well as the input parameters for the calculations are presented in Appendix 3.

For calculating the required thickness, two different stress levels were chosen 1) at 0.6 of the yield strength of the material and 2) with a factor of safety of 3. The respective thickness obtained for the ballast tank pressure hulls were 1 mm and 2 mm with mild steel. The respective thickness obtained for the hydraulic and electric-electronics pressure hulls were 1 mm and 0.5

mm with mild steel. For all calculations the density variations of the surrounding water with temperature and depth were neglected. For the ballast tanks, a stiffener spacing of 0.3 m was used. The dimension of the rectangular stiffener chosen was, width of stiffener = 5 mm and thickness or height of stiffener = 50 mm. The same spacing and stiffener dimensions were used for the hydraulic and electric-electronics modules also.

Table 2.2 and Table 2.3 show the estimated critical pressures for the ballast tanks and hydraulic and electric-electronics modules respectively.

Table 2. 2 Estimated critical pressures and corresponding operating depths for ballast tanks (Thickness of pressure hull = 3 mm)

Failure Criteria	Critical Pressure (kPa)	Operating Depth (m)
Unstiffened cylinder	618	61
Stiffened cylinder		
a) Axisymmetric yielding	1214	124
b) Lobar buckling	630	64
c) General instability		
n = 2	25132	2561
n = 3	33951	3460
n = 4	61496	6268
n = 5	98074	9997

Table 2. 3 Estimated critical pressures and corresponding operating depths for hydraulic and electric-electronics modules (Thickness of pressure hull = 2 mm)

Failure Criteria	Critical Pressure (kPa)	Operating Depth (m)
Unstiffened cylinder	825	82
Stiffened cylinder		
a) Axisymmetric yielding	2474	252
b) Lobar buckling	1843	188
c) General instability		
n = 2	83902	8552
n = 3	216149	22033
n = 4	404875	41271
n = 5	647744	66029

It can be concluded that with the chosen dimensions of shell-stiffener combination, the depths corresponding to the critical pressures are not less than the design operating depth. Hence the vehicle can operate safely.

2.4 Design of the Hull

The main body frame is fabricated from longitudinal tubular mild steel pipes and gusset plates, strengthened by transverse tubular mild steel pipes. The main body frame is shown in Figure 2.8. The ballast tanks are constructed from rolled 3 mm mild steel sheets and strengthened by external ring stiffeners. The hydraulic and electric-electronics modules are made from 6 mm thick, 300 mm nominal bore mild steel pipes.

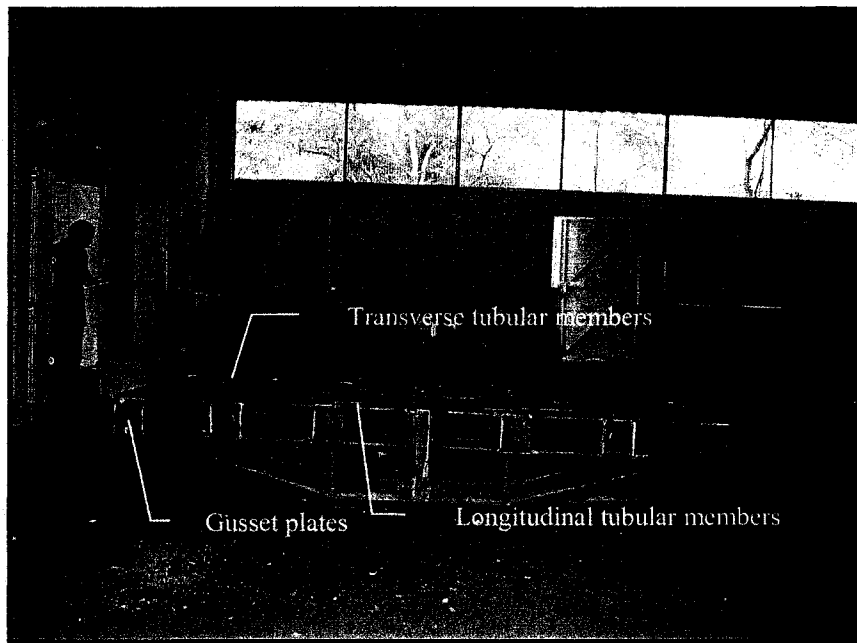


Figure 2.8 Main body frame

The unique trapezoidal shape of the main body frame has several advantages. A cambered sheet with ribs is to be fixed on the bottom of the main body frame, with which the vehicle can slide on its belly over very soft soil. The ribs will prevent vacuum generation, when the vehicle is on

its belly. While resting on its belly, if the vehicle sinks, the designed trapezoidal shape increases the area of contact and thus the soil reaction also. Thus the chances of the vehicle capsizing due to low soil bearing capacities are highly reduced. This main body frame shape helps in maintaining 'stable equilibrium' of the vehicle, thereby enabling the vehicle body to return to its equilibrium position after it has been displaced slightly. A disturbance was longitudinally given to the main body frame and the damping time recorded was 6 seconds. This was done to test the stability of the frame.

The geometry of the main body frame is defined by the length to width ratio, the camber angle and the camber height. The definitions of the different terms are shown in Figure 2.9. It is necessary to find the optimum values of the length to width ratios of the main body frame and also the camber geometry for a given weight of the designed vehicle in order to increase the area of contact.

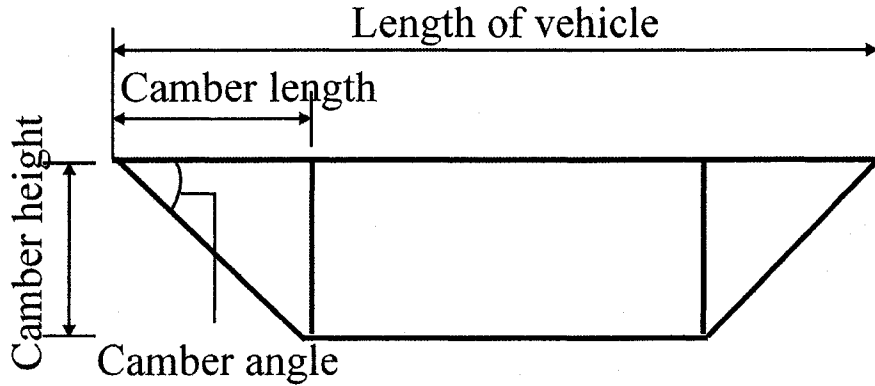


Figure 2.9 Main body frame definition

The contact area of the vehicle belly with the soil for a given sinkage is deduced,

$$A_{belly} = \left[(L_{vehicle} - 2 * L_{camber}) + \left(\frac{2 * \Delta h_{belly} * h_{camber}}{\tan(\alpha_{camber})} \right) \right] * B_{vehicle} \quad \text{[Equation 2.7]}$$

where, A_{belly} is the area of contact of the vehicle belly with the soil [m^2], $B_{vehicle}$ is the width of the vehicle [m], L_{camber} is the length of the camber [m], $L_{vehicle}$ is the length of the vehicle [m], h_{camber} is the height of the camber [m], Δh_{belly} is the sinkage of the vehicle belly [%] and α_{camber} is the camber angle of the main body frame [degree].

The camber angle was varied while the camber height, length to width ratio of the vehicle main body frame and the weight of the vehicle were kept constant. The area of contact was plotted against the camber angles for different sinkage percentages (Figure 2.10). The camber length was calculated from the camber angle and the camber height, while the length of the vehicle was assumed to be 3.5* camber length.

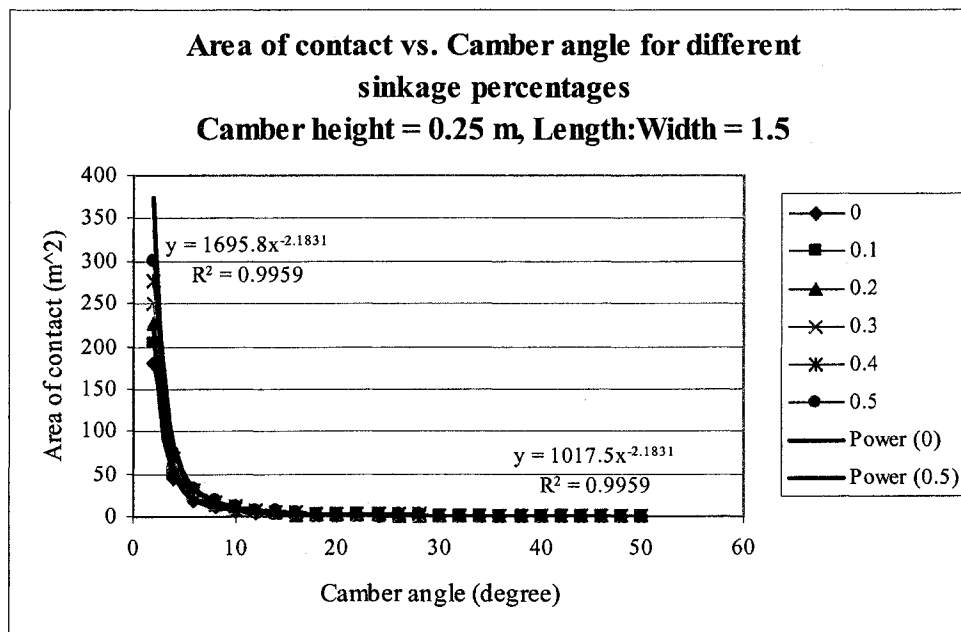


Figure 2.10 Optimum camber angle for the main body frame

It is observed from Figure 2.10, that for a fixed camber height and ratio between the length and width of the vehicle main body frame, the contact area of the vehicle belly decreases rapidly up to a camber angle of 10 degrees. With further increase in the camber angle, the contact area

remains more or less constant. The numerical values of the contact area vary with the dimensions of the vehicle and camber height, but the same trend was observed for other values of camber height and length to width ratio of the vehicle main body frame. The different curves shown in Figure 2.10 are plotted for different sinkage percentages of the vehicle belly. In very soft working terrain, the camber angle of the designed vehicle should not exceed 10 degrees.

The total weight, buoyancy and net weight of the different components of the prototype vehicle were either calculated or weighed and are given in Table 2.4. The total weight of the prototype vehicle in air is roughly 3 tons and has a net weight of 2.2 tons in water. The vehicle will descend under its own weight when lowered slowly in water, which is helpful for submersible bottom moving vehicles.

Table 2. 4 Weight and buoyancy of the prototype vehicle ‘Golden Tortoise’

Part description	Total weight (kN)	Total buoyancy (kN)	Net weight (kN)
Main body frame	5.29	2.31	2.98
Ballast Tank	4.46	0.46	4.00
Leg & Foot Assy.	5.76	2.56	3.20
Hydraulic Module	4.64	0.13	4.51
Control Module	2.56	2.49	0.07
Dredge pump	2.01	Buoyancy not known	2.01
Eductor pump	1.29	Buoyancy not known	1.29
Pipelines	0.37	Buoyancy not known	0.37
Ladder Trunnion Assy.	1.16	0.41	0.75
Cutter System	1.59	0.39	1.20
Ladder Boom Assy.	1.62	0.47	1.15
Ladder Dipper Assy.	0.66	0.18	0.48
Total	31.40	9.40	22

The total weight of the vehicle determines the magnitude of the static load incident at the different foot/ soil interfaces and hence the stability of the vehicle due to soil bearing capacity.

These are further discussed and estimated in section 3.5.

2.5 System Excavation

2.5.1 Design of the Cutter and the Ladder Assembly

The twin drum cutter system with a suction mouth in between is not a common excavation system in surface floating dredgers. The submersible diamond miner used by NAMCO in South Africa for exploitation of offshore diamonds uses a twin drum cutter system with the suction mouth situated in the middle. The same concept was adopted while developing the design of the excavation system in this research. The cutter module attached to the dipper by temporary fasteners is shown in Figure 2.11. Because of their modularity, the cutters can be assembled and interchanged very easily.

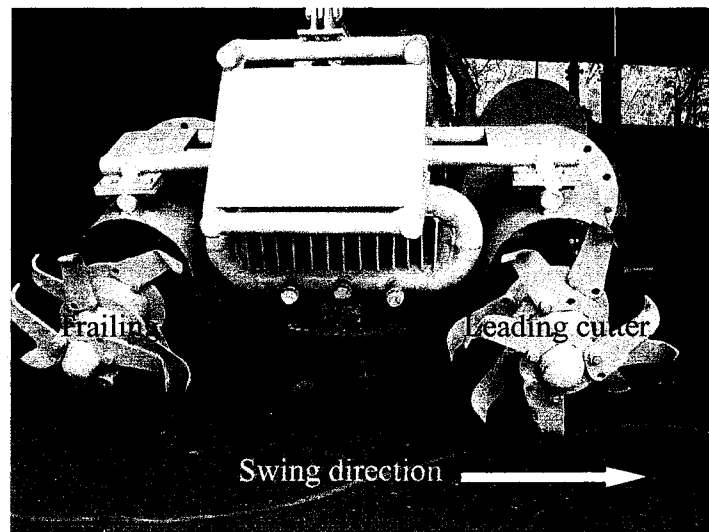


Figure 2.11 Cutter module using two drum cutters

The cutter axes are parallel to the vehicle longitudinal axis. The cutters consist of a tapered drum, which is expected to help in easy penetration and maintains a greater contact area with the excavated soil. Rings were welded to the cutter drum. L-shaped blades manufactured by EEM (P) Ltd. are attached to these rings. These L-shaped blades can be replaced by other type of blades, teeth or picks. The number of blades in a ring and the number of rings are of primary importance

in determining the cutter performance, which are discussed in section 4.2.3. The designed system is likely to generate less spillage in a single swing cycle when compared with a single cutter system. This is because the trailing cutter will excavate the material left as spillage by the leading cutter. The gear-hydraulic motor combination driving the cutter is shown in Figure 2.12.

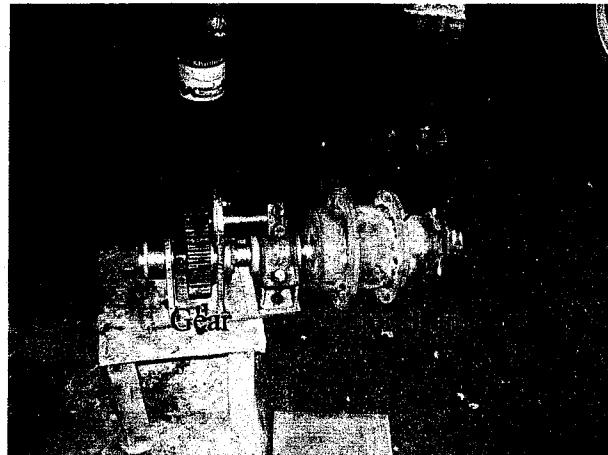


Figure 2. 12 Hydraulic drive for cutter

The leading cutter should perform ‘overcutting’, while the trailing cutter should perform ‘undercutting’ in order to bring the excavated material in front of the suction mouth and thus facilitate in effective gathering, mixing and transport. The definitions of ‘overcutting’ and ‘undercutting’ are shown in Figure 2.13. The leading and trailing cutter during the swinging of the ladder in a particular direction are shown in Figure 2.11.

Two hydraulic cylinders are used to lift/ lower the ladder boom and a third hydraulic cylinder to lift/ lower the dipper. The movement of the dipper helps in adjusting the angle of cut of the cutters. The required depth of cut is achieved by the movement of the ladder boom. Two hydraulic cylinders will be used to rotate the yoke and thus swing the ladder assembly from one side to the other. Currently one hydraulic cylinder is being used to swing the ladder assembly.

Two hydraulic cylinders are responsible for the pitching motion of the cutters and suction mouth assembly using the dipper and ladder boom.

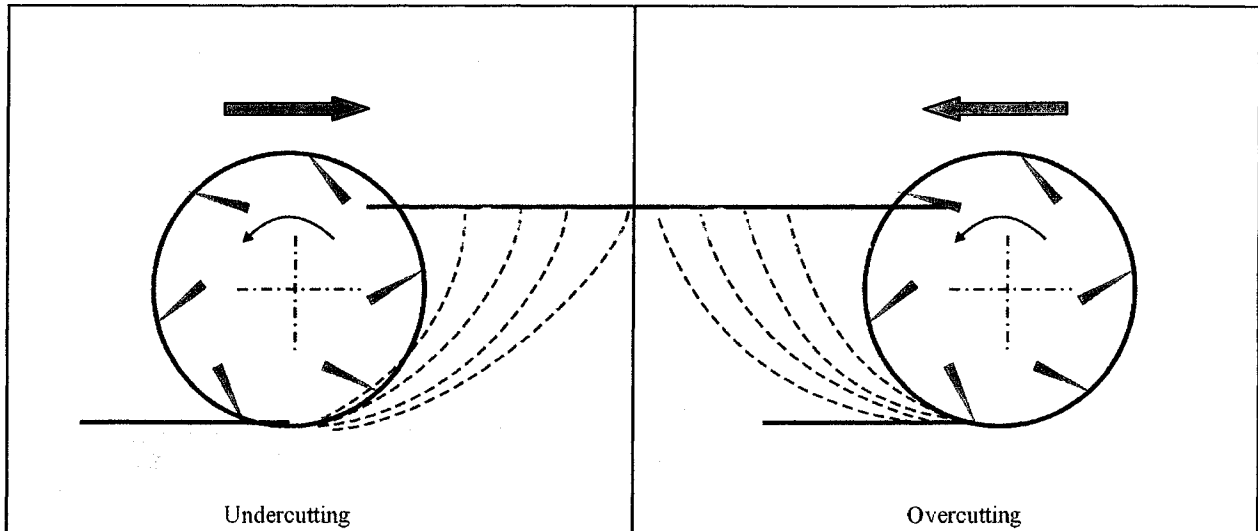


Figure 2. 13 Overcutting and Undercutting

The hydraulic cylinders operating the ladder assembly and the legs were specially designed for underwater operation by EEM (P) Ltd., and manufactured by a machine shop in Calcutta, India.

2.5.2 Functionality Tests for the Excavation System

Ladder Lifting/ Lowering Trials

The lifting / lowering operation of the ladder assembly was initially performed by one hydraulic cylinder. The single cylinder was unable to lift/ lower the ladder assembly smoothly and there were lots of vibrations. Thus two cylinders were used to lift/ lower the ladder assembly. Two cylinders were operated by one directional control (DC) valve as there was a limitation in the number of DC valves available in the designed hydraulic circuit. The number of DC valves can however be increased in the future. The test set up is shown in Figure 2.14.

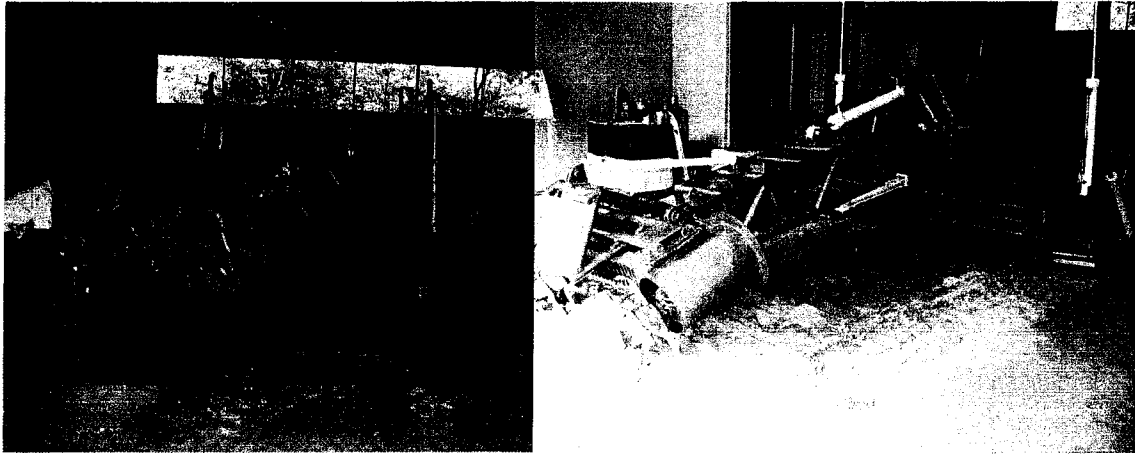


Figure 2. 14 Ladder lifting/ lowering and swinging trials

Two different types of cylinder connections were used while the cylinders were operated by one DC valve (Figure 2.15). In the first arrangement (Figure 2.15(a)), same cylinder ports were interconnected, so that oil coming into one cylinder was pushed into the other.

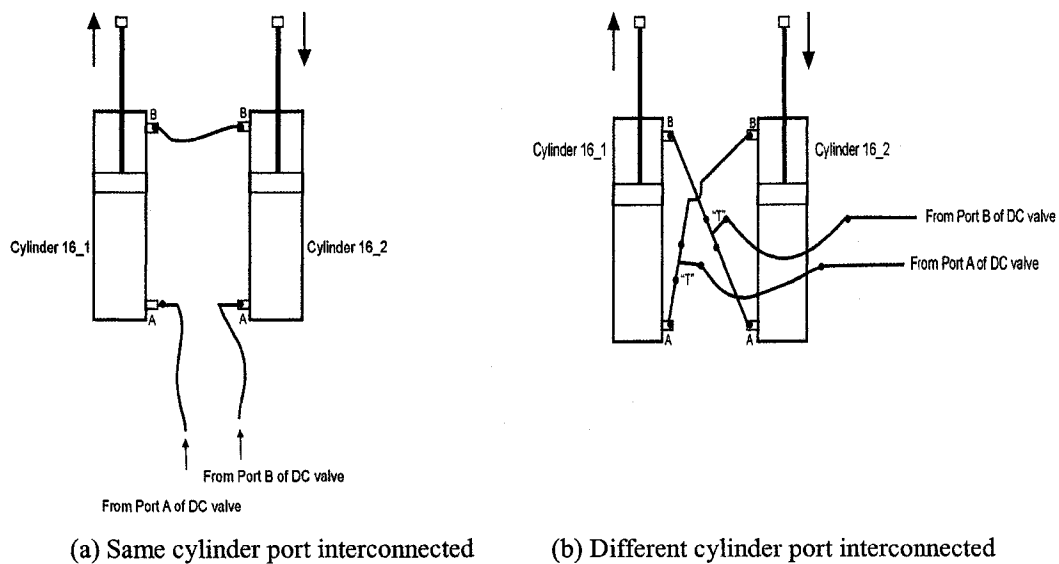


Figure 2. 15 Arrangements for ladder lift/ lower cylinder connections

With this arrangement one cylinder will expand while the other retracts producing the same direction of movement of the ladder assembly. The hydraulic oil pressure was kept at 50 kPa for

the tests, but can be increased to 100 kPa for the designed hydraulic circuit. During the operation there was too much lag between the cylinders and hence this arrangement was abandoned.

In the second arrangement, different cylinder ports were interconnected with 'T' connections (Figure 2.15(b)). With this arrangement the hydraulic oil coming from the hydraulic pump was divided between the two cylinders, and one was expanding while the other was retracting. First a single stabilizer-converter circuit was used to supply the 12 V DC to the solenoid of the directional control valve actuating the hydraulic cylinders, but sufficient current was not available. Hence two sets of stabilizer-converter circuits were used to perform the following tests

- 1) ladder lifting/ lowering tests were conducted without the dipper and the cutter modules, and
- 2) ladder lifting/ lowering tests were conducted with the dipper and cutter modules. The hydraulic oil pressure was kept at 60 kPa but can be increased to 100 kPa for the designed hydraulic circuit.

The ladder assembly is attached to the rotating yoke by two pins to have a pitching motion. The yoke can also give a swinging motion to the ladder assembly. The ladder is of fixed length and not telescopic. The ladder swing motion was performed by one swing cylinder. In the actual design two cylinders were envisaged. Another cylinder will be used in the future in order to reduce the variations of the turning moment. The ladder assembly was lowered to different heights and then swinging motions were performed from one side to the other. The ladder was observed to accelerate and decelerate during the swinging motions. The ladder slowed down in the middle (at swing angle = 0 degree). This is because of the change in cylinder ports. It is necessary to refine the hydraulic circuits in the future as there are problems with the actuator responses leading to vibrations of the ladder.

The maximum width of cut achieved during the ladder swing trials was $B_{cut} = 4700$ mm, which was greater than the width of the designed vehicle. This is necessary since the designed vehicle will perform locomotion on the excavated channel. The length of the ladder (as measured from the ladder yoke pin and the tip of last blade of cutter) was $L_{ladder} = 2800$ mm. Thus the maximum angle of ladder swing, achieved by the designed ladder assembly was,

$$\tan(\alpha_{swing}) = \frac{0.5 * B_{cut}}{L_{ladder}} \text{ i.e. } \tan(\alpha_{swing}) = 0.8393 \text{ i.e. } \alpha_{swing} \approx 40^\circ \text{ (Figure 2.16).}$$

The ladder swing angle of cutter suction dredgers is 30° [Training Institute for Dredging (TID), The Netherlands, Dredging handbook].

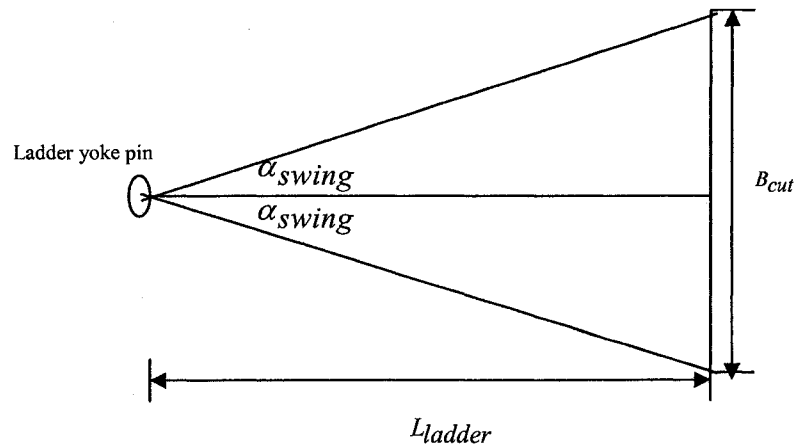


Figure 2.16 Ladder swing angle (Plan view)

Cutter Rotation Trials

Under this trial each cutter was operated by a solenoid operated DC valve actuating a hydraulic motor. The cutters were rotated both in clockwise and counter-clockwise directions. The test set up is shown in Figure 2.17.

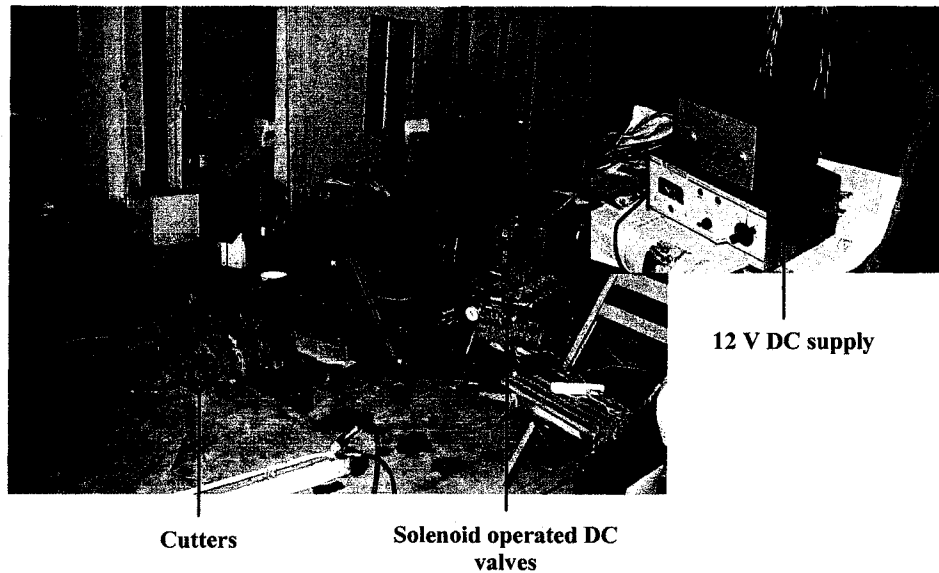


Figure 2. 17 Cutter rotation trials

2.6 System Transport

The centrifugal dredge pumps manufactured by EEM (P) Ltd. will be used to transport the excavated material to the surface by pipelines. The centrifugal dredge pumps considered were 1) capacity = 19.5 l/sec = 0.0195 m³ / sec = 70 m³/ hr, and 2) capacity =70 lit/ s = 0.07 m³/ s = 252 m³/ hr. The rpm for both the pumps is 1450. The centrifugal pump was placed on mountings fixed to the main body frame.

An assisting eductor pump will be used to prevent the chances of pipeline blockage and generation of vacuum on the suction side of the dredge pump. The annular eductor pump used is a special design developed by EEM (P) Ltd., India, which they have used in different dredging projects. The eductor pump is attached to the ladder assembly. The trapezoidal suction mouth with rectangular cross section is also attached to the ladder assembly. The centrifugal dredge pump and the eductor pump used are shown in Figure 2.18. The performance evaluation models and the results for the centrifugal dredge pump-pipeline system are discussed in chapter 6.

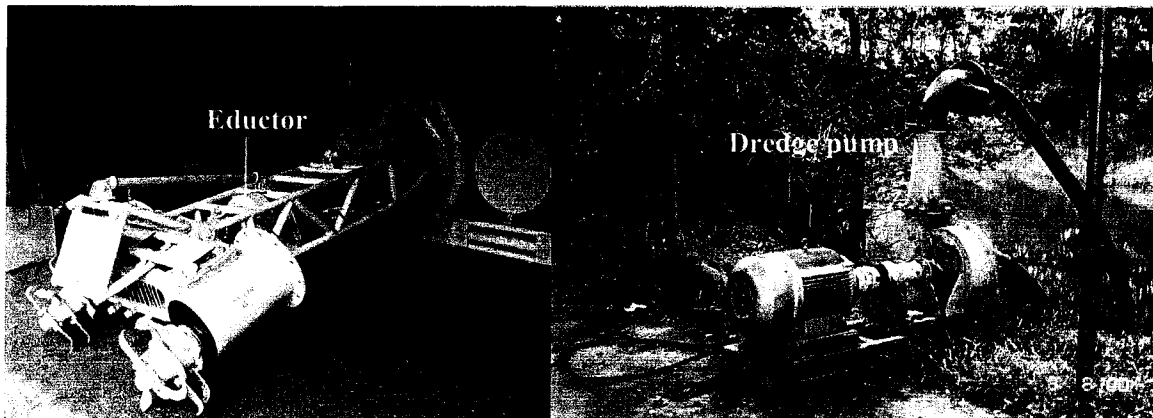


Figure 2.18 Eductor and Dredge pumps

2.7 System Locomotion

2.7.1 Terrain of Locomotion

The designed vehicle should exhibit both straight line and curvilinear locomotion on submerged natural terrain. The natural terrain was subdivided into 1) level terrain where the slope of the terrain is zero and 2) sloped terrain where the slope of the terrain is not zero. Each of these terrains can be either reasonably flat or undulating. A unique method of locomotion and non-uniform periodic gait plans were developed for straight line and curvilinear locomotion on a given terrain. The method of locomotion of the designed vehicle was inspired by the belly crawling motion of a tortoise or turtle, which is very effective in moving in different terrain especially very soft terrain (Figure 2.19).



Figure 2.19 Turtle performing belly crawling motion on very soft muddy terrain

The leg linkage design, method of locomotion, advantages of the proposed method of locomotion and the task planning for the designed vehicle are discussed in the subsequent sections. The functionality tests performed to observe the operational limitations of the designed locomotion system are also presented in this section.

2.7.2 Leg Linkage Design

Four hydraulically operated legs with pinned foot were used to achieve the simulated belly crawling motion of a tortoise or turtle on submerged ground and also on land if necessary. The conceptual design of the leg linkage is shown in Figure 2.20.

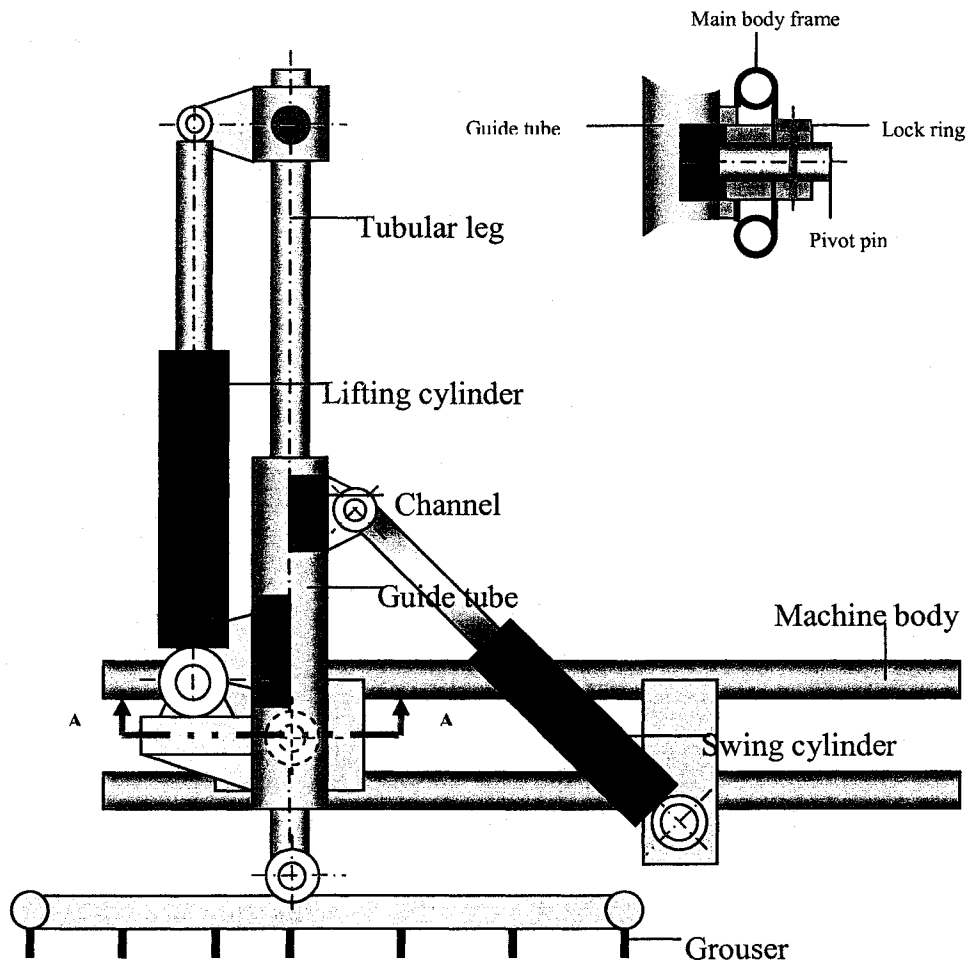


Figure 2. 20 Conceptual design of the leg linkage of ‘Golden Tortoise’

The 'lift hydraulic cylinder' is used to lift/ lower the designed leg linkage, while the 'swing hydraulic cylinder' is used to swing the leg linkage and thus advance the designed vehicle through a desired step size. Each foot has a honeycomb structure made from flats and covered with sheet plating (Figure 2.21). Strengthening members are used at the connection of the foot with the leg. Grousers present on the underside of each foot provide greater friction and reduce the chances of vacuum generation.

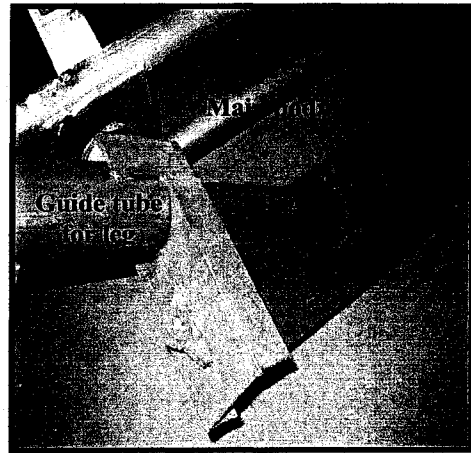
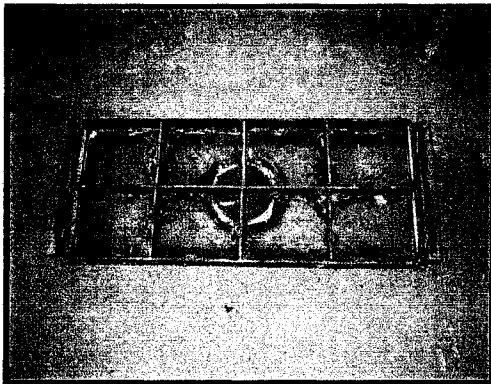


Figure 2. 21 Foot construction (Left Inner construction of the foot, Right Leg with foot)

The leg constructed is shown in Figure 2.22.

The maximum lifting/ lowering distances depend on the stroke of the hydraulic cylinder. The maximum and minimum angles of swing were measured during the prototype tests, keeping in mind the practical operational problems which might occur during actual field operation. These are discussed in the section 2.7.6.

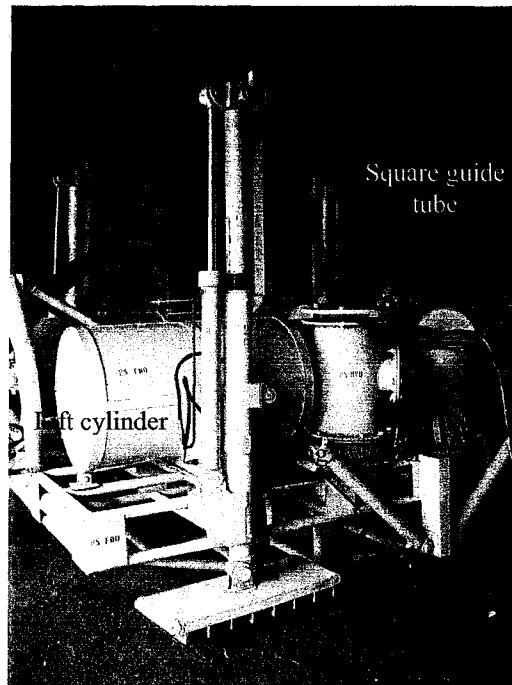


Figure 2. 22 Designed leg of the prototype vehicle of ‘Golden Tortoise’

2.7.3 Mode of Locomotion

Two different modes of locomotion were proposed for the designed vehicle 1) legged locomotion and 2) belly sliding.

During legged locomotion, the designed vehicle rests on its belly before the commencement of the locomotion cycle and at the end of the locomotion cycle. The vehicle body is lifted off the ground and moved forward through a desired distance by the four legs during the locomotion cycle. During the locomotion cycle the vehicle body is supported on the four feet.

In belly sliding mode, the vehicle belly is in constant contact with the ground during the entire locomotion cycle. The vehicle weight is thus always supported by the belly. The sliding motion of the vehicle belly can be generated by the swinging motions of the four legs, in which case a very small portion of the vehicle weight is supported by the four feet. Alternatively, the sliding motion of the belly can be achieved by anchoring the ladder assembly with the cutters and then

swinging the ladder assembly. The swinging of the ladder results in the sliding of the belly in the opposite direction exhibiting a turning behavior of the vehicle around the pivot point defined by the position of the cutters. When the belly sliding is achieved by swinging of the ladder assembly, the four legs are lifted off the ground. This is shown in Figure 2.23. Belly sliding is especially effective in very soft soil conditions, where sufficient soil bearing capacity may not be available.

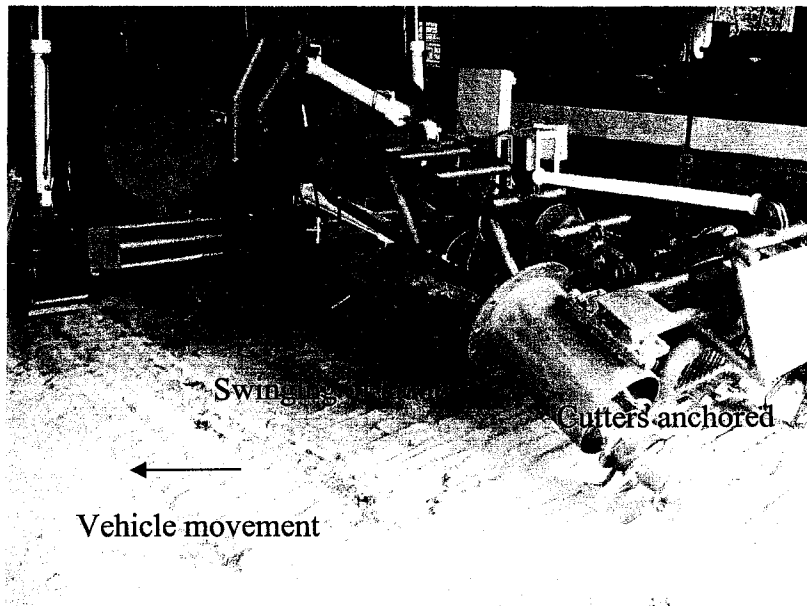


Figure 2. 23 Belly sliding with the swinging of ladder assembly

The matrix between the mode and type of locomotion and the terrain type is shown in Table 2.5.

Table 2. 5 Locomotion vs. Terrain

Locomotion	Level – Reasonably flat	Level – Undulating	Sloped – Reasonably flat	Sloped – Undulating
Belly sliding – Straight line locomotion				
Belly sliding – Curvilinear locomotion				
Legged locomotion – Straight line locomotion				
Legged locomotion – Curvilinear locomotion				

Shaded boxes in Table 2.5 indicate that the particular mode and the type of locomotion is possible in the given terrain.

2.7.4 Method of Locomotion

A unique method of locomotion was developed for the designed vehicle, which solves various problems of other legged locomotion as was discussed in chapter 1. The various steps of the locomotion cycle are shown in Figure 2.24.

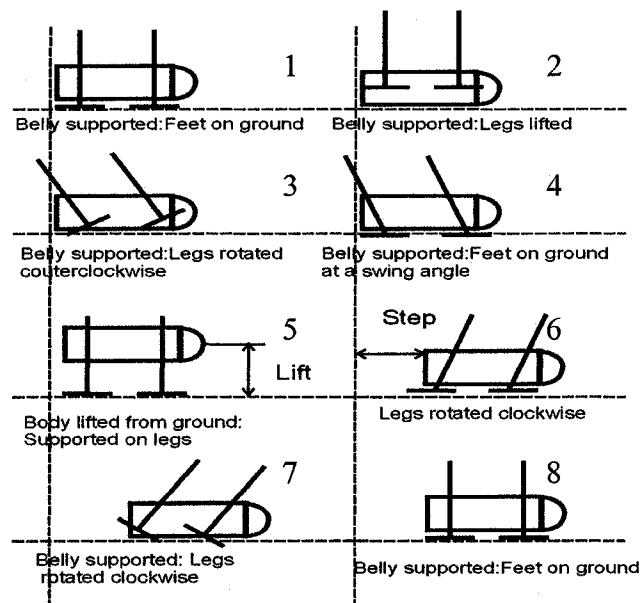


Figure 2. 24 Method of locomotion

This periodic gait can be used for straight line and curvilinear locomotion on any terrain. Non-periodic gaits are common on natural terrain. The ‘support phase’ and the ‘transfer phase’ of each leg coincide with one another. The transfer phases of the legs start when the vehicle is supported on its belly. The steps shown in Figure 2.24 are followed for all successive locomotion cycles, but the swing angles of the legs may vary depending upon the required step size of the individual legs and that of the vehicle. The gait is thus defined as a non-uniform periodic gait.

The static stability margin is not a major concern for the proposed mode of locomotion as the vehicle is always supported on the four legs. The centre of gravity of the designed vehicle is moving together with the legs. The ground reactions conveyed through the legs are transmitted to the main body frame at the leg pin joints, which are responsible for the vehicle movement. The vehicle rests on its belly when the position of the centre of gravity due to dredging has been changed.

With the designed leg linkage, individual leg movements are possible, which allows the designed vehicle to traverse on uneven terrains. The designed vehicle body can be kept horizontal by individual movements of the legs, which is necessary in order to move the ladder assembly and the cutters along the desired trajectory. Both forward and backward motions and obstacle avoidance are possible with the designed leg linkage. Forward and backward motions and obstacle avoidances are possible with the leg linkage. For obstacle avoidance 1) the foot can be placed in a different place, 2) the vehicle can be lifted off the ground with the aid of the legs, and 3) thrusters can be used to help the vehicle in swimming.

The feet positions do not change during the vehicle frame movement (Figure 2.24). This facilitates easy computations of the joint parameters for the feet placement (inverse kinematics) and easy control, essential for any submersible walking dredger/ miner. During successive locomotion cycles the deviation from the proposed path of locomotion can be corrected at the end of each locomotion cycle, as continuous locomotion is not envisaged. No dredging or mining activities are executed during a locomotion cycle. During a dredging cycle the vehicle is either supported on its belly or on its four legs depending on the soil conditions. During the support phases of the legs, the load incident at each leg determines the soil reaction and thus the stability of the vehicle in terms of the soil bearing capacity. The area of contact and the soil reaction

increases when the vehicle is supported on its belly. The stability of the vehicle due to soil bearing capacity is discussed in Appendix 1 and in section 3.5.

2.7.5 Task Planning

The main task of the designed vehicle is to perform locomotion and dredging/ mining operations in a given workspace present within the working area. Geological and geophysical surveys of the working area are to be performed prior to the commencement of any dredging/ mining operations. The working area can thus be considered as a partially unstructured terrain. Obstacles present in the workspace can be classified as 1) non-negotiable slopes for the designed vehicle, 2) abrupt raised or depressed contours, and 3) material unsuitable for excavation, transportation or locomotion for the designed vehicle. Obstacles are either to be avoided or in extreme cases the mission is to be abandoned. Within the scope of this research all analyses were performed for a single continuous workspace without any obstacle.

For dredging/ mining and locomotion operations the workspace is to be divided into rectangular strips of equal width. The width of the rectangular strips depends on the 1) maximum length of the ladder assembly, 2) swing angle of the ladder assembly, and 3) joint angles of the ladder assembly.

The maximum depth of dredging will also depend on these parameters and the maximum depth over which the legs can move. A 'ray-like' locomotion pattern to cover the entire workspace is proposed for the designed vehicle (Figure 2.25). With this locomotion pattern the umbilical cables will be less stressed during the to and fro motion of the vehicle. The chances of formation of knots due to circular or curvilinear motion are also lowered.

The vehicle will start excavation from segment 1, moving to segment 4, and then will turn in the other direction to perform excavation in segment 5, segment 6 and so on till the gaps left during excavation are covered. Detailed discussion on the dredging sequence is given in section 4.2.2.

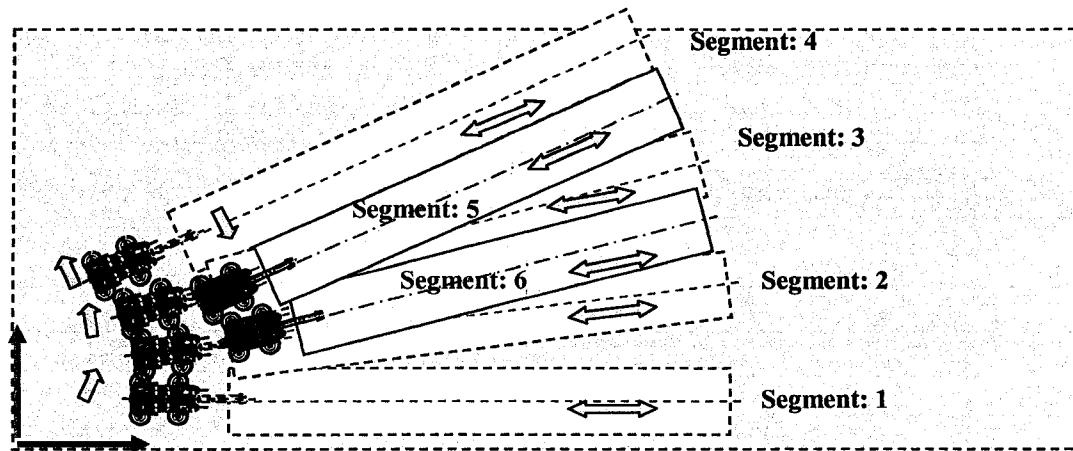


Figure 2. 25 Locomotion pattern in a given workspace

2.7.6 Functionality Tests for the Locomotion System

The lifting/ lowering and swinging motions of the legs were tested separately. Two sets of stabilizer-converter circuits (12 V DC) were used for operating the portside (PS) and starboard side (SBS) legs. The hydraulic oil pressure was kept at 70 kPa for the PS and SBS hydraulic circuits. Individual leg lifting/ lowering operations were performed first. This was followed by lifting the vehicle off the ground while the legs reached their maximum lowering distances. This is shown in Figure 2.26. Stability of the vehicle was maintained in this position.

Trials for the swinging of individual legs while the vehicle was on its belly were performed. It was attempted to move the vehicle along a curvilinear path by swinging one leg. The vehicle was lifted up by lowering the starboard side forward leg and then swinging the leg in the forward direction. While performing the turning action with one leg, the leg pin (pin with which the leg is attached to the main body frame) damaged the main body frame. This was because, the foot of

the leg was fixed on the ground and the vehicle was moving. The movement of the leg is restricted due to the presence of the square guide tube. The restricted movement of the leg caused the leg pin to hit the main body frame and be damaged. Two grousers on the foot of the starboard side forward leg bent due to the same reasons.

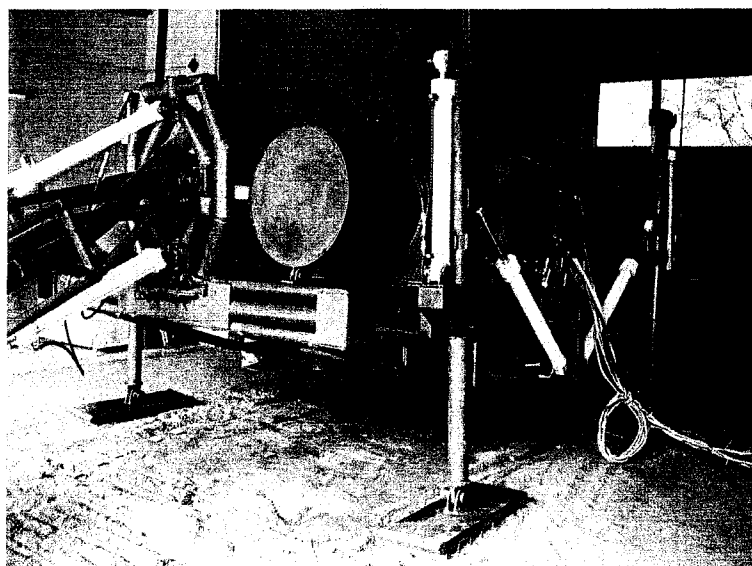


Figure 2. 26 Trials for prototype vehicle supported on its four legs

This problem did not arise for straight line locomotion, but is potentially prevalent for curvilinear locomotion. The solutions to this problem are 1) keeping the swing angle of the legs within safe limits by the use of a mechanical lock, 2) never using a single leg for turning of the vehicle, and 3) designing a new pin with greater tolerance.

The maximum angle of swing achieved by the forward legs was $29 \pm 1^\circ$. The maximum swing angle achieved by after legs was 50° . The discrepancy is because of the way the swing cylinders are attached to the main body frame. One cylinder rod is expanding and the other is retracting while turning the legs through the same swing angle in the same direction. The maximum leg

swing angles were considered while designing the test matrices for gait planning and leg load tests, which are presented in chapter 4.

2.8 Design Power

The primary electrical power was taken from a main supply line (440 V AC, 50 Hz cycle). The electric induction motors driving the dredge pump, eductor pump and hydraulic pumps required 440 V AC, while the solenoids of the directional control (DC) valves operating the hydraulic actuators required 12 V DC. Initially a stabilizer-converter circuit was used for supply of the 12 V DC, which was later replaced by a 12 V battery together with a battery charger. Figure 2.27 shows the schematic of the power supply for the prototype vehicle. There are two different electrical circuits including the PS electrical circuit and the SBS electrical circuit.

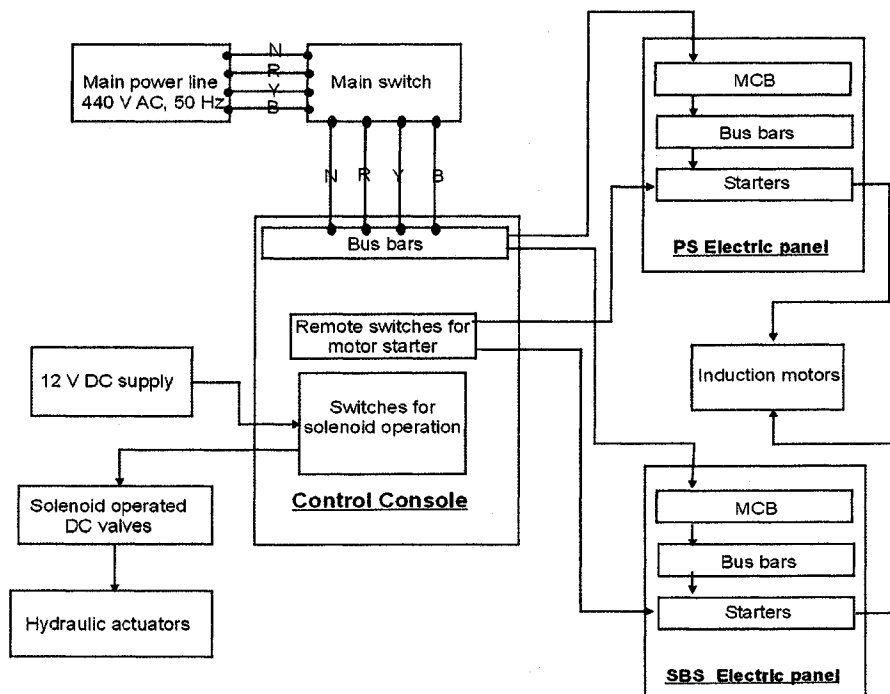


Figure 2. 27 Schematic of the power supply for the prototype vehicle⁸

⁸ MCB Moulded circuit breaker
 N Neutral power line
 R Red phase line
 Y Yellow phase line
 B Blue phase line

The specifications of the different components of the two electrical circuits are shown in Table 2.6.

Table 2.6 Electrical circuits

Electrical circuit: Port Side	Electrical circuit: Starboard side
Dredge pump drive motor: 10 HP (7.5 kW), 3 phase squirrel cage induction motor, 1450 rpm, 440 V AC, 50 Hz	Eductor pump drive motor: 10 HP (7.5 kW), 3 phase squirrel cage induction motor, 2850, 440 V AC, 50 Hz
Hydraulic pump drive motor for port side hydraulic circuit: 1.5 HP (3.75 kW), 3 phase squirrel cage induction motor, 1450 rpm, 440 V AC, 50 Hz	Hydraulic pump drive motor for star board side hydraulic circuit: 1.5 HP (3.75 kW), 3 phase squirrel cage induction motor, 1450 rpm, 440 V AC, 50 Hz
Power supply to a stabilizer-converter circuit for stepping down 220 V AC, 50 Hz to 12 V DC stabilized supply for operation of solenoids actuating hydraulic actuators of the PS hydraulic circuit	Power supply to a stabilizer-converter circuit for stepping down 220 V AC, 50 Hz to 12 V DC stabilized supply for operation of solenoids actuating hydraulic actuators for the SBS hydraulic circuit

The stabilizer-converter circuit (schematic) and the battery with the charger for 12 V DC supply used for operation of the solenoids actuating the DC valves of the hydraulic actuators are shown in Figure 2.28. The solenoids were connected in parallel and thus had the same supply voltage of 12 V DC. The hydraulic circuits designed are shown in Figure 2.29.

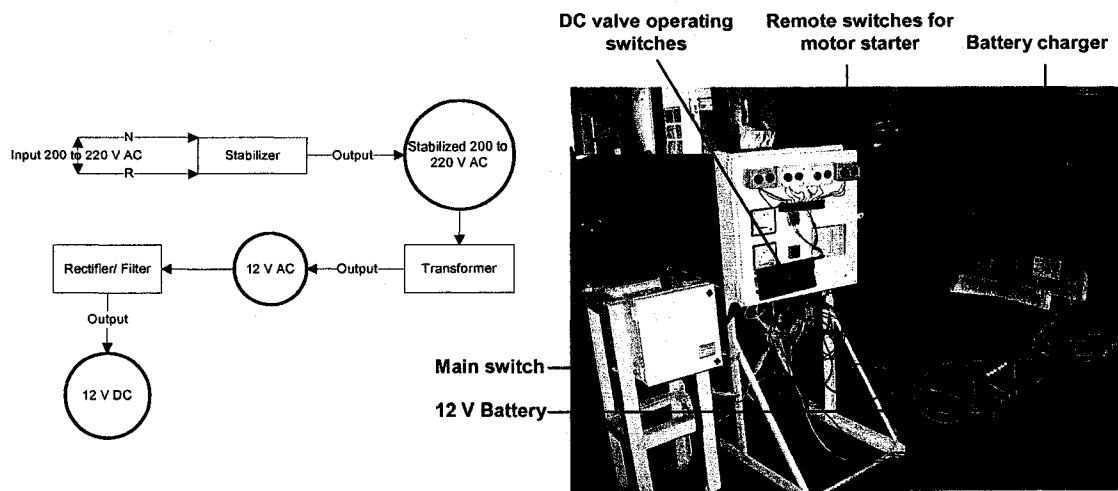


Figure 2.28 Power supply for operation of the Directional Control Valves (12 V DC)

Hydraulic circuit for Golden Tortoise (Portside)

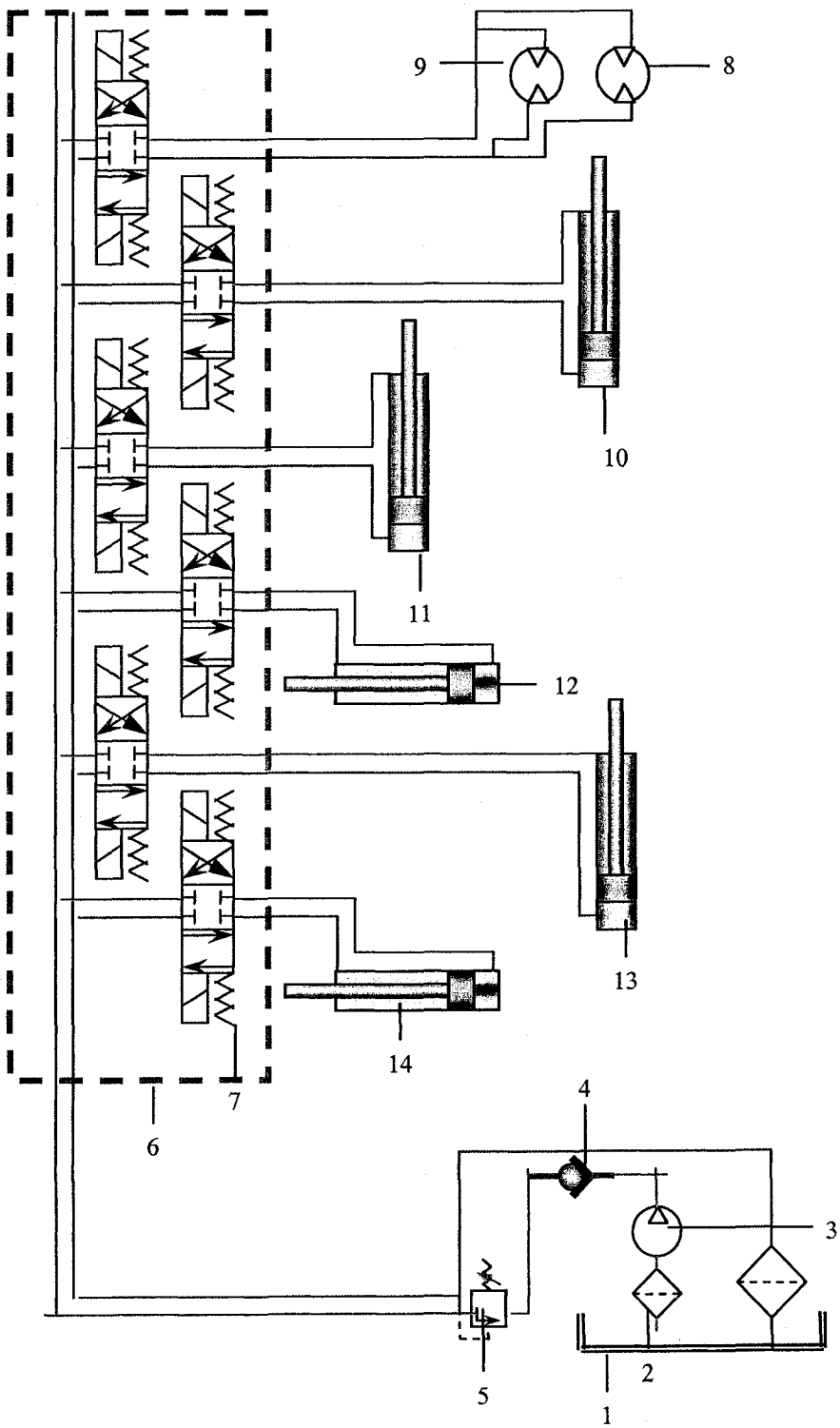


Figure 2. 29 (a) Hydraulic circuits designed (PS)

Hydraulic circuit for Golden Tortoise (Starboard)

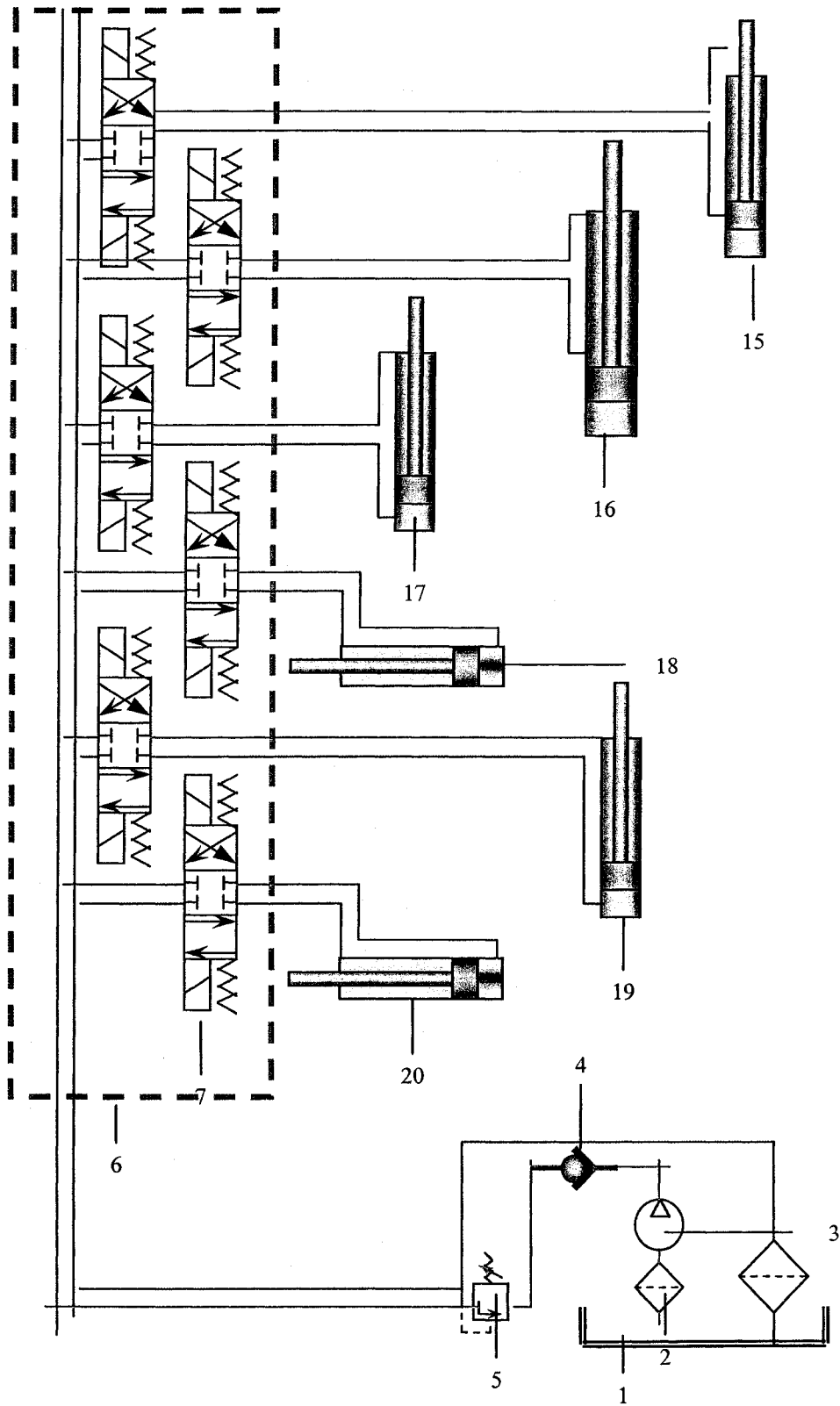


Figure 2.29 (b) Hydraulic circuits designed (SBS)

Legends for Figure 2.29

1. Reservoir
2. Suction strainer
3. Pump, Hydraulic
4. Check valve
5. Pressure relief valve
6. Manifold, 6 station
7. Solenoid operated spring centered Directional Control Valve

PS Hydraulic circuit

8. Hydraulic motor, Cutter drive, PS
9. Hydraulic motor, Cutter drive, SBS
10. Dipper lift cylinder
11. Leg lift cylinder, PS, FWD
12. Leg swing cylinder, PS, FWD
13. Leg lift cylinder, PS, AFT
14. Leg swing cylinder, PS, AFT

SBS Hydraulic circuit

15. Boom lift cylinder
16. Boom swing cylinder
17. Leg lift cylinder, SBS, FWD
18. Leg swing cylinder, SBS, FWD
19. Leg lift cylinder, SBS, AFT
20. Leg swing cylinder, SBS, AFT

Vertical dry pressure hulls house the electrical motors, hydraulic circuits and electronics. The electrical motor driving the hydraulic pump is immersed in a hydraulic oil tank (Figure 2.30). There is a separate hydraulic return tank, which is connected with the hydraulic delivery tank. This helps in reducing the amount of impurities entering from the return line to the pressure line. The same arrangement is repeated on either side of the catamaran hull.



Figure 2. 30 Hydraulic oil tanks

The power supplies should be modified in the future, when the vehicle will operate under water. Primary electrical power supplied through an umbilical cable will drive the secondary hydraulic circuits. The main electrical power will be a 440 V/ 220 V, 50 Hz AC electrical power supplied through an umbilical cable. The power source will be either from an onshore support station or from an appropriate alternator placed onboard the support vessel.

2.9 Comparison between Tracked and Designed Legged Vehicle

This section presents the comparisons between the different models of the ‘Caterpillar’ tracked vehicles and the designed legged vehicle. The relevant data used for these comparisons are presented in Appendix 4. ‘Caterpillar’ tracks are used in unprepared natural terrain both on land and in subsea conditions. The following comparisons between the different performance evaluation parameters of ‘Caterpillar’ tracked vehicles and the designed legged vehicle thus helps in the evaluation of this new design. The graphical results are presented next. The model numbers of the different ‘Caterpillar’ tracked vehicles used for the comparisons are shown on the X axis of Figures 2.31, 2.32 and 2.33. ‘GT01’ represents the prototype vehicle of the ‘Golden Tortoise’. The contact areas of the four feet for GT01 were considered for all the comparisons presented in this section.

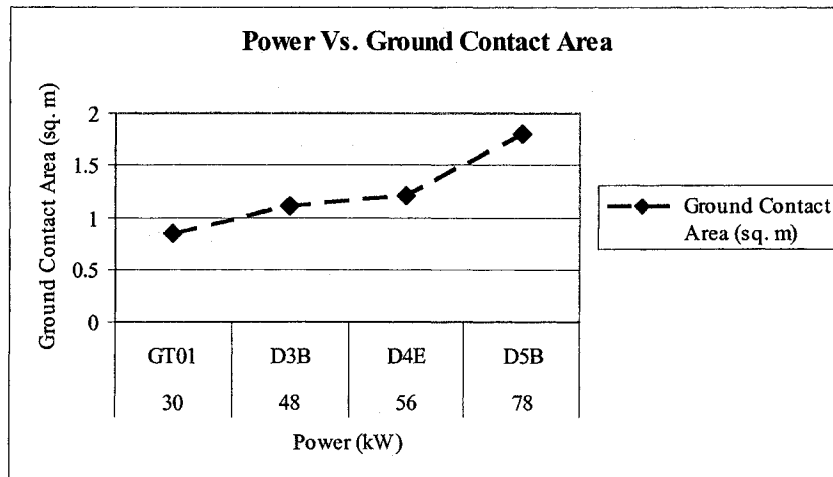


Figure 2. 31 Power vs. ground contact area for ‘Caterpillar’ tracked vehicles and the designed legged vehicle

The excavation and transportation power of the designed prototype vehicle was considered for all the comparisons.

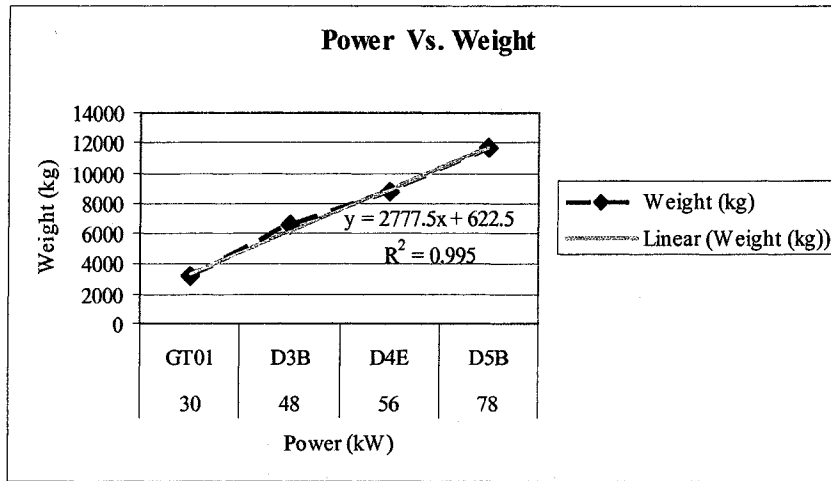


Figure 2. 32 Power vs. weight for ‘Caterpillar’ tracked vehicles and the designed legged vehicle

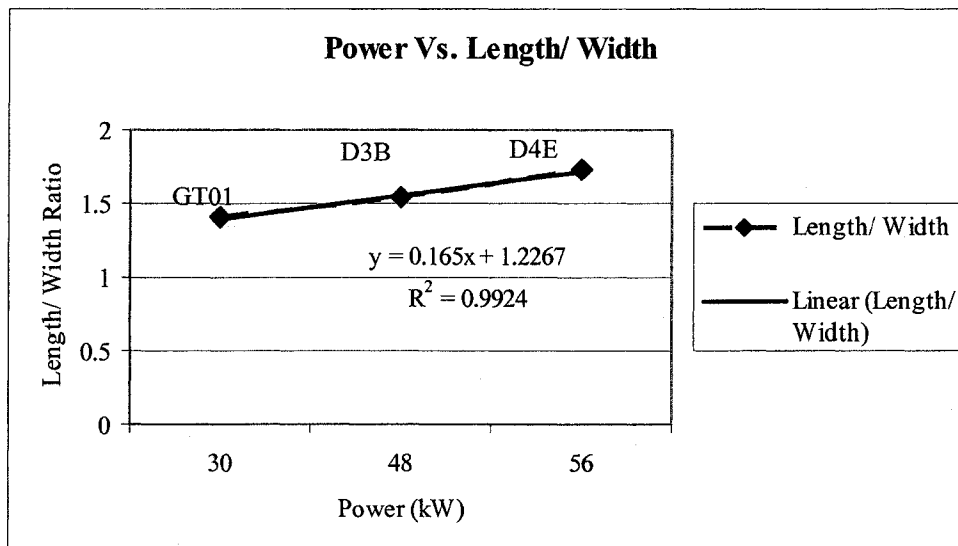


Figure 2. 33 Power vs. length/ width ratio for ‘Caterpillar’ tracked vehicles and the designed legged vehicle

The ratio of the ground contact area / kW for ‘Caterpillar’ tracked vehicles was approximately calculated as 0.022 (Figure 2.31). The same ratio for the designed walking dredger was kept at about 0.028 to have less ground pressure (Figure 2.31). The acceptable ground pressure for ground operated ‘Caterpillar’ tracked vehicles was calculated to be 50 to 51 kPa. The ground pressure as calculated in air for the prototype vehicle was 37 kPa, which is much lower than the

'Caterpillar' tracked vehicles. Hence the designed vehicle is expected to be able to perform locomotion and the designed tasks in soils with low soil bearing capacities. Weights may be added to increase ground pressure and the ballast tanks may be emptied for reducing the ground pressure. The average weight/ kW ratio for 'Caterpillar' tracked vehicles is approximately 148 kg (Figure 2.32). The same ratio for the walking dredger is 107 kg (Figure 2.32). This indicates less cost per unit power.

The average length/ width ratio for 'Caterpillar' tracked vehicles is approximately 1.6, whereas, that for the designed walking dredger it is 1.4 (Figure 2.33).

2.10 Concluding Remarks

The design of the active legged submersible dredger/ miner discussed in this chapter is a very modular design, where each module or component can be dismantled and interchanged very easily. This facilitates easy transportation and assembly of the designed vehicle. The interchangeability options will help in using the designed vehicle under different operational and environmental conditions. The functionality tests discussed in this chapter proved that the different systems were working properly. The gait plans developed for straight line and curvilinear locomotion were validated by suitable on-land prototype tests, to investigate the suitability of the designed leg linkage and the proposed simulated belly crawling motion over unprepared natural terrain. The theoretical gait plans developed and the experiments executed are discussed in the next chapter.

CHAPTER 3

PERFORMANCE EVALUATION MODELS FOR LOCOMOTION

3.1 Introduction

In developing the parametric performance evaluation models for locomotion, the design parameters of the vehicle including the overall geometry, the leg and foot geometry, the leg joint parameters, the number and geometry of the grousers and the location of the centre of gravity of the vehicle were considered. The required soil properties of the terrain, the bearing capacity, and the shearing characteristics of the terrain were also considered. The soil mechanical aspects are discussed in Appendix 1. The performance of the designed vehicle was judged by the effectiveness of the gait plan in executing a particular type of locomotion, the locomotion cycle time required to perform a particular gait plan, the stability issues due to soil reaction forces and the tractive forces generated during the locomotion process. Experimental validations of the gait plans, the locomotion cycle time and the static load incident at each leg were performed.

3.2 Gait Plan for Straight Line Locomotion

The magnitude of the step size of individual leg determines whether the designed vehicle will exhibit straight line or curvilinear locomotion. The step sizes of all the legs and the centre of gravity of the designed vehicle must be equal for straight line locomotion. A step generator was developed to predict the step size of the leg as a function of the leg joint parameters. The step generator was further modified to accommodate the level difference due to terrain or submergence at the foot/ soil interface. The slip action at the foot/ soil interface was also considered. The slip for the designed vehicle is due to the shearing action at the foot/ soil interface and not due to the frictional force as is common in other legged vehicles. This is because the feet are kept fixed during the entire locomotion cycle for the designed vehicle as

opposed to other legged vehicles. Comparisons between the predicted step sizes without and with slip conditions and experimental step sizes were done to observe the percentage of slip occurring at the foot/ soil interface during legged locomotion. The slip was also estimated from the experimental data.

3.2.1 Step Generator

The step generator for the designed legged vehicle is shown in Figure 3.1.

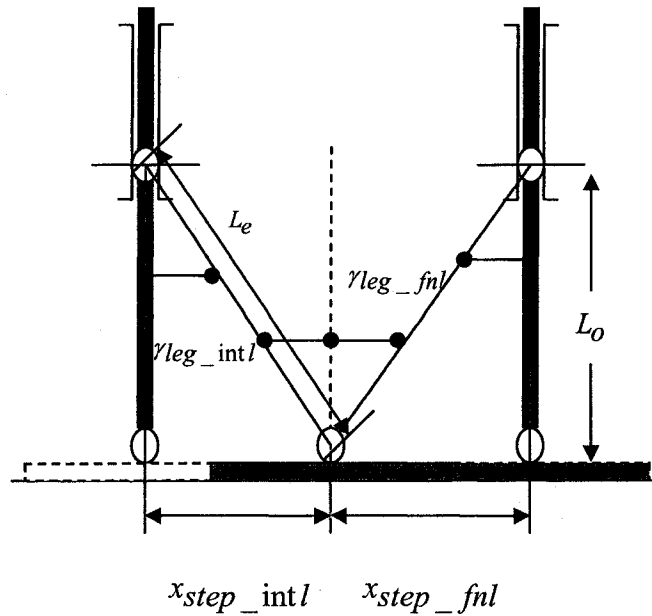


Figure 3.1 Step generator

The step generator without any level difference, submergence or slip at the foot/ soil interface is deduced,

$$x_{step_intl} = L_o * \tan(\gamma_{leg_intl}) \quad \text{[Equation 3.1]}$$

$$x_{step_fnl} = L_o * \tan(\gamma_{leg_fnl}) \quad \text{[Equation 3.2]}$$

$$x_{step} = x_{step_intl} + x_{step_fnl} \quad \text{[Equation 3.3]}$$

where, L_o is the perpendicular distance between the leg pin centre and the foot hinge pin centre [m], x_{step_intl} is the step size due to initial swing angle of the leg [m], x_{step_fnl} is the step size due to final swing angle of the leg [m], x_{step} is the total step size of individual leg [m], γ_{leg_intl} is the initial angle of leg swing [degree], and γ_{leg_fnl} is the final angle of leg swing [degree]. Unless otherwise stated, the term ‘swing angle’ for leg, used in this thesis represents ‘half swing angle’ of the leg i.e. either γ_{leg_intl} or γ_{leg_fnl} . The sum of the initial and final swing angle is denoted as the ‘total swing angle’.

Figure 3.2 shows two legs present at two different levels denoted by L_1 and L_2 [m], with a level difference of (+) Δh_{leg} [m].

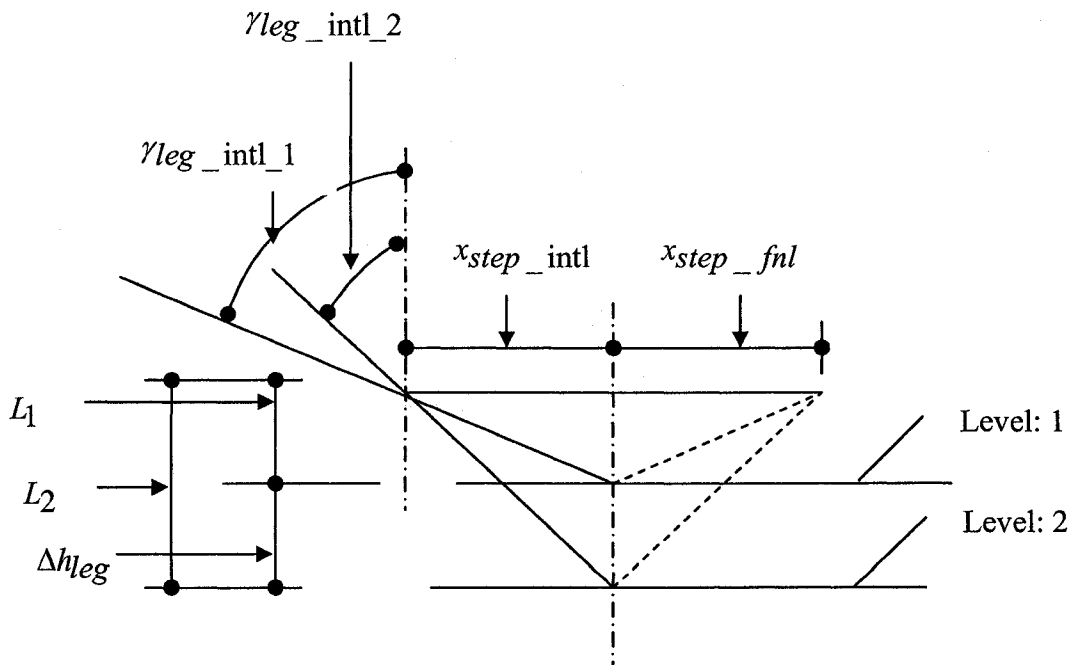


Figure 3. 2 Step generator with level difference or submergence

If the initial and final swing angles of individual legs are equal, the step generator deduced in Equations 3.1 to 3.3 is modified,

$$x_{step_intl} = x_{step_fnl} = L_1 * \tan(\gamma_{leg_intl_1}) \quad [\text{Equation 3.4}]$$

$$x_{step_intl} = x_{step_fnl} = L_2 * \tan(\gamma_{leg_intl_2}) = (L_1 + \Delta h_{leg}) * \tan(\gamma_{leg_intl_2}) \quad [\text{Equation 3.5}]$$

$$\gamma_{leg_intl_2} = \tan^{-1} \left[\frac{L_1}{(L_1 + \Delta h_{leg})} * \tan(\gamma_{leg_intl_1}) \right] \quad [\text{Equation 3.6}]$$

where, the subscripts 1 and 2 represent two different legs. If there is submergence of Δh_{foot} [m] at any foot/ soil interface, the term Δh_{leg} [m] must be replaced by $(\Delta h_{leg} + \Delta h_{foot})$ [m] in the above equations. When there is a slip of Δx [m] along the longitudinal direction of the vehicle at any foot/ soil interface, the final leg swing angle of the leg which slips, needs to be modified in order to achieve the same step size for all the legs. Figure 3.3 shows two legs, one of which slips in the direction opposite to the vehicle motion.

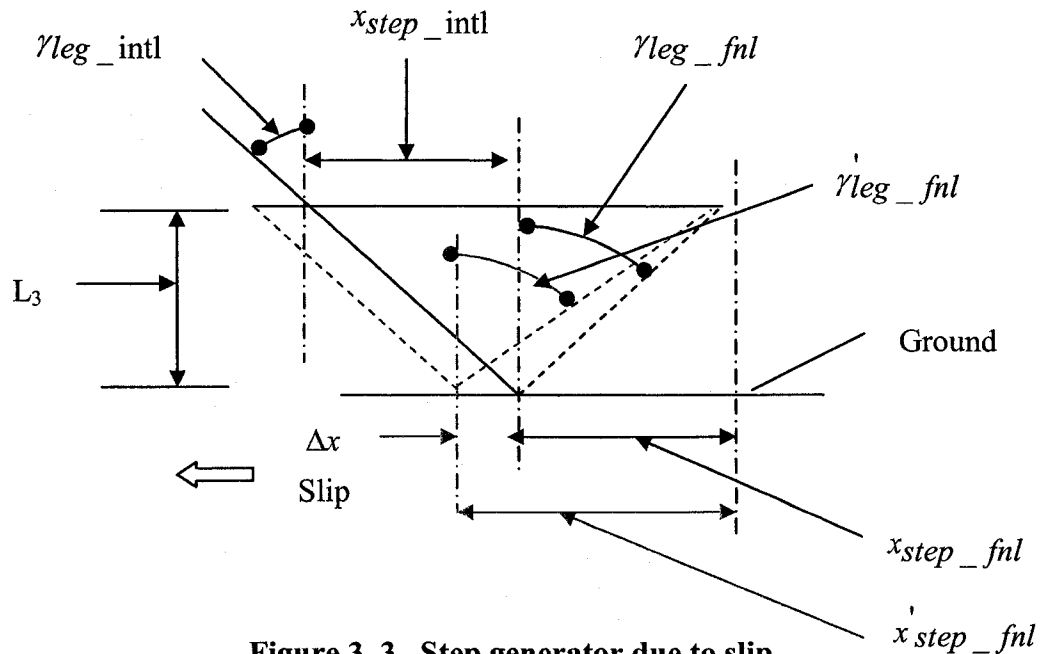


Figure 3.3 Step generator due to slip

The final swing angle of the leg which slips is deduced,

$$\gamma'_{leg_fnl} = \tan^{-1} \left(\frac{x_{step_fnl} + \Delta x}{L_3} \right) \quad [\text{Equation 3.7}]$$

where, γ'_{leg_fnl} is the final angle of leg swing due to slip [degree].

With simultaneous level difference of the legs (Δh_{leg}) [m] and/ or submergence (Δh_{foot}) [m] and slip (Δx) [m], the initial swing angle of the leg concerned will be $\gamma_{leg_intl_2}$ [degree] and the final swing angle of the leg will be γ'_{leg_fnl} [degree].

3.2.2 Experimental and Predicted Results for Straight Line Locomotion

Full scale on land prototype tests for both forward and backward straight line locomotion were carried out on level and relatively flat terrain. The experimental set up, measuring techniques, and measuring instruments are discussed in Appendix 5. The test matrices and the experimental and predicted data are given in Appendix 6. The initial and final leg swing angles, the step size and the time required to lift and swing the legs were measured for straight line and curvilinear locomotion tests. The perpendicular distance between the leg swing pin centre and the foot hinge pin centre (L_o), was kept at 340 mm during all the locomotion tests.

The experimental step sizes were first compared with step sizes predicted by using Equations 3.1 to 3.3, which do not consider the slip at the foot/ soil interface. The graphical results are presented in Figure 3.4 to 3.11.

The prototype vehicle was remotely operated on land by manually controlling the electronic switches actuating the solenoids of the directional control (DC) valves of the hydraulic cylinders.

It was thus difficult to accurately control the final swing angle of the legs. Due to human operational errors, the deviations between the experimental and predicted results existed.

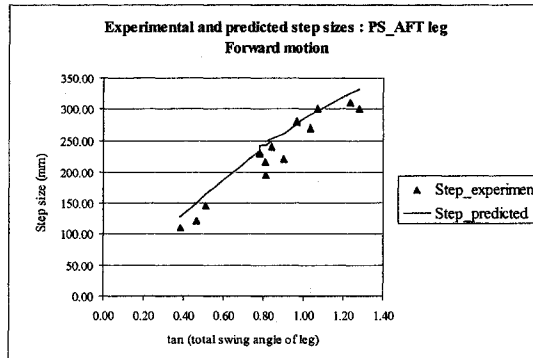


Figure 3. 4 Experimental step size and predicted step size without slip for PS_AFT leg during forward straight line locomotion

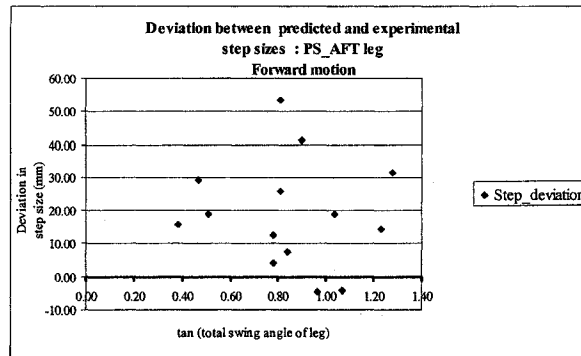


Figure 3. 5 Deviation between predicted and experimental step sizes for PS_AFT leg during forward straight line locomotion

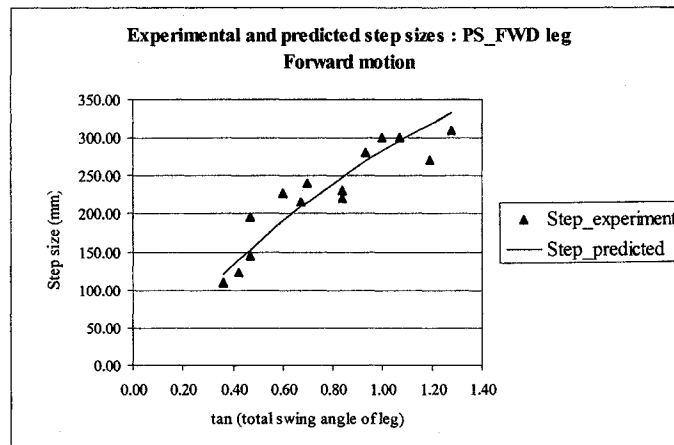


Figure 3. 6 Experimental step size and predicted step size without slip for PS_FWD leg during forward straight line locomotion

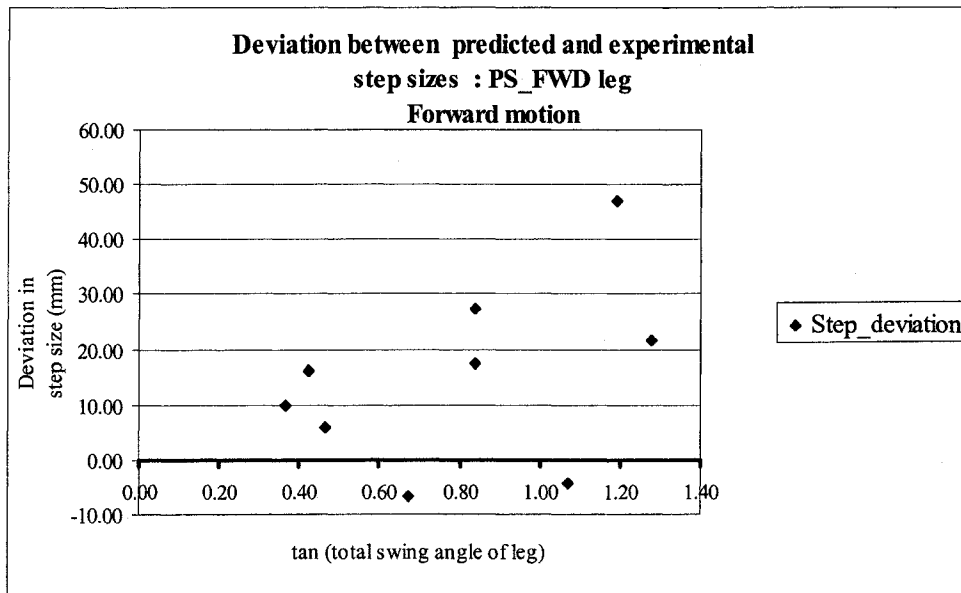


Figure 3. 7 Deviation between predicted and experimental step sizes for PS_FWD leg during forward straight line locomotion

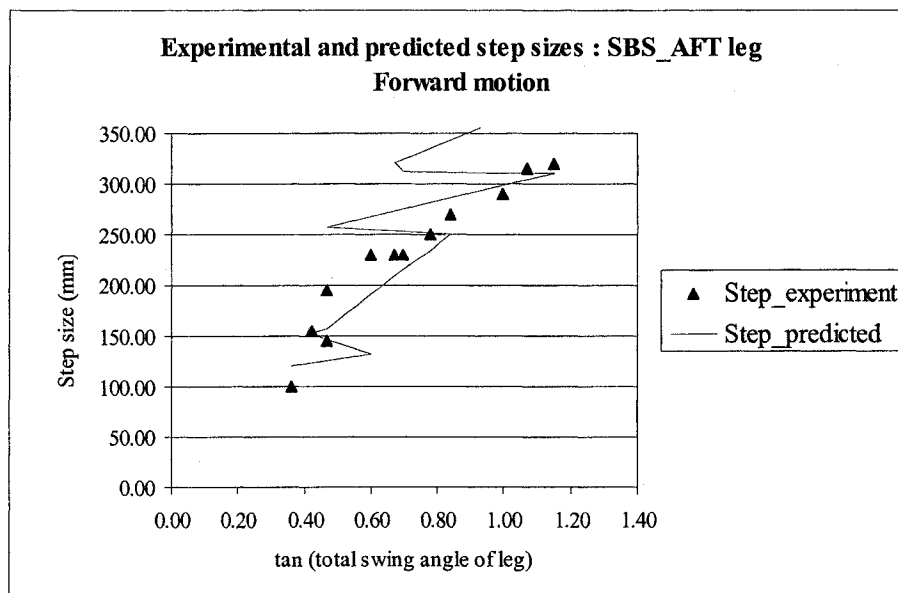


Figure 3. 8 Experimental step size and predicted step size without slip for SBS_AFT leg during forward straight line locomotion

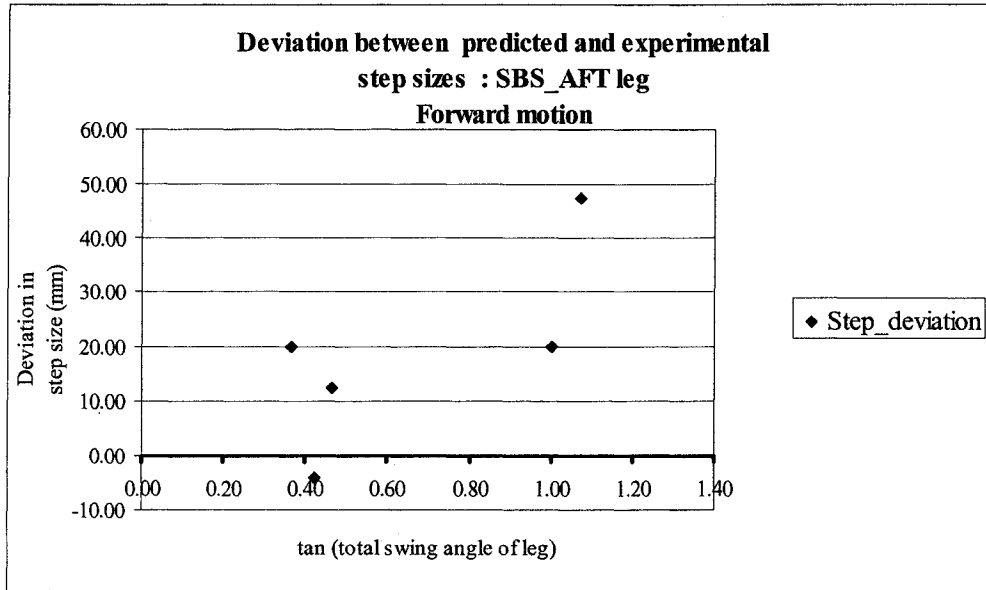


Figure 3.9 Deviation between predicted and experimental step sizes for SBS_AFT leg during forward straight line locomotion

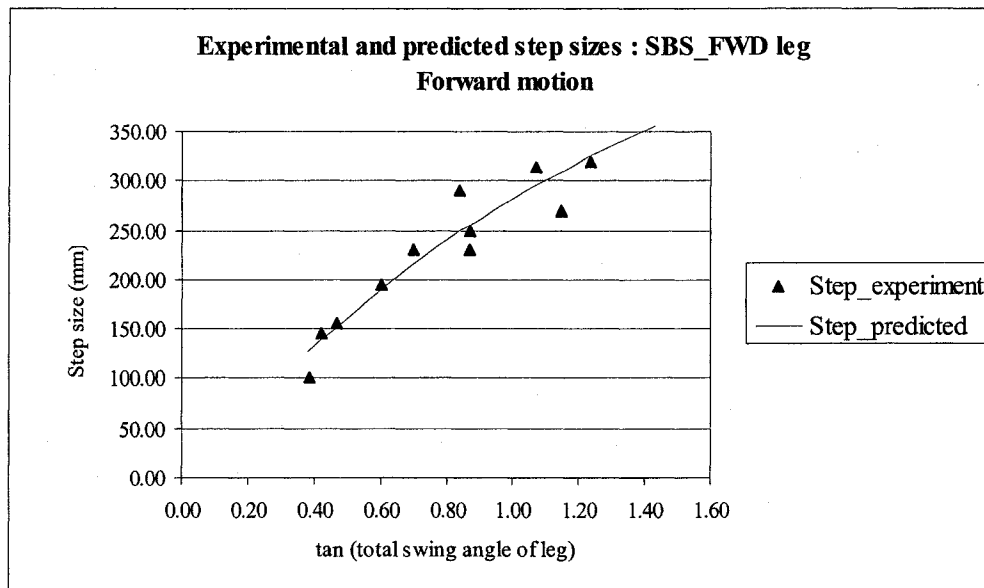


Figure 3.10 Experimental step size and predicted step size without slip for SBS_FWD leg during forward straight line locomotion

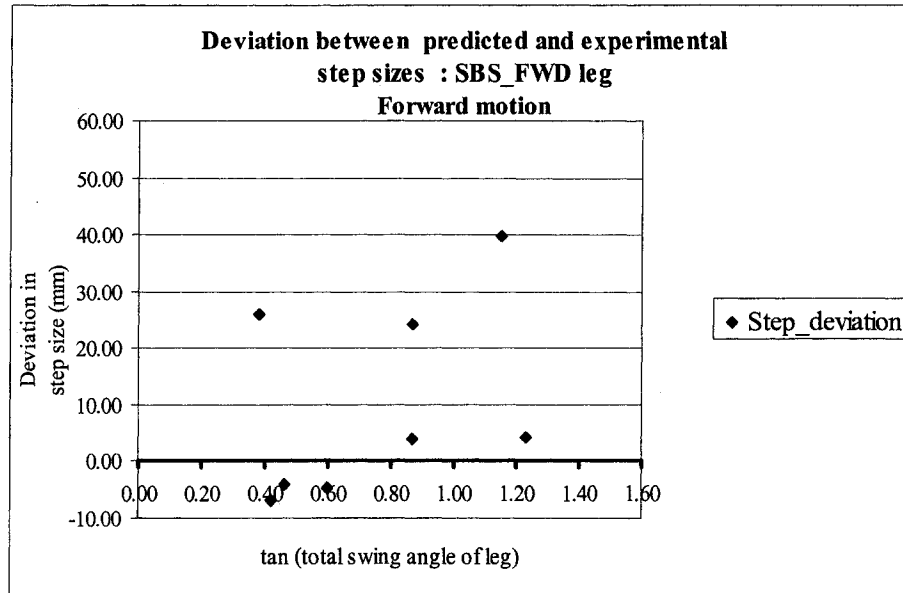


Figure 3. 11 Deviation between predicted and experimental step sizes for SBS_FWD leg during forward straight line locomotion

The deviation and the percentage deviation were respectively calculated as

$$(\text{Calculated value} - \text{Experimental value}) \text{ and } \left[\left(\frac{\text{Calculated value} - \text{Experimental value}}{\text{Experimental value}} \right) * 100 \right].$$

The average percentage deviations for the different legs for the forward straight line locomotion tests are presented in Table 3.1. It is observed from Table 3.1, that the average percentage deviations of the AFT legs were very close. The same was true for the FWD legs. The deviations between the experimental and predicted results can also be explained due to the presence of the slip at the foot/ soil interfaces. The presence of the ladder assembly and the direction of movement of the vehicle explain the discrepancies observed between the average deviation percentages for the AFT and the FWD legs. The FWD legs are under predicted, since the ladder assembly tries to drag the FWD legs (in the direction of the vehicle motion) more as compared to the AFT legs during the forward straight line locomotion. Hence the experimental step sizes for the FWD legs were higher compared to the predicted step sizes. The FWD legs will thus exhibit

both slip and skid actions during forward straight line locomotion. The AFT legs will exhibit greater slip compared to the FWD legs during forward straight line locomotion, since the ladder assembly generates resistance to motion of the AFT legs. Hence the AFT legs show over predicted values of step sizes.

Table 3.1 Average deviation percentage for forward straight line locomotion

Leg	Average deviation percentage
PS_AFT	10 %
PS_FWD	- 5 %
SBS_AFT	9 %
SBS_FWD	- 6 %

The experimental step sizes for forward straight line locomotion were next compared with the predicted step sizes which considered the slip at the foot/ soil interface (Figure 3.12). Such comparisons help to estimate the slip percentage occurring at the different foot/ soil interfaces for the particular soil on which the locomotion tests were performed. The soil consisted of relatively dry medium to fine sand. The effective leg lengths, the angular and the linear velocities of the legs at different slip percentages were calculated from the experimental data. The step sizes were predicted from the linear velocities of the legs and the time required swinging the leg through the total swing angle.

It is observed from Figure 3.12, that the experimental step sizes are close to the predicted step sizes with a slip of 10 % for the PS_AFT leg. In case of the SBS_AFT leg, the experimental step sizes are close to the predicted step sizes with slips of 10 % and 20 %. The average slip percentage calculated from the experimental results for the PS_AFT leg was 12 % and that for the SBS_AFT leg was 17 %. From the predicted and experimental results it can be concluded that the slip percentage for the designed leg and foot in medium to fine relatively dry sand varies between 10 to 20 % for forward straight line locomotion. Manual operation of the prototype,

presence of the ladder assembly and the lagging or leading effects of the PS and the SBS hydraulic circuits explains the differences between the slip percentages for the PS_AFT and the SBS_AFT legs.

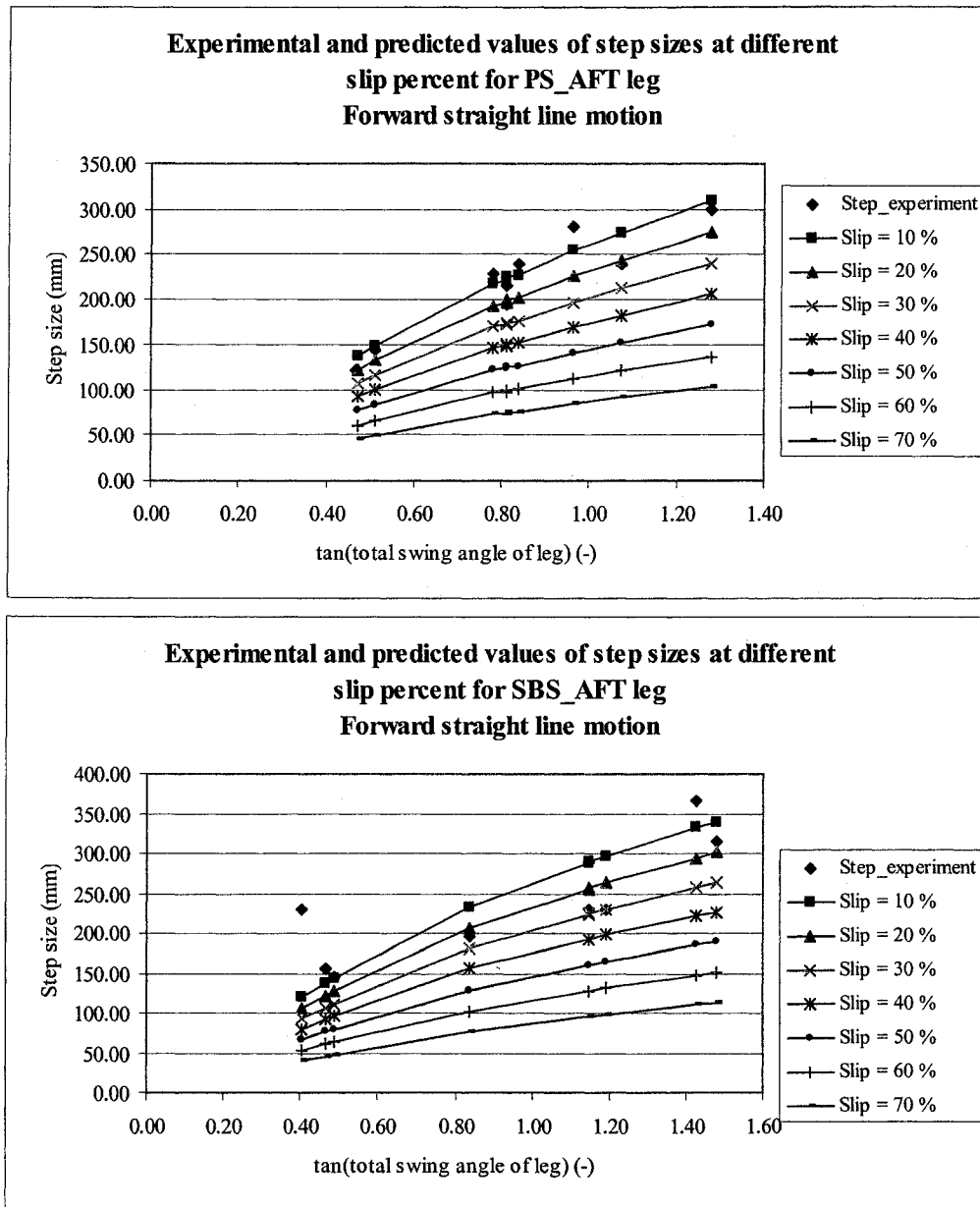


Figure 3. 12 Experimental and predicted step sizes with different slip percentages during forward straight line locomotion

The graphical results for backward straight line locomotion are presented next. The experimental step sizes were first compared with the predicted step sizes without any slip at the foot/ soil interface (Figure 3.13 to 3.20)

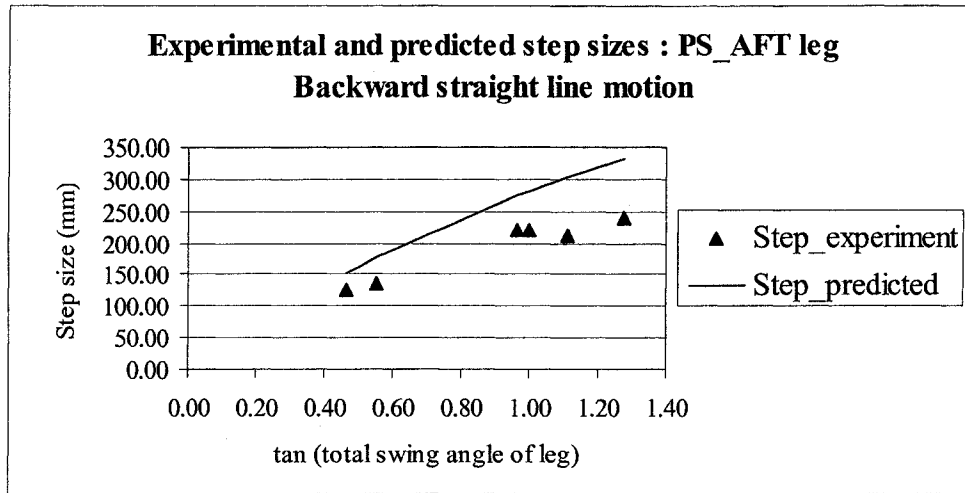


Figure 3. 13 Experimental step size and predicted step size without slip for PS_AFT leg during backward straight line locomotion

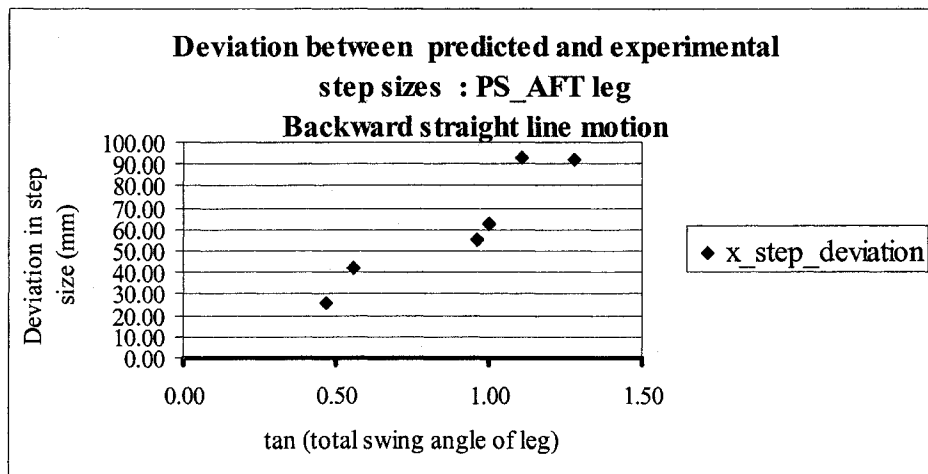


Figure 3. 14 Deviation between predicted and experimental step sizes for PS_AFT leg during backward straight line locomotion

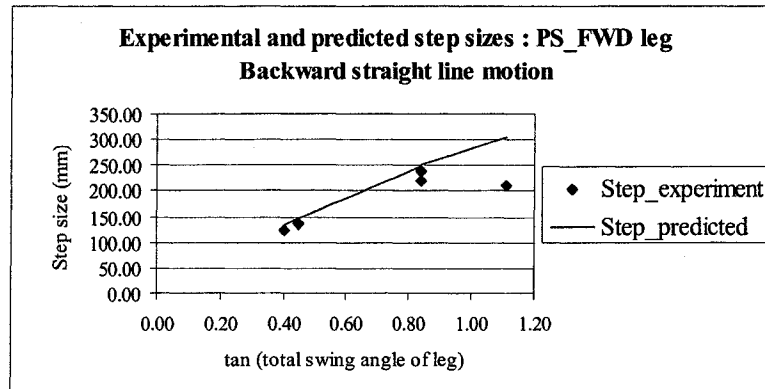


Figure 3.15 Experimental step size and predicted step size without slip for PS_FWD leg during backward straight line locomotion

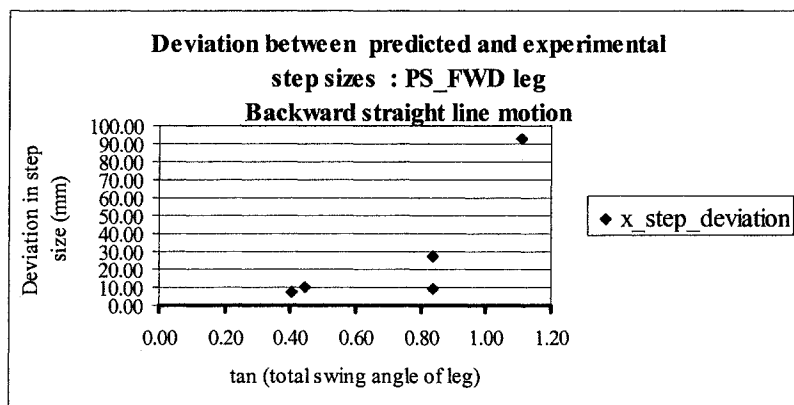


Figure 3.16 Deviation between predicted and experimental step sizes for PS_FWD leg during backward straight line locomotion

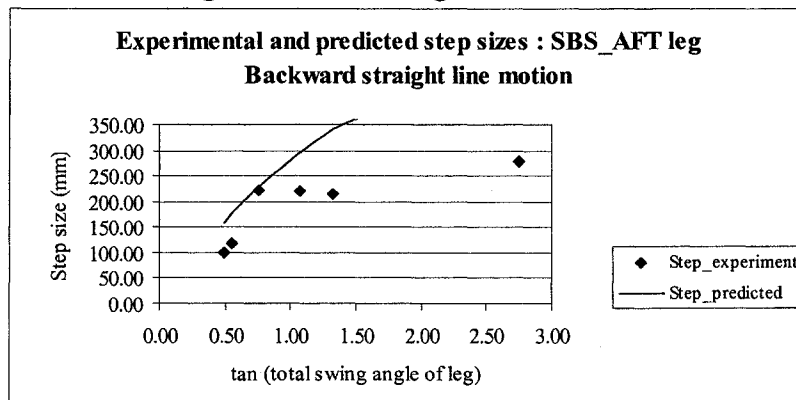


Figure 3.17 Experimental step size and predicted step size without slip for SBS_AFT leg during backward straight line locomotion

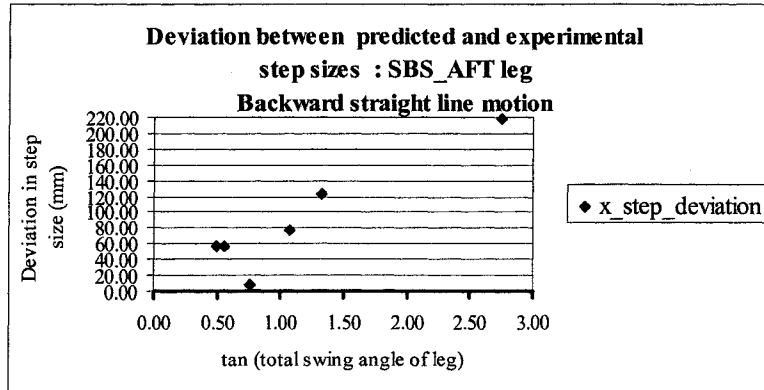


Figure 3. 18 Deviation between predicted and experimental step sizes for SBS_AFT leg during backward straight line locomotion

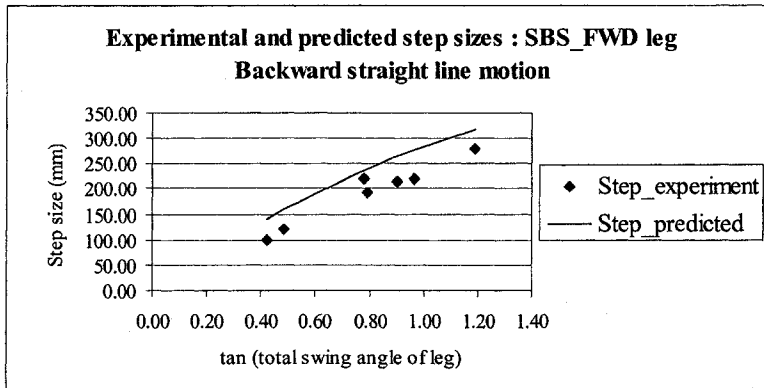


Figure 3. 19 Experimental step size and predicted step size without slip for SBS_FWD leg during backward straight line locomotion

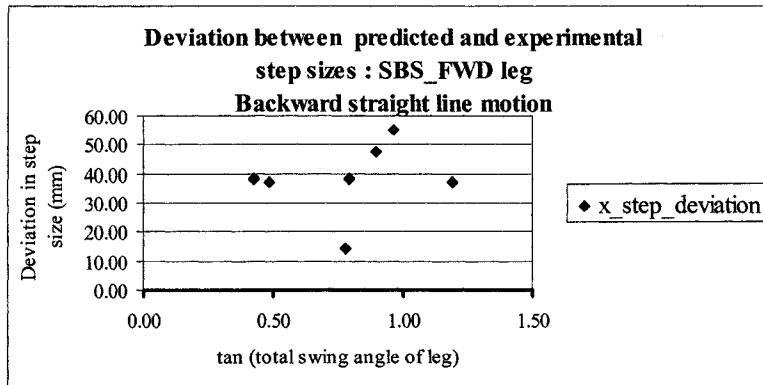


Figure 3. 20 Deviation between predicted and experimental step sizes for SBS_FWD leg during backward straight line locomotion

The deviations between the experimental and predicted step sizes are much higher for the backward locomotion tests than the forward locomotion tests. The average deviation percentages for the different legs are presented in Table 3.2.

Table 3.2 Average deviation percentage for backward straight line locomotion

Leg	Average deviation percentage
PS AFT	31 %
PS FWD	14 %
SBS AFT	46 %
SBS FWD	23 %

The legs were over predicted during backward straight line locomotion. The average deviation percentages for the AFT legs were however higher than the FWD legs. The presence of the ladder assembly results in higher slip percentages for the AFT legs than the FWD legs. The deviations for the AFT legs were thus higher compared to the FWD legs. The ladder assembly also generates motion resistance to the FWD legs. Hence, the FWD legs will also slip. The chances of skid for the FWD legs are lower during backward straight line locomotion. The outliers in Figures 3.15 and 3.17 represent data points from the same test run, where the final swing angle of the SBS_AFT leg was almost twice the initial swing angle of the same leg. The SBS_AFT leg was exhibiting swinging action long after the other legs stopped swinging. This resulted in unusual movement of the prototype vehicle. The outlier in Figure 3.12 is also due to the lack of control of the final swing angle of the leg.

The comparisons between the experimental and predicted step sizes for the backward straight line locomotion with slip conditions at the foot/ soil interface are shown in Figure 3.21.

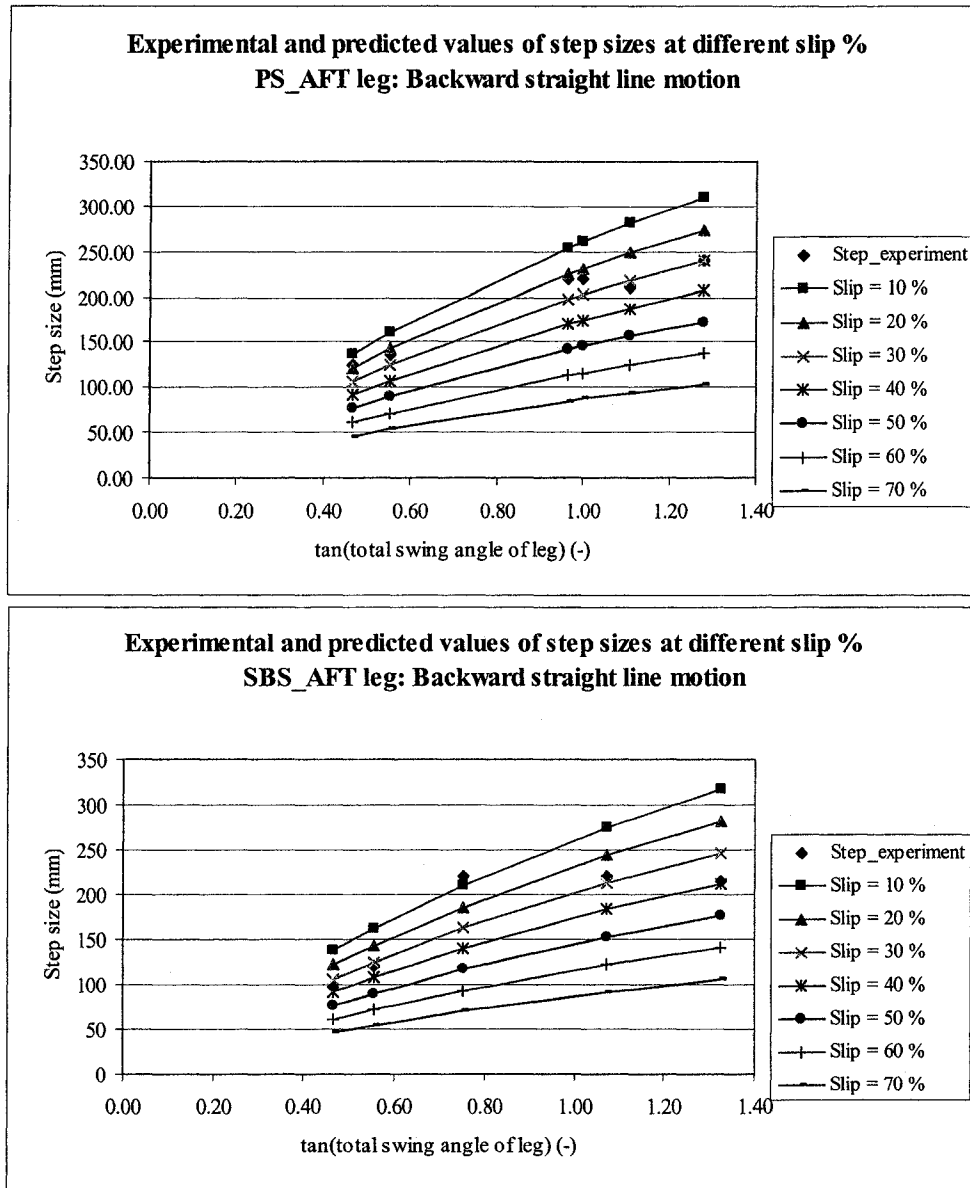


Figure 3. 21 Experimental and predicted step sizes with different slip percentages for backward straight line locomotion

For the PS_AFT leg, the experimental results are closer to the predicted results with a slip of 20 %. Two experimental data points however coincide with the predicted values of 30 % slip. For the SBS_AFT leg, the majority of the data points coincide with predicted results of 30 % slip. The average slip percentage calculated from the experimental results for the PS_AFT leg was 25 % and that for the SBS_AFT leg was 30 %.

From the predicted and experimental results, it can be concluded that the maximum percentage of slip for forward straight line locomotion is 20 % and that for backward straight line locomotion is 30 % in relatively dry medium to fine sand. The slip percentage for the SBS_AFT leg is higher than the PS_AFT leg. The higher slip percentage for the SBS_AFT leg may be due to the 1) time delay factors of the designed hydraulic circuit, and 2) human operational errors. The slip occurring due to shearing action is a function of the grouser geometry, number of grousers, soil type and the hydraulic cylinder force available.

The trajectory of the prototype vehicle during straight line locomotion was drawn in AutoCAD and is presented in Figure 3.22. The step sizes and the headings measured by scales and tapes during the prototype tests were used to draw the vehicle trajectory. The deviation of the vehicle from the proposed straight line path was measured from the AutoCAD drawing. The deviation was given by the perpendicular distance between the proposed straight line path and the actual vehicle trajectory.

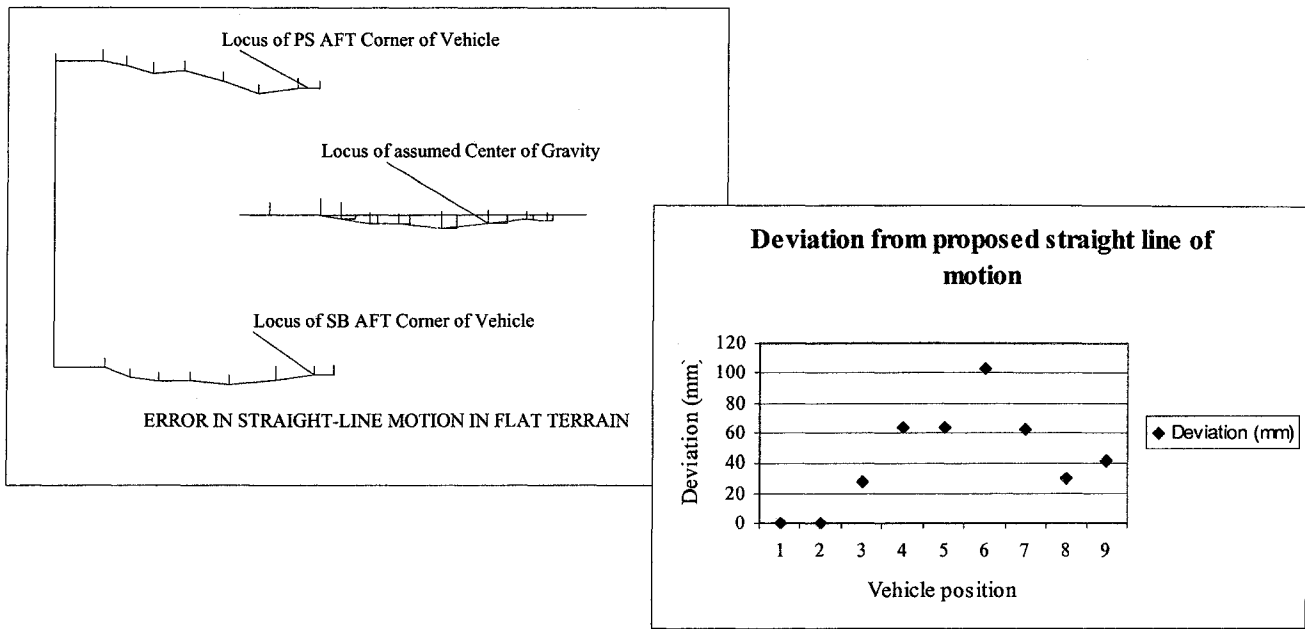


Figure 3.22 Vehicle trajectory and deviation from proposed path during straight line locomotion

As is observed from Figure 3.22, the minimum deviation was 28 mm, while the maximum deviation was 103 mm. Such deviation values are acceptable for dredging or mining operations.

The maximum level difference negotiable and the maximum submergence possible at a particular foot/ soil interface are dependent on the 1) stroke of the hydraulic cylinders used for lifting/ lowering and swinging of the leg, and 2) the allowable tilt for the designed vehicle in the longitudinal and transverse directions. For the designed vehicle the maximum swing angles achieved by the FWD legs are different from that of the AFT legs, which was discussed in section 2.7.6. The maximum allowable slip is also determined by the stroke of the hydraulic cylinder used for swinging the leg and the maximum swing angle achievable for that particular leg. The predicted ratios between the swing angles of the AFT to FWD legs were plotted against

the swing angle of the AFT legs for different level differences between the AFT and the FWD legs (Figure 3.23).

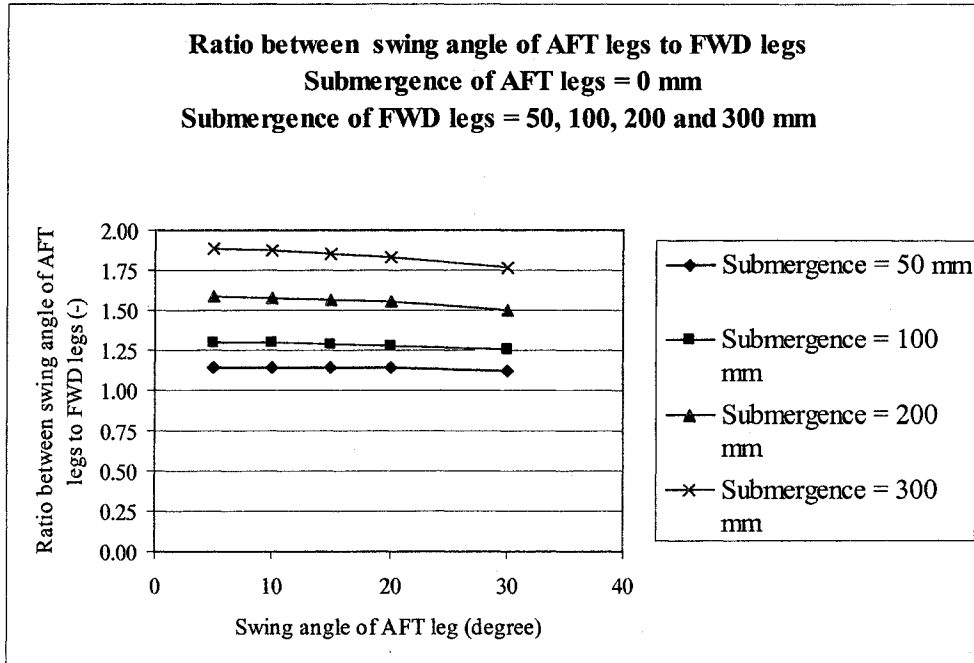


Figure 3. 23 Ratio between swing angles of AFT and FWD legs for different submergences of the FWD legs and zero submergence of AFT legs

The AFT legs were assumed to touch the ground with zero submergence. The FWD legs were assumed to have submergences of 50 mm, 100 mm, 200 mm and 300 mm. Thus the FWD and the AFT legs were present at two different ground levels.

It was discussed in section 2.7.6, that the maximum swing angle for the FWD legs was 30 degrees, while the maximum swing angle achieved by the AFT legs was 50 degrees. Thus a level difference of 300 mm between the FWD and AFT legs (Figure 3.2), equal to half the hydraulic cylinder stroke of 600 mm, is possible. The same conclusion is valid for the PS and SBS legs. The vehicle tilts under the given conditions are tabulated below, which are within the design limit i.e. < 10 degrees. The same ratio between the swing angles of the AFT and FWD legs is to be maintained during the occurrence of slip at the foot/ soil interface.

Table 3.3 Longitudinal tilt of vehicle for different level differences between AFT and FWD legs

Level difference (mm)	Longitudinal tilt (degree)
50	1.30
100	2.60
200	5.20
300	7.77

Table 3.4 Transverse tilt of vehicle for different level differences between PS and SBS legs

Level difference (mm)	Longitudinal tilt (degree)
50	1.2
100	2.4
200	4.8
300	7.2

Obstacles of diameter ≤ 300 mm can also be negotiated by the prototype vehicle, assuming the vehicle performs locomotion in a relatively flat and level terrain with scattered boulders of diameter ≤ 300 mm.

3.3 Gait Plan for Curvilinear Locomotion on Level Terrain

3.3.1 Principle of Curvilinear Motion

The principle of skid steering is used for tracked vehicles where one track is driven faster than the other, causing the vehicle to turn towards the slower track. A new principle of skid steering is applied to the designed legged vehicle where differential step sizes are applied to the inner and outer legs as a result of which the vehicle turns towards the inner legs with lower step sizes.

Differential step sizes can be achieved in two ways using 1) inner legs with equal initial swing angles ($\gamma_{leg_intl_in} \neq 0^\circ$) and outer legs with equal initial swing angles ($\gamma_{leg_intl_out} \neq 0^\circ$), where, $\gamma_{leg_intl_out} > \gamma_{leg_intl_in}$, and 2) inner legs with zero initial swing angles ($\gamma_{leg_intl_in} = 0^\circ$) and outer legs with equal initial swing angles ($\gamma_{leg_intl_out} \neq 0^\circ$). For ease of operation the initial and the final swing angles should be equal for all the legs. The swing

angle of the leg is assumed zero, when the leg is vertical. When the top of the leg points towards the vehicle AFT, the swing angle of the leg is denoted as a positive angle. The principle of curvilinear locomotion is shown in Figure 3.24.

The two rectangles represent the positions of the main body frame of the vehicle before and after turning. The centre of gravity of the vehicle is assumed at the mid-point of the vehicle main body frame. The instantaneous centre of rotation is given by the point of intersections of the perpendiculars drawn to the longitudinal centre lines of the main body frame at the assumed centre of gravity. The turning radius for any point is given by the linear distance between the instantaneous centre of rotation and the point under consideration.

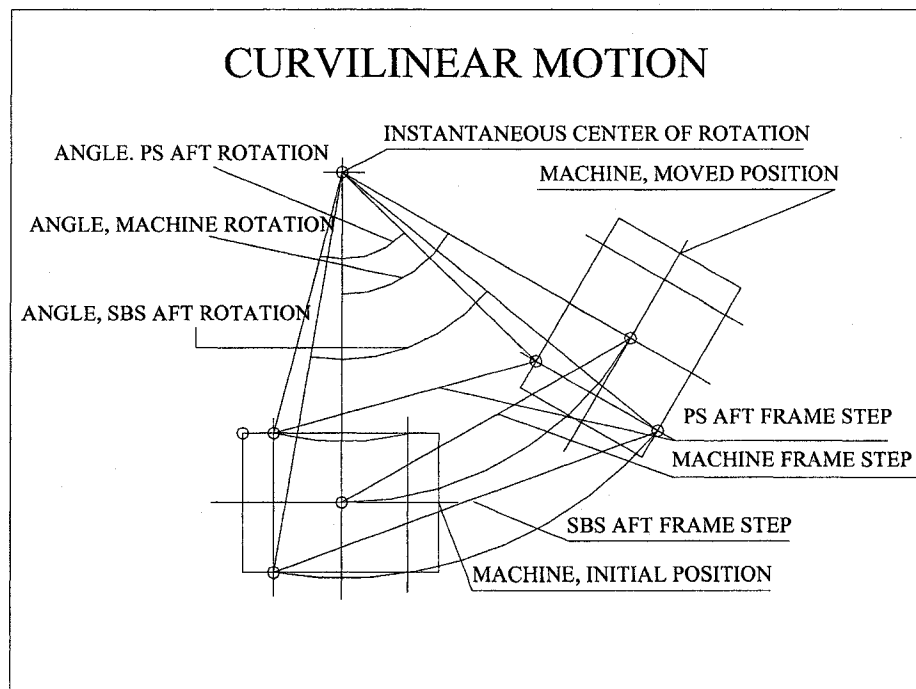


Figure 3. 24 Principle of curvilinear motion

According to the design, two separate hydraulic circuits are used to drive the inner and the outer legs. If the hydraulic oil flows of both the circuits are the same, the time required by the outer legs to swing will be higher than the inner legs. The inner legs might slip or skid under the given

circumstances. The hydraulic oil flows may be adjusted for the two separate hydraulic circuits, so that both the inner and outer legs have the same swinging time irrespective of the swing angles.

3.3.2 Kinematics of Skid Steering for the Legged Vehicle

A two-dimensional model for curvilinear locomotion on level and relatively flat terrain was developed. Figure 3.25 shows the designed legged vehicle turning about an instantaneous centre of rotation O_i [-], with a turning radius of R_{turn} [m] and a yawing velocity of $\Omega_{vehicle}$ [rad/sec]. It was assumed that the outer legs had an equal angular velocity of Ω_{leg_out} [rad/sec] while the inner legs also had an equal angular velocity of Ω_{leg_in} [rad/sec]. It was assumed that during turning there was no slip or skid at the foot/ soil interface.

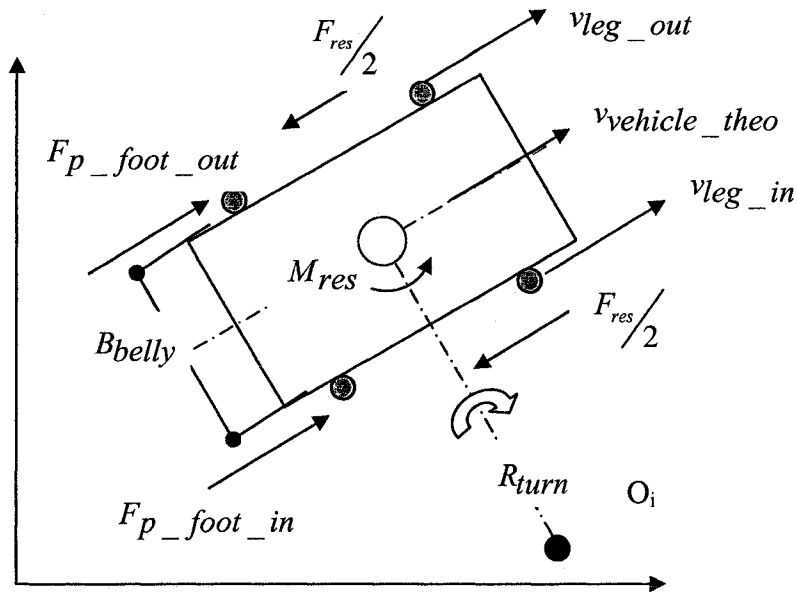


Figure 3. 25 Principle of skid steering for the legged vehicle

The turning behavior of the designed legged vehicle using skid-steering depends on the step sizes of the outer and inner legs, (x_{step_out}) [m] and (x_{step_in}) [m], the resultant resisting force

(F_{res}) [kN], the moment of turning resistance (M_{res}) [kN-m] exerted on the feet by the ground and the vehicle design parameters e.g. width of the vehicle $(B_{vehicle})$ [m], dimensions of the foot, and linear velocities of the outer and inner legs, (v_{leg_out}) [m/sec] and (v_{leg_in}) [m/sec] respectively.

For a small turning angle and with a greater turning radius, the outer and inner step sizes, $x_{step_out} = L_{e_out} * \Omega_{leg_out} * t$ [m] and $x_{step_in} = L_{e_in} * \Omega_{leg_in} * t$ [m] may be assumed to be straight lines (Figure 3.24 and 3.26), where L_{e_out} [m] and L_{e_in} [m] are the effective leg lengths of the outer and inner legs respectively.

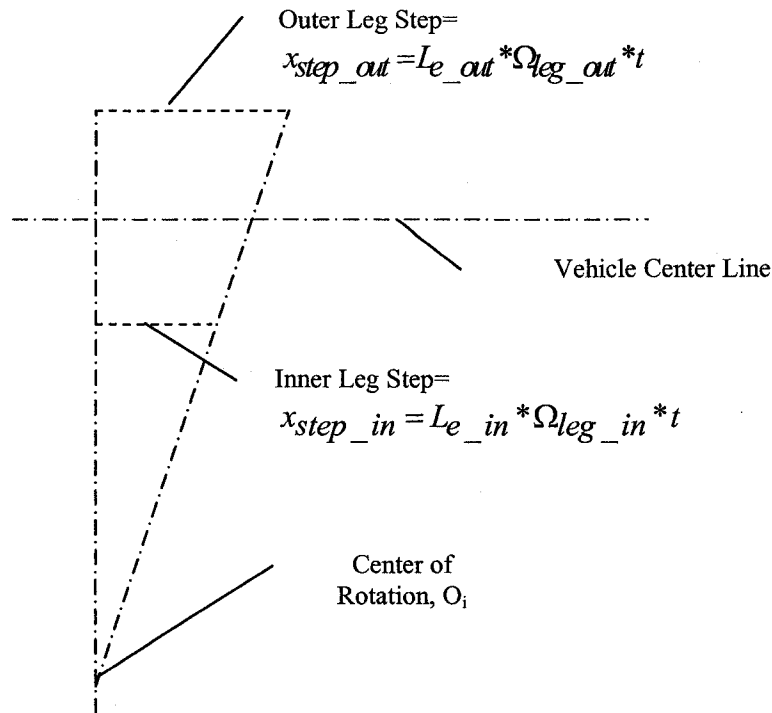


Figure 3. 26 Step sizes for inner and outer legs for curvilinear locomotion

If the feet do not slip (or skid), the turning radius (R_{turn}) [m] and the yaw velocity of the vehicle $(\Omega_{vehicle})$ [rad/sec] are deduced,

$$R_{turn} = \frac{B_{vehicle} \left(L_{e_out} \Omega_{leg_out} + L_{e_in} \Omega_{leg_in} \right)}{2 \left(L_{e_out} \Omega_{leg_out} - L_{e_in} \Omega_{leg_in} \right)} \quad [\text{Equation 3.8}]$$

When $L_{e_out} = L_{e_in}$, Equation 3.8 is modified,

$$R_{turn} = \frac{B_{vehicle} (K_{leg} + 1)}{2 (K_{leg} - 1)} \quad [\text{Equation 3.9}]$$

where, $K_{leg} [-]$ is the ratio of the angular velocities of the outer and inner legs. In level and relatively flat terrain, $L_{e_out} \neq L_{e_in}$, since the swing angles of the outer and inner legs are different. The perpendicular distance between the leg swing pin centre and the foot hinge pin centre (L_o) [m] is however equal for all the legs in level and relatively flat terrain. In sloped or uneven terrain, the effective lengths of the outer and inner legs are equal when the following condition is satisfied,

$$\frac{L_{o_in}}{L_{o_out}} = \frac{\cos(\gamma_{leg_intl_in})}{\cos(\gamma_{leg_intl_out})} \quad [\text{Equation 3.10}]$$

The yawing velocity of the vehicle is deduced as,

$$\Omega_{vehicle} = \frac{L_{e_out} \Omega_{leg_out} + L_{e_in} \Omega_{leg_in}}{2R_{turn}} \quad [\text{Equation 3.11}]$$

When $L_{e_out} = L_{e_in}$, the yawing velocity is obtained,

$$\Omega_{vehicle} = \frac{L_{e_out} \Omega_{leg_in} (K_{leg} - 1)}{B_{vehicle}} \quad [\text{Equation 3.12}]$$

The no slip or skid conditions are ideal conditions. In reality, slip and skid at the foot/ soil interface will be common. Slip occurs when there is a swing velocity of the leg and the foot slips

over the ground in a direction opposite to vehicle motion, but the swing pin centre does not move.

The slips at the inner and outer feet/ soil interface are defined,

$$i_{in} = \left(1 - \frac{v}{L_{e_in} \Omega_{leg_in}} \right) * 100\%$$

[Equation 3.13]

$$or, i_{out} = \left(1 - \frac{v}{L_{e_out} \Omega_{leg_out}} \right) * 100\%$$

where, v is the actual linear velocity of the vehicle body frame at the swing pin for the respective leg [m/sec]. The terms $L_{e_in} \Omega_{leg_in}$ and $L_{e_out} \Omega_{leg_out}$ represent the theoretical linear velocities of the inner and outer legs respectively [m/sec].

Skid occurs when there is no swing velocity of the leg, but the swing pin centre moves along with the leg and the foot in the direction of the vehicle motion. The skids for the inner and outer legs are given in equation 3.14.

$$i_{in} = \left(1 - \frac{L_{e_in} \Omega_{leg_in}}{v} \right) * 100\%$$

[Equation 3.14]

$$or, i_{out} = \left(1 - \frac{L_{e_out} \Omega_{leg_out}}{v} \right) * 100\%$$

The definitions of slip and skid are schematically shown in Figure 3.27.

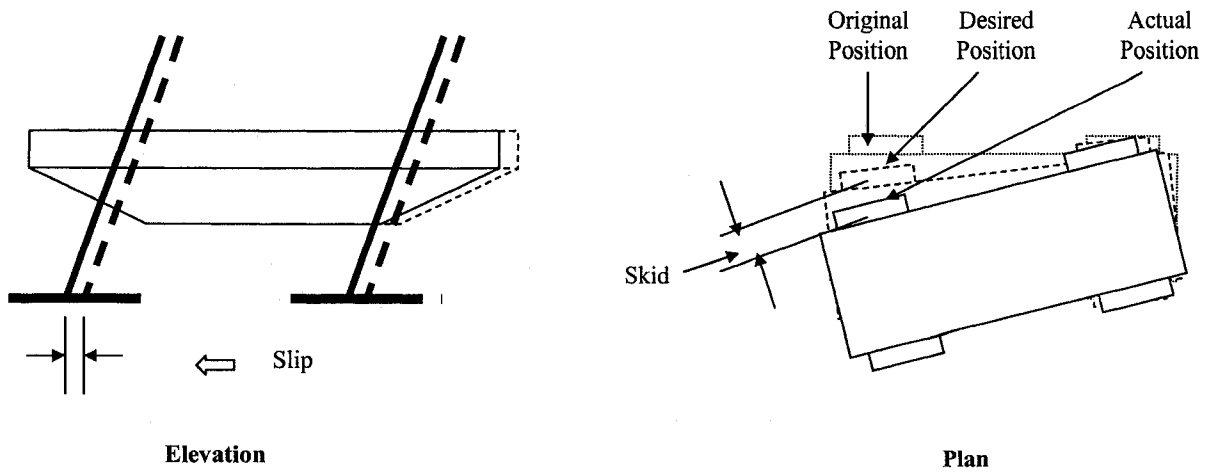


Figure 3.27 Definitions of slip and skid

In case of a tracked vehicle during a turning maneuver, an appropriate thrust or braking force is applied to the track. As a result the track will either slip or skid, depending on whether a forward thrust or a braking force is applied [Wong, 1993]. The outside track always develops a forward thrust and therefore slips [Wong, 1993]. The inside track may develop a forward thrust or a braking force depending on the magnitude of the turning resistance moment, the total resisting force, and the dimensions of the vehicle and tracks [Wong, 1993]. Unlike tracked vehicles, the slipping or skidding may occur at any of the four feet of the designed legged vehicle depending on whether the leg has a swing velocity or not. Since the main body frame of the vehicle is rigid and the inner legs have equal swing angles during turning, the inner legs were assumed to have equal slip or skid. The same assumption was made for the outer legs. The modified turning radius R'_{turn} [m] and the modified yawing velocity $\Omega'_{vehicle}$ [rad/sec], when the slip or skid at the foot/ soil interface is taken into consideration are given below,

$$R'_{turn} = \frac{B_{vehicle} * [L_{e_out} \Omega_{leg_out} (1 - i_{out}) + L_{e_in} \Omega_{leg_in} (1 - i_{in})]}{2 [L_{e_out} \Omega_{leg_out} (1 - i_{out}) - L_{e_in} \Omega_{leg_in} (1 - i_{in})]} \quad [\text{Equation 3.15}]$$

$$\Omega'_{vehicle} = \frac{[L_{e_out}\Omega_{leg_out}(1-i_{out}) + L_{e_in}\Omega_{leg_in}(1-i_{in})]}{2R'_{turn}} \quad [\text{Equation 3.16}]$$

With $L_{e_out} = L_{e_in}$, the modified turning radius and the modified yawing velocity are given in the next two equations,

$$R'_{turn} = \frac{B_{vehicle} * [K_{leg}(1-i_{out}) + (1-i_{in})]}{2[K_{leg}(1-i_{out}) - (1-i_{in})]} \quad [\text{Equation 3.17}]$$

$$\Omega'_{vehicle} = \frac{L_{e_out}\Omega_{leg_in}[K_{leg}(1-i_{out}) - (1-i_{in})]}{B_{vehicle}} \quad [\text{Equation 3.18}]$$

where i_{out} and i_{in} are the slip (or skid) of the outer and inner legs respectively.

The relationship between the turning angle (γ_{turn}) of the vehicle [degree], the turning radius (R_{turn}) [m] and the step size (x_{step}) for any point on the vehicle [m] is given in Equation 3.19 (Figure 3.24).

$$x_{step} = 2 * R_{turn} * \sin\left(\frac{\gamma_{turn}}{2}\right) \quad [\text{Equation 3.19}]$$

3.3.3 Experimental and Predicted Results for Curvilinear Locomotion

The test matrices and the experimental and predicted data for the curvilinear locomotion tests are given in Appendix 7. The comparisons between the experimental and predicted results with unequal outer and inner leg swing angles are presented first. The different positions of the vehicle during successive locomotion cycles were drawn on an AutoCAD drawing (Figure 3.28). The points in the figure represent the positions of the instantaneous centers of rotation. The final heading was achieved by turning the vehicle through successive small angles. The definition of instantaneous centre of rotation is shown in Figure 3.24.

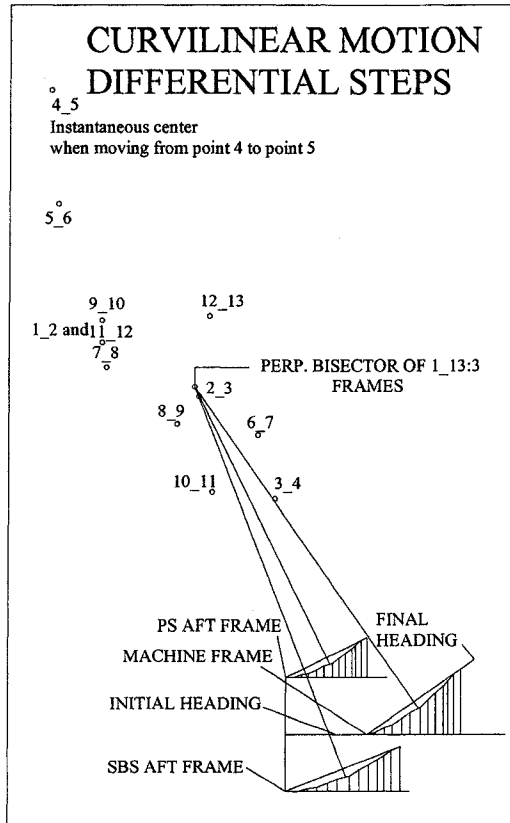


Figure 3. 28 Vehicle trajectory for curvilinear locomotion on flat terrain with unequal swing angles of outer and inner legs

The experimental turning radii, turning angle and the step size of the assumed centre of gravity, PS_AFT and SBS_AFT corners were measured from the AutoCAD drawing. The procedure is discussed in Appendix 7. The step size for given experimental turning radius and turning angle was predicted by using Equation 3.19. This is the predicted step size.

The comparisons between the experimental and predicted step sizes for a given turning radius and turning angle are shown in Figure 3.29. The deviations between the predicted and experimental step size results for the PS_AFT and SBS_AFT legs are shown in Figure 3.30 and 3.31. The deviation was the predicted value minus the experimental value.

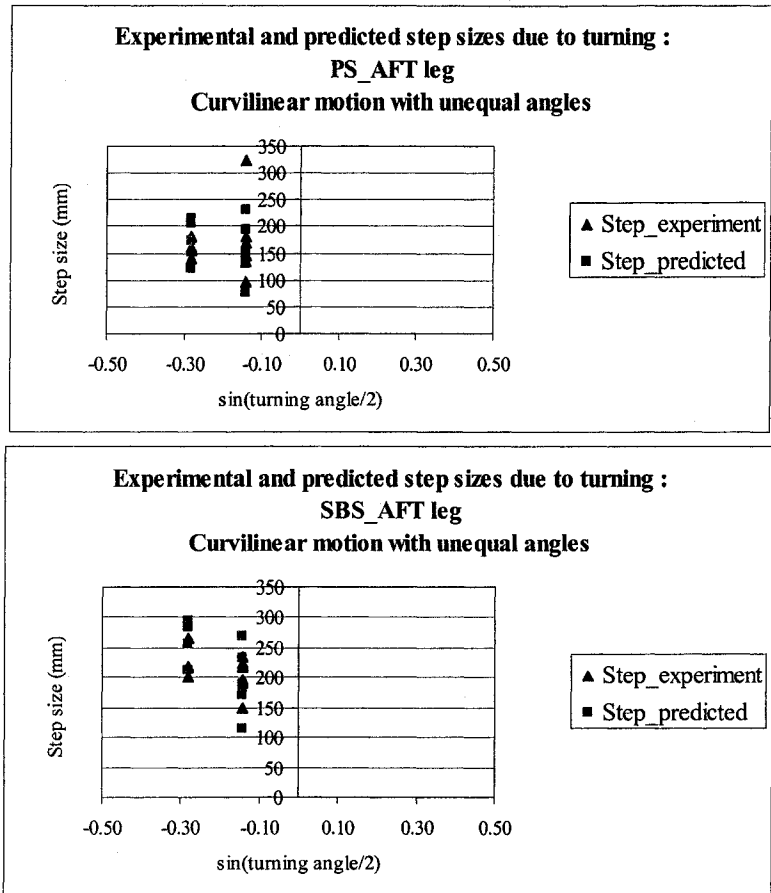


Figure 3. 29 Experimental and predicted step size vs. turning angle of vehicle for curvilinear locomotion with unequal angles (AFT legs)

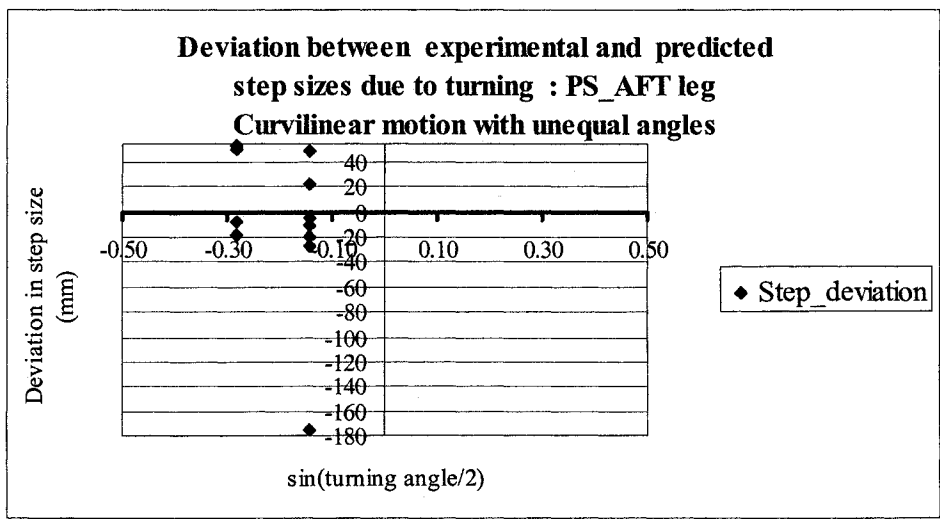


Figure 3. 30 Deviation between predicted and experimental step size value for curvilinear locomotion with unequal angles (PS_AFT leg)

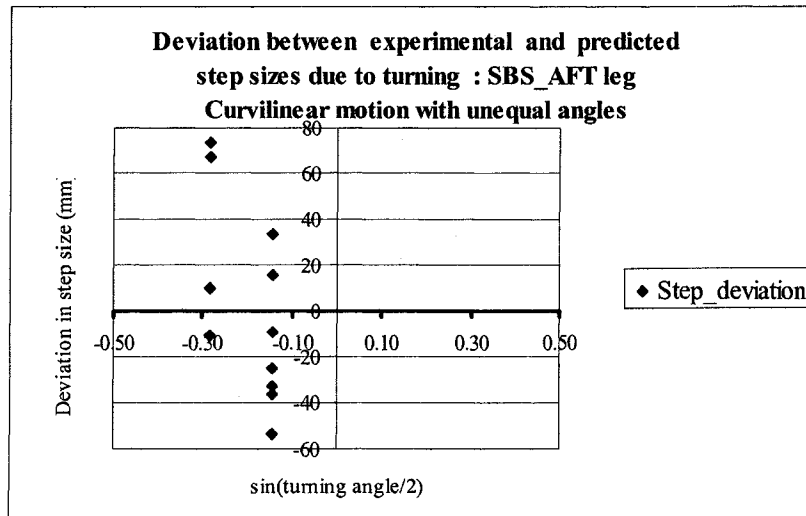


Figure 3. 31 Deviation between predicted and experimental step size value for curvilinear locomotion with unequal angles (SBS_AFT leg)

The turning angles measured were either 1 degree or 2 degrees, while the turning radii varied from approximately 3.5 m to 13 m. Since the step size and the deviation were plotted against the $\sin\left(\frac{\text{turning angle}}{2}\right)$, the data points are parallel to the Y axis in Figures 3.29, 3.30 and 3.31.

The experimental and predicted step sizes of the assumed centre of gravity of the vehicle were plotted against the turning radii of the vehicle (Figure 3.32). The deviations between the predicted and experimental step sizes for the assumed centre of gravity of the vehicle are shown in Figure 3.33.

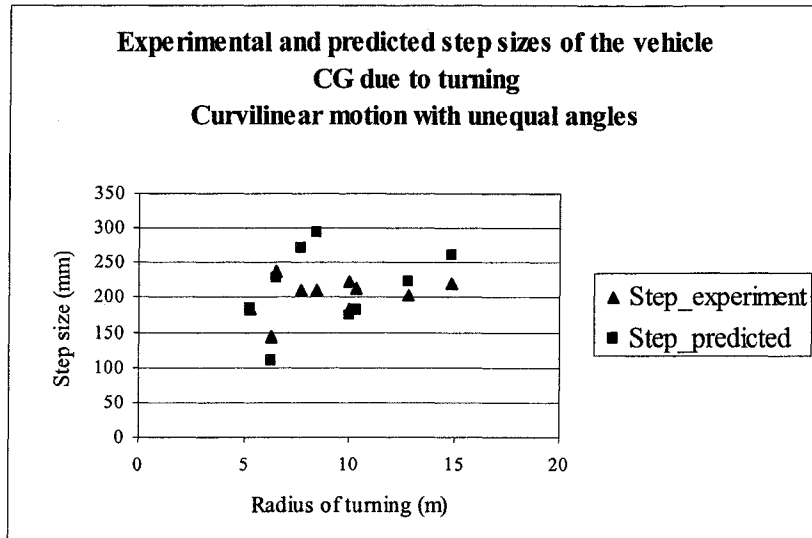


Figure 3. 32 Experimental and predicted step size of the vehicle centre of gravity vs. turning radius of vehicle for curvilinear locomotion with unequal angles

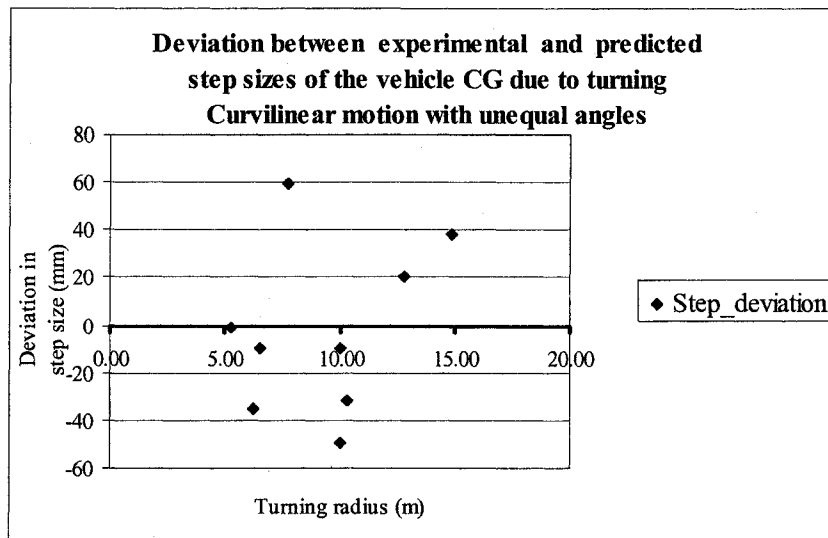


Figure 3. 33 Deviation between predicted and experimental step size of the vehicle centre of gravity for curvilinear locomotion with unequal angles

Figure 3.32 shows the predicted step sizes lay along two distinct curves. This is because the turning angle of the assumed centre of gravity of the vehicle was either 1 degree or 2 degrees during all the successive locomotion cycles, while the turning radius varied.

It is observed from Figure 3.30, the experimental and predicted step sizes for the PS_AFT leg, are relatively close to each other. Most of the deviations are within 0 to (-) 20 mm. The SBS_AFT leg shows both positive and negative deviations and most of the deviations vary between (+) 40 to (-) 40 mm. The PS_AFT leg was thus exhibiting a minor amount of skidding during turning. Since the PS legs were the inner legs during turning, skidding action can occur. The SBS leg showing both over predicted and under predicted step sizes must be exhibiting slip as well as skid at the foot/ soil interfaces during turning.

It is observed from Figure 3.33, that most of the deviations for the assumed centre of gravity of the vehicle are negative and vary from 0 to (-) 40 mm. The minimum, maximum and average values of the experimental and predicted step sizes and the deviations are presented in Table 3.5. It is observed that the step sizes of the assumed centre of gravity of the vehicle are closer to the SBS_AFT leg.

Table 3.5 Representative values of step size and deviation for curvilinear locomotion with unequal angles

Step size (mm)						
Values	PS_AFT		SBS_AFT		Machine_CG	
	Experimental	Predicted	Experimental	Predicted	Experimental	Predicted
Minimum	95	75.5	150	113	144	109
Maximum	325	230	265	293	238	293
Average	169	147	214	215	204	191
Deviation (mm / percentage)						
Values	PS_AFT		SBS_AFT		Machine_CG	
	Experimental		Experimental		Experimental	
Minimum	- 176/ - 54		-53/ -24		- 49 / - 22	
Maximum	53/ 33		73 / 33		82/ 39	
Average	-22/ - 9.5		3 / 0.6		6 / 2	

The deviations between the experimental and predicted step sizes are due to 1) manual operation of the electronic switches actuating the solenoids of the directional control valves operating the hydraulic actuators, 2) slip or skid at the foot/ soil interface, and 3) absence of oil flow control system in the designed hydraulic circuits.

Due to manual operation, it was extremely difficult to control the final swing angles of the legs. Sometimes one or more leg was still swinging while the others stopped their movements. The manual operation posed problems in accurately following the theoretical gait plans developed and as a result the vehicle exhibited fairly complex turning behaviors. This resulted in unusual slip or skid actions at the foot/ soil interfaces too. As long as there is a leg swing velocity, the respective foot has a tendency to slip. When there is no swing velocity of the inner legs, the inner feet have tendencies to both slip and skid. This occurs when the inner legs have stopped swinging and the outer legs still exhibit swinging motion. Due to the absence of a flow control system in the hydraulic circuits and unequal leg swing angles of the inner and outer legs, these phenomena will occur frequently leading to deviations between experimental and predicted results. With the present experimental set up, the deviations between the experimental and predicted values are unavoidable but the results do show the general performance of the vehicle.

The turning radius was predicted by using Equation 3.8, where slip or skid at the foot/ soil interface was neglected. The predicted turning radius was compared with the experimental turning radius measured from the AutoCAD drawing (Figure 3.28). The comparisons are shown in Figure 3.34. No correspondence is observed between experimental and predicted results. The reasons discussed above for the deviations between the experimental and predicted step sizes are also applicable for the turning radii.

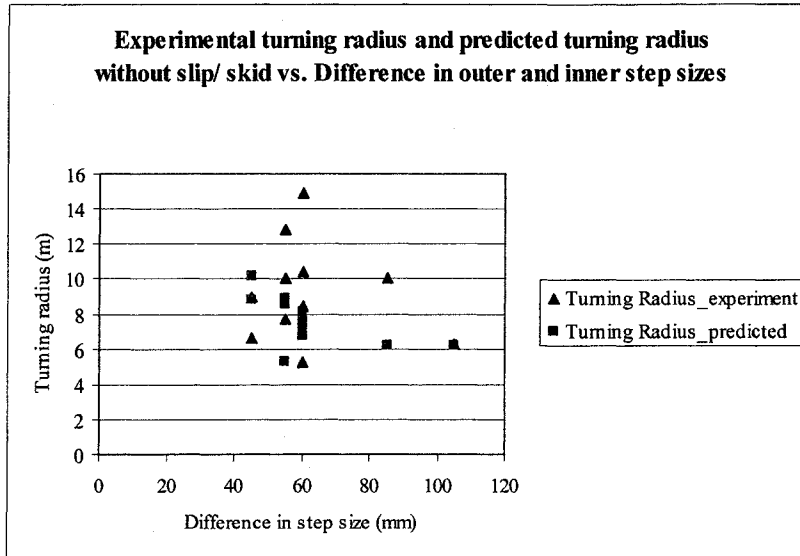


Figure 3. 34 Experimental turning radius and predicted turning radius without slip/ skid at the foot/ soil interface

The turning angle of the vehicle was predicted by using Equation 3.11, which neglects the effect of slip/ skid at the foot/ soil interface. The comparison between the experimental and predicted turning angles of the vehicle is shown in Figure 3.35.

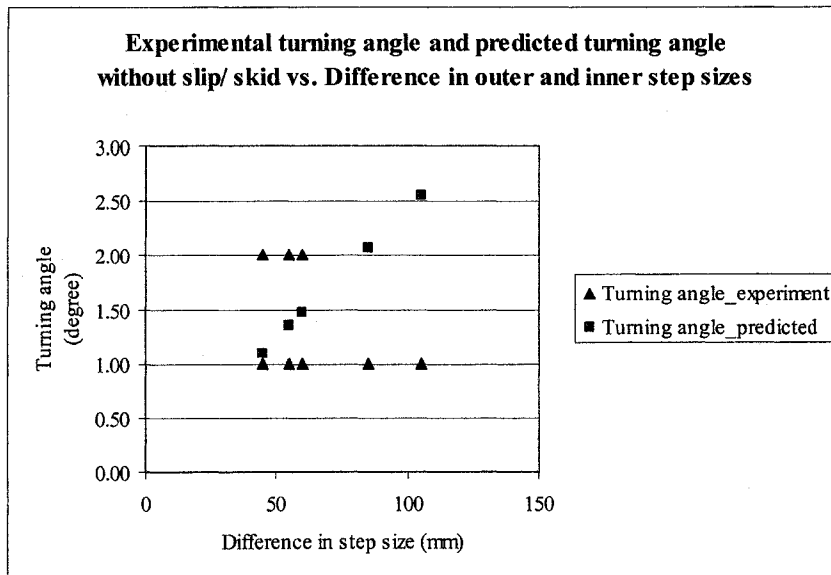


Figure 3. 35 Experimental turning angle and predicted turning angle without slip/ skid at the foot/ soil interface

The vehicle turning angles were very small and hence the deviation observed was also of the order of 0.5 degree. Such deviations can be neglected under the given experimental set up and measuring techniques used.

The modified turning radius and turning angle were predicted by using Equations 3.15 and 3.16. It was assumed that only slipping action was occurring at the foot/ soil interfaces. When skid occurs i_{out} and i_{in} will be negative in Equations 3.15 and 3.16. Two different scenarios were considered for predicting the modified turning radii and the modified turning angles with slip conditions 1) slip of the outer legs is > slip of the inner legs, and 2) slip of the inner legs is > slip of the outer legs. Figure 3.36 and 3.37 show the comparisons between the experimental and predicted values of the turning radius and turning angle for different slip conditions.

The different series shown in Figure 3.36 and 3.37 are explained in Table 3.6. The slip values in Table 3.6 were based on the step size results for straight line locomotion (Figure 3.12 and Figure 3.21).

Table 3. 6 Different series of Figure 3.36 and Figure 3.37

Inner slip < Outer slip		
Series	Inner slip/ skid (-)	Outer slip/ skid (-)
Series 1	0.1	0.2
Series 2	0.1	0.3
Series 3	0.2	0.3
Series 4	0.1	0.3
Inner slip > Outer slip		
Series	Inner slip/ skid (-)	Outer slip/ skid (-)
Series 1	0.3	0.1
Series 2	0.3	0.2
Series 3	0.4	0.2
Series 4	0.2	0.1

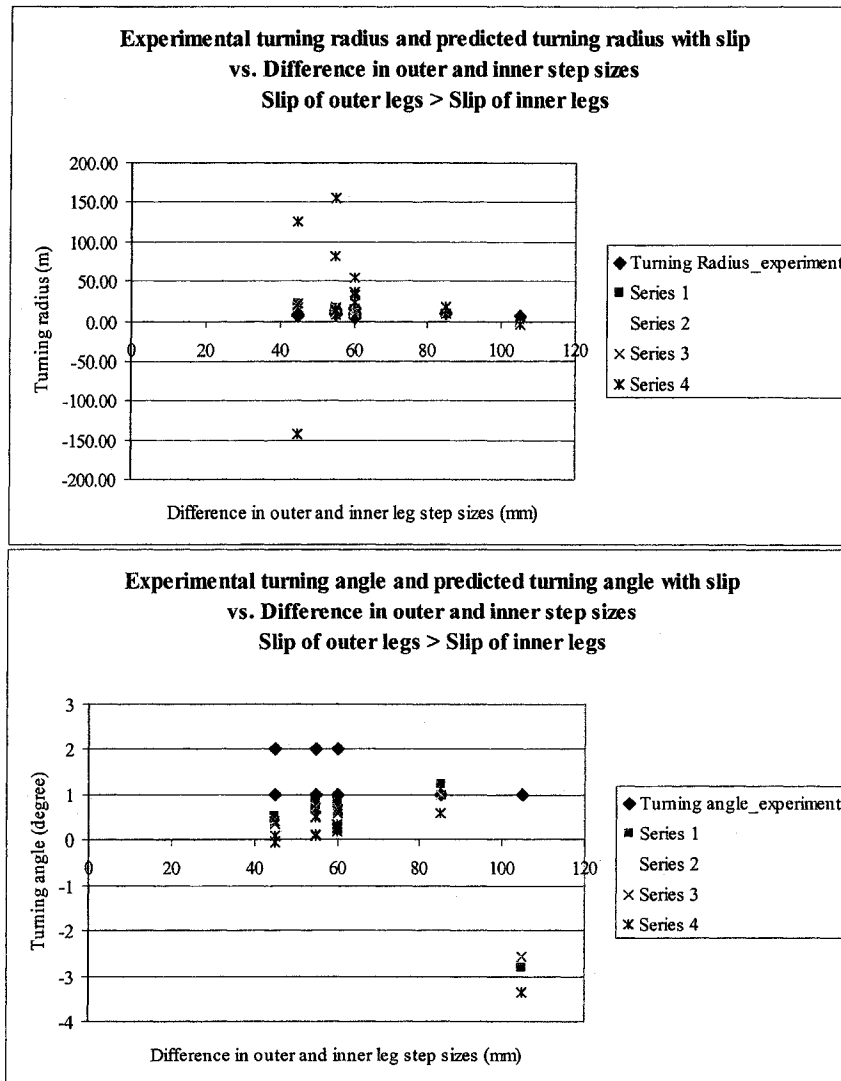


Figure 3.36 Experimental and predicted values of turning radii and turning angles with slip (slip of outer legs is > slip of inner legs)

Figure 3.36 shows that the experimental values are close to the predicted values represented by Series 1 and Series 3. Good matching of experimental and predicted values of the turning radii and turning angles was not obtained for the cases where slip of inner legs was > slip of outer legs (Figure 3.37).

It was possible to calculate the slip or skid percentages occurring at the different foot/ soil interfaces from the measured positions of the vehicle for the straight line locomotion tests. This is presented in section 3.2.2. The vehicle exhibited very complex turning behavior during the

curvilinear tests due to manual operation of the electronic switches actuating the solenoids of the DC valves of the hydraulic cylinders. Hence, it was not possible to assess the slip or skid percentages during the curvilinear tests from the vehicle positions.

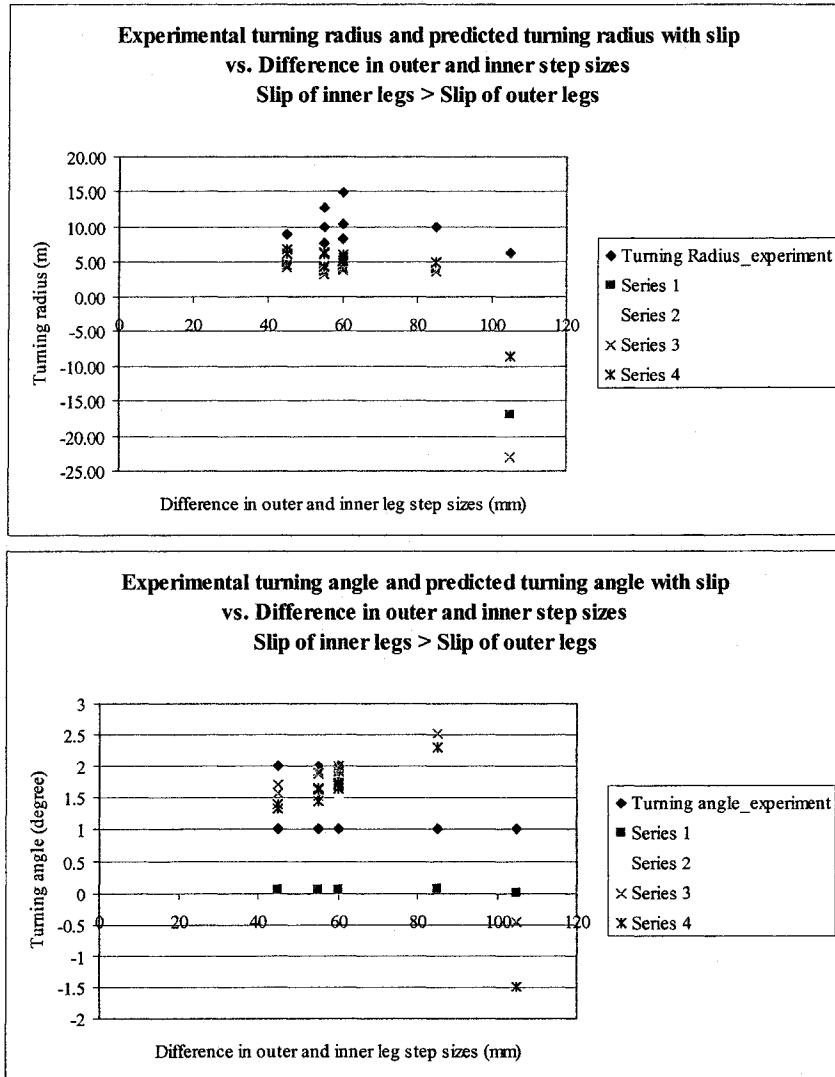


Figure 3. 37 Experimental and predicted values of turning radii and turning angles with slip (slip of inner legs > slip of outer legs)

The vehicle trajectory for curvilinear locomotion with inner legs fixed is shown in Figure 3.38.

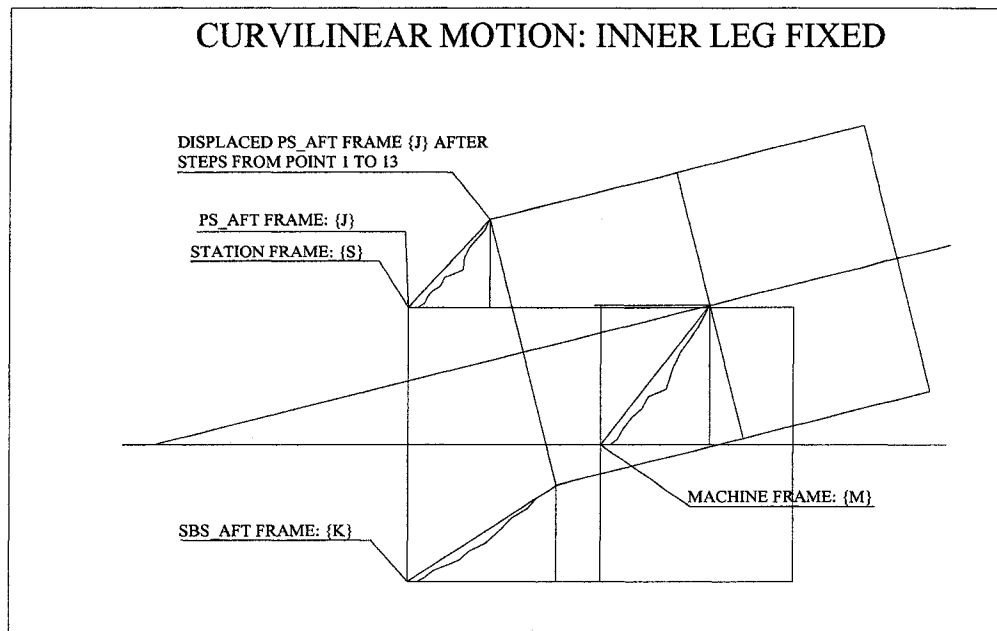


Figure 3. 38 Vehicle trajectory for curvilinear locomotion on flat terrain with inner legs fixed

The experimental step sizes of the different legs for the curvilinear locomotion with inner legs fixed are shown in Figure 3.39. The PS legs were the inner legs with zero swing angles. Hence the data points for the PS legs clustered on the Y axis. This figure gives an idea of the magnitude of the step sizes achieved for the given set of test. The PS_FWD leg has the lowest step size. Theoretically, the step sizes of the inner legs should be zero, but due to slip and skid, the inner legs exhibited minor movements. During the execution of the test, the final swing angle of the SBS_AFT leg always became more due to the operational error. Human operational error crept in during this set of tests, but the tests proved that it is possible to turn the vehicle by keeping the inner angles fixed.

It is easier to control curvilinear locomotion with the inner legs fixed as only two legs are operated at a time. But the magnitude of slip or skid at the inner foot/ soil interface will be much

higher since the inner legs are always fixed. Higher stresses in the legs, feet and soil might also be generated as a result of this type of movement.

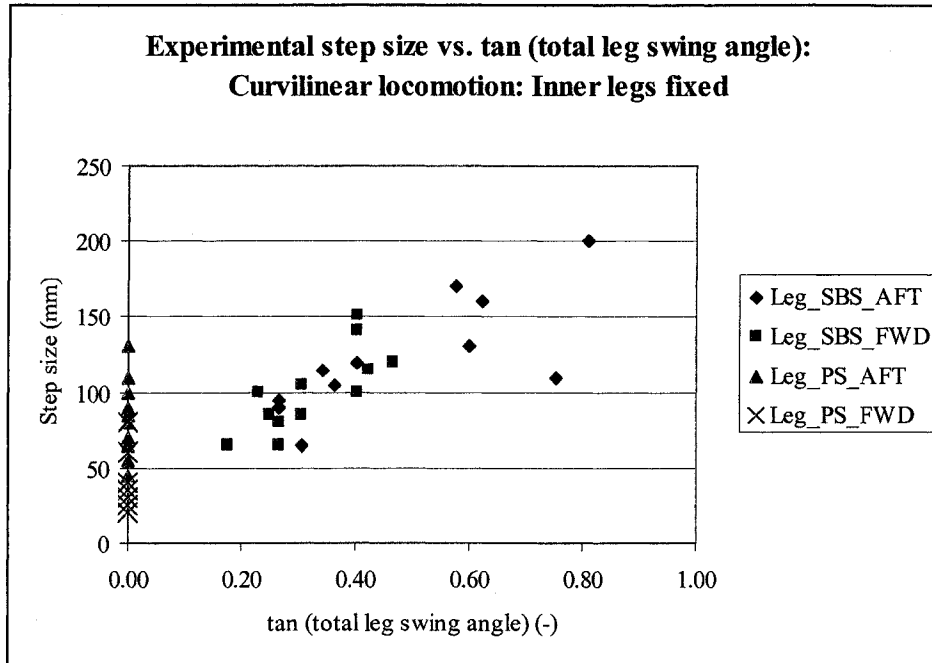


Figure 3.39 Experimental step sizes for curvilinear locomotion with inner legs fixed

The magnitude of the slip generated at the foot/ soil interface determines the tractive force available for the vehicle movement, which are further discussed in section 3.6.1, 3.6.2 and 3.6.3.

The theoretical turning radius of the vehicle was plotted against 1) the ratio between the step sizes of the outer and inner legs, and 2) the ratio between the angular velocities of the outer and inner legs for different inner leg step sizes (Figure 3.40). The slip or skid at the foot/ soil interface was neglected. The perpendicular distance between the leg swing pin centre and the foot hinge pin centre (L_o) was assumed to be 340 mm. The skidding of the belly was not included in these analyses, since during the curvilinear tests the belly was not in contact with the soil.

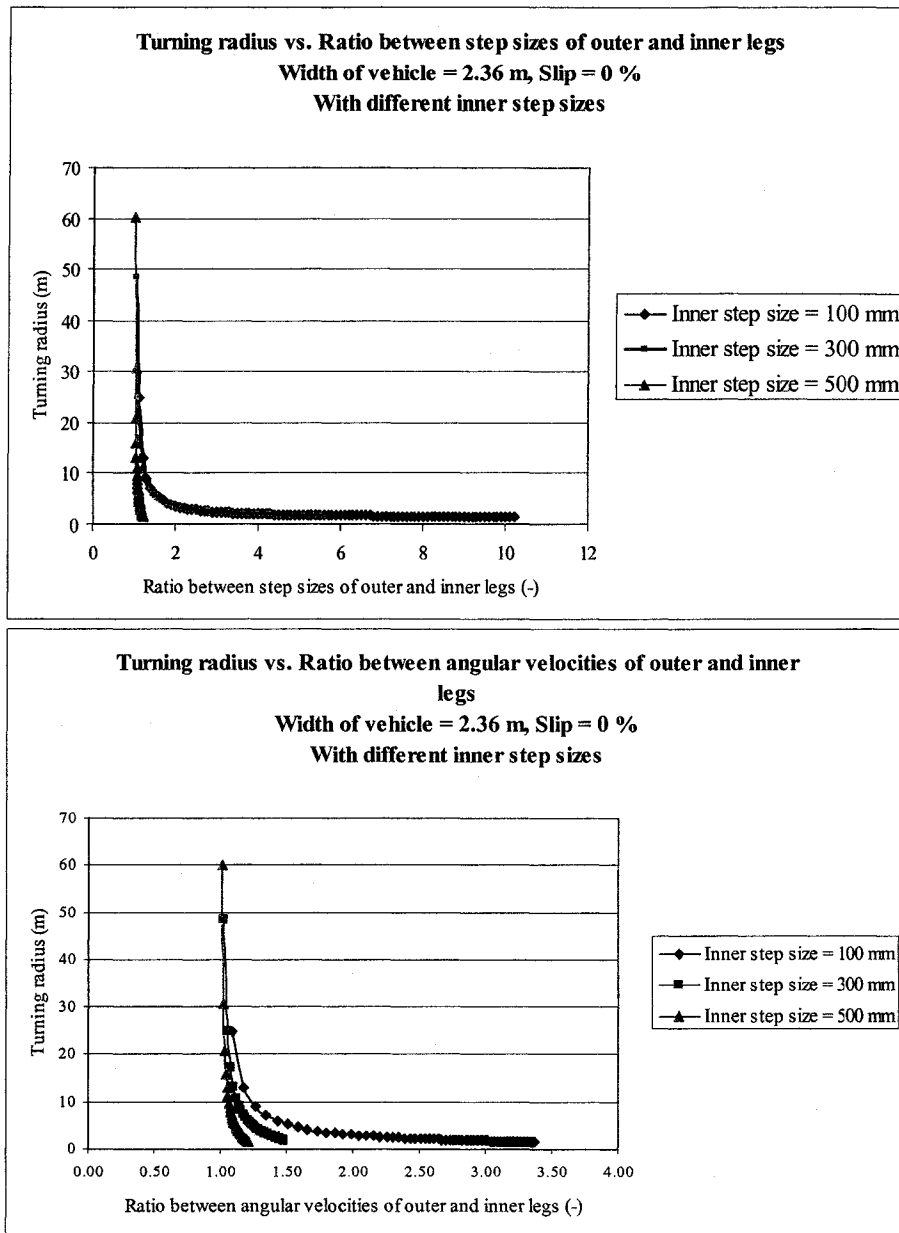


Figure 3. 40 Predicted turning behavior under no slip condition

It is observed from Figure 3.40, the turning radius becomes almost constant after attaining a particular value of the ratio between step sizes or angular velocities between outer and inner legs. With increase in the step size of the inner leg, the value of this particular ratio decreases. The ratio between the step sizes of the outer and inner legs should be varied from 1 to 2, beyond which the turning radius attains a constant value. The ratio between the angular velocities of the

outer and inner legs must be varied from 1 to 1.75. The inner leg step size was varied from 100 to 500 mm.

The turning angle of the vehicle under no slip conditions was plotted against the ratio of the step sizes and angular velocities of the outer and inner legs (Figure 3.41 and 3.42). The perpendicular distance between the leg swing pin centre and the foot hinge pin centre L_O was kept at 340 mm.

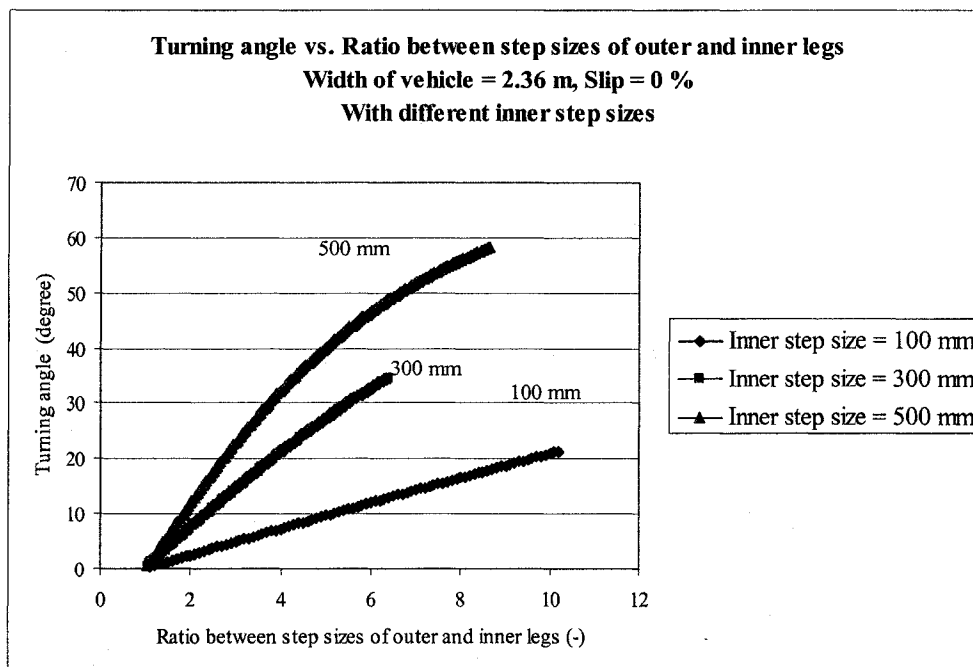


Figure 3.41 Predicted turning angle under no slip condition vs. ratio between step sizes of outer and inner legs

The ratio between the angular velocities of the outer and inner legs can be varied over a range to obtain different turning angles with lower values of inner leg step size. The turning angle changes very rapidly with a minor change in the ratio between the angular velocities when the inner leg step size is increased.

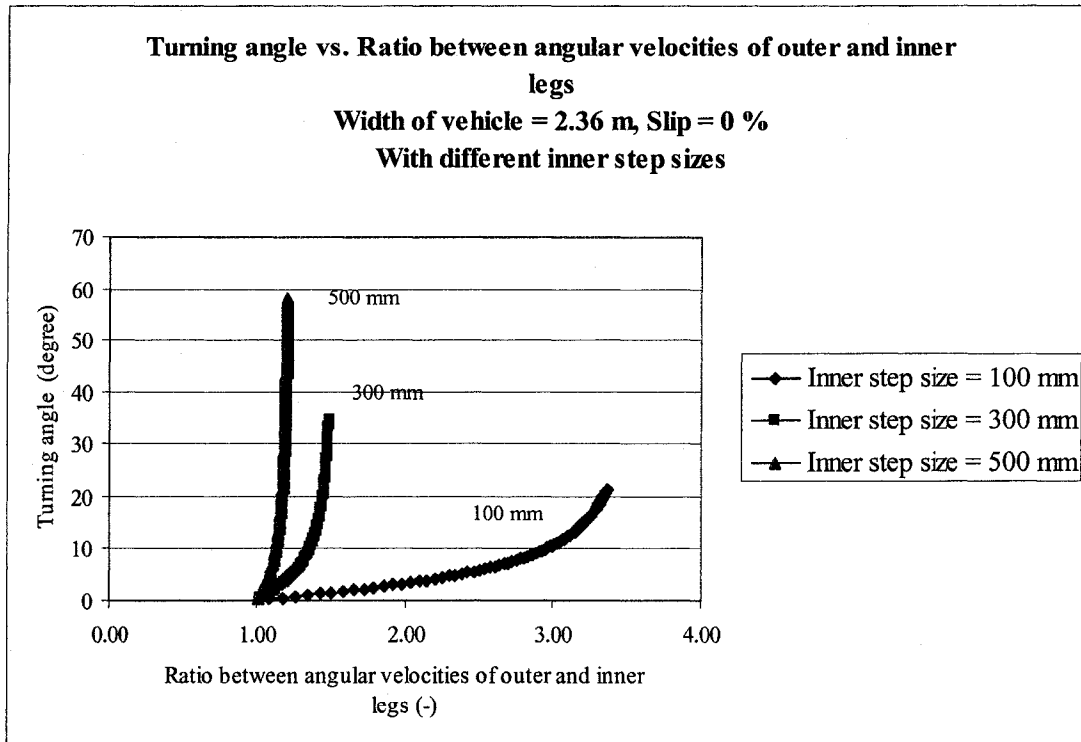


Figure 3. 42 Predicted turning angle under no slip condition vs. ratio between angular velocities of outer and inner legs

The turning behavior of the vehicle was predicted with slip occurring at both the outer and inner feet/ soil interfaces. The step size of the inner leg was considered to be equal to 100 mm, while the step size of the outer leg was varied from 110 to 1020 mm with an increment of 10 mm. The perpendicular distance between the leg swing pin centre and the foot hinge pin centre L_o was kept at 340 mm. The slip of the inner leg was considered to be 10 %, while the slip of the outer leg was varied from 20 to 50 % with an increment of 10 %. The different series in Figure 3.43 represent the difference between the outer and the inner slip percentages. It was observed from Figure 3.36, that a good match existed between the experimental results and the predicted results with the slip of outer legs being $>$ the slip of inner legs. Hence only this condition was considered for the following predicted results shown in Figure 3.43.

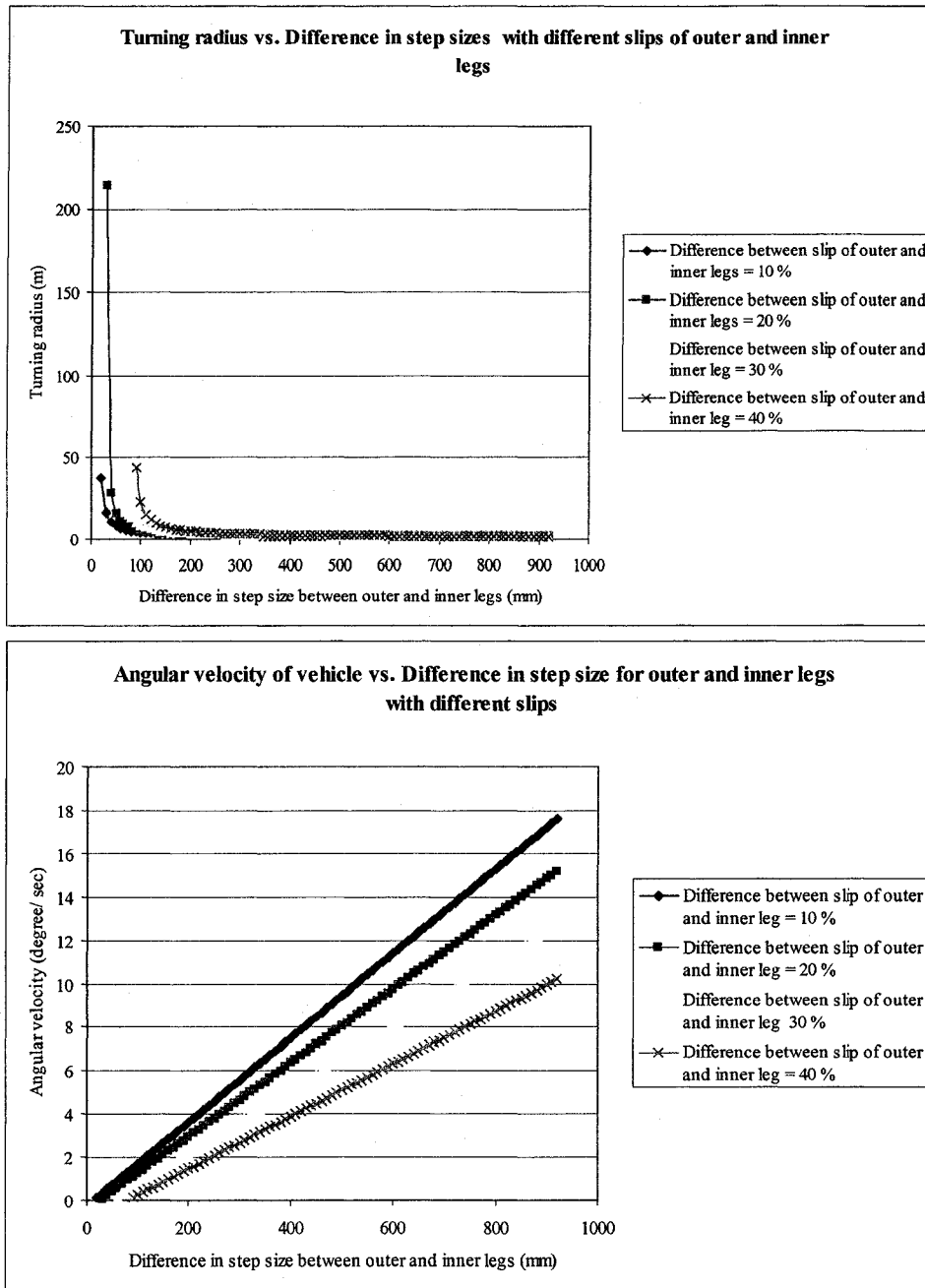


Figure 3. 43 Predicted turning behavior of the designed vehicle with slip

To achieve the same turning radius, with increase in slip difference between the outer and inner legs, the difference between the outer and inner step sizes needs to be increased also. With the same difference in step size, the angular velocity of the vehicle decreases with the increase in the difference in the slip percent between the outer and the inner legs.

Uncertainty analyses for the gait planning tests were performed, which are presented in Appendix 8. The following results were obtained from such analyses.

For forward straight line locomotion the confidence limit for the calculated step sizes of the portside after leg is 10.07 mm with 95 % confidence level and 11 samples. The confidence limit for the experimental step sizes for the portside after leg is 32 mm with 95 % confidence level and 14 samples. The mean experimental step size for the portside after leg was found to be 226 mm. The confidence limit indicates that the mean step size will be 226 ± 32 mm with a 95 % confidence level. The confidence limit for the calculated step sizes for the portside forward leg is 5 mm with 95 % confidence level and 11 samples. The confidence limit for the calculated step sizes for the starboard side after leg is 11.3 mm with 95 % confidence level and 10 samples. The confidence limit for the experimental step sizes for the starboard side after leg is 35.9 mm with 95 % confidence level and 14 samples. The mean experimental step size for the starboard side after leg was 237.5 mm. The confidence limit for the calculated step sizes for the starboard side forward leg is 6.7 mm with 95 % confidence level and 10 samples. The experimental step sizes of the forward legs were determined from the machine geometry and the experimental step sizes measured for the after legs. Hence the experimental step sizes of the portside after and portside forward and that for the starboard side after and starboard side forward were equal.

In case of backward straight line locomotion, the confidence limit for the calculated step sizes of the portside after leg is 35.8 mm with 95 % confidence level and 5 samples. The confidence limit for the experimental step sizes for the portside after leg is 44.1 mm with 95 % confidence level and 6 samples. The mean experimental step size for the portside after leg was found to be 191.6 mm. The confidence limit for the calculated step sizes for the portside forward leg is 88.7 mm with 95 % confidence level and 3 samples. The confidence limit for the calculated step sizes for

the starboard side after leg is 34.5 mm with 95 % confidence level and 5 samples. The confidence limit for the experimental step sizes for the starboard side after leg is 40.9 mm with 95 % confidence level and 6 samples. The mean experimental step size for the starboard side after leg was 175.8 mm. The confidence limit for the calculated step sizes for the starboard side forward leg is 25.6 mm with 95 % confidence level and 5 samples.

For curvilinear locomotion with unequal angles to the inner and outer legs, the confidence limits for the experimental step sizes of the portside after and starboard side after legs were calculated. The confidence limit for the experimental step sizes for the portside after leg is 29.7 mm with 95 % confidence level and 11 samples. The mean experimental step size for the starboard side after leg was 175.9 mm. The confidence limit for the experimental step sizes for the starboard side after leg is 16.6 mm with 95 % confidence level and 11 samples. The mean experimental step size for the starboard side after leg was 211.8 mm. The confidence limits for the turning radius and turning angle of the assumed centre of gravity of the designed vehicle were also estimated. The confidence limit for the experimental turning radius of the assumed centre of gravity of the prototype vehicle is 1641.7 mm with 95 % confidence level and 11 samples. The mean value of the turning radius was 9211.6 mm. The confidence limit for the experimental turning angle of the assumed centre of gravity of the prototype vehicle is 0.29 degree with 95 % confidence level and 11 samples. The mean value of the turning radius was 1.36 degree.

3.4 Locomotion Cycle Time

This section describes the parametric model developed to evaluate the locomotion cycle time for the designed submersible walking vehicle. When the vehicle performs straight line locomotion on level and relatively flat terrain, the locomotion cycle time is identical for all the four legs. The locomotion cycle time however will be different for the four legs, when the vehicle performs

straight line locomotion on uneven terrain or curvilinear locomotion on any terrain. The cycle time of the leg, which takes the maximum time to finish the locomotion cycle will be considered under such circumstances.

The motion of one leg is simulated to predict the locomotion cycle time of the vehicle. The locomotion cycle was divided into four separate sub-cycles of 1) preparatory cycle, 2) motion cycle, 3) idle cycle, and 4) finishing cycle.

The details of the parametric locomotion cycle model are discussed in Appendix 8.

3.4.1 Experimental Results for Locomotion Cycle Time

The different steps followed during the straight line and curvilinear locomotion tests are discussed in Appendix 6 and 7. The experimental data for the locomotion cycle time are presented in Appendix 8. Because of the manual operation of the solenoid actuating the electronic switches of the DC valves, it was possible to measure t_3, t_4 and t_5 [sec], as defined in Appendix 6 and 7. The time required to lower the leg is denoted by t_3 seconds. The legs take t_4 seconds to move through an angle of $(\gamma_{leg_intl} + \gamma_{leg_fnl})$ [degree], where γ_{leg_intl} is the initial is angle of leg swing [degree] and γ_{leg_fnl} is the final angle of leg swing [degree]. The time required to lift the leg is denoted by t_5 seconds. The cycle times t_1 and t_2 were estimated from t_4 and the total angle moved by the leg.

The locomotion cycle time for different legs was plotted for successive locomotion cycles for a particular set of gait planning tests. The results for the forward straight line locomotion are shown in Figure 3.44.

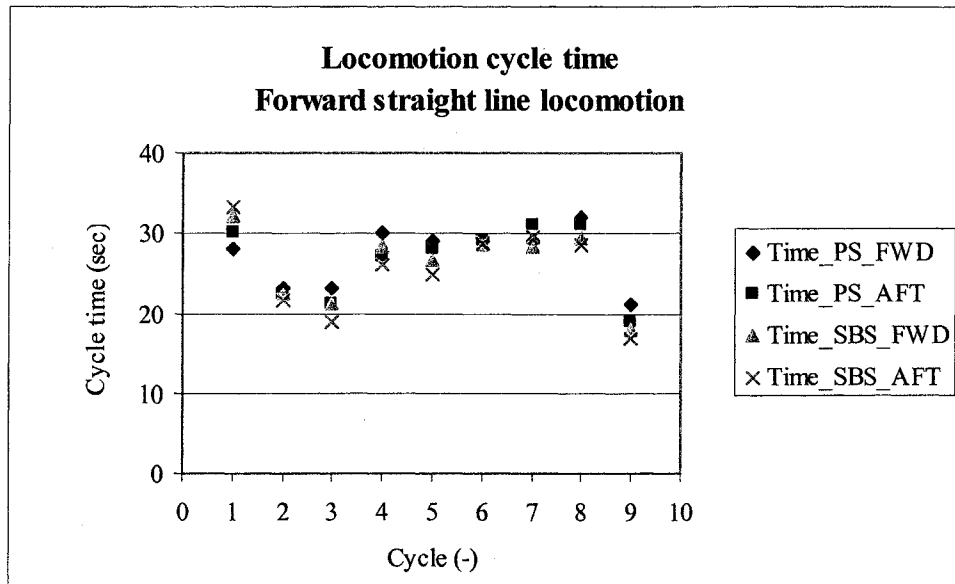


Figure 3. 44 Locomotion cycle time for forward straight line locomotion

The total distance moved by the PS corner during the entire locomotion test (forward straight line) was 2025 mm and that by the SBS corner was 2155 mm. It was thus estimated that the vehicle moved an average distance of 2090 mm during the particular locomotion test. The average speed of the vehicle was calculated from the average distance moved by the vehicle and the average locomotion cycle time. The calculated average speed of the vehicle is approximately 0.01 m/sec which is low compared with other submersible tracked or legged dredgers. The average locomotion cycle time in each test for the AFT legs is greater than that of the FWD legs. This is possibly because of the presence of the ladder assembly.

In general the locomotion cycle time increased with the increase in the step size of the leg. But, it was also observed that the locomotion cycle time increased even for the same step size, or the

locomotion cycle time decreased with the increase in the step size. These discrepancies can be explained due to the manual operation of the electronic switches and slip/ skid at the foot/ soil interface.

The graphical results for backward straight line locomotion are shown in Figure 3.45.

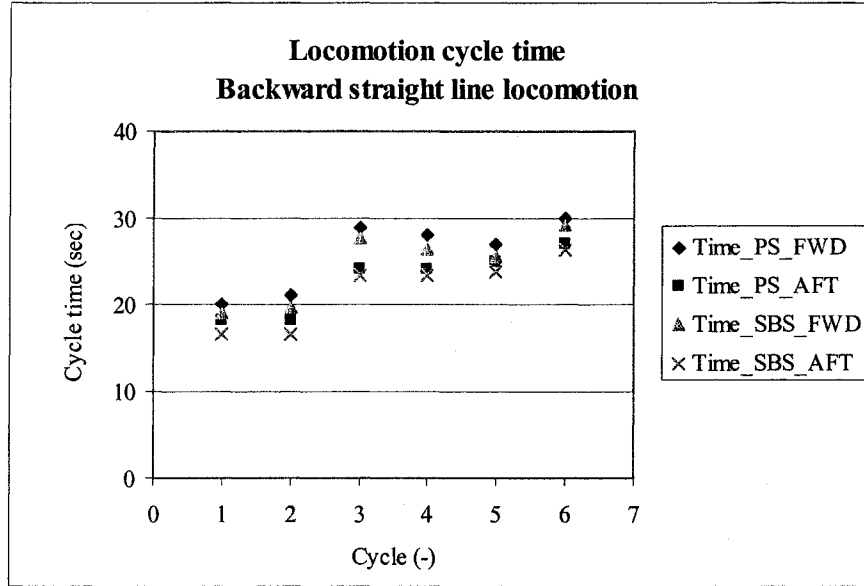


Figure 3. 45 Locomotion cycle time for backward straight line locomotion

The average locomotion cycle time for the FWD legs is higher compared to the AFT legs during backward straight line locomotion. The direction of movement and the presence of the ladder assembly has an influence on the locomotion cycle time of the FWD and AFT legs.

The same trend with the leg swing angle and the locomotion cycle time or with the step size of the leg and the locomotion cycle time was observed in both forward and backward straight line locomotion. The discrepancies can be explained due to the same reasons as was given for the forward straight line locomotion.

The total locomotion cycle times for forward and backward straight line locomotion are given in Table 3.7. The number of steps for backward straight line locomotion tests was less than the number of steps for forward straight line locomotion tests. Hence the total locomotion cycle time for forward test is larger than backward straight line locomotion test.

Table 3.7 Total locomotion cycle time during the entire locomotion test for straight line locomotion

Forward straight line locomotion (sec)				Backward straight line locomotion (sec)			
PS AFT	PS FWD	SBS AFT	SBS FWD	PS AFT	PS FWD	SBS AFT	SBS FWD
238.00	244.00	228.80	234.55	136.00	155.00	130.50	147.40

The graphical results for curvilinear locomotion with inner legs fixed are given in Figure 3.46.

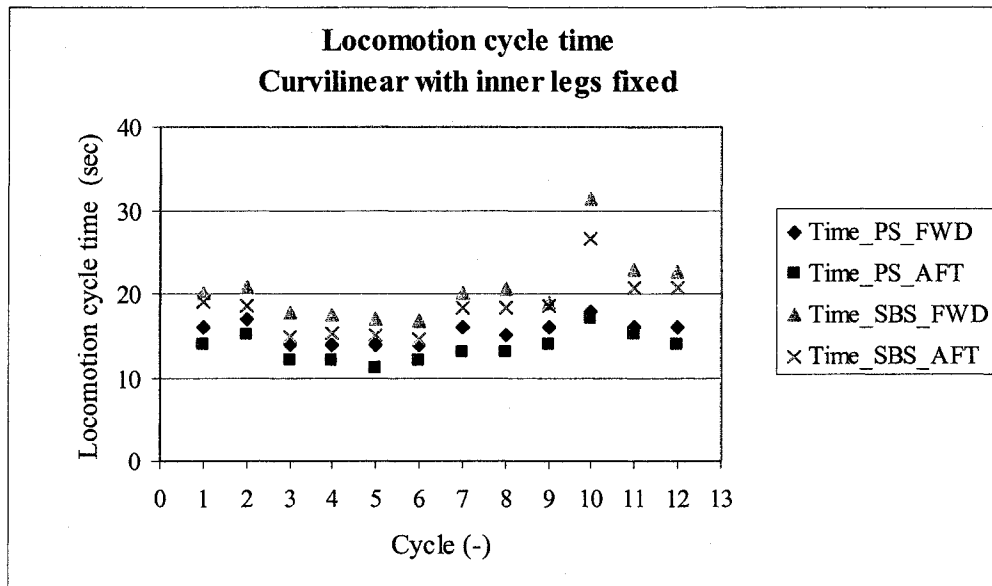


Figure 3.46 Locomotion cycle time for curvilinear locomotion with inner legs fixed

Because of the manual operation, it was difficult to control the final swing angles of the legs. The locomotion cycle time for each cycle is similar for both straight line and curvilinear locomotion.

The graphical results for curvilinear locomotion with unequal inner and outer leg angles are given in Figure 3.47. The locomotion cycle time for curvilinear locomotion with unequal angles was greater than that of curvilinear locomotion with inner legs fixed. The vehicle trajectories for both types of curvilinear locomotion should be checked to select the suitable one for executing the curvilinear locomotion.

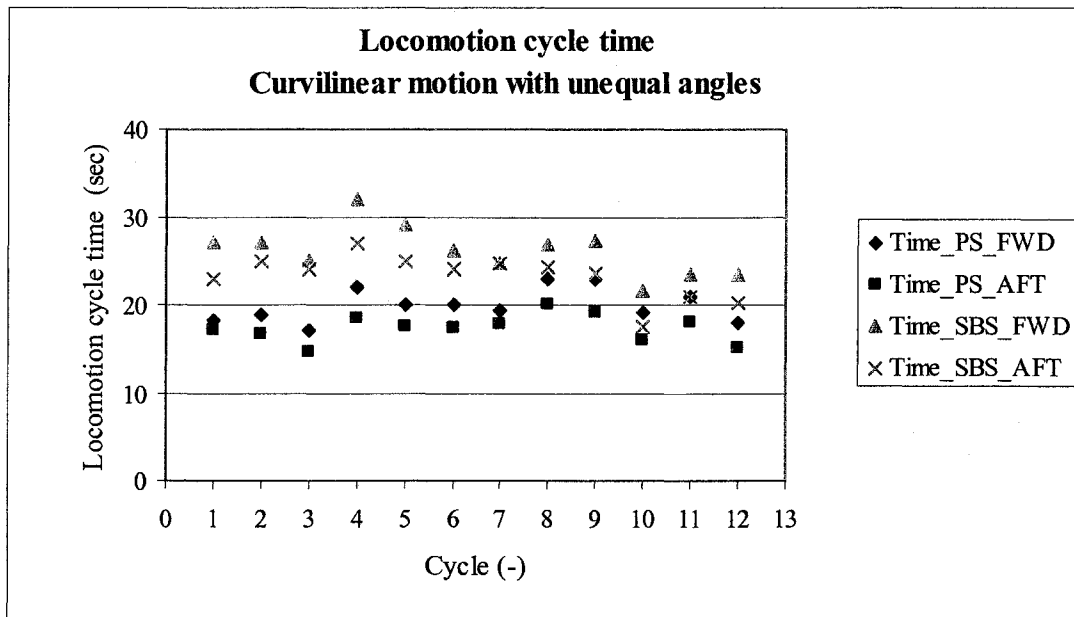


Figure 3. 47 Locomotion cycle time for curvilinear locomotion with unequal angles

3.5 Soil Pressure and Stability

3.5.1 Soil Response Models

To develop the soil response models, each foot was treated as a shallow foundation of variable configuration resting on the soil without any overburden (Figure 3.48). The ground slope was neglected for the analyses. The soil was assumed to behave as an ideal elasto-plastic material and the soil failure was described by the Mohr-Coulomb failure criterion.

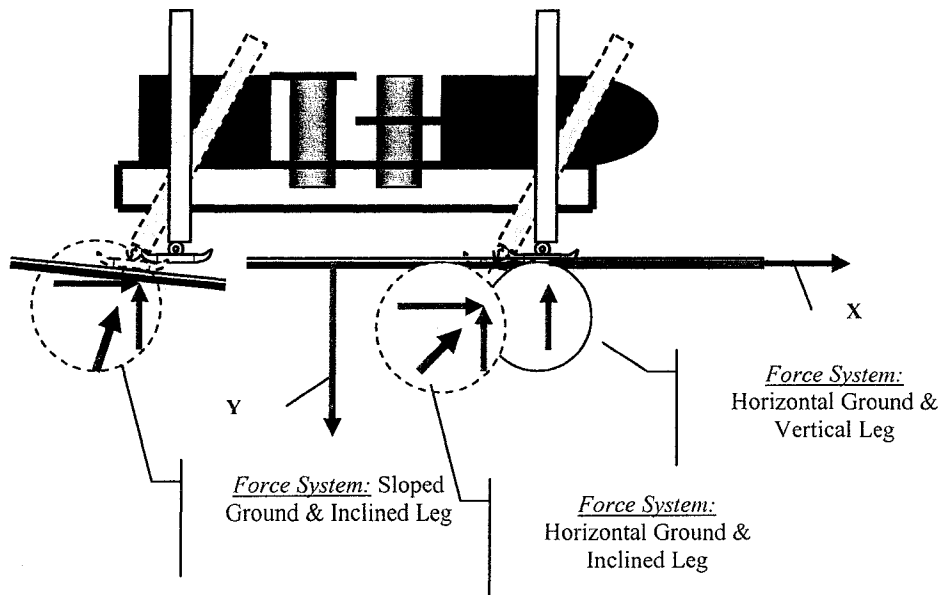
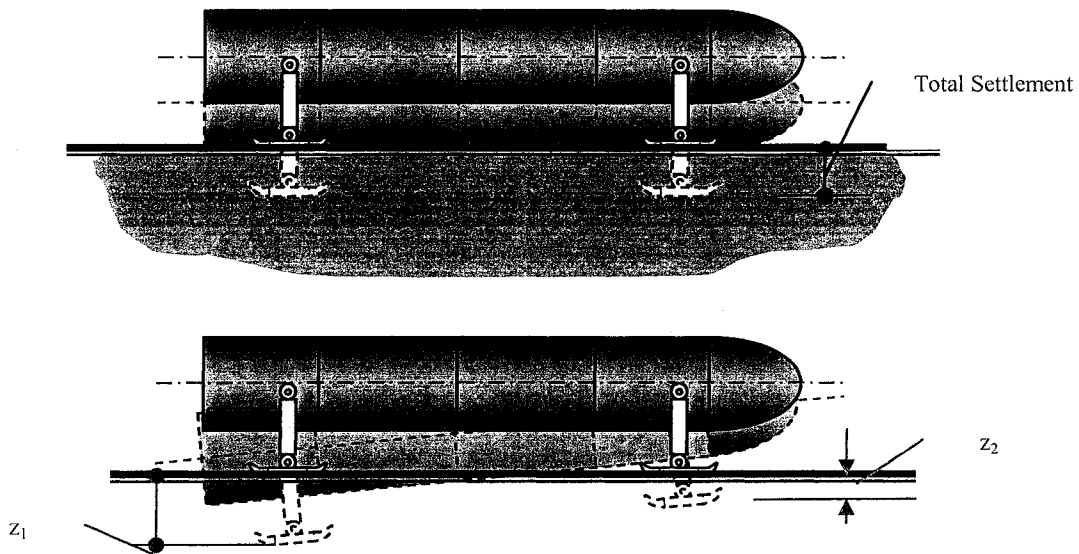


Figure 3. 48 Soil response force system during locomotion

The main design considerations for the designed vehicle were the 1) safety of the vehicle and its components, 2) functional utility, and 3) dependability. These can be achieved by 1) safety against soil failure, 2) tolerable settlements, and 3) sufficient strength of the sub-soil.

The safety against the soil failure at the foot/ soil interface is concerned with the bearing capacity of the soil, which is discussed in Appendix 1. The requirement of tolerable settlement is concerned with the total and differential settlements at the foot/ soil interface (Figure 3.49). Only immediate and primary settlement criteria are applicable to the designed legged vehicle. In case of an ideal elasto-plastic soil, when the normal load is light, the soil beneath it may be in a state of elastic equilibrium. With the increase in load, a point is reached when the soil beneath the foot will pass into a state of plastic flow, and the settlement of the foot will increase abruptly resulting in failure. At the point of failure, the soil beneath the foot can be divided into three different zones as shown in Figure 3.50. Zone I is defined as the ‘active Rankine zone’, Zone II is the ‘Prandtl zone’ and Zone III is the ‘passive Rankine zone’. Zone I pushes Zone II sideways and Zone III upwards.



$z_1 = z_2$, Total settlement, $z_1 \neq z_2$, Differential settlement

Figure 3. 49 Total and differential settlement

In the Figure 3.50, AC and DE are straight lines, inclined at $45^\circ + \frac{\phi_{soil}}{2}$ and $45^\circ - \frac{\phi_{soil}}{2}$ with the horizontal respectively. The shape of CD varies from a logarithmic spiral to a circle depending on the values of ϕ_{soil} and $\gamma_{soil} * \frac{B_{foot}}{p_{soil_surcharge}}$, where B_{foot} is the width of the foot [m], $p_{soil_surcharge}$ is the soil surcharge [kPa] (additional soil load), γ_{soil} is the specific weight of the soil [kN/m^3], and ϕ_{soil} is the angle of internal friction of the soil [degree].

The total allowable settlement for the designed vehicle was considered to be equal to the maximum lift of the designed leg. The maximum tilt of the designed vehicle should not exceed 10° in transverse and longitudinal directions, when differential settlements occur at different feet/soil interfaces. Allowable ultimate normal pressure q_0 [kPa] may be assumed on the basis of the allowable settlement.

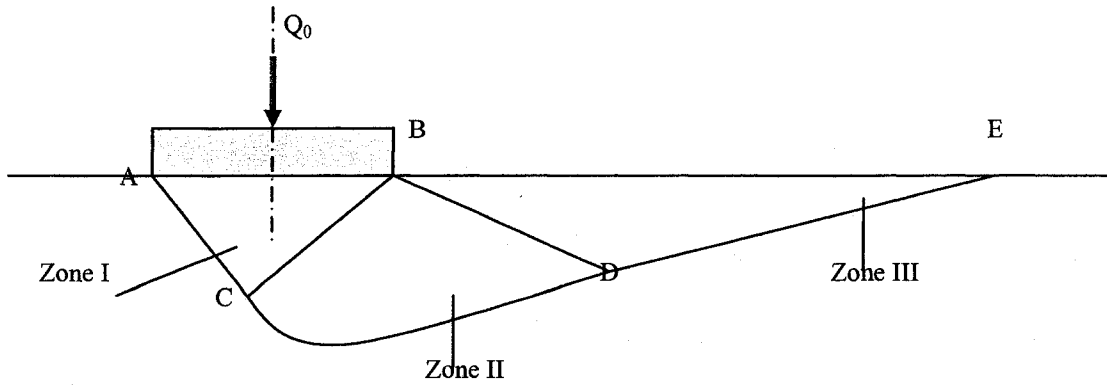


Figure 3. 50 Failure pattern under the foot

The strength of the sub-soil is important and with increase in the normal load, the pressure bulbs extend to greater depths. In order to predict the required sub-soil strength, the stress distribution characteristics in an elastic medium due to a uniform pressure p_{soil_normal} [kPa] applied over a strip of infinite length and of constant width (B_{strip}) [m] was considered. At a depth equal to the width of the strip, the vertical stress under the centre of the loading area is approximately 50 % of the applied pressure and practically vanishes at a depth equal to twice the width of the strip [Bekker, 1956; Wong, 1993].

3.5.2 Static and Dynamic Load at Foot/ Soil Interface

The determination of the normal load at the foot/ soil interface as a function of the static and the dynamic forces acting on the designed vehicle is a very complex problem. In this thesis, the normal load was expressed only as a function of the static vehicle weight and the dynamic load generated by the leg swing hydraulic cylinder. Two-dimensional parametric models were formulated separately to express the normal load as a function of the static and dynamic loads acting on the vehicle.

The static and dynamic forces acting at the foot/ soil interface can be categorized into 1) equipment related forces, and 2) environment related forces. The static equipment related forces include the gravity forces of all the components of the vehicle at different orientations of the vehicle either due to operation (e.g. position of the leg) or due to the ground condition (e.g. slope). The dynamic equipment related forces can be harmonic, periodic or impulsive in nature and are due to the operations of the different actuators. The static environment related forces include the buoyant forces at different orientations of the vehicle. The dynamic environmental forces are created by currents, waves and collisions with other submerged bodies or animals.

Only the static forces (gravity and buoyancy) and the dynamic forces due to the operation of the leg actuators were considered in developing the designed vehicle–terrain interaction models and the soil response models.

3.5.3 Static Load

The static load due to the weight of the different components of the designed vehicle is a vertical load and is transferred through the leg swing pins to the feet/ soil interfaces (Figure 3.51).

If $F_{prp_vert_leg}$ is the proportional vertical static load transferred to a particular leg swing pin [kN], then the vertical and horizontal force components acting at the foot/ soil interface are given in Equation 3.20.

$$F_{prp_vert_leg_vert} = F_{prp_vert_leg} * \cos^2(\gamma_{leg})$$

$$F_{prp_vert_leg_hor} = F_{prp_vert_leg} * \cos \gamma * \sin(\gamma_{leg})$$

[Equation 3.20]

where, γ_{leg} is the swing angle of the leg [degree].

The proportional vertical static load ($F_{prp_vert_leg}$) [kN] for the prototype vehicle was estimated by formulating a two-dimensional model based on simply supported beam theory. Because of the vehicle symmetry, the following assumptions were made when the legs are vertical and the ladder is horizontal with zero swing and pitch angles 1) the normal load at the FWD legs were equal, and 2) the normal load at the AFT legs were equal.

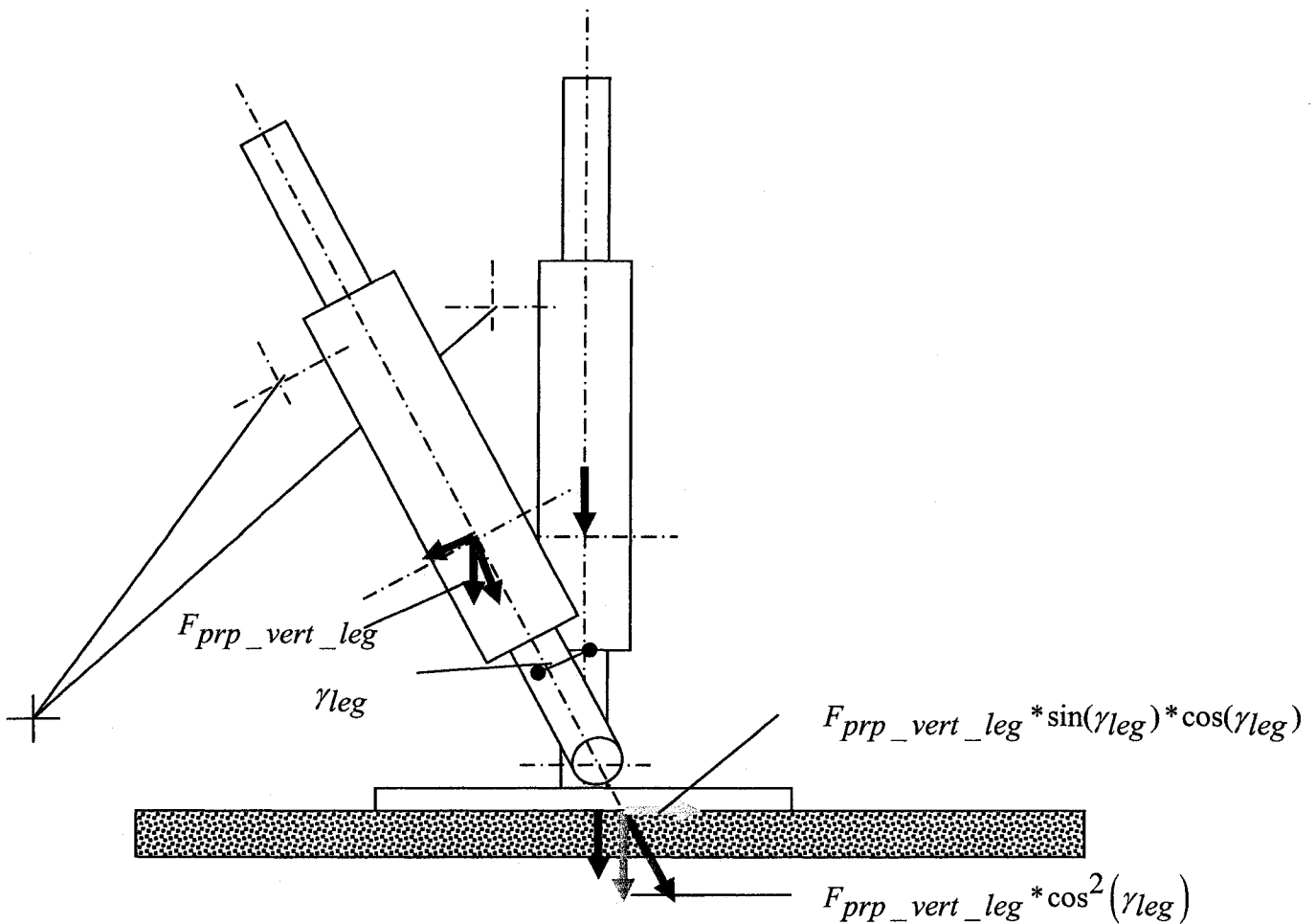


Figure 3. 51 Static load due to weight at the foot/ soil interface

The distance of a particular component from the vehicle AFT, the weight of the component and the type of load distribution assumed for the particular component are shown in Table 3.8.

Moments of the different components were taken about the AFT leg swing pin centre, to predict the proportional vertical static load transferred to the FWD and AFT legs.

Table 3. 8 Design properties of different components of the vehicle

Component	Start from body aft (m)	Finish from body aft (m)	Length (m)	Total weight (kN)	Add 5 % to weight (kN)	Weight/Length (kN/ m)	Remarks Type of load assumed
1. Main frame	0.00	3.30	3.30	5.04	5.29	1.60	Distributed
2. Ballast tanks	0.05/ 2.25	1.05/ 3.25	1.00	4.25	4.46	2.23	Dist. half
3. Leg and foot	0.55/ 2.75	0.55/ 2.75	NA	5.49	5.76	2.88	Concentrated
4. Hyd. module	1.81	2.14	0.33	4.42	4.64	7.14	Distributed
5. Control module	1.16	1.49	0.33	2.44	2.56	3.94	Distributed
6. Dredge pump	0.00	1.10	1.10	1.91	2.01	1.82	Distributed
7. Eductor pump	1.10	2.20	1.10	1.23	1.29	1.17	Distributed
8. Pipelines	1.00	3.30	2.30	0.35	0.37	0.16	Distributed
9. Ladder trunnion	3.30	3.30	NA	1.1	1.16	1.16	Concentrated
10. Cutter system	2.96	3.78	0.82	1.51	1.59	1.95	Distributed
11. Ladder boom	0.00	2.25	2.25	1.54	1.62	0.72	Distributed
12. Ladder dipper	2.25	3.35	1.1	0.63	0.66	0.60	Distributed

The magnitude of the moment arm and the moment for the different components of the designed vehicle are presented in Table 3.9.

Table 3. 9 Moment arm and moment for the different components of the vehicle

Component	Moment arm (m)	Load (kN)	Moment (kN-m)
Ballast Tanks AFT	0.00	2.23	0.00
LFC AFT	0.00	2.88	0.00
Dredge Pump	0.00	2.02	0.00
Control Module	0.87	2.56	2.23
Main Frame	1.10	5.28	5.81
Eductor Drive Pump	1.10	1.29	1.42
Hydraulic Module	1.33	4.64	6.17
Pipeline	1.60	0.37	0.59
Ballast Tanks FWD	2.20	2.23	4.91
LFC FWD	2.20	2.88	6.34
Trunnion, Ladder Assy.	2.75	1.16	3.19
Ladder Assy.	2.75	3.86	10.62
Total		31.40	41.26

The proportional vertical static loads ($F_{prp_vert_leg}$) [kN] transferred to the FWD and AFT leg swing pin centers, when the legs were vertical and the ladder assembly was horizontal with

zero swing and pitch angles were estimated as 1) FWD two legs are 18.76 kN, and 2) AFT two legs are 12.64 kN.

When the legs are vertical i.e. the swing angle of the leg, $\gamma_{leg} = 0^\circ$, and the proportional vertical static load transferred at the leg swing pin centre ($F_{prp_vert_leg}$) [kN], is equal to the vertical force acting at the foot/ soil interface ($F_{prp_vert_leg_vert}$) [kN]. The vertical force acting at the foot/ soil interface ($F_{prp_vert_leg_vert}$) was calculated as a function of the swing angle of the leg (γ_{leg}) [degree]. These predicted values were compared with experimental results.

The experimental set up, measuring techniques and calibration curves of the measuring instruments are discussed in Appendix 5. Hydraulic load cells (rubber tubes filled with water) were used to measure the normal load incident at each leg. The principle of transducing the force to a fluid pressure and then measuring the pressure with a pressure gage was followed in designing the hydraulic load cell. The hydraulic load cells designed and constructed are also discussed in Appendix 5. A mechanical ring load cell with a full Wheatstone bridge strain gage circuit was designed and constructed to measure the load incident at each leg. The experimental and predicted vertical forces acting at the foot/ soil interface ($F_{prp_vert_leg_vert}$) [kN] are presented in Appendix 9.

Figure 3.52 shows the comparisons between the predicted and experimental results for the vertical force acting at the foot/ soil interface ($F_{prp_vert_leg_vert}$) [kN] plotted as a function

of the $\cos^2(\gamma_{leg})$, where γ_{leg} is the swing angle of the leg [degree]. The percentage deviations between the predicted and experimental results are shown in Table 3.10.

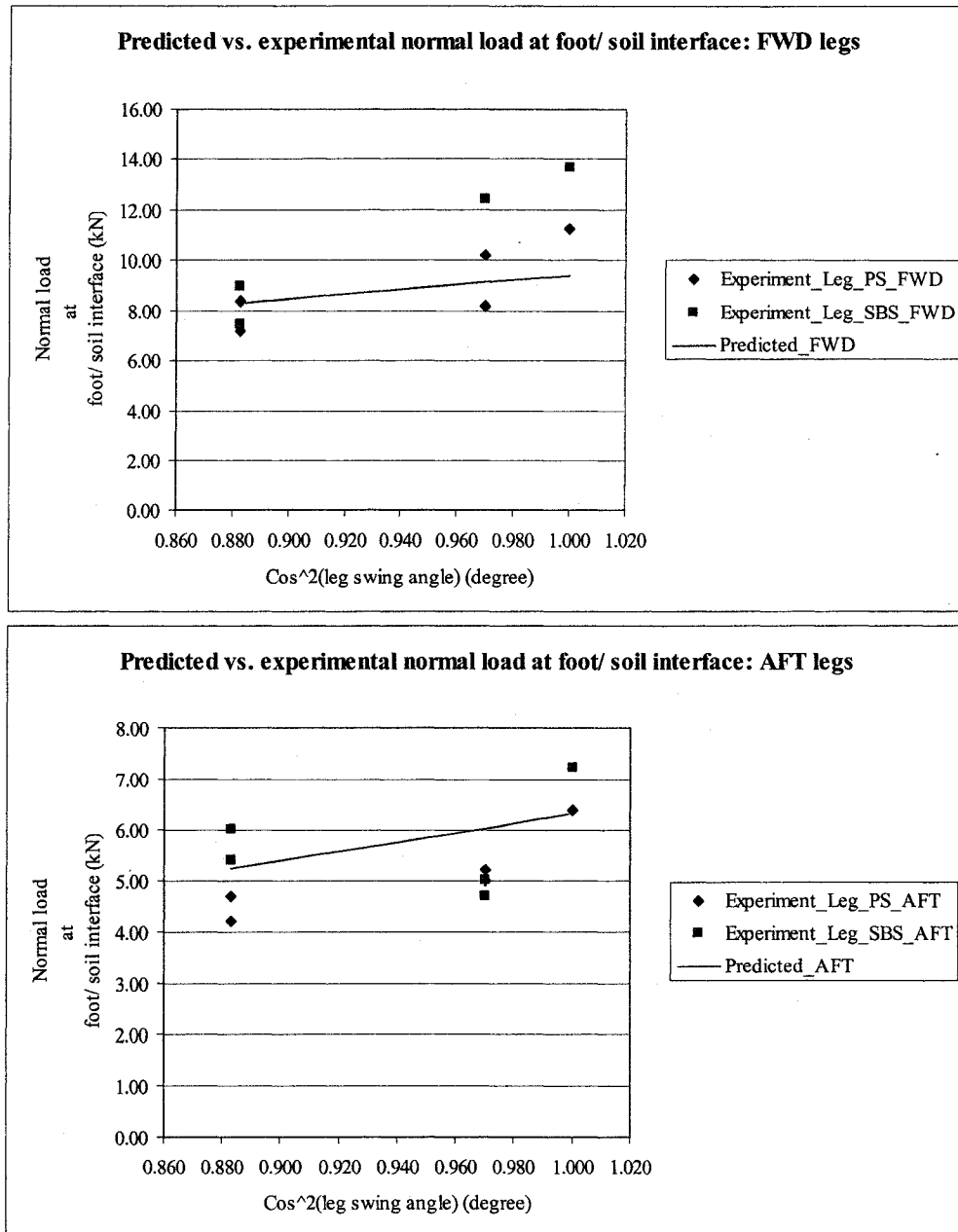


Figure 3. 52 Predicted and experimental vertical load at foot/ soil interface

Table 3. 10 Deviations for vertical force at foot/ soil interface

PS_FWD (%)	PS_AFT (%)	SBS_FWD (%)	SBS_AFT (%)
40.30	49.37	27.16	43.04
54.92	56.95	31.75	58.61
56.52	59.96	55.22	48.52
43.93	58.61	31.75	61.09
49.28	55.20	46.17	42.80

The deviations between the predicted and experimental vertical loads at the foot/ soil interface are due to the following reasons,

1. Some error is due to the experimental set up. The vertical force at the foot/ soil interface ($F_{prp_vert_leg_vert}$) [kN] was measured for one leg at a time. Since the vehicle was operated manually, it was difficult to control the leg movements accurately. As a result some legs touched the ground earlier than others, leading to the transfer of higher instantaneous proportional vertical static loads ($F_{prp_vert_leg}$) [kN] through the leg swing pins. The leg, for which measurements were taken, was lowered in steps because of the manual operation of the vehicle. The pressure gage reading thus varied during the lowering operation of the particular leg. During measurements, efforts were made to note the highest reading, but sometimes human errors crept in.
2. The two-dimensional model proposed for the prediction of the proportional vertical static load ($F_{prp_vert_leg}$) [kN] does not consider the level difference of the terrain as also the slope of the terrain. During experimental measurements, the terrain over which the vehicle was operated was relatively flat, but level differences cannot be neglected.
3. Instrumental sensitivity was also another problem. Different hydraulic load cells were used to measure the vertical force at the foot/ soil interface for different legs. As a result the

deviations of the measured values from the predicted values are different for the four legs. The pressure gages used were not sensitive enough to record changes in pressure reading very accurately. Measurement errors might have occurred. Height of the hydraulic load cell is approximately 100 mm, which is not the same as the foot height.

4. The deviations are also due to oversimplification of the theoretical model. The two-dimensional parametric model developed for prediction of the proportional vertical static loads ($F_{prp_vert_leg}$) [kN] is a very simplified model based on simply supported beam theory.

The ratios between the vertical forces at the foot/ soil interface ($F_{prp_vert_leg_vert}$) of FWD legs to that of the AFT legs were plotted against the square of the cosine of the leg swing angle, (γ_{leg}) [degree] (Figure 3.53).

At higher leg swing angles, the deviations between the experimental and predicted values are less for both PS and SBS legs. The average value of such ratios for the PS legs was 1.77, while that for SBS legs was 1.98. The average value of such ratios for predicted results was 1.53. The deviation percentage between the measured average value for the PS legs and the predicted average value is approximately 16 %. The deviation percentage between the measured average value for the SBS legs and the predicted average value is approximately 29 %.

The calculated weight of the vehicle was compared with the weight calculated from experimental measurements. The summation of the vertical forces ($F_{prp_vert_leg_vert}$) [kN] at the feet/ soil interfaces of the four legs for a particular leg swing angle should be equal to the weight of

the designed vehicle. The weight of the vehicle calculated from the experimental results is shown in Table 3.11.

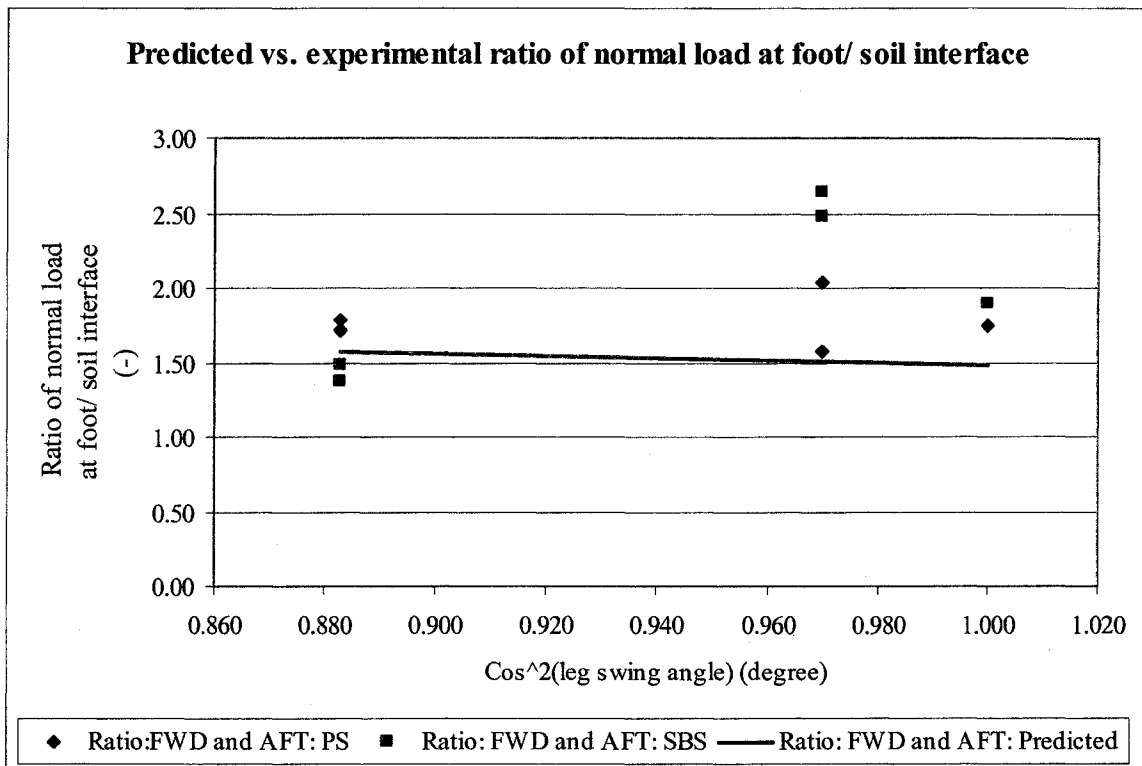


Figure 3. 53 Predicted and experimental values of ratios between vertical force of FWD and AFT legs

Table 3. 11 Weight of vehicle calculated from experimental results

Leg swing angle (degree)	Weight of the vehicle (from experimental measurements) (kN)
0	38.47
10	30.82
20	24.22
-10	32.32
-20	28.02

The discrepancies in the weight of the vehicle for different leg swing angles is due to the fact that the vertical forces for different legs were not measured simultaneously, but were measured one at a time. The reasons mentioned before, for explaining the deviations between the predicted and experimental results of vertical force at the foot/ soil interface also applies here. The average

value of the weight of the vehicle as calculated from the experimental results is approximately 31 kN, which is close to the calculated value of 31.4 kN, mentioned in Table 3.9.

The maximum value of the vertical force at the foot/ soil interface obtained from the experimental results was used to calculate the required soil strength for stability purposes.

3.5.4 Dynamic Load

The dynamic force due to the operation of the hydraulic cylinder swinging the leg was considered to determine the soil reactions. The hydraulic oil pressure was assumed to be constant and hence the forces generated by the hydraulic cylinder during expansion and retraction were constant. The leg linkage and the hydraulic cylinder form a four bar mechanism. The angles between the different linkages change during the cylinder operation. As a result the horizontal and vertical components of the hydraulic cylinder force changes with time.

It is thus necessary to perform the linkage synthesis and analyses of this four bar mechanism to determine the angles between the linkages at various positions. The horizontal and vertical dynamic force components acting at the foot hinge pin were expressed as a function of the hydraulic cylinder force and the angles between the linkages for various positions.

The free body diagram for this four bar mechanism is shown in Figure 3.54. The foot hinge pin is denoted by the point 'O' and was assumed as the point where all the static and dynamic forces were acting. The point 'A' denotes the pin centre for the hydraulic cylinder. The point 'B' represents the positions of the instantaneous rod pin centre 'C' of the hydraulic cylinder during the cylinder rod movements.

The swing angle of the leg is denoted as a positive angle when the leg rotates towards the AFT of the vehicle and is denoted as a negative angle when the leg rotates towards the FWD direction of the vehicle. In order to swing the legs through a given positive angle, the hydraulic cylinders for the AFT legs expand, while the hydraulic cylinders of the FWD legs retract. The rod pin centre of the hydraulic cylinder of the leg when the cylinder is at half stroke and the respective leg is vertical is denoted by the point 'C' in Figure 3.54. The point 'D' represents the swing pin centre of the leg in Figure 3.54.

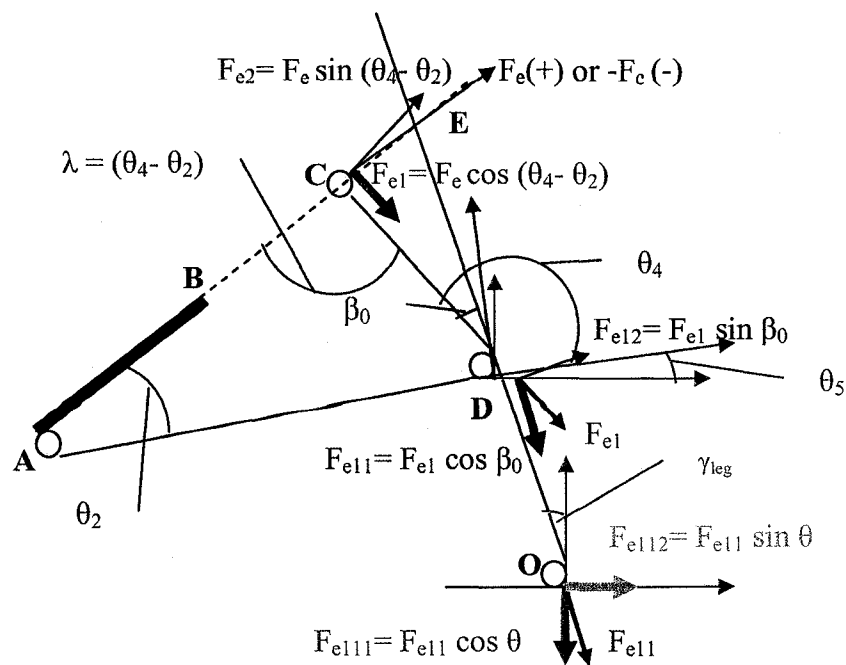


Figure 3. 54 Dynamic force transfer at the foot/ soil interface

- A) Swing cylinder pin centre, C) Swing cylinder rod pin centre, D) Leg swing pin centre, O) Foot hinge pin centre

It was assumed that initially the leg was vertical and the hydraulic cylinder was at half stroke. The hydraulic cylinder started from rest and accelerated to the constant velocity of v_{shc_leg} [m/sec] and then decelerated to zero. The swing angle of the leg varied from $(+)\gamma_{leg}$ to

(-) γ_{leg} degrees.

The expanding and retracting force of the hydraulic cylinder (F_e or F_r) [kN] acts at an angle of $\lambda = (\theta_4 - \theta_2)$ [degree] with the link 'CD'. The expanding force of the hydraulic cylinder was considered as positive, while the retracting force was considered as negative.

The vertical and horizontal dynamic force components acting at the foot hinge pin when the slope of the terrain = 0° were deduced respectively as (Figure 3.54) given below,

$$F_{e11} = F_{e11} \cos \theta = F_e \cos(\theta_4 - \theta_2) \cos \beta_0 \cos \gamma_{leg} \quad [\text{Equation 3.21}]$$

$$F_{e12} = F_{e11} \cos \theta = F_e \cos(\theta_4 - \theta_2) \sin \beta_0 \sin \gamma_{leg}$$

The hydraulic cylinder forces are given below,

$$F_e = a_{hc} * p_{ho} * A_{hc} \quad [\text{Equation 3.22}]$$

$$F_r = a_{hc} * p_{ho} * (A_{hc} - A_{hc_rod}) \quad [\text{Equation 3.23}]$$

where, A_{hc} is the area of the swing cylinder [m^2], A_{hc_rod} is the area of the swing cylinder rod [m^2], a_{hc} is an arbitrary loss factor [-], F_e and F_r are respectively the expansion and retraction forces of the hydraulic cylinder swinging the leg [kN], and p_{ho} is the hydraulic oil pressure [kPa].

In order to determine the values of the different angles shown in Figure 3.54, for different positions of the hydraulic cylinder rod and the leg linkages, position analyses [Norton, 1999] was performed. The position analyses of this four bar mechanism is given in Appendix 10.

3.5.5 Total Load

The total vertical and horizontal forces acting at the foot hinge pin, due to the static and dynamic loads of leg operation are given below,

$$Q_o = F_{prp_vert_leg} \cos^2 \gamma_{leg} + F_e \cos(\theta_4 - \theta_2) \cos \beta_0 \cos \gamma_{leg} \quad [\text{Equation 3.24}]$$

$$P = F_{prp_vert_leg} \sin \gamma_{leg} \cos \gamma_{leg} + F_e \cos(\theta_4 - \theta_2) \sin \beta_0 \sin \gamma_{leg}$$

3.5.6 Allowable Load

The allowable ground pressure $\left(q_o = \frac{Q_o}{B_{foot} * L_{foot}} \right)$ [kPa], can be determined by the

Buismann–Terzaghi equation modified by De Beer and Vesic. This is discussed in Appendix 1.

In case of inclined loading the problem is more complicated due to presence of the horizontal force component (P) [kN]. Failure can occur either due to the 1) sliding of the foot along AB (if there is no grouser) or 2) by general shear failure of the under laying soil (with grousers).

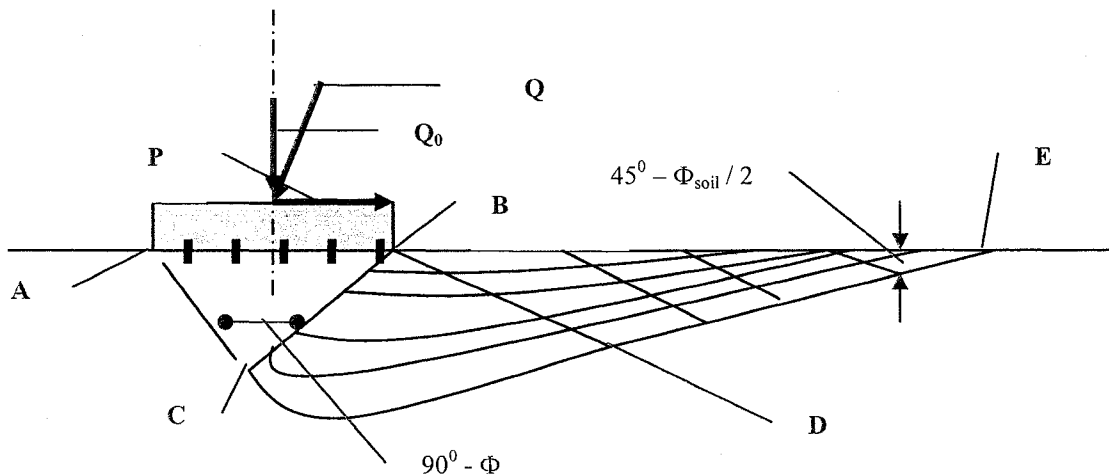


Figure 3.55 Inclined loading on foot

Just at the point of sliding, the force P is maximum (P_{max}) [kN], and is balanced by the frictional and adhesive forces,

$$P_{\max} = Q_0 * \tan(\delta_{soil_foot}) + A_{foot} * a \quad [\text{Equation 3.25}]$$

where, A_{foot} is the contact area of the foot [m^2], a is the adhesion between the soil and the foot [kPa], and δ_{soil_foot} is the angle of friction between soil and foot [degree]. Adhesion in soft clays is equal to their undrained shear strength.

For inclined legs (Figure 3.55), the bearing capacity equation is multiplied by the ‘inclination factors’ (ζ_{ci}, ζ_{qi} and $\zeta_{\gamma i}$) [-] and the bearing capacity equation is modified [Vesic,1970],

$$q_0 = Q_0 / (B_{foot} * L_{foot}) = c * N_c * \zeta_c * \zeta_{ci} + h_{\text{surcharge}} * \gamma_{soil} * N_q * \zeta_q * \zeta_{qi} + \frac{1}{2} * \gamma_{soil} * B_{foot} * N_{\gamma} * \zeta_{\gamma} * \zeta_{\gamma i} \quad [\text{Equation 3.26}]$$

As suggested by Vesic [1970], ζ_{qi} and $\zeta_{\gamma i}$ should be,

$$\zeta_{qi} = \left[1 - \frac{P}{(Q + B_{foot} * L_{foot} * c * \cot \phi_{soil})} \right]^m$$

$$\zeta_{\gamma i} = \left[1 - \frac{P}{(Q + B_{foot} * L_{foot} * c * \cot \phi_{soil})} \right]^{m+1} \quad [\text{Equation 3.27}]$$

$$\zeta_{ci} = 1 - \frac{m * P}{B_{foot} * L_{foot} * c * N_c * \cot \phi_{soil}}$$

The exponent m [-] in the longitudinal direction is given [Vesic,1970],

$$m_L = \frac{\left(2 + \frac{L_{foot}}{B_{foot}} \right)}{\left(1 + \frac{L_{foot}}{B_{foot}} \right)} \quad [\text{Equation 3.28}]$$

3.5.7 Results and Discussions for Soil Response

The required soil strength in granular and cohesive soils was calculated for the designed legged vehicle with rectangular, square and circular foot shape. The required soil strength for a Caterpillar tracked vehicle with similar overall dimensions and weight was also calculated and compared with the results of the designed legged vehicle.

The constants used for the calculations and the results are given in Appendix 10.

The vertical and horizontal components of the dynamic forces at the foot/ soil interface for the designed leg linkage were estimated first. The vertical dynamic force acting at the foot hinge pin was plotted for two different leg swing angles of 0 and 30 degrees (Figure 3.56). The horizontal dynamic force acting at the foot hinge pin was plotted for swing angles of leg = 10 and 30 degrees (Figure 3.57). The vertical and horizontal dynamic forces were plotted against the displacement of the hydraulic cylinder rod. The vertical and horizontal dynamic forces were plotted for both hydraulic cylinder expansion and retraction.

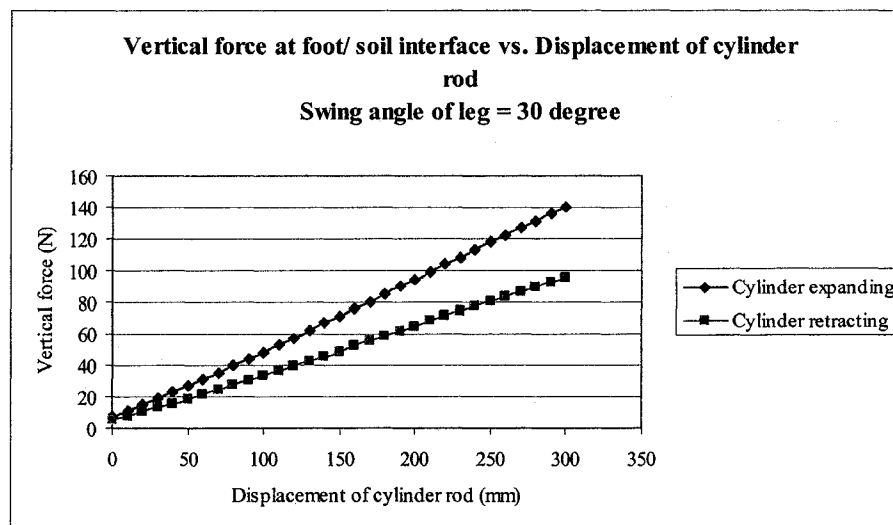
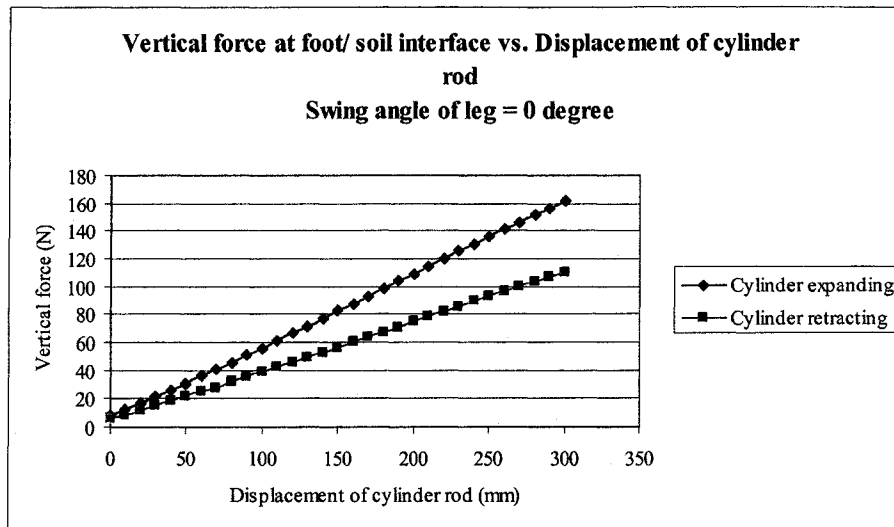


Figure 3. 56 Vertical dynamic force at foot/ soil interface

When the swing angle of the leg is 0 degrees, the magnitude of the vertical component of the dynamic force is maximum. The vertical component of the dynamic force is observed to vary from approximately 7 to 160 N during hydraulic cylinder expansion and approximately 5 to 108 N during hydraulic cylinder retraction (Figure 3.56). The magnitude of the dynamic vertical force acting at the foot hinge pin is negligible when comparing 150 N with 4 to 14 kN (Figure 3.52).

When the swing angle of the leg is 0 degrees, the magnitude of the vertical component of the dynamic force is maximum. The vertical component of the dynamic force is observed to vary from approximately 7 to 160 N during hydraulic cylinder expansion and approximately 5 to 108 N during hydraulic cylinder retraction (Figure 3.56). The magnitude of the dynamic vertical force acting at the foot hinge pin is negligible when comparing 150 N with 4 to 14 kN (Figure 3.52).

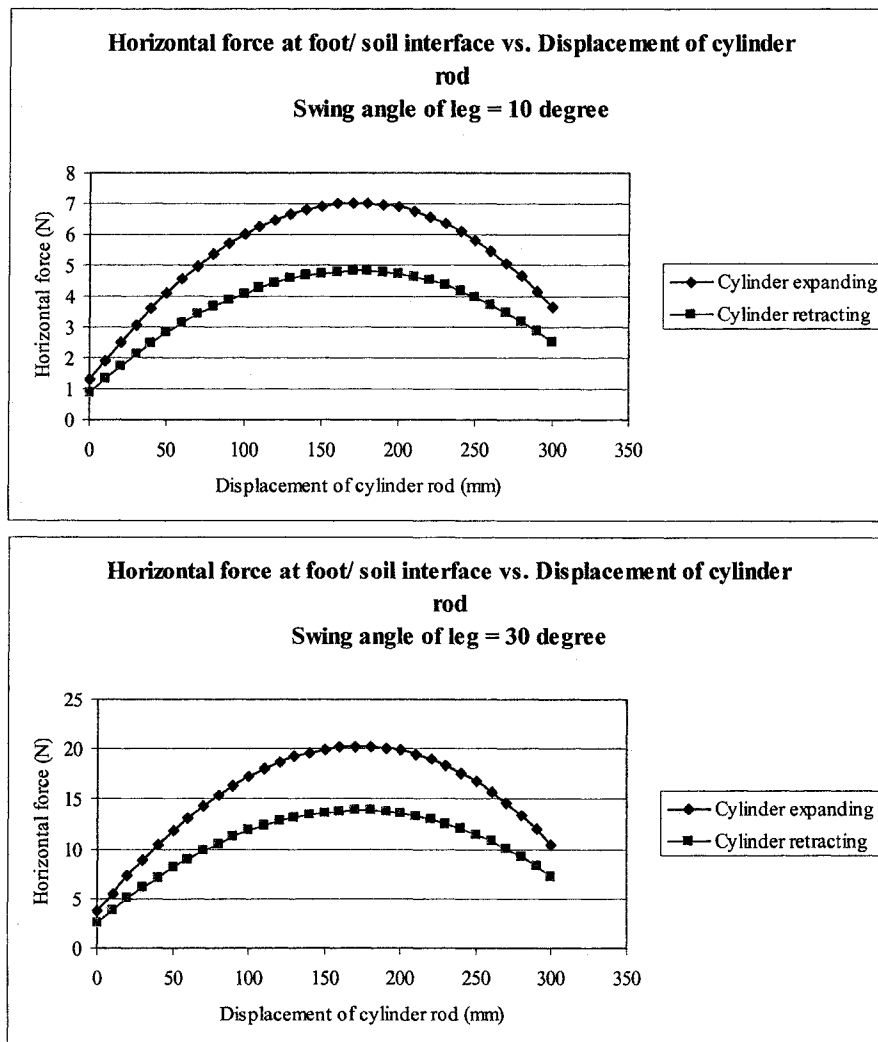


Figure 3. 57 Horizontal dynamic force at the foot/ soil interface

The horizontal component of the dynamic force at the foot hinge pin will increase with the increase in the swing angle of the leg. The maximum swing angle of the leg considered for the

designed vehicle was 30 degrees on either side of the vertical. The horizontal component of the dynamic force at the foot hinge pin is observed to increase from approximately 4 N to a peak value of 20 N and then decrease to 10 N during cylinder expansion. The forces are much lower during cylinder retraction. These are shown in Figure 3.57.

The experimental value of the vertical static force acting at the foot hinge pin was a maximum for the SBS_FWD leg, when the swing angle of the leg was 0 degrees (13.67 kN). The vertical component of the dynamic force acting at the foot hinge pin was also a maximum when the swing angle of the leg was 0 degrees. The maximum vertical total load was estimated from the maximum values of the vertical static and dynamic loads, since these are the most critical conditions in terms of soil bearing capacity. The total vertical force acting at the foot hinge pin and hence the foot/ soil interface is shown in Figure 3. 58. From Figure 3.58, it can be concluded that the maximum vertical total force which can come at any foot hinge pin is approximately 13 to 14 kN.

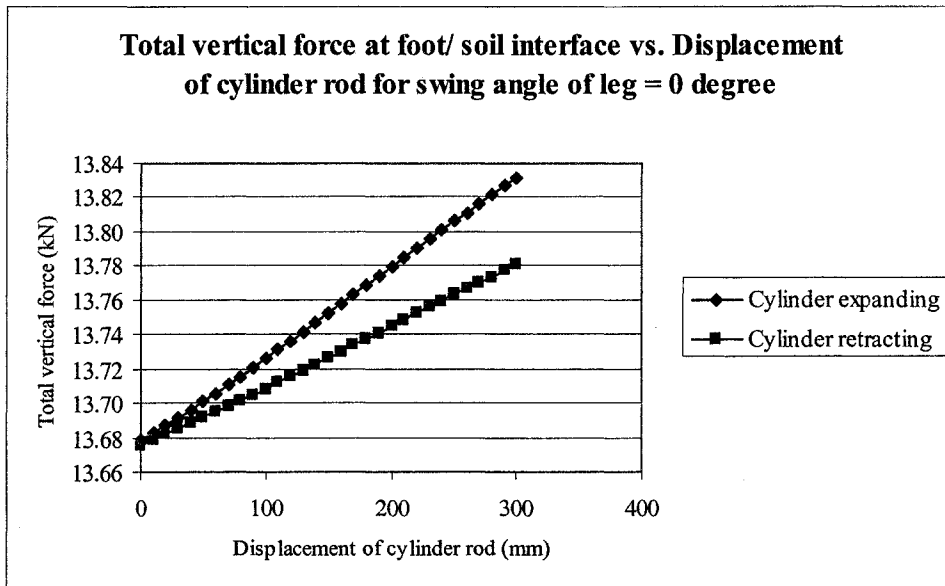


Figure 3. 58 Total force at the foot/ soil interface

To estimate the required soil pressure, the total vertical force at the foot/ soil interface (Q_o) was assumed to be 12 kN. The assumed soil properties chosen for the granular soil [Wong, 1993] are adhesion, $a = 4$ kPa, dimensionless bearing capacity factors, $N_c = 35.49$, $N_q = 23.18$ and $N_\gamma = 30.22$, angle of internal friction, $\phi_{soil} = 32^\circ$, angle of friction between soil and foot, $\delta_{soil_foot} = \frac{2}{3} * \phi_{soil}$, and specific weight of soil, $\gamma_{soil} = 10$ kN/ m³. For saturated cohesive soils, the angle of internal friction of soil, ϕ_{soil} is 0 degrees, the dimensionless bearing capacity factors are $N_c = 5.14$, $N_q = 1$, and $N_\gamma = 0$. It was assumed that there was no surcharge of soil. Due to other dynamic loading on the designed vehicle, a factor of safety of 1.5 was assumed for estimating the required soil bearing capacity in both granular and cohesive soils. The areas of the feet of different shapes were kept nearly identical and the dimensions were chosen according to the area assumed. The graphical results for the required bearing capacity of the soil are shown in Figure 3.59.

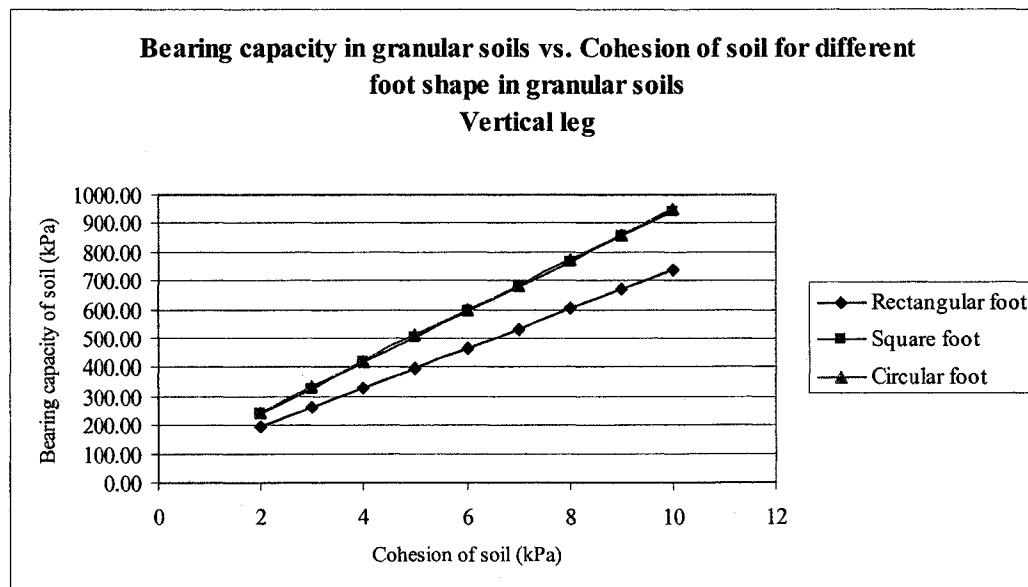


Figure 3.59 Bearing capacity in granular soil for different foot shape

The constants used for the calculations and the calculated results are shown in Appendix 10.

The bearing capacity is not a limiting factor for granular soils. The undrained shear strength of soft to very soft clays can vary from 2 to 15 kPa with specific weight of 16 to 18 kN/ m³. Thus bearing capacity or soil strength can be a major limitation for the operation of submersible vehicles in cohesive soils. In case of weaker soils, the submersible weight of the vehicle must be reduced by using air tanks or fixed buoyancy blocks.

It is observed from Figure 3.60, that the bearing capacity requirements for rectangular, square or circular foot shapes in cohesive soils are nearly identical for vehicle weights up to 400 kN. In very soft soil with limited bearing capacity, the designed vehicle can perform locomotion by belly sliding.

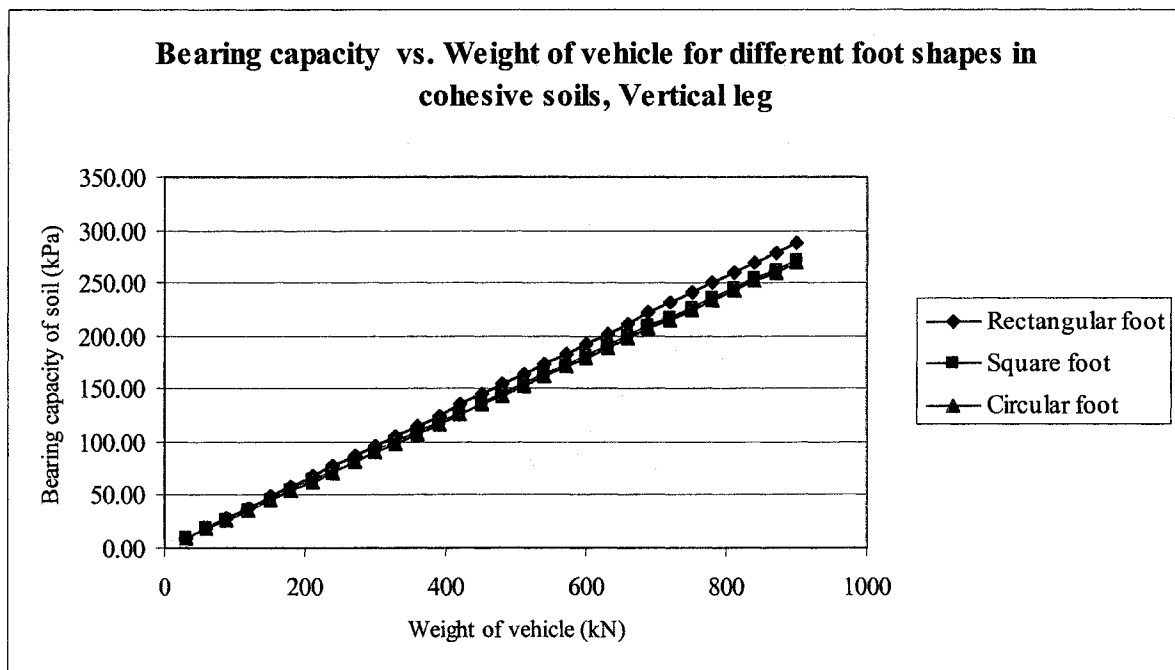


Figure 3. 60 Bearing capacity in cohesive soil for different foot shape

The Caterpillar tracked vehicle D3B was chosen for the comparison with the designed legged vehicle. The specifications of the Caterpillar tracked vehicle D3B is given in Appendix 4. Figure

3.61 shows that with the given rectangular foot dimensions and with the increase in vehicle weight, the required soil strength for the designed legged vehicle is greater than the soil strength required for a tracked vehicle of the same weight. The foot dimensions need to be increased if the designed legged vehicle weight is to be increased. In Figure 3.60 and 3.61, the weight of the vehicle is assumed up to 1000 kN for prospective bigger vehicles in the future.

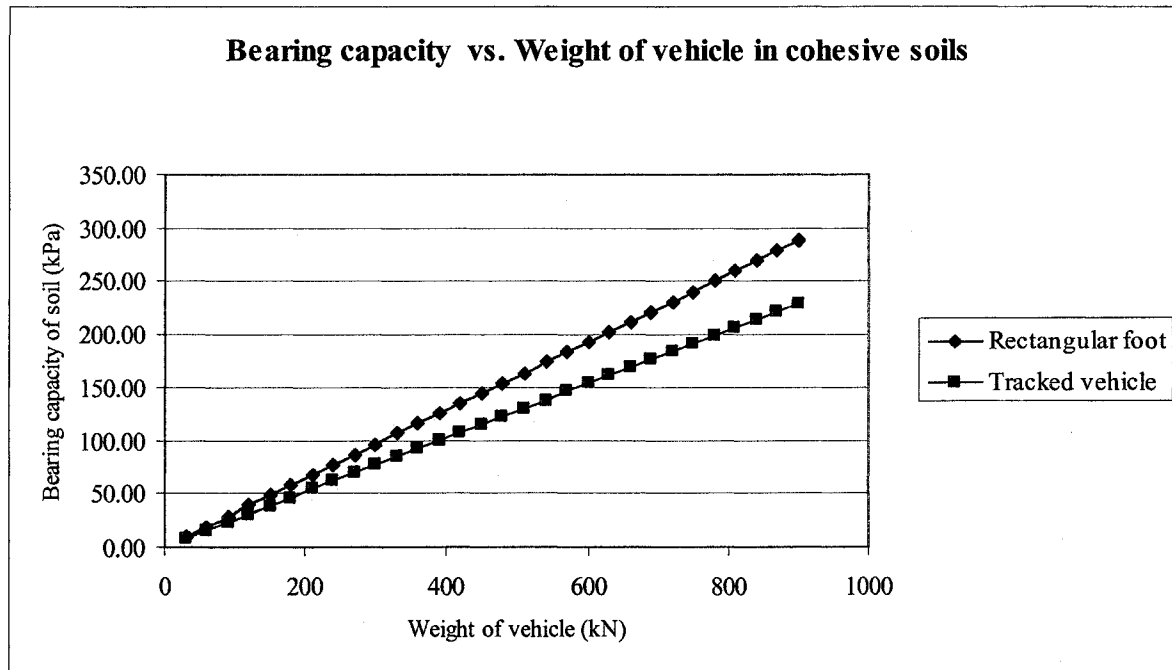


Figure 3. 61 Comparisons between required soil strength for cohesive soil for tracked and designed legged vehicle

3.6 Tractive Force Generated by the Designed Legged Vehicle

This section presents the parametric models developed for the evaluation of the tractive force generated by the grousers and the foot during legged locomotion and the tractive force generated by the belly during belly sliding.

The theory of passive earth pressures was used to develop the model for the prediction of the tractive force generated by the grousers of the designed foot. The maximum tractive force that

can be developed by the foot and the belly is determined from the maximum shear strength of the terrain (τ_{\max}) [kPa] and the contact area (A_{contact}) [m²].

The static load due to the weight of the vehicle and the dynamic load due to the operation of the hydraulic cylinder swinging the leg were considered in developing the parametric models for estimation of the tractive forces. The geometry of the grouser, the foot and the vehicle belly as well as the soil type affects the tractive forces generated. The variation of the tractive force due to slip was also included in the parametric models.

3.6.1 Tractive Force at the Grousers

A two-dimensional parametric model was developed to evaluate the tractive forces generated by the grousers based on the theories of passive earth pressures. The turning force generated by the hydraulic cylinder swinging the leg (F_{e2}) [kN] is balanced by an equal reaction force (F_{e2}') [kN] at the foot/ soil interface (Figure 3.62). The turning force is given in Equation 3.29.

$$F_{e2} = F_{e2}' = F_e \sin(\theta_4 - \theta_2) \quad [\text{Equation 3.29}]$$

The horizontal and vertical components of the turning force acting at the foot hinge pin are ($F_{e2}'_1$) [kN] and ($F_{e2}'_2$) [kN]. The horizontal (P) [kN] and vertical (Q_o) [kN] components of the total static and dynamic loads acting at the foot hinge pin are deduced in Equation 3.30 and 3.31.

$$P = (F_{prp_vert_leg}) \sin \gamma_{leg} \cos \gamma_{leg} + F_e \cos(\theta_4 - \theta_2) \sin \beta_o \sin \gamma_{leg} \quad [\text{Equation 3.30}]$$

$$Q_o = F_{prp_vert_leg} \cos^2 \theta + F_e \cos(\theta_4 - \theta_2) \cos \beta_o \cos \gamma_{leg} \quad [\text{Equation 3.31}]$$

Neglecting the spring and damping effect of the locomotion system, the tractive force available at the foot/ soil interface is given in Equation 3.32.

$$F_{p_foot} = (P \pm F_{e2}' \cdot 1) \quad \text{[Equation 3.32]}$$

This equation is valid only when the soil does not fail under the given conditions.

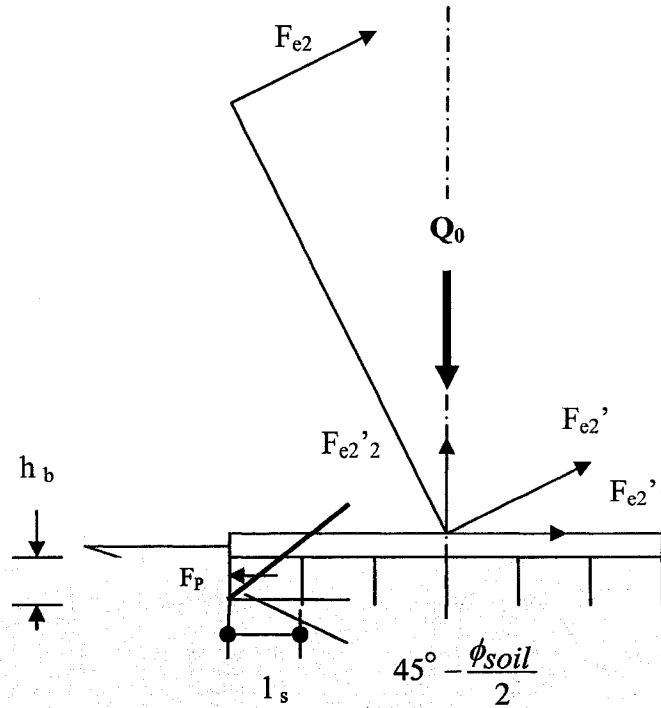


Figure 3.62 Tractive force without soil failure

The soil present in between the grousers may fail by the Rankine passive failure criteria as was discussed in section 3.5.1. Assuming the tractive force (F_{p_foot}) [kN] is equally divided

between all the grousers, the tractive force available at each grouser will be $\frac{F_{p_foot}}{z_{grouser}}$ [kN],

where $z_{grouser}$ is the number of grousers [-], each of width $B_{grouser}$ [m].

The rupture distance between two grousers (l_s) [m] (Figure 3.62) is given in Equation 3.33.

$$l_s = \frac{h_{grouser}}{\tan\left(45^\circ - \frac{\phi_{soil}}{2}\right)} \quad [\text{Equation 3.33}]$$

The rupture distances were calculated for non-cohesive granular soil and cohesive soil, for height of grouser ($h_{grouser}$) = 40 mm. These are presented in Table 3.12 and Table 3.13.

Table 3.12 Rupture distance for grousers in granular soil

ϕ_{soil} (degree)	20	25	30	35	40
l_s (mm)	57	63	69	77	86

Table 3.13 Rupture distance for grousers in cohesive soil

ϕ_{soil} (degree)	0	5	10	15	20
l_s (mm)	40	44	48	52	57

The spacing between the designed grousers is 94 mm. Thus there is a possibility of soil failure in between the grousers in accordance to the Rankine passive failure criteria. The soil failure will however first initiate in front of the leading grouser.

If the grouser spacing is too small, the space between the grousers will be filled up with soil and shearing will occur at the tips of the grousers. The dominant mode of failure will be the shearing of the soil around the grouser edges (i.e. two sides and bottom of grouser). The length of the shear plane for each grouser (l_{sp}) [m] is deduced in Equation 3.34.

$$l_{sp} = (2 * h_{grouser} + B_{grouser}) \quad [\text{Equation 3.34}]$$

The total length of the shear plane is thus given as $(2 * h_{grouser} + B_{grouser}) * z_{grouser}$ [m].

Both the shear planes need to be calculated and the lower value should be considered for calculation of the tractive force generated by the grousers, when the grouser spacing is too small.

The grousers of the foot are vertical and are being pushed against the soil when the turning force is applied by the hydraulic cylinder. The soil in front of the grouser will be brought into a state of passive failure. Since the ratio of the width of the grouser to the height of the grouser is large, the situation can be considered as two-dimensional. The grouser is vertical and hence the normal pressure exerted by the grouser on the soil will be the major principle stress and is equal to the passive earth pressure (σ_p) [kPa]. The resultant force acting on the grouser per unit width ($F_{p_grouser}$) [kN] can be calculated by integrating the passive earth pressure (σ_p) [kPa] over the height of the grouser ($h_{grouser}$) [m]. The details of such calculations are given by Wong [1993].

Since the width of the grouser is equal to the width of the foot, there is a surcharge on the soil surface behind the leading grouser due to the total vertical load at the foot hinge pin (Q_o) [kN].

The tractive force generated per unit width of the grouser is given in Equation 3.35.

$$(F_{p_grouser}) = \frac{1}{2} \gamma_{soil} (h_{grouser})^2 N_{\phi} + (p_{soil_surcharge}) (h_{grouser}) N_{\phi} + 2c (h_{grouser}) \sqrt{N_{\phi}} \quad [\text{Equation 3.35}]$$

where, c is the soil cohesion [kPa], N_{ϕ} is called the flow value and is equal to

$$\tan^2 \left(45^\circ + \frac{\phi_{soil}}{2} \right) [-], p_{soil_surcharge} \text{ is the soil surcharge [kPa] due to the total vertical load}$$

(Q_o) [kN], γ_{soil} is the specific weight of the soil [kN/m³], and ϕ_{soil} is the angle of internal

friction of the soil [degree]. This model neglects the surface roughness of the grousers and the friction and/ or adhesion between the grouser and the soil.

The tractive force that a grouser in vertical position can develop is given by equation 3.36.

$$\frac{F_{p_foot}}{z_{grouser}} = (B_{grouser}) \left(\frac{1}{2} \gamma_{soil} (h_{grouser})^2 N_{\phi} + (p_{soil_surcharge}) (h_{grouser}) N_{\phi} \right) + 2c (h_{grouser}) \sqrt{N_{\phi}}$$

[Equation 3.36]

3.6.2 Tractive Force and Slip of Foot

The maximum tractive effort which may be developed by a foot is given in equation 3.37.

$$F_{p_foot_max} = A_{foot} * \tau_{max} = A_{foot} * (c + p_{soil_normal} * \tan \phi_{soil})$$

$$= A_{foot} * c + Q_o \tan \phi_{soil}$$

[Equation 3.37]

where, A_{foot} is the contact area of the foot [m²], c is the soil cohesion [kPa], (Q_o) is the total vertical load [kN], p_{soil_normal} is the normal pressure exerted on the soil [kPa], and ϕ_{soil} is the angle of internal friction of the soil [degree].

In dry sand, the cohesion of soil c [kPa] is negligible. The total vertical load (Q_o) [kN] thus determines the maximum tractive effort available for the designed leg. In saturated clay, the second term due to the angle of internal friction of the soil ϕ_{soil} [degree] can be neglected and hence the tractive force will depend on the contact area of the foot.

To predict the relationship between the tractive force generated by a foot and slip at the foot/ soil interface, it is necessary to examine the shear displacement j [m] beneath a foot, since the shear stress is a function of the shear displacement j [m]. The shear displacement j [m] will be the

same for all the grousers. The shear stress–shear displacement relationships for various types of soil are discussed in Appendix 1.

The relationship between the slip and the shear displacement for the designed legged vehicle are deduced in equation 3.38.

$$i = 1 - \frac{v}{L_e * \Omega_{leg}} = 1 - \frac{v}{v_{vehicle_theo}} \quad [Equation 3.38]$$

$$= \frac{v_{vehicle_theo} - v}{v_{vehicle_theo}} = \frac{v_j}{v_{vehicle_theo}}$$

where, v is the actual velocity of the vehicle with respect to the ground [m/sec], v_j is the speed of slip of the foot in a direction opposite to the direction of vehicle motion, $v_{vehicle_theo}$ is the theoretical velocity of the vehicle = $L_e * \Omega_{leg}$ [m/sec] with L_e being the effective leg length [m] and Ω_{leg} the angular velocity of the leg [rad/sec].

The shear displacement is given in equation 3.39.

$$j = v_j * t_{swing_leg} = v_j * \frac{x_{step}}{v_{vehicle_theo}} = i * x_{step} \quad [Equation 3.39]$$

where, t_{swing_leg} is the time required for swinging the leg [sec] and x_{step} is the theoretical step size of the leg [m]. It is observed from Equation 3.39, that the shear displacement linearly varies with the step size of the leg.

The shear stress–shear displacement relationship proposed by Janosi and Hanamoto [Wong, 1993] as described in Appendix 1 was used to predict the tractive force developed by the foot.

The tractive force generated by the foot under a given slip is deduced in Equation 3.40.

$$F_{p_foot} = (A_{foot} * c + Q_o \tan \phi_{soil}) \left[1 - \frac{K}{i * x_{step}} \left(1 - e^{-\left(i * x_{step} / K \right)} \right) \right]_{x_{step_min}}^{x_{step_max}}$$

[Equation 3.40]

where, x_{step_max} and x_{step_min} are the maximum and minimum step sizes respectively [m] during a particular locomotion cycle.

3.6.3 Tractive Force and Slip of Vehicle Belly

During belly sliding, the speed of slip v_j [m/sec] is the same at every point of the belly in contact with the terrain. When belly sliding is performed with the aid of legs, the displacement of the belly is assumed to be equal to the step size of the leg i.e. x_{step} [m]. The relationship deduced between shear displacement, slip and step size for the designed leg linkage in the previous section thus also holds for the belly sliding motion. The contact area of the foot however is to be replaced by the contact area of the belly.

$$A_{belly} = B_{belly} * L_{belly} \quad \text{[Equation 3.41]}$$

where, A_{belly} is the area of contact of the belly with the soil [m²], B_{belly} is the width of the vehicle belly in contact with the soil [m] and L_{belly} is the length of the vehicle belly in contact with the soil [m].

3.6.4 Tractive Effort and Slip of a Track

The tractive effort of a track under different slip percentages was deduced by Wong [1993]. It was shown by Wong [1993] that the shear displacement beneath a flat track increases linearly

from the front to the rear of the contact area. The shear displacement and the slip for a track are thus related [Wong, 1993].

$$j = i * x_j \quad \text{[Equation 3.42]}$$

where i is the slip [%] and x_j is the distance of the point at which shear displacement is considered from the front of the contact area of the track [m].

The relationship between the tractive effort of the track and the slip of the track when the Janosi and Hanamoto equation [Wong, 1993] for shear stress–shear displacement is used is given in Equation 3.43.

$$F_{p_track} = (A_{track} * c + F_W \tan \phi_{soil}) \left[1 - \frac{K}{i * L_{track}} \left(1 - e^{-\left(\frac{i * L_{track}}{K} \right)} \right) \right] \quad \text{[Equation 3.43]}$$

where, A_{track} is the contact area of the track [m²], F_W is the normal load due to weight of the vehicle [kN], i is the slip [%], and L_{track} is the length of the track [m].

3.6.5 Results and Discussions for Tractive Force and Slip

The tractive force generated by the Caterpillar tracked vehicle D3B as a function of the slip percentage of the track was compared with the tractive force generated by the designed legged vehicle expressed as a function of the slip percentage of the foot. Granular and cohesive soils were considered for the comparisons. The soil mechanical parameters and the design parameters of the tracks, grousers, feet and vehicle belly are presented in Appendix 11.

It was assumed for all the calculations that the weight of the tracked vehicle was equally distributed between the two tracks. The same assumption was made for the designed legged

vehicle, where the weight of the vehicle was assumed to be equally distributed between the four legs. From the predicted and experimental data presented in section 3.5.3, it was observed that the load incident at the FWD and AFT legs were different. Equal distribution of weight was assumed in order to simplify the problem. Uniform pressure distribution was assumed at the vehicle running gear–terrain interfaces.

The tractive force generated in granular soil with different slip percentages for the Caterpillar tracked vehicle varied from approximately 13 to 24 kN as is observed from Figure 3.63.

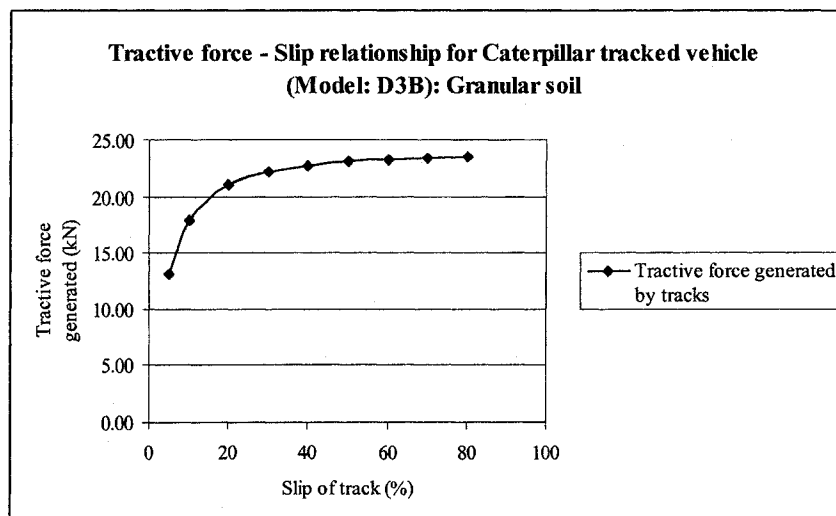


Figure 3. 63 Tractive force generated vs. slip for ‘Caterpillar’ tracked vehicle D3B in granular soil

The tractive force generated by the four feet without grousers for the designed legged vehicle is shown in Figure 3.64. The tractive force generated by the four feet without grousers in granular soil is not sufficient for vehicle movement, since the weight of the vehicle is 31 kN. The vehicle will not move without the grousers and the foot will slip, which was also found during the experiments.

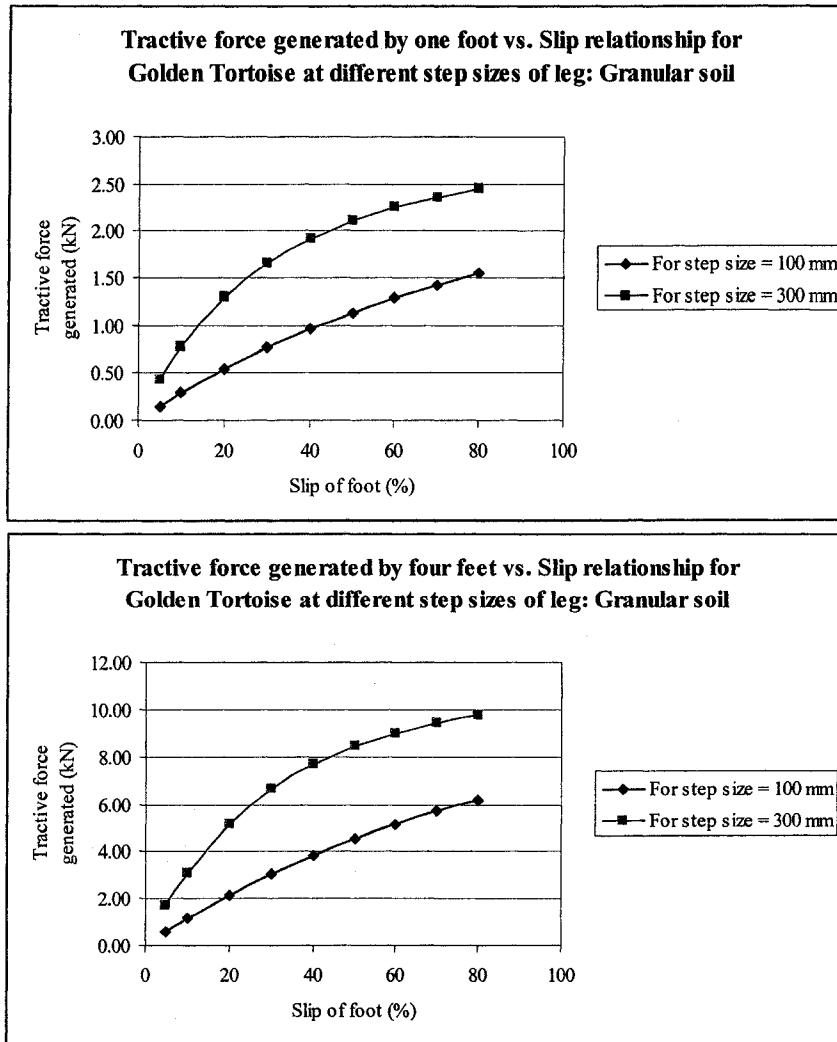


Figure 3. 64 Tractive forces generated by four feet of the designed legged vehicle under different slip percentages in granular soil (without grouser)

The tractive force generated by the grousers in granular and cohesive soils were estimated. The tractive force generated by one grouser in granular soil was estimated as 0.96 kN, while that in cohesive soil was estimated as 1.1 kN. There are 8 grousers attached to each foot. Hence the total tractive force generated by each foot in granular soil is 7.7 kN, while that in cohesive soil is 8.8 kN.

It is observed from Figure 3.63, that with a slip of > 5 % the total traction available from the four feet with the eight grousers in granular soil is just able to overcome the vehicle weight for lower step size of the vehicle. With the increase in step size of the leg, higher traction is available from the foot, which increases the total traction available from the foot and the grousers.

The tractive effort generated by the tracked vehicle in cohesive soil is shown in Figure 3.65.

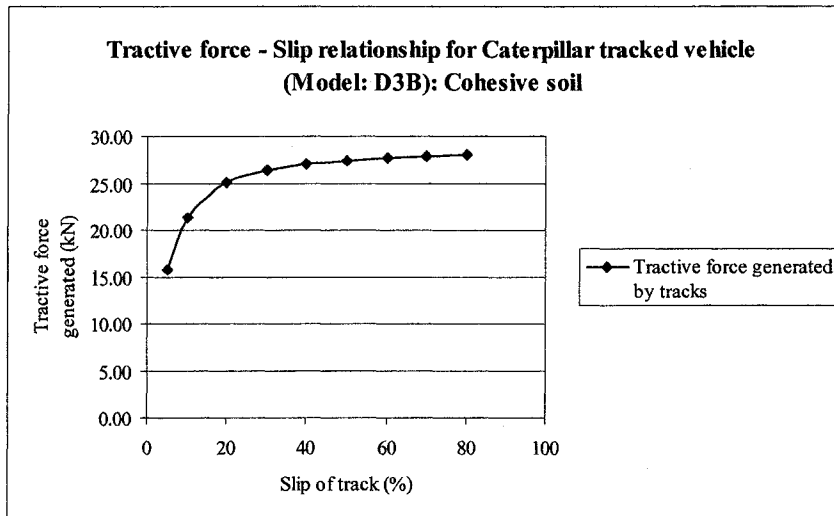


Figure 3. 65 Tractive force generated vs. slip for ‘Caterpillar’ tracked vehicle D3B in cohesive soil

Comparisons between Figure 3.65 and Figure 3.66 show that the designed legged vehicle generates more tractive effort compared to the tracked vehicle in cohesive soil. In cohesive soil the weight of the vehicle is not important in the generation of the maximum tractive effort, but the area of contact is important in developing traction at the vehicle running gear–terrain interface. Though the area of contact of the legged vehicle (0.84 m²) is lower than the tracked vehicle (1.11 m²), the presence of the grousers develop sufficient traction to overcome the vehicle weight and any other resistances. The step size of the legged vehicle should be increased to generate more tractive force in order to overcome greater resistances (e.g. water drag).

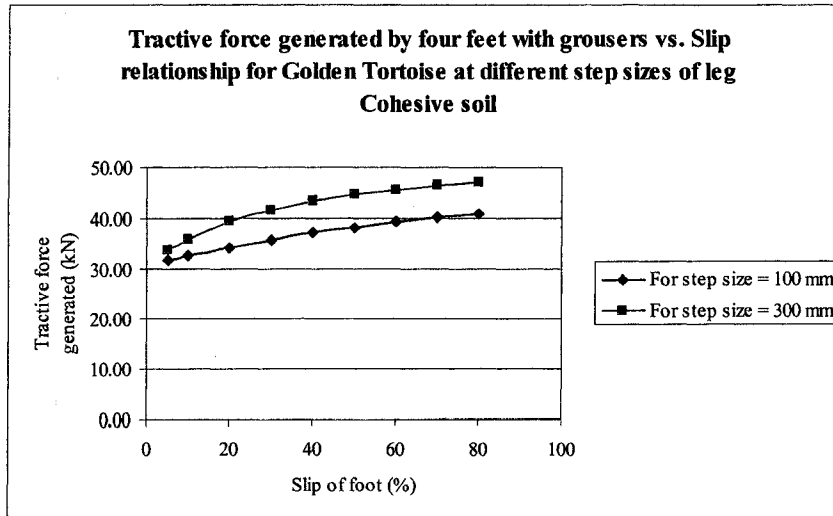


Figure 3. 66 Tractive forces generated by the designed legged vehicle under different slip percentages in cohesive soil (with grousers)

During belly sliding the area of contact with the terrain of locomotion is increased, thereby increasing the tractive force generated in cohesive soil. This is shown in Figure 3.67. The tractive force generated due to belly sliding is about seven times of the tractive force generated by the four feet in cohesive soil. Higher tractive force is necessary in very soft soil.

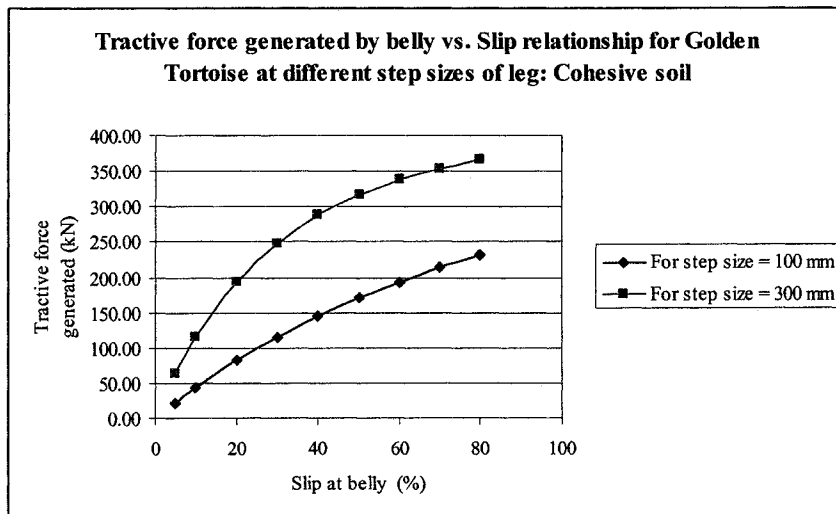


Figure 3. 67 Tractive force generated during belly sliding

3.7 Concluding Remarks

The validation of the theoretical gait planners which considers the slip at the foot/ soil interface with the experimental results for straight line and curvilinear locomotion showed good matching between the two. The designed vehicle was able to follow the theoretical gait planners with acceptable accuracy, even with manual operation of the electronic switches of the solenoids of the directional control valves. Such results show the effectiveness of using the designed leg linkage and the proposed method of locomotion for submersible legged dredgers/ miners. Comparisons between the bearing capacity requirements of tracked and the designed legged vehicle shows nearly identical results in cohesive soils up to a vehicle weight of 200 kN. The tractive force generated by the foot and grousers of the designed legged vehicle in cohesive soil is much higher compared to tracked vehicle. The bearing capacity requirements and the tractive force generated by the designed legged vehicle shows the effectiveness of the design in cohesive soils. Mobility over cohesive soils is always critical compared to granular soils.

The parametric performance evaluation models for the excavation and transportation systems are discussed in the next chapters.

CHAPTER 4

PERFORMANCE EVALUATION MODELS FOR EXCAVATION

4.1 Introduction

In crown cutters the suction mouth is situated within the cutter. The cutter mechanically excavates the soil and forms a soil/ water mixture within the cutter. For the designed excavation system, the mixture formation occurs in the suction influence zone located in front of the suction mouth. The processes of gathering and mixing of the excavated material and hence the generation of the spillage is different for the crown cutter and the designed twin drum cutter system. The spillage is defined as the soil cut by the cutter but not sucked in by the suction mouth. Prediction of the amount of soil cut and the spillage generated is thus very important for accurate excavation production estimation. The factors influencing spillage are 1) the shape, geometry and type of the cutter, 2) soil characteristics, 3) operational parameters of the ladder assembly and the cutter, and 4) suction force.

This chapter presents the parametric performance evaluation models developed to predict the design constraints, the limiting operating conditions, the volume of soil loosened by the leading and trailing cutters, and the cutter power required for the designed drum cutter in different soil types.

4.2 Loosening Production

Loosening production (P_{loose}) [m^3/sec] is defined as the volume of soil mechanically dislodged by the cutter per unit of time (t) [sec]. It is a function of the 1) type, shape and geometry of the cutter, 2) rpm and power/ torque installed on the cutter, 3) geometry, orientation and swing velocity of the ladder assembly, and 4) soil properties. Correlations between the loosening

production of the designed drum cutter and the 1) number of cutter blades, 2) cutter rpm and direction of cutter rotation, and 3) swing velocity and orientation of the ladder assembly are presented in this section. Correlations between the installed cutter power/ torque, the soil properties and the loosening production for the designed cutter are discussed in section 4.4.

4.2.1 Assumptions for Loosening Production

The assumptions made for the evaluation of the loosening production were 1) the ground was level, 2) axis of the cutter was horizontal, 3) cutter was assumed cylindrical with diameter D_{cutter} [m] and radius R_{cutter} [m], 4) number of rows of cutter blades present along the length of the cutter were z_{cutter_row} [-], 5) each row has equal number of blades, z_{blade} [-], 6) each blade was of same width, B_{blade} [m], 7) interaction effects between the blades were neglected, and 8) swing velocity of the ladder assembly (v_{swing_ladder}) [m/sec] and the cutter rpm (rpm_{cutter}) [-] were known.

4.2.2 Working Principle during Dredging

The working principle during the dredging operation is shown in Figure 4.1. The ladder assembly swings to one end and is then lowered. The dipper is rotated with respect to the ladder boom to make the desired angle with the cutting face. The cutters start rotating and the ladder assembly swings to the other end, while excavating the soil on the first layer of cut. The angle between the dipper and the ladder boom is kept constant during the swing cycle. The cutter tip thus maintains a constant radius of rotation with the centre of rotation at the pivot point of the ladder assembly (R_{swing_cutter}) [m]. The ladder is lowered to achieve the next layer of cut and the swing cycle is repeated as above. When the workspace is exhausted the vehicle moves to

the next dredging setting. The maximum step size should never exceed the length of the drum cutter. The maximum dredging depth depends on the geometry of the designed vehicle and the stroke of the leg-lift hydraulic cylinder.

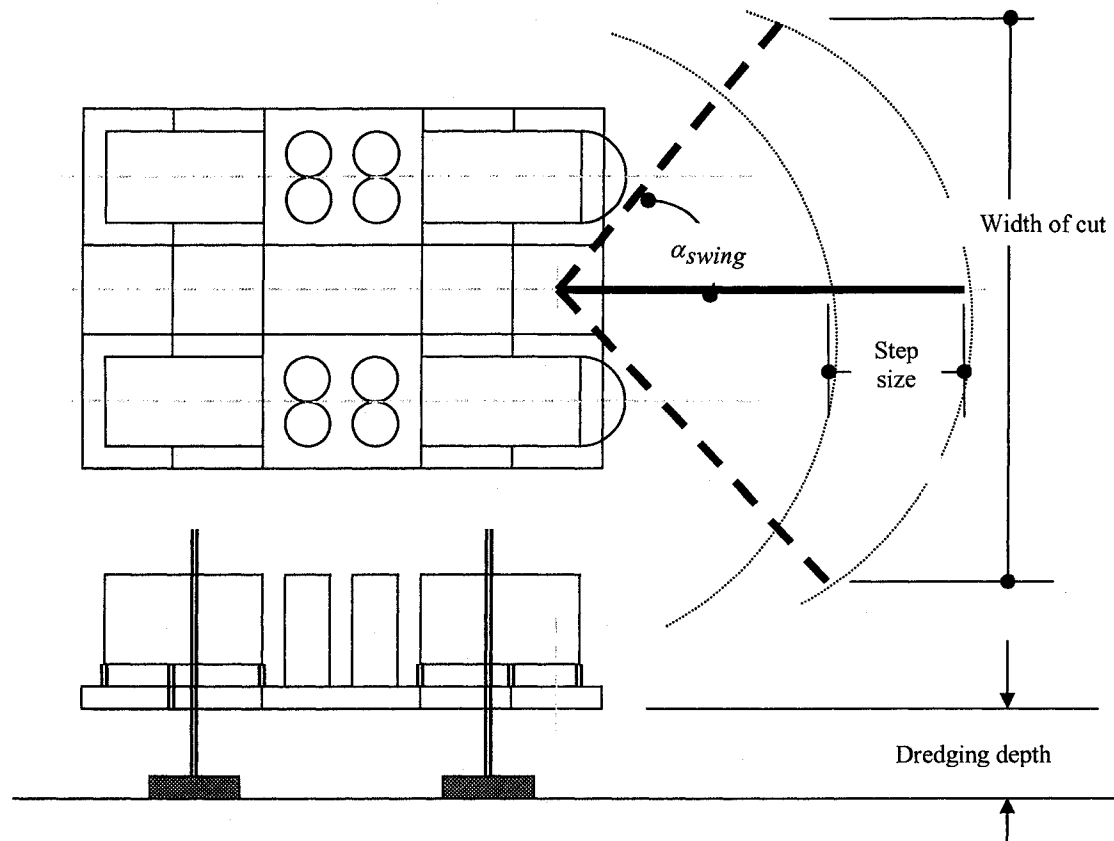


Figure 4.1 Working principle during excavation

4.2.3 Volume of Soil Excavated

The volume of soil dislodged by the designed drum cutter during 'overcutting' and 'undercutting' were evaluated in this section. Two different methods were followed to estimate the volume of soil dislodged which are 1) area integration method, and 2) feed of cutter method.

The cross sectional area of the soil wedge excavated by successive cutter blades in a row was calculated by integrating the area bounded by the successive cutter blade trajectories and the straight line representing the top of the soil layer which is being excavated. The volume of the

soil wedge was obtained by multiplying the cross sectional area with the maximum width of the cutter blade. The total volume of the soil loosened by the designed drum cutter was obtained by multiplying the volume of the soil wedge with the number of blades in a row and the number of rows (Figure 4.2).

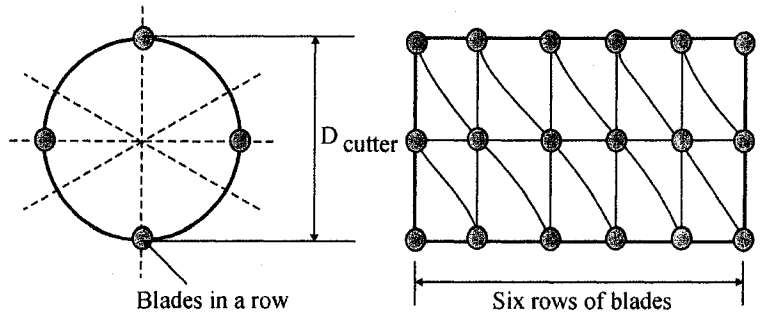


Figure 4.2 Lacing of blades on cutter drum

Individual cutter blades of a drum cutter execute a complex motion consisting of a relative rotary motion around the axis of the cutter drum, with a velocity ($v_{cutter} = R_{cutter} * \Omega_{cutter}$) [m/sec] and a translatory motion with a velocity (v_{swing_cutter}) [m/sec] (Figure 4.3). The translatory velocity of the cutter (v_{swing_cutter}) [m/sec] represents a component of the swing velocity of the ladder assembly (v_{swing_ladder}) [m/sec] acting in a horizontal direction. This is due to the cutter offset from the point of rotation of the ladder assembly. The trajectory of motion of the cutter blade is determined by the ratios of the rotary and translatory velocities of the cutter

$$\left(\lambda_{cutter} = \frac{v_{cutter}}{v_{swing_cutter}} \right) [\text{Yatsuk et al., 1971}].$$

The parametric equations of the tip of two successive cutter blades in a row (A and B in Figure 4.3), when the centre of the cutter drum was taken as the origin were deduced based on theories of earth moving machineries [Yatsuk et al., 1971].

where, R_{cutter_edge} is the radius of the circle described by the cutter edge during rotation [m],

$\left(\Omega_{cutter} = \frac{2\pi * rpm_{cutter}}{60} \right)$ is the angular velocity of the cutter [rad/sec] and

$\left(\phi_{blade} = \frac{2\pi}{z_{blade}} \right)$ is the angle between two successive cutter blades [radians]. It was assumed

that $R_{cutter_edge} = R_{cutter}$.

The cross sectional area of the soil wedge was obtained by integrating the area bounded by the curves represented in equations 4.1 to 4.4 and the straight line representing the top of the depth of cut (Figure 4.3). The equation of the straight line was deduced,

$$y = (R_{cutter} - h_{cut}) \quad \text{[Equation 4.5]}$$

where h_{cut} is the depth of cut [m].

The cross sectional area of the soil wedge was also calculated from the feed of the cutter (S) [m] and the depth of cut (h_{cut}) [m]. The feed of cutter (S) [m] (Figure 4.4) is a function of the cutter rpm and the translatory velocity of the cutter (v_{swing_cutter}) [m/sec]. The feed of the cutter is the linear distance covered when the cutter rotates through an angle of $\left(\frac{2\pi}{z_{blade}} \right)$ [radians]. If (t) [sec] denotes the time required by the cutter to rotate through the said angle, then the feed of the cutter is obtained [Yatsuk et al., 1971],

$$S = v_{swing_cutter} * t \quad \text{[Equation 4.6]}$$

$$S = \frac{2\pi * R_{cutter}}{z_{blade} * \lambda_{cutter}} \quad \text{[Equation 4.7]}$$

or,

$$S = \frac{60 * v_{swing_cutter}}{z_{blade} * rpm_{cutter}} \quad \text{[Equation 4.8]}$$

The cross sectional area of the soil wedge was approximated (Figure 4.4),

$$A_{soilwedge} = S * h_{cut} \quad \text{[Equation 4.9]}$$

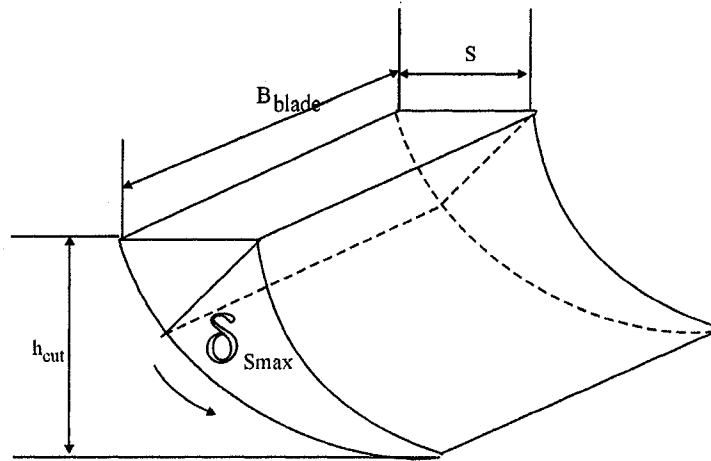


Figure 4.4 Feed and depth of cut

The translatory velocity of the cutter (v_{swing_cutter}) [m/sec] was expressed as a function of the swing velocity of the ladder assembly (v_{swing_ladder}) [m/sec] and the translatory velocity of the hydraulic cylinder rod swinging the ladder assembly (v_{shc_ladder}) [m/sec]. These relations given in Appendix 12 were used to estimate the cross sectional area of the soil wedge formed.

The total volume of soil dislodged by the cutter per unit of time was deduced as follows,

$$V_{soil_total} = A_{soilwedge} * B_{blade} * \frac{rpm_{cutter}}{60} * z_{blade} * z_{cutter_row} \quad \text{[Equation 4.10]}$$

where, $A_{soilwedge}$ is the cross sectional area of the soil wedge dislodged by two successive cutter blades [m²].

4.2.4 Results and Discussions for Loosening Production

The constants and the variables chosen for the simulations are presented in Appendix 12. The values of the constants and the variables were based on the prototype vehicle.

The translatory velocity of the cutter (v_{swing_cutter}) [m/sec] was calculated as a function of the hydraulic oil flow (Q_{shc_ladder}) [m³/sec], angle which the ladder boom makes with the horizontal (α) [degree], half angle of swing of the ladder assembly (α_{swing}) [degree], angle which the dipper makes with the horizontal (β) [degree] and the angle between the axis of the ladder swing cylinder and the central axis of the vehicle (γ_{ladder}) [degree]. The definitions of the angles are schematically shown in Appendix 12. A 2-level full factorial design was performed with these 5 factors using the software 'Design Expert' [Montgomery, 2005]. For a 2-level full factorial design all the factors were studied at two levels, a high level and a low level. The levels can either be quantitative or qualitative. The high and the low values chosen for each factor are given in Appendix 12.

The calculated values of the translatory velocity of the hydraulic cylinder rod swinging the ladder assembly (v_{shc_ladder}) [m/sec], the swing velocity of the ladder assembly (v_{swing_ladder}) [m/sec] and the translatory velocity of the cutter (v_{swing_cutter}) [m/sec] for the different test runs are presented in Appendix 12. It was observed from the results, that the

minimum value of the translatory velocity of the cutter (v_{swing_cutter}) was 0.48 m/sec while the maximum value was 2.64 m/sec for the prototype vehicle.

The relationship between the translatory velocity of the cutter (v_{swing_cutter}) [m/sec] and the angle which the ladder boom makes with the horizontal (α) [degree] is shown in Figure 4.5. The maximum value of the swing velocity of the ladder assembly (v_{swing_ladder}) for the prototype vehicle was 0.18 m/sec, which was used for Figure 4.5. The angle which the ladder boom makes with the horizontal (α) [degree] was varied from 5° to 60° and the angle which the dipper makes with the horizontal (β) [degree] was kept at two constant values of 5° and 10°. Figure 4.5 shows that the swing velocities of the cutter are nearly identical for $\beta = 5^\circ$ and 10° . The range of the angle β [degree] is very small and hence the translatory velocity of the cutter (v_{swing_cutter}) [m/sec] can be considered as independent of the angle β [degree].

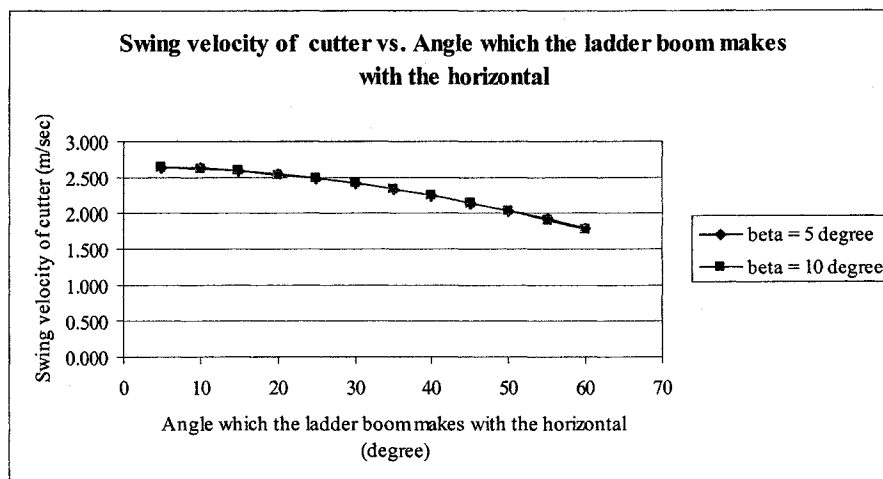


Figure 4.5 Swing velocity of cutter and the angle between ladder boom and horizontal (Swing velocity of the ladder = 0.18 m/sec)

The same plot is shown in Figure 4.6, for a value of swing velocity of the ladder of $v_{swing_ladder} = 0.035$ m/sec, which is the minimum value of this parameter.

The maximum value, minimum value and variation between the maximum and minimum values of the translatory velocity of the cutter (v_{swing_cutter}) [m/sec] as obtained from Figure 4.5 and 4.6 are shown in Table 4.1. The volume of the soil wedge dislodged and hence the loosening production is a function of the translatory velocity of the cutter. Thus it was necessary to estimate the variation of the translatory velocity of the cutter with the change in the angle which the ladder boom makes with the horizontal (α) [degree].

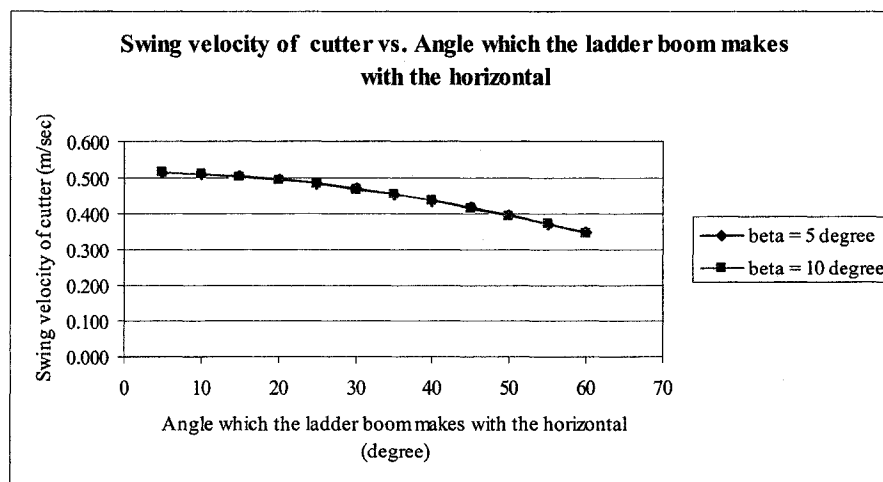


Figure 4.6 Swing velocity of cutter and the angle between ladder boom and horizontal (Swing velocity of the ladder = 0.035 m/sec)

Table 4.1 Variations in translatory velocity of cutter

β (deg)	v_{swing_ladder} (m/sec)	v_{swing_cutter} (Min) (m/sec)	v_{swing_cutter} (Max) (m/sec)	Variation (m/sec)
5	0.035	0.346	0.513	0.167
10	0.035	0.344	0.511	0.167
5	0.18	1.78	2.64	0.86
10	0.18	1.77	2.63	0.86

The cutter blade trajectories under various operating conditions during ‘overcutting’ and ‘undercutting’ are presented next. The location of the point of intersection of the successive cutter blade trajectories determines the chances of formation of the soil wedge during cutter rotations. It also determines the height of the soil ridge formed during excavation. The soil ridge height is defined as the perpendicular distance between the point of intersection of the successive cutter blade trajectories and the straight line joining the lower culmination points of the cutter blade trajectories. The ridge height is shown as h_{ridge} [m] in Figure 4.3. The height of the soil ridge must be kept to a minimum, resulting in a relatively smooth excavated surface and efficient loosening production. The maximum allowable ridge height was assumed as 10 cm for the designed vehicle ‘Golden Tortoise’.

The values of the different variables used for the simulations in the ‘overcutting’ mode and the respective figure numbers are presented in Table 4.2.

Table 4.2 Parameters for cutter blade trajectories during overcutting

$$\alpha = 30^\circ, \alpha_{swing} = 30^\circ, \beta = 10^\circ, \gamma_{ladder} = 10^\circ$$

Parameters						Figure number
Hydraulic oil flow [m ³ /sec]	rpm_{cutter} [-]	z_{blade} [-]	h_{cut} [m]	Ω_{cutter} [rad/sec]	v_{swing_cutter} [m/sec]	
2.0000e-004	50	3	0.1000	5.23	2.40	Figure 4.7(a)
2.0000e-004	90	4	0.2000	9.42	2.40	Figure 4.7(b)
5.0000e-005	50	2	0.1000	5.23	0.60	Figure 4.7(c)
5.0000e-005	90	3	0.2000	9.42	0.60	Figure 4.7(d)

Figure 4.7 shows that the number of blades in a row z_{blade} [-] as well as the ratio between the rotary and translatory velocities of the cutter $\left(\lambda_{cutter} = \frac{v_{cutter}}{v_{swing_cutter}} \right)$ [-] determines the thickness of the soil wedge generated as well as the height of the soil ridge formed. Thinner soil

wedges help to create easy gathering and mixing processes. Increase of the number of blades in a row will produce thinner soil wedges.

The ratio λ_{cutter} for Figure 4.7 (a) is 0.63, that for Figure 4.7 (b) is 1.14, that for Figure 4.7 (c) is 2.53 and that for Figure 4.7 (d) is 4.55. For the given operating conditions in Table 4.2, the ratio λ_{cutter} should be > 0.63 , in order to have soil ridge height lower than 50 cm. Increase in the number of blades lowers the soil ridge height, but the number of blades which can be attached in a row depends on the diameter of the cutter. A maximum of three blades can be attached in a row for the designed cutter installed to the prototype vehicle (Figure 2.11 and 2.18). For the cutter installed on the prototype vehicle with three blades in a row and with the translatory velocity of the cutter (v_{swing_cutter}) varying from 0.6 to 2.4 m/sec, the ratio $\lambda_{cutter} > 1.00$ should be maintained during 'overcutting' in order to keep the soil ridge height < 10 cm. The value of λ_{cutter} must be optimized in order to have maximum loosening production in a particular soil type without any waste of the cutter power available.

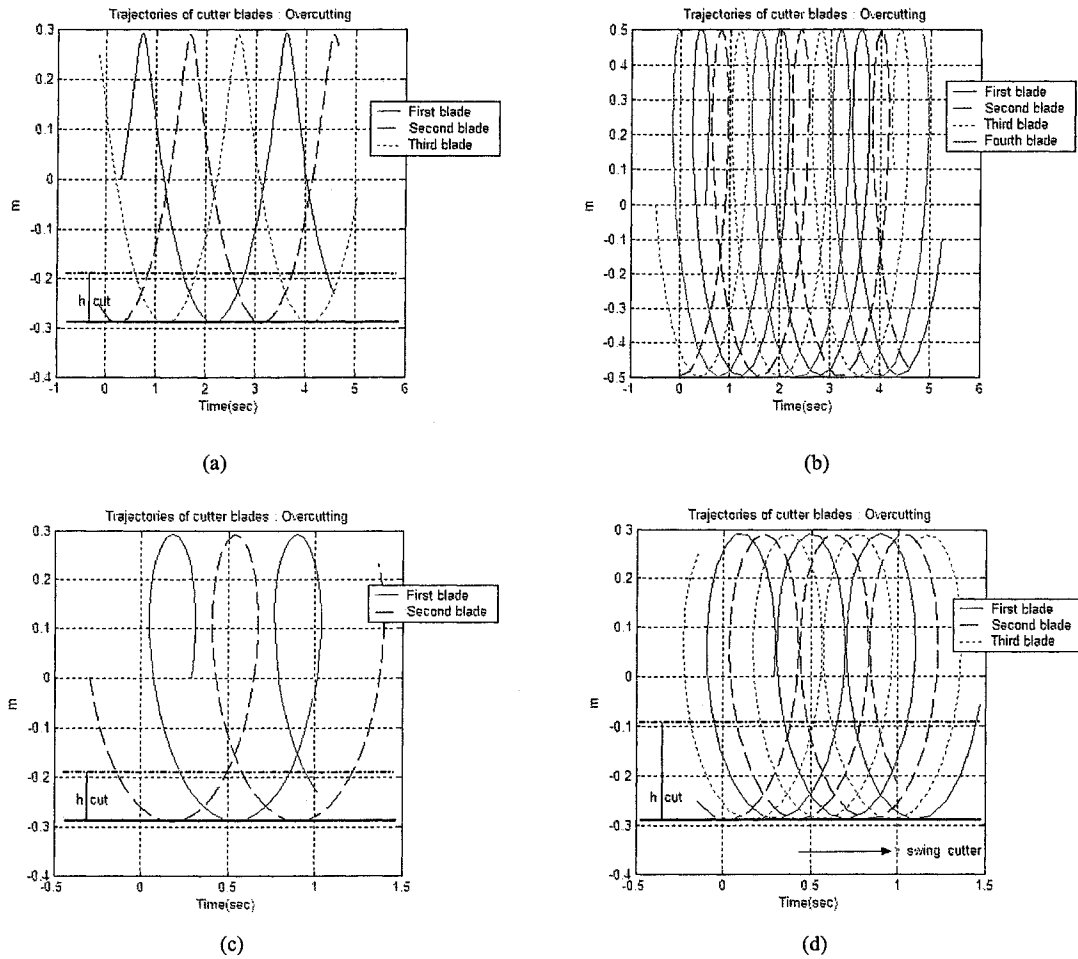


Figure 4.7 Cutter blade trajectories during ‘overcutting’

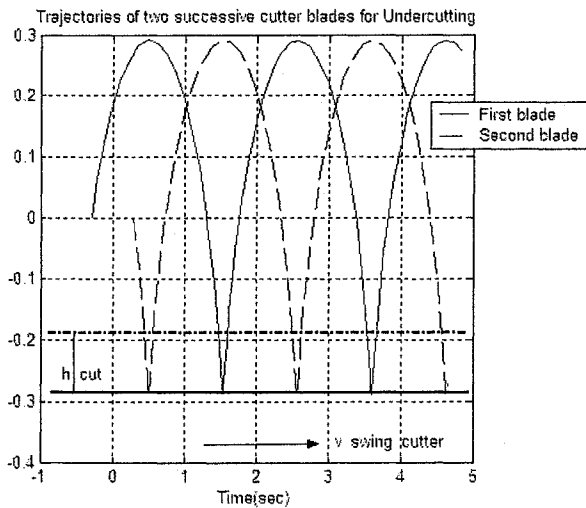
The cutter blade trajectories for ‘undercutting’ are presented next. The values of the different variables used for the simulations in the ‘undercutting’ mode and the respective figure numbers are presented in Table 4.3.

In order to form the soil wedge during undercutting, the limiting value for the translatory velocity of the cutter (v_{swing_cutter}) is ≤ 0.6 m/sec for the prototype cutter. The cutter rpm can be varied from 50 to 90. In order to increase the swing velocity of the designed cutter, the radius of the cutter needs to be increased. The value of λ_{cutter} when soil wedge formation takes place (Figure 4.9 (b) and (c)) are 2.53 and 4.55 respectively.

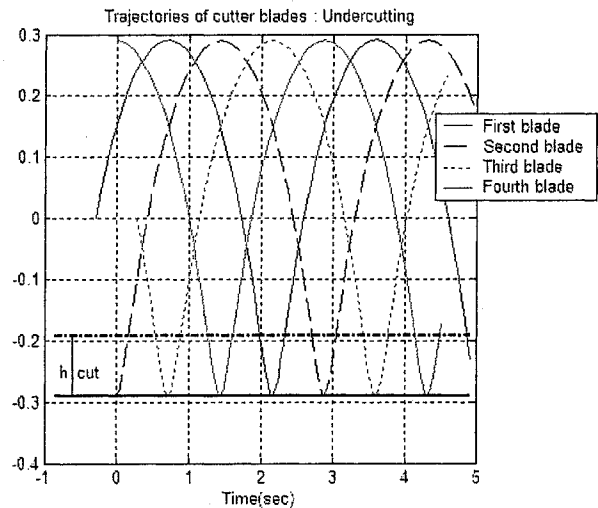
Table 4.3 Parameters for cutter blade trajectories during undercutting

$$\alpha = 30^\circ, \alpha_{swing} = 30; \beta = 10; \gamma_{ladder} = 10^\circ$$

Parameters						Figure number
Q_{shc_ladder} [m ³ /sec]	rpm_{cutter} [-]	z_{blade} [-]]	h_{cut} [m]	Ω_{cutter} [rad/sec]	v_{swing_cutter} [m/sec]	
2.0000e-004	90	2	0.1000	9.42	2.40	Figure 4.8(a)
2.0000e-004	50	4	0.1000	5.23	2.40	Figure 4.8(b)
1.0000e-004	90	3	0.2000	9.42	1.20	Figure 4.9(a)
5.0000e-005	50	3	0.2000	5.23	0.60	Figure 4.9(b)
5.0000e-005	90	3	0.2000	9.42	0.60	Figure 4.9(c)



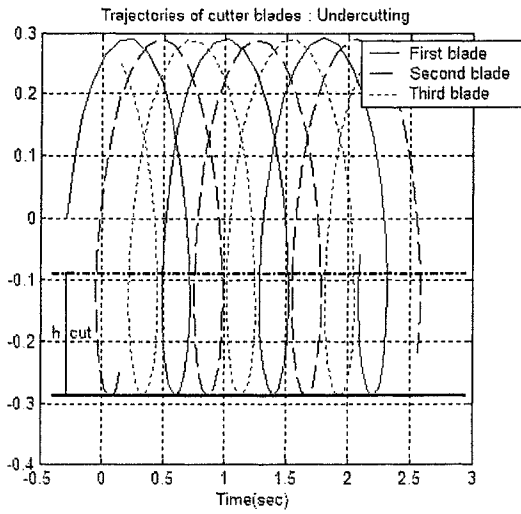
(a)



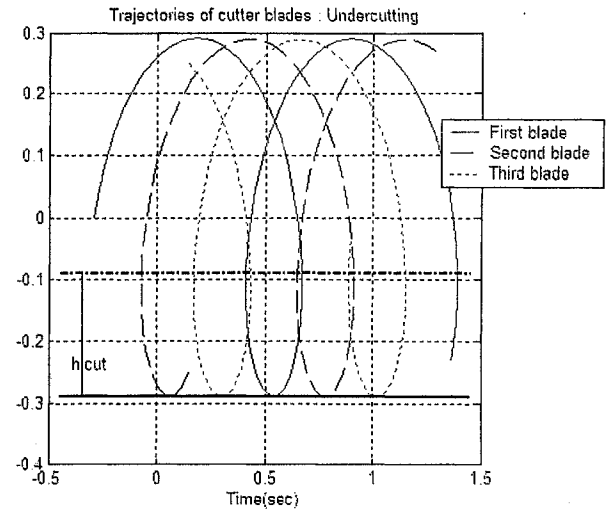
(b)

Figure 4.8 Cutter blade trajectories during ‘undercutting’

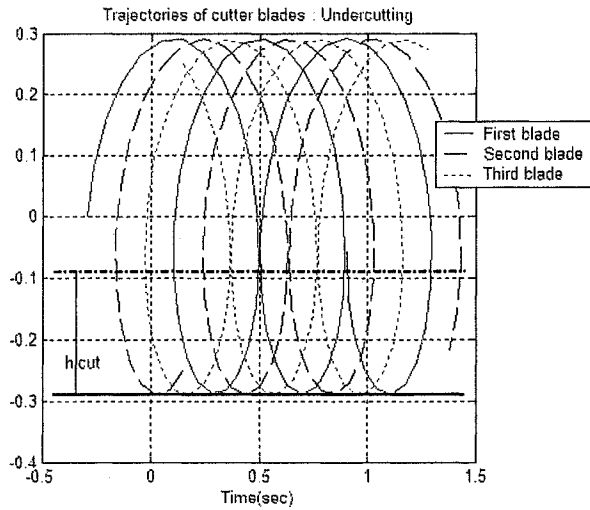
The swing velocity of the leading and trailing cutters must be equal. For efficient gathering, the leading cutter performs ‘overcutting’ while the trailing cutter performs ‘undercutting’. The lower value of the limiting translatory velocity of the leading and trailing cutter must be used while operating the prototype vehicle.



(a)



(b)



(c)

Figure 4.9 Cutter blade trajectories during ‘undercutting’

In order to estimate the loosening production for the designed drum cutter, the translatory velocity of the cutter (v_{swing_cutter}) was thus assumed as 0.6 m/sec, while the cutter rpm was varied from 50 to 90. The depth of cut was assumed to be 0.1 and 0.2 m. The number of cutter blades in a row was considered to be 3, while the number of rows of cutter blades was also

assumed to be 3. The loosening productions calculated by the methods of area integration and feed of cutter, for a single drum cutter during ‘overcutting’ are shown in Tables 4.4 and 4.5.

Table 4.4 Loosening production calculated by the method of area integration

Depth of cut = 0.1 m		
Cutter rpm (-)	Area of soil wedge (m ² /sec)	Loosening production (m ³ /hr)
50	0.042	79.56
60	0.033	74.88
70	0.026	69.12
80	0.021	64.80
90	0.018	59.40
Depth of cut = 0.2 m		
Cutter rpm (-)	Area of soil wedge (m ² /sec)	Loosening production (m ³ /hr)
50	0.091	172.08
60	0.073	165.60
70	0.060	159.12
80	0.051	154.44
90	0.043	148.68

Table 4.5 Loosening production calculated by the method of feed of cutter

Depth of cut = 0.1 m		
Cutter rpm (-)	Area of soil wedge (m ² /sec)	Loosening production (m ³ /hr)
50	0.0240	45.38
70	0.0172	45.38
90	0.0133	45.38
Depth of cut = 0.2 m		
Cutter rpm (-)	Area of soil wedge (m ² /sec)	Loosening production (m ³ /hr)
50	0.0480	90.77
70	0.0343	90.77
90	0.0267	90.77

It is observed from Table 4.5, that when the loosening production is estimated from the feed of the designed cutter and the depth of cut, the variation in loosening production due to the change in the cutter rpm is not detected. The method of area integration however shows the variation in the loosening production as a function of the cutter rpm.

4.3 Gathering Production

Gathering production (P_{gather}) [m³/sec] is defined as the volume of soil entering the suction mouth for further transportation by the pump-pipeline system.

In crown cutters the gathering action is performed by the combined effect of the cutter and the suction force generated by the centrifugal dredge pump. The gathering action is primarily performed by the suction force generated by the dredge pump in case of the designed excavation system. The suction influence zone is established in front of the suction mouth. The soil loosened by the drum cutters must fall within the suction influence zone in order to be picked up by the suction mouth for transportation to the surface through the delivery pipeline. The trajectory of motion and the velocity of the soil lumps/ particles are thus very important in determining the probability of the soil lumps/ particles being picked up by the suction mouth. The forces acting on the soil lump/ particle ejected by the drum cutter into water were identified. A two-dimensional mass-damper model was formulated to predict the soil lump/ particle trajectory and the velocity as a function of time. When the velocity of the ejected soil lump/ particle is less than the settling velocity, the particle settles back on the soil-water interface. The suction influence zone was established for the designed excavation system based on the work of Apgar [1973]. The position of the soil lump/ particle was compared with the position of the suction mouth and the velocity of the soil lump/ particle was compared with the suction velocity in order to determine the chances of the soil particle being picked up by the suction mouth. The percentage of spillage was estimated for the designed drum cutter as a function of the radius and rotational velocity of the cutter and the suction velocity of the centrifugal dredge pump. Prediction of the spillage helped in estimating the gathering production of the suction mouth and thus the delivery production at the delivery end of the pipeline.

4.3.1 Assumptions made for Gathering Production

The assumptions made for the estimation of the gathering production were 1) soil wedge loosened was homogeneous and uniform in nature and was of constant density, 2) soil wedge

was disintegrated into discrete lumps/ particles when thrown in the water by the cutter, 3) granular and partly cohesive soils were considered for the model, where formation of discrete lumps/ particles is common, 4) interactions between soil lumps/ particles and the surrounding water was neglected, 5) soil and water were considered non-elastic and incompressible, thus eliminating the spring factors from the model developed, 6) resultant velocity v_r [m/sec] (a function of the rotational velocity and the translatory velocity of the cutter), with which the soil lumps/ particles leaves the cutter was known, 7) angle which the tangential velocity of the cutter due to cutter rotation makes with the horizontal was known, and 8) initial distance between the soil lump/ particle and the origin of a fixed reference frame was known at the time of emergence into water.

4.3.2 Forces Acting on the Soil Lump/ Particle

The forces acting on a soil lump/ particle loosened by a cutter determine the trajectory of motion and the velocity of the same. The dominant forces acting on relatively large soil particles in a crown cutter are the gravitational force, the centrifugal force and the suction force [Burger et al., 1999]. The dominant forces identified to act on the soil lump/ particle formed by the disintegration of the soil wedge loosened by the designed drum cutter are shown in Figure 4.10.

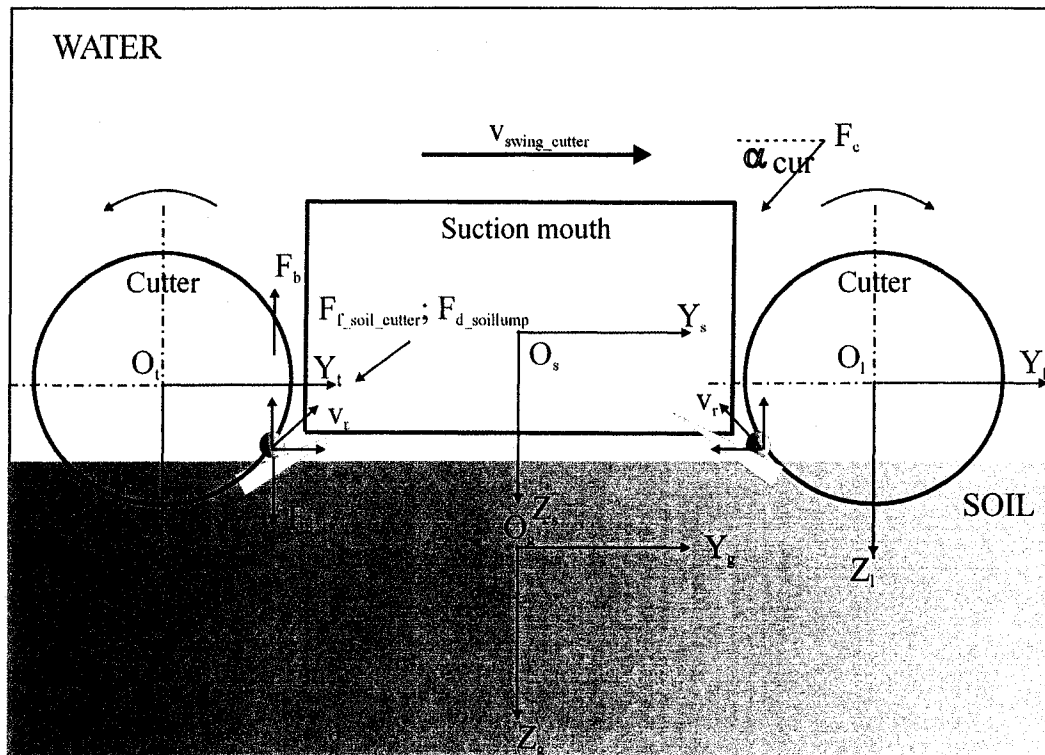


Figure 4. 10 Forces acting on a soil lump/ particle

The forces include 1) frictional force ($F_{f_soil_cutter}$) [kN] between the soil lump/ particle and the cutter blade, acting along the direction of the resultant velocity (v_r) [m/sec] but opposing the motion, 2) drag force ($F_{d_soillump}$) [kN], acting along the direction of the resultant velocity (v_r) [m/sec] but opposing the motion, 3) current force (F_{cur}) [kN], acting at an angle α_{cur} with the horizontal, 4) gravitational force (F_g) [kN], acting in a vertically downward direction, and 5) buoyancy force (F_b) [kN], acting in a vertically upward direction. All the forces were resolved in the Y and Z directions and the equations of motions were obtained for the Y and Z directions (Figure 4.10).

An arbitrary frame $\{O_s\}$ was attached to the mid point of the suction bell mouth. Two other frames $\{O_l\}$ and $\{O_t\}$ were attached to the centers of the leading and trailing cutters. An arbitrary ground frame $\{O_g\}$ is attached to the soil, whose origin lies in the same line as the origin of the frame $\{O_s\}$. The frame $\{O_s\}$ is a translating frame with respect to the ground frame $\{O_g\}$. The frames $\{O_l\}$ and $\{O_t\}$ are translating as well as rotating with respect to the ground frame $\{O_g\}$. The translation motions of the frames $\{O_l\}$, $\{O_t\}$ and $\{O_s\}$ with respect to the ground frame $\{O_g\}$ determine the position of the cutter centers and the suction mouth with time.

The resultant velocity with which the soil lump/ particle emerges into the water was derived,

$$v_{r,i} = \sqrt{\left(v_{swing_cutter}\right)^2 + \left(v_{cutter,i}\right)^2 + 2 * \left(v_{swing_cutter} * v_{cutter,i} * \cos(\psi)\right)} \quad \text{[Equation 4.11]}$$

where, i is the subscript for the leading or trailing cutter [-], $v_{cutter,i}$ is the tangential velocity of the cutter due to cutter rotation [m/sec], where $v_{cutter,i} = \Omega_{cutter,i} * R_{cutter}$ and ψ is the angle between the tangential velocity of the cutter and the horizontal [degree].

The angle which the resultant velocity (v_r) [m/sec] makes with the horizontal (θ_r) [degree] was deduced as follows,

$$\tan(\theta_r) = \frac{v_{cutter,i} * \sin(\psi)}{v_{swing_cutter} + v_{cutter,i} * \cos(\psi)} \quad \text{[Equation 4.12]}$$

The mass of a spherical soil lump/ particle ($m_{soillump}$) [kg] was obtained,

$$m_{soillump} = \frac{4}{3}\pi * (R_{soillump})^3 * \rho_{soil} \quad [\text{Equation 4.13}]$$

where, $R_{soillump}$ is the radius of the soil lump/ particle [m] and ρ_{soil} is the density of soil [kg/m³].

Gravitational and Buoyancy Forces

The gravitational and buoyancy forces (F_g and F_b) [kN] acting on the soil lump/ particle are given respectively,

$$F_g = m_{soillump} * g$$

$$F_b = \frac{4}{3}\pi (R_{soillump})^3 * \rho_{fT} * g \quad [\text{Equation 4.14}]$$

where, ρ_{fT} is the density of water at T °C [kg/m³].

Frictional Force

The frictional force acting between the soil and the blade $F_{f_soil_cutter}$ [kN] is,

$$F_{f_soil_cutter} = \mu_{soil_blade} * (F_g - F_b) * \cos(\theta_r) \quad [\text{Equation 4.15}]$$

where, μ_{soil_blade} is the coefficient of friction between the soil and the blade [-].

Drag and Current Force

The drag force acting on the soil lump/ particle $F_{d_soillump}$ [kN] is as follows,

$$F_{d_soillump} = \frac{1}{2} \rho_{fT} C_{d_fa} A_{fa} (v_r)^2 \quad [\text{Equation 4.16}]$$

The current force F_{cur} [kN] is deduced,

$$F_{cur} = \frac{1}{2} \rho_{fT} C_{d_fa} A_{fa} (v_{cur})^2 \quad [\text{Equation 4.17}]$$

where, A_{fa} is the projected frontal area of the spherical soil lump/ particle [m^2], C_{d_fa} is the drag co-efficient based on projected frontal area [-], and v_{cur} is the velocity of current [m/sec].

Equations of Motion

The equation of motion in the Y direction,

$$m_{soillump} \ddot{y} - F_{f_soil_cutter} \cos(\theta_r) - \left(\left(\frac{1}{2} \rho_{fT} C_{d_fa} A_{fa} \right) (v_r \cos(\theta_r) + v_{cur} \cos(\alpha_{cur})) \right) \dot{y} = 0 \quad [\text{Equation 4.18}]$$

The equation of motion in the Z direction,

$$m_{soillump} \ddot{z} - \left(\left(\frac{1}{2} \rho_{fT} C_{d_fa} A_{fa} \right) (v_r \sin(\theta_r) + v_{cur} \sin(\alpha_{cur})) \right) \dot{z} - \pi (R_{soillump})^2 g (\rho_{soil} - \rho_{fT}) z = 0 \quad [\text{Equation 4.19}]$$

The trajectory and the velocity of the soil lump/ particle are obtained by solving equations 4.18 and 4.19.

4.3.3 Suction Influence Zone

The suction velocity generated by the centrifugal dredge pump decreases with the increase in horizontal as well as vertical distances from the suction pipe or the suction bell mouth. The suction influence zone is defined by the velocity profile in front of the suction pipe or suction bell mouth. The suction velocity within the suction influence zone will be sufficient enough to suck in the excavated material for further transportation by the dredge pipeline system.

In order to establish the suction influence zone in front of the designed suction mouth, it was assumed that the ladder assembly together with the suction mouth and the twin drum cutter module was swinging with a velocity equal to the swing velocity of the ladder assembly (v_{swing_ladder}) [m/sec]. The size and velocity of the soil lump/ particle ejected into water by the cutter determine whether it will remain suspended or settle on the soil/ water interface. The suction velocity at the suction mouth as well as at the suction pipe must be greater than the settling velocity of the soil lump/ particle.

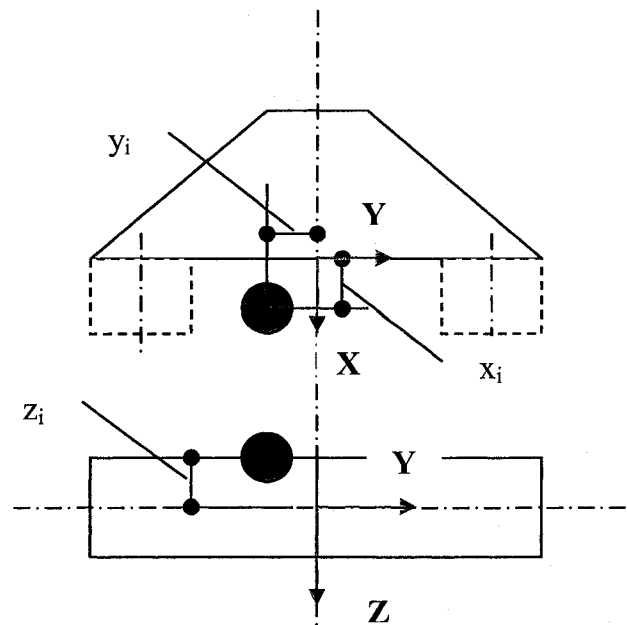


Figure 4.11 Soil particle position with respect to suction mouth (Top Plan view, Bottom Front view)

The suction velocity at the suction pipe entry $v_{pipe_suc_entry}$ [m/sec] is,

$$v_{pipe_suc_entry} = \frac{Q_m}{\left(\frac{\pi}{4} * (D_{pipe_suc})^2\right)} \quad \text{[Equation 4.20]}$$

The equivalent pipe diameter for the suction mouth of rectangular cross section (D_{eq_sm}) [m] was calculated,

$$D_{eq_sm} = \sqrt{\frac{4}{\pi} * (L_{sm} * B_{sm})} \quad [\text{Equation 4.21}]$$

The velocity at the suction mouth was estimated,

$$v_{sm} = \frac{Q_m}{\left(\frac{\pi}{4} * (D_{eq_sm})^2\right)} \quad [\text{Equation 4.22}]$$

The condition for the soil lump/ particle to be picked up by the suction mouth was given,

$$v_{sm} \geq a_{sm} * v_{setl_maxsize} \quad [\text{Equation 4.23}]$$

and

$$(v_{pipe_suc_entry}) \geq (v_{setl_maxsize}) \quad [\text{Equation 4.24}]$$

where, a_{sm} is a factor dependent on the grating at suction mouth entry, surface finish etc.[-], B_{sm} is the width of suction mouth [m], D_{pipe_suc} is the diameter of suction pipe [m], L_{sm} is the length of suction mouth [m], Q_m is the mixture flow rate [m³/sec], $v_{pipe_suc_entry}$ is the suction velocity at the suction pipe entry [m/sec], $v_{setl_maxsize}$ is the settling velocity of the largest diameter soil lump/ particle [m/sec], and v_{sm} is the velocity at the suction mouth [m/sec].

The flow velocity of the water into the suction pipe decreases rapidly as the distance to the suction mouth increases [Apgar, 1973]. The suction influence zone for a circular suction pipe was plotted based on the work of Apgar [1973]. The ratio between the flow velocity of the material into the suction mouth (v_o) and the swing velocity of the ladder assembly

(v_{swing_ladder}) is plotted against the ratio between distance of the particle from centre of the suction mouth in horizontal direction (r) [m] and diameter of suction pipe (D_{pipe_suc}) [m]. The vertical distance of the suction mouth from the soil bed is denoted by a [m]. This plot is shown in Figure 4.12. Exponential trend lines were fitted to these plots. The R^2 values varied from 0.975 to 0.996. The fitted equations for

$$\frac{a}{D_{pipe_suc}} = 0.1 \text{ is } y = 0.002e^{0.4792x} \quad \text{[Equation 4.25]}$$

$$\frac{a}{D_{pipe_suc}} = 1 \text{ is } y = 0.0025e^{0.3727x} \quad \text{[Equation 4.26]}$$

$$\frac{a}{D_{pipe_suc}} = 2 \text{ is } y = 0.0026e^{0.2337x} \quad \text{[Equation 4.27]}$$

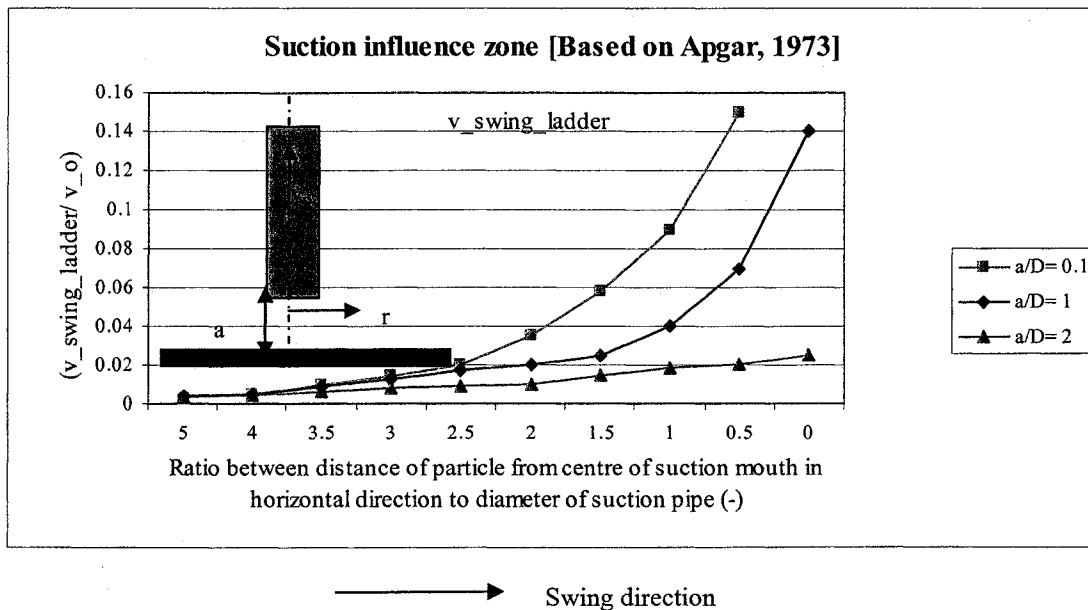


Figure 4.12 Suction influence zone[Based on Apgar, 1973]

Equations 4.25, 4.26 and 4.27 were used to establish the suction influence zone in front of the designed suction mouth.

4.3.4 Spillage

The spillage is given as [Vlasblom, 1999; den Burger et al., 1999],

$$Spillage = \left[1 - 0.4 * \frac{v_{sm}}{R_{cutter} * \Omega_{cutter}} \right] \quad \text{[Equation 4.28]}$$

The relationship between the loosening production (P_{loose}) [m^3/sec] and gathering (P_{gather}) [m^3/sec] or suction production is [Vlasblom, 1999],

$$P_{loose} = \frac{P_{gather}}{Spillage} \quad \text{[Equation 4.29]}$$

4.3.5 Results and Discussion for Gathering Production

The results showing the soil lump/ particle trajectory and velocity when ejected into water by the leading and trailing cutters in Z and Y directions (Figure 4.10) are shown next. In the following figures the trajectory of the soil lump/ particle is represented by the solid line and the velocity by the dashed line. Leading is the cutter which is leading in the swing direction and is performing ‘overcutting’. Trailing cutter is the cutter following the leading cutter and is performing ‘undercutting’. The leading and the trailing cutters were given different rpm, in order to observe the difference in the soil lump/ particle trajectories and velocities for the two cutters. Each cutter can be controlled separately and thus can be given different rpm.

The values of the different parameters used for simulation are given in Appendix 12. The soil lumps/ particles were assumed as spherical. The angle between the tangential velocity of the cutter ($v_{cutter} = R_{cutter} * \Omega_{cutter}$) [m/sec] and the horizontal was assumed to be equal for the leading and trailing cutters. Two different soil lump/ particle sizes were considered for the simulations with diameters of 2 mm and 20 mm. The simulation results for the leading and

trailing cutters showing the soil lump/ particle trajectory and velocity in the Z direction are shown in Figure 4.13 and 4.14.

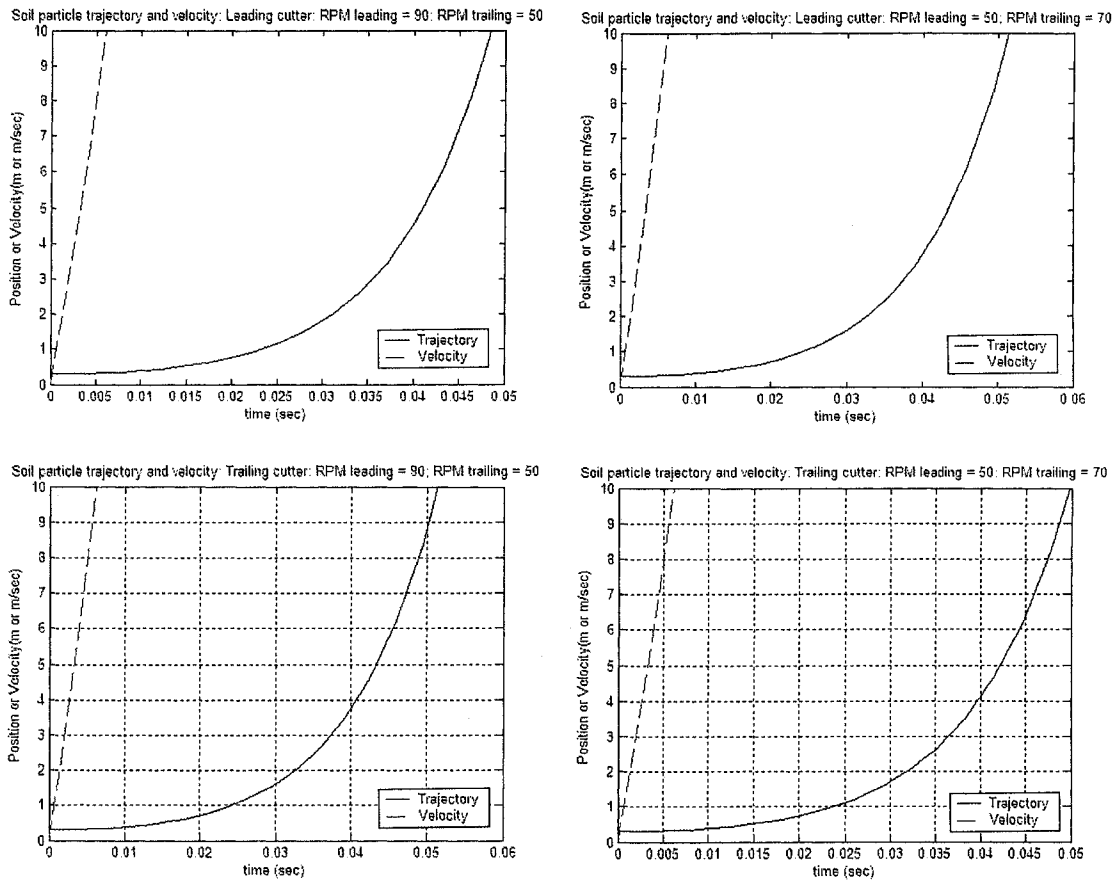


Figure 4. 13 Soil lump/particle trajectory and velocity with diameter of soil lump/ particle = 2 mm in the Z direction

It is observed from Figure 4.13 and Figure 4.14 that smaller soil lumps/ particles leave the suction influence zone much faster than the larger ones. The position or velocity values represent the upward position or velocity values of the soil particles/ lumps from the soil/ water interface in the Z direction. The terminal settling velocity of the soil particle with diameter 2 mm is 0.004 m/sec and the terminal settling velocity of the soil particle/ lump with diameter 20 mm is 0.359 m/sec. The terminal settling velocity of the soil lump/ particle was obtained by using the Stokes equation. The velocity of the soil lump/ particle in the Z direction is much higher than the

terminal settling velocity of the same. The chances of the soil lump/ particle being picked up by the suction mouth is most when the soil lumps/ particles are within a distance of the width of the suction mouth in the Z direction.

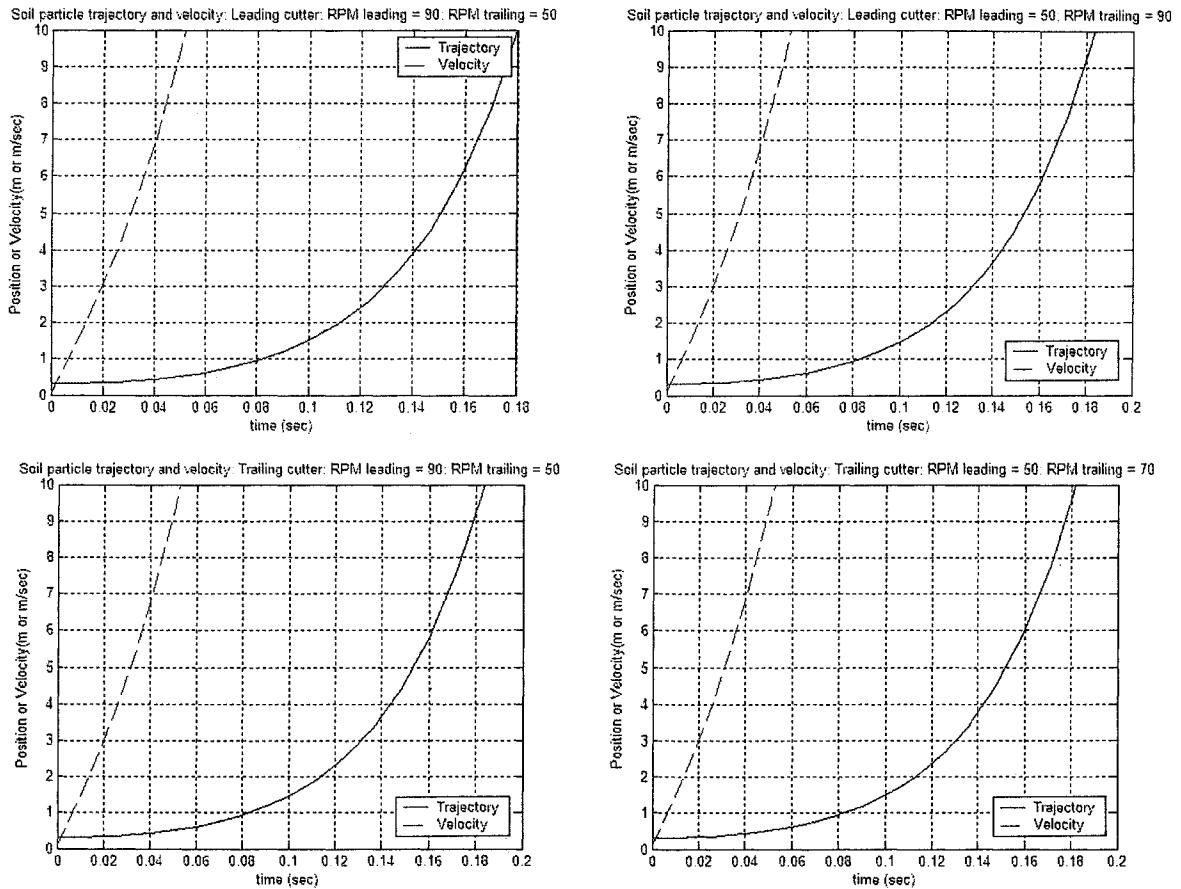


Figure 4.14 Soil lump/ particle trajectory and velocity with diameter of soil lump/ particle = 20 mm in the Z direction

The positions and velocities of the soil lump/ particle with respect to the suction mouth and the cutters in the Y direction were also determined, which are shown in Figure 4.15 and Figure 4.16. The simulations were carried out for both the leading and trailing cutters. In all the Figures 4.13 to 4.17, the initial condition for the position of the soil lump/ particle was defined with respect to the arbitrary fixed reference frame $\{O_g\}$.

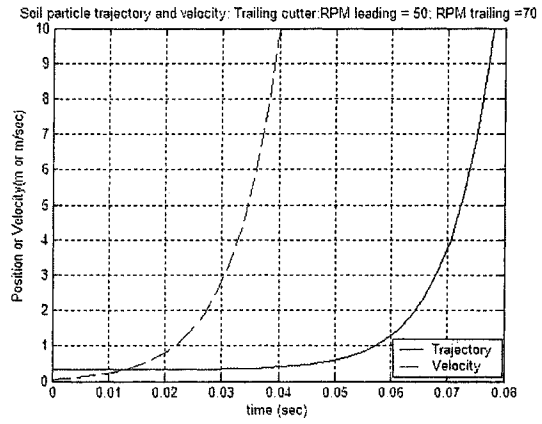
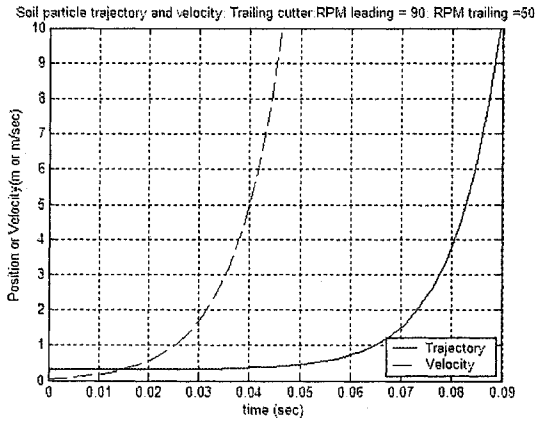
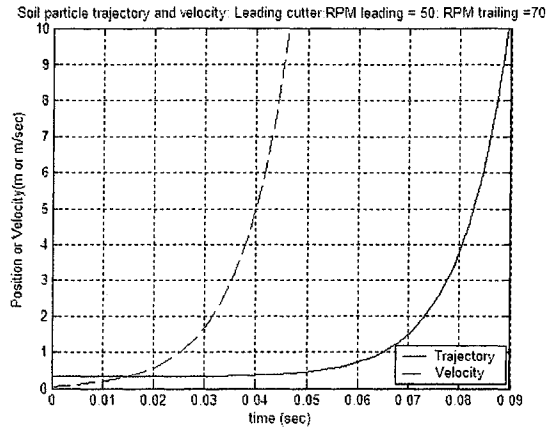
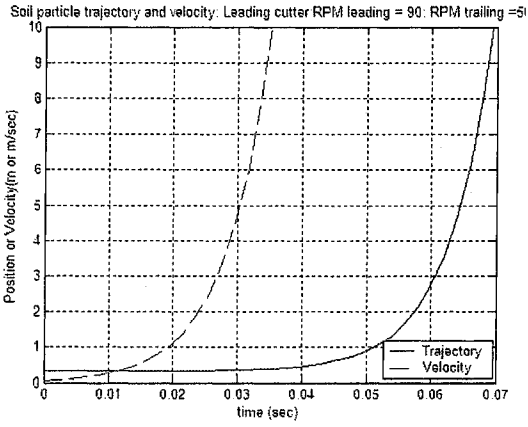


Figure 4. 15 Soil lump/ particle trajectory and velocity with diameter of soil lump/ particle = 2 mm in the Y direction

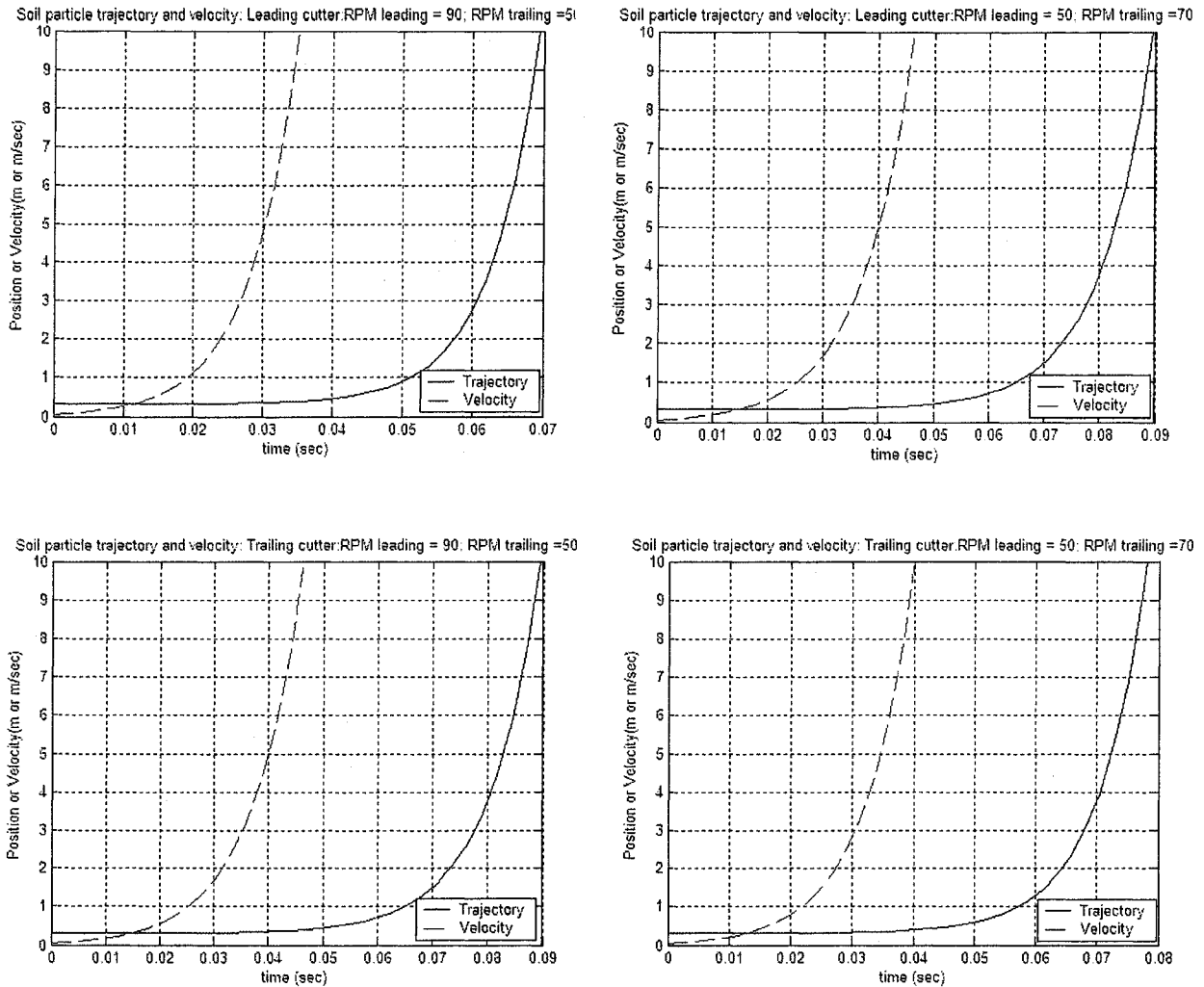


Figure 4. 16 Soil lump/ particle trajectory and velocity with diameter of soil lump/ particle = 20 mm in the Y direction

The positions of the centers of the suction mouth, the leading and the trailing cutters with respect to the arbitrary fixed reference frame $\{O_g\}$ are shown in Figure 4.17. The slopes of the three lines represented in Figure 4.17 represent the swing velocity of the ladder assembly. The figure shows that, if the soil lump/ particle ejected by the leading or trailing cutter stays for a period of 2 seconds within a distance of the length of the suction mouth in the Y direction and within the width of the suction mouth in the Z direction, it has the chance of being picked up by the suction mouth. The soil lumps/ particles considered in Figure 4.13 to Figure 4.16 must be picked up

within 0.01 to 0.02 seconds after they are ejected into the surrounding water by the leading and trailing cutters. The suction velocity however must be greater than the settling velocity of the soil lump/ particle.

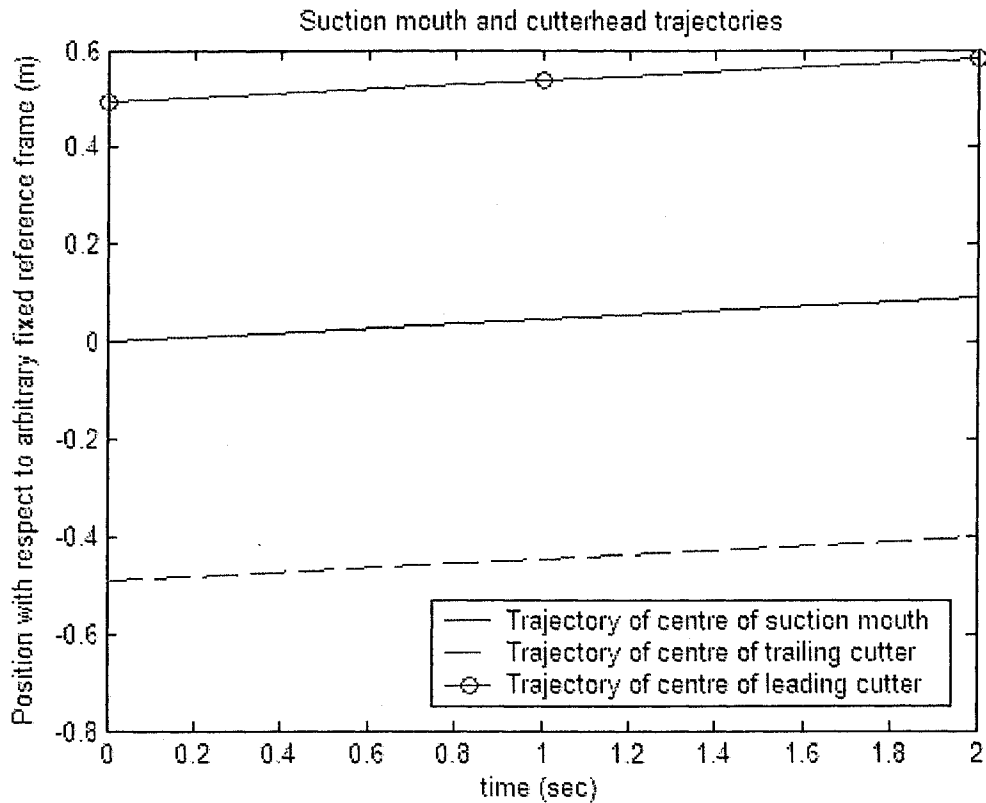


Figure 4. 17 Position of centers of suction mouth, leading and trailing cutters

The flow velocity into the suction mouth was plotted as a function of the distance from the centre line of the suction mouth (Figure 4.18). Such plots were based on the work of Apgar [1973] as discussed in section 4.3.3. Apgar assumed a vertical pipe of circular cross-section, positioned above the soil bed. For the designed suction mouth of rectangular cross section with rounded corners, the equivalent diameter of the suction mouth represents the diameter of the pipe as used by Apgar. The designed suction mouth is trapezoidal in plan view. The suction pipe is parallel to the soil bed in case of Apgar’s work. For the designed suction mouth, though the suction mouth

has different inclinations, the agitated material and the suction zone are always parallel to the transverse section of the suction mouth. Hence the use of Apgar's work in developing the parametric model is justified.

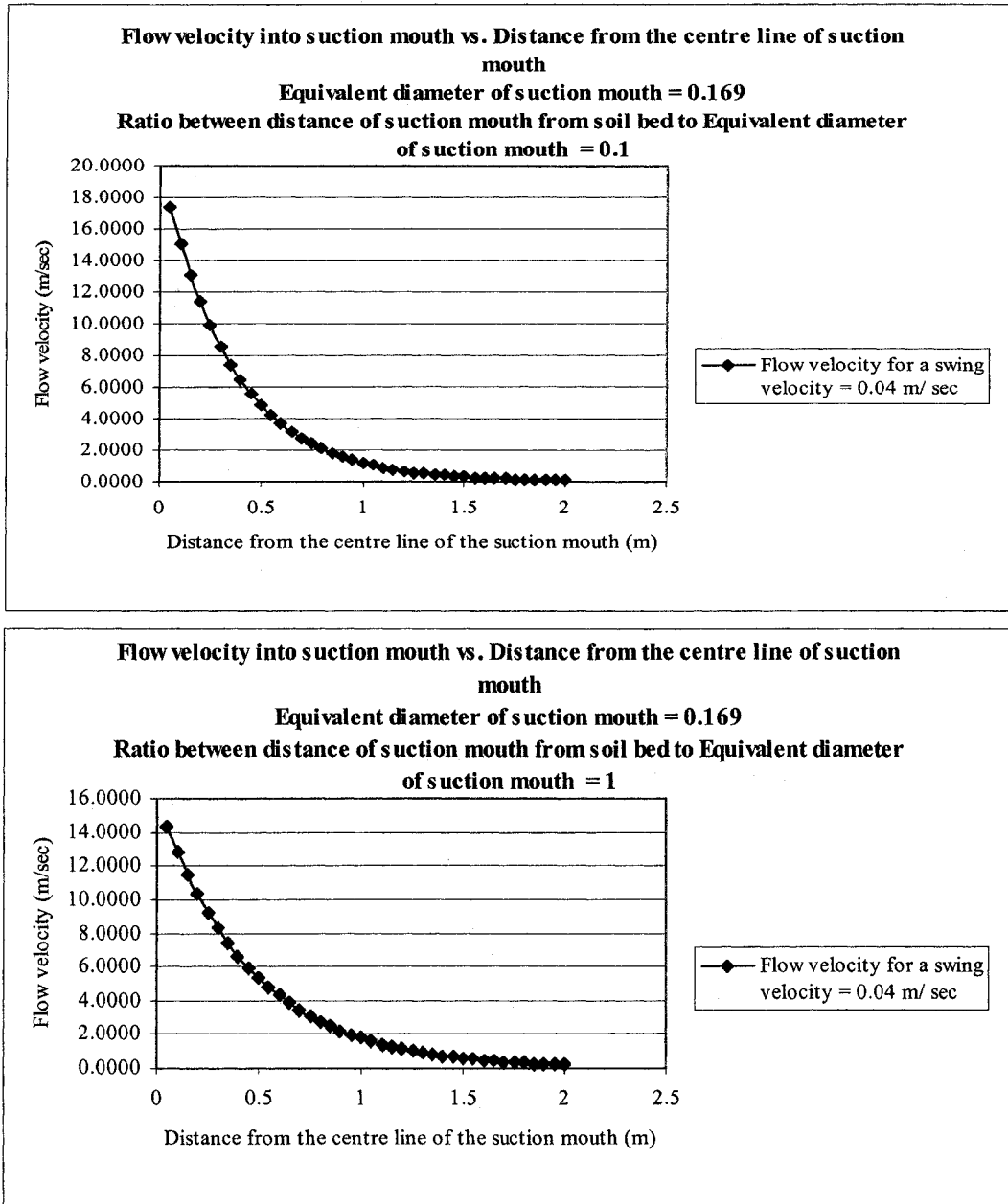


Figure 4. 18 Suction influence zone in front of the suction mouth of rectangular cross section

The flow velocity at a distance of 0.5 m from the centre of the suction mouth is close to 4 m/sec, which is greater than the settling velocities of the soil lump/ particle concerned. Hence they will be picked up by the suction mouth. The length of the suction mouth in the Y direction is 0.3 m and the width of the suction mouth in the Z direction is 0.075 m. This parametric model represents a very basic model and further work needs to be done on this model to more accurately predict the soil lump/particle trajectory and velocity.

The percentage of spillage for the designed drum cutter was estimated. The cutter diameter is 0.29 m and the suction velocity of the suction mouth was assumed as 2 m/sec. The cutter rpm was varied from 30 to 90. The results are presented in Table 4.6.

Table 4.6 Spillage percent as a function of cutter rpm

Cutter RPM	Spillage percent
30	0.12
40	0.34
50	0.47
60	0.56
70	0.62
80	0.67
90	0.71

4.4 Specific Energy

The excavation processes of granular non-cohesive soils under non-cavitating and cavitating conditions were discussed in Appendix 1.

The similarity between the blades of a crown cutter and the designed drum cutter blades is shown in Figure 4.19.

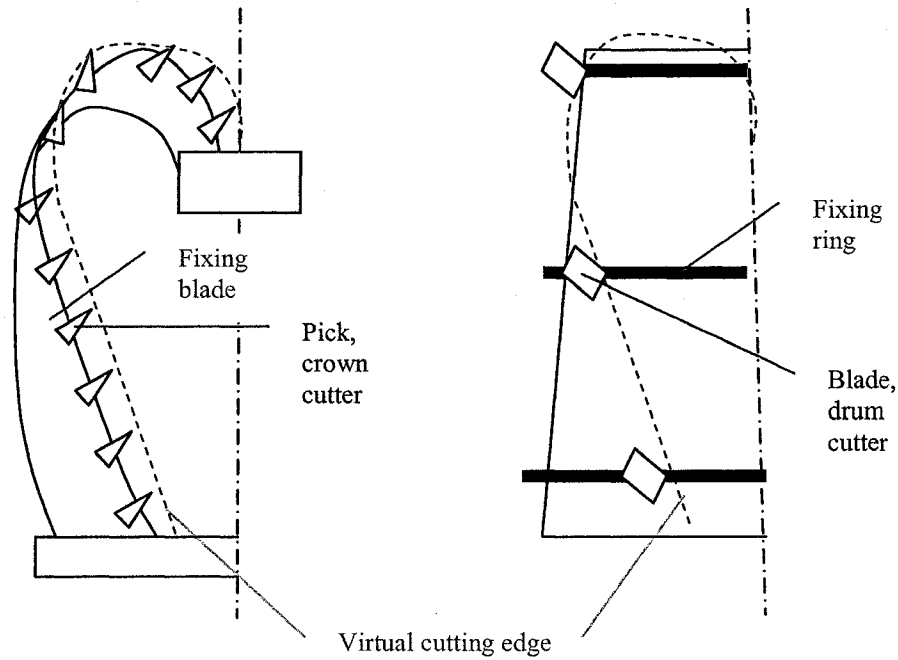


Figure 4.19 Similarity between crown cutter pick points and the virtual blades of drum cutter (Left Crown cutter, Right Drum cutter)

The specific energy requirement in case of non-cohesive granular material under non-cavitating condition $E_{s_gran_nc}$ [kJ/ m³] can be estimated as [Report: Paragon International bv, The Netherlands to EEM (P) Ltd., 1994],

$$E_{s_gran_nc} = 0.013 * (\rho_{rel_soil})^{1.15} * \frac{(v_{swing_ladder} * D_{cutter})}{(z_{blade} * k)} \quad \text{[Equation 4.30]}$$

The specific energy requirement in case of non-cohesive granular material under cavitating condition $E_{s_gran_c}$ [kJ/ m³] can be estimated as [Report: Paragon International bv, The Netherlands to EEM (P) Ltd., 1994],

$$E_{s_gran_c} = (1.8h_w + 17.6) * (\rho_{rel_soil})^{0.7} \quad \text{[Equation 4.31]}$$

where, D_{cutter} is the diameter of the cutter [m], ρ_{rel_soil} is the relative density of soil [%],

h_w is the depth of water or depth of operation [m], k is the permeability of soil [m/sec],

v_{swing_ladder} is the swing velocity of the ladder assembly [m/sec] and z_{blade} is the number of cutter blades or the number of pick lines in the horizontal direction [-].

The specific energy for cohesive soil E_{s_coh} [kJ/ m³] can be estimated by the following relationship, [Report: Paragon International bv, The Netherlands to EEM (P) Ltd., 1994]

$$E_{s_coh} = 307.15 \ln(S_u) - 880.46 \quad \text{[Equation 4.32]}$$

where, S_u is the undrained shear strength of cohesive soil [kPa]. This relationship is valid only for undrained shear strength values of $S_u < 300$ kPa.

The required average cutting power N_{cutter_av} [kW] is estimated [Vlasblom, 1999],

$$N_{cutter_av} = \frac{E_s}{P_{loose}} \quad \text{[Equation 4.33]}$$

where, E_s is the specific energy for a cutter in a given soil [kJ/ m³] and P_{loose} is the loosening production [m³/sec].

The cutting force is not constant during the excavation process. Hence the average cutting power N_{cutter_av} [kW] must be multiplied by several factors depending upon the material excavated and the cutter configuration.

Depending on the operating condition (irregularities in the soil conditions and the possible occurrence of different materials e.g. stones and other obstacles), the average cutter power required must be multiplied with a 'service factor' (a_{serv_cutter}) [-]. A service factor of 1.3 was chosen [EEM internal report, 1990]. Another factor which needs to be considered is the

'recirculation factor' (a_{rcrc_cutter}) [-] due to the extra energy required for recirculation of the excavated material within a drum cutter or around a rotavator cutter. In extreme cases it may be 50% to 60% of the average energy requirement as calculated (N_{cutter_av}) [kW] [EEM internal report, 1990]. A material factor (a_{soil_cutter}) [-] of 1.3 for excavating sand was chosen. The dredging service factors are mostly empirical and chosen on the basis of experiences and unpublished knowledge. There are scopes for their modifications.

So, the power required for actual cutting process (N_{cutter}) [kW] will be,

$$N_{cutter} = N_{cutter_av} * a_{serv_cutter} * a_{rcrc_cutter} * a_{soil_cutter} \quad \text{[Equation 4.34]}$$

The simulation results for specific energy and cutter power requirement for non-cohesive, granular and cohesive soils are presented in Figures 4.20 to 4.22.

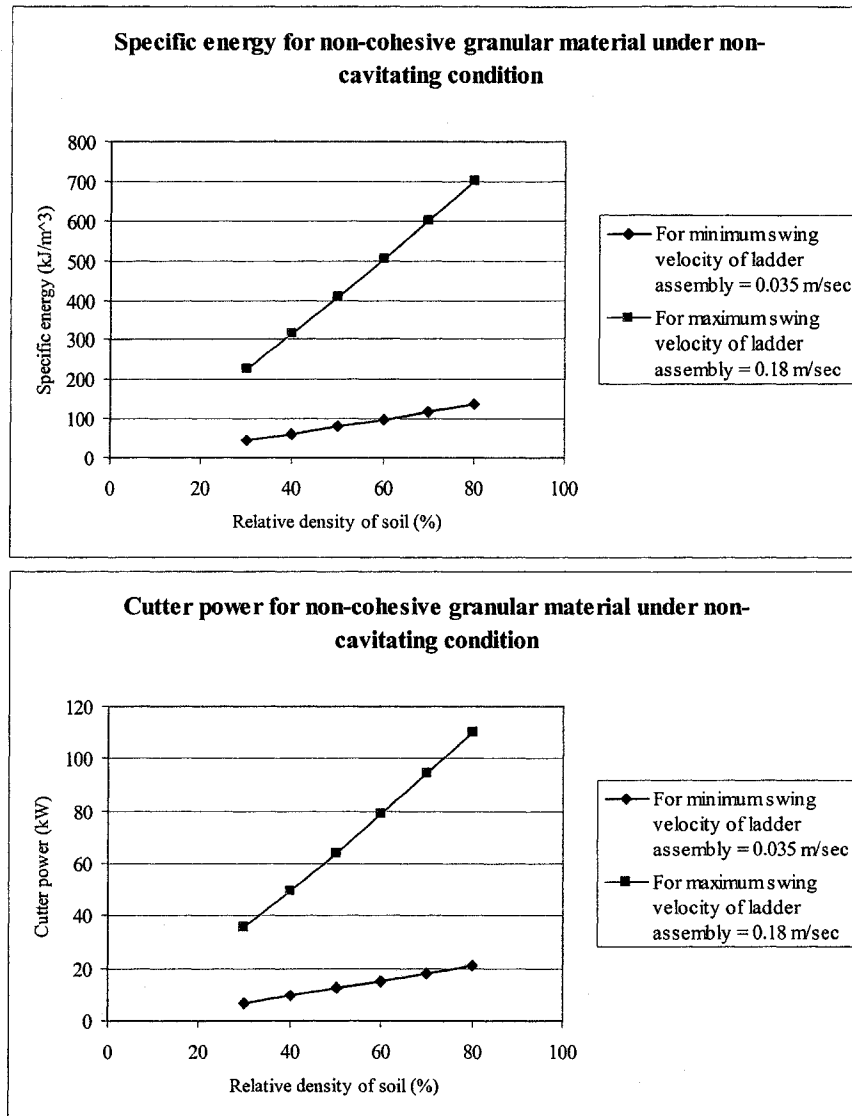


Figure 4. 20 Specific energy and cutter power for non-cohesive granular material under non-cavitating condition

The estimated cutter power required is too high. The cutter diameter needs to be increased in order to increase the excavation production. With increase in the excavation production, the required cutter power will be decreased.

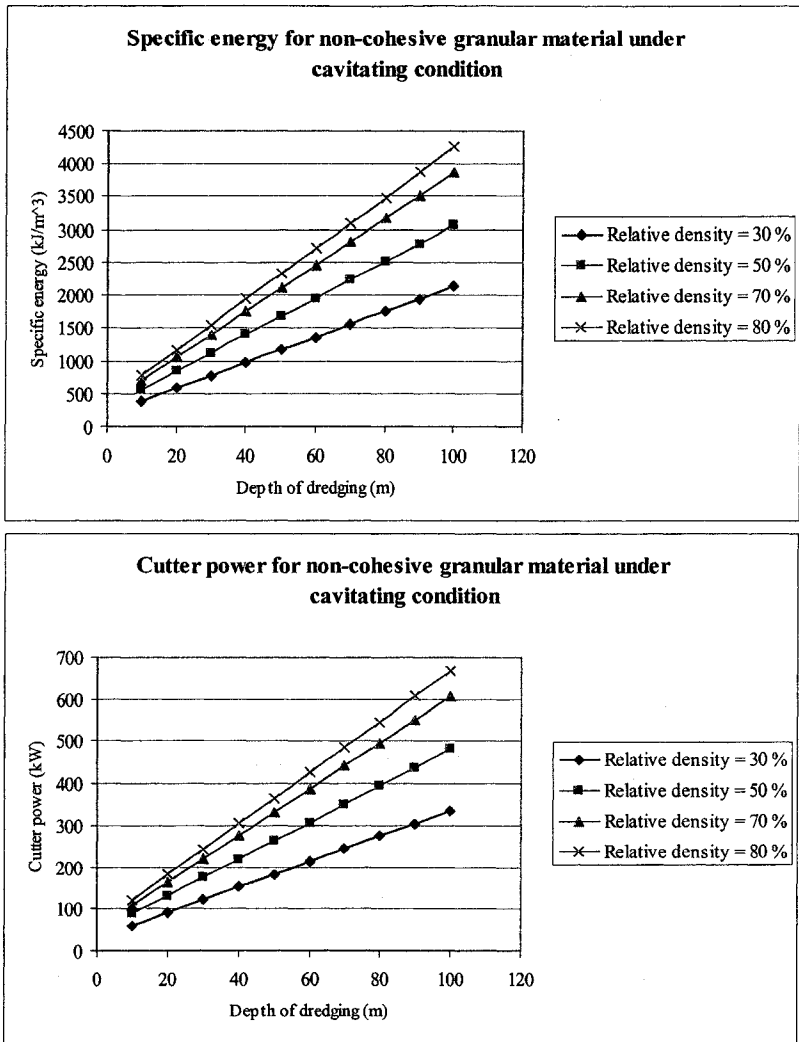


Figure 4.21 Specific energy and cutter power in granular and non-cohesive material under cavitating condition

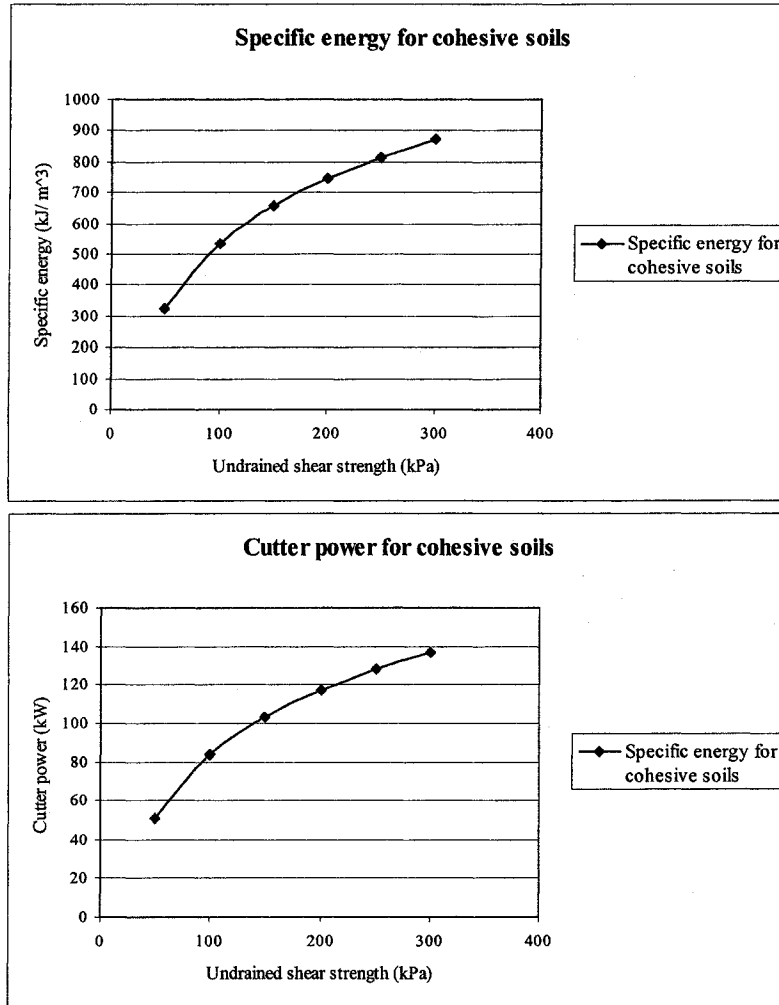


Figure 4. 22 Specific energy and cutter power for cohesive soils

4.5 Concluding Remarks

The loosening and gathering production, the spillage generated and the excavation power required were estimated for the designed twin drum cutter system with the suction mouth in between. The gathering production should match with the delivery production at the pipeline delivery end. The next chapter evaluates the delivery production of the designed centrifugal dredge pump–pipeline system and also the limiting operating conditions of the dredge pump–pipeline system.

CHAPTER 5

PERFORMANCE EVALUATION MODELS FOR TRANSPORTATION

5.1 Introduction

The designed transport system starts at the trapezoidal suction bell mouth with rectangular cross-section, which is connected to the annular eductor pump. A flexible suction hose connects the eductor pump and the centrifugal dredge pump. The centrifugal dredge pump adds energy to the solid-liquid mixture, which increases the pressure of the mixture. The pressurized mixture travels through the delivery pipeline, connected to the delivery point of the centrifugal dredge pump. The delivery pipeline will be a flexible hose of appropriate strength. There will be a funnel shaped guard attached to the vehicle, through which the delivery pipeline will pass. This guard will help to reduce the pipeline angular movement and thus will reduce stresses. There will be a submerged inclined portion of the delivery pipeline to cater for the working depth. A horizontal floating portion of the delivery pipeline will facilitate the movement of the submersible dredger, while not affecting the onboard or onshore pipeline portion. An almost vertical or inclined portion of the pipeline is necessary to climb to the supporting vessel or the bank. Depending on the requirement horizontal/ vertical/ inclined onboard or onshore pipelines will be used. There will be different types of pipeline fittings e.g. bends, elbows, 'T', ball joints etc. in the pipeline. The pressurized slurry comes out at the delivery point of the pipeline system. The drive supplying the energy to the pump is also a part of the transport system. The boundary conditions thus always start under water and terminate above water, normally in the atmospheric condition. The designed transport system configuration together with the pressure, energy and velocity profiles are schematically shown in Figure 5.1.

The performance of the designed centrifugal dredge pump-pipeline system is determined by the delivered volumetric solid rate available for a given centrifugal pump power. The performance is also judged by the possibility of pipeline blockage due to settling of the solid particles within the pipeline system. Parametric performance models based on two-phase flow theories deduced by previous researchers were developed for the evaluation of the designed transport system. The two-phase flow theories discussed in sections 5.2 to 5.9 were integrated to predict the power required by the centrifugal dredge pump and the limiting mean mixture velocity in the pipeline to avoid pipeline blockage. The design parameters, operational, environmental and soil parameters can be varied to evaluate the performance of the designed centrifugal dredge pump-pipeline system.

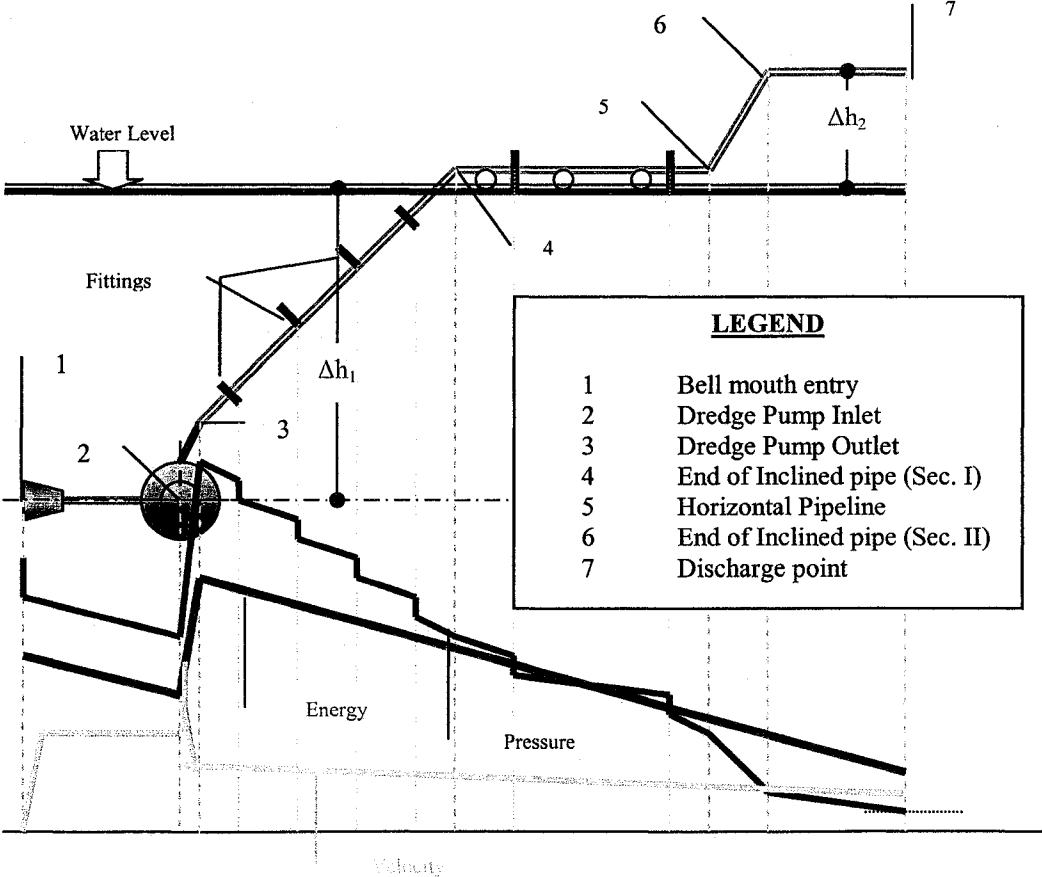


Figure 5. 1 Transport system

5.2 Working Principle of Centrifugal Dredge Pump-Pipeline System

The rotating impeller of a centrifugal dredge pump adds mechanical energy to the medium flowing through the pump [Stepanoff, 1965]. The nominal velocity of the fluid depends on the energy imparted by the pump to the fluid. As a result of energy addition a pressure differential occurs in the pumped medium between the inlet and outlet of a pump. The pressure or the energy added depends on the speed (rpm) of an impeller and on the flow rate of medium through the pump. For each pump the characteristics curves give the relationship between the manometric head [m]-flow rate [m^3/sec] ($H_{man} - Q_{pump}$), pump power [kW]-flow rate [m^3/sec] ($N_{pump} - Q_{pump}$) and pump efficiency [-]-flow rate [m^3/sec] ($\eta_{pump} - Q_{pump}$) relationships for constant pump rpm. Affinity laws are used to produce pump characteristics for different pump speeds. For dredge pumps the characteristics may change over time as the flow conditions within the pump are influenced by the wear of the impeller and pump housing. The pump efficiency drops while pumping a mixture. The ratio of pump efficiencies when pumping a mixture to pumping water is a measure of the manometric pressure reduction and output power reduction. This ratio is denoted by fc . Stepanoff [1965] gave a relationship between the mean particle size (d_{50}) [mm] and the delivered volumetric concentration (C_{vd}) [-] of transported solids with fc . The original Stepanoff equation does not consider the effect of impeller size. Miedema [1999] revised the original Stepanoff equation by including the impeller diameter.

For a pump-pipeline system operation, the manometric pressure (or head) of a dredge pump must overcome the total loss in transporting the mixture through the pipeline connected to the pump. The total pipeline losses consist of the 1) major and minor losses due to flow friction in a suction pipeline, 2) loss due to change in elevation of a suction pipeline, 3) major and minor losses due

to flow friction in a discharge pipeline, 4) loss due to change in elevation of a discharge pipeline, and 5) losses due to mixture acceleration in a pipeline i.e. entry and exit losses. The operating point of a designed pump-pipeline system for pumping water is given by the cross-point of a pump manometric head [m] – flow rate [m^3/sec] ($H_{man} - Q_{pump}$) curve and the pipeline resistance curve (head [m]-flow rate curve [m^3/sec]). The cross point gives the velocity at which a balance is found between the energy provided by the pump and the energy required overcoming flow resistance in a pipeline and a change in the geodetic height between the pipeline inlet and outlet. In dredging instead of a single working point there is a working range. This is because of the change in mean mixture velocity due to fluctuation of mixture density. To obtain constant delivered solids in production the pump speed is to be controlled. The working point and working range of a pump-pipeline system is shown in Figure 5.2.

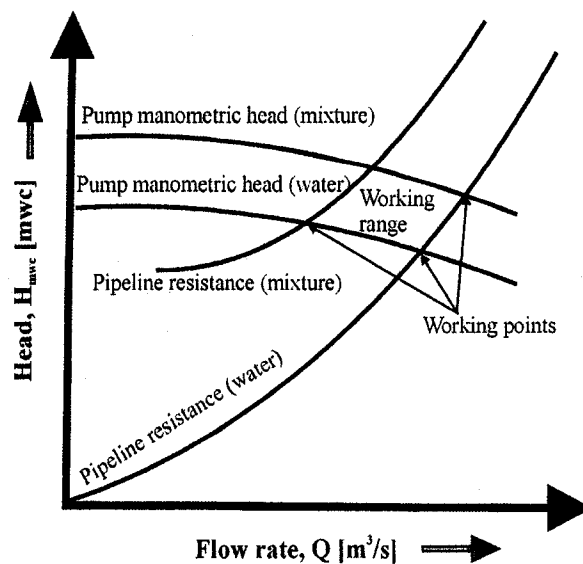


Figure 5.2 Working point and working range of a pump-pipeline system

It is observed from Figure 5.2, that with the increase in concentration (i.e. from water to mixture) the required pump manometric head increases. This will require more pump power. If a

hydraulic motor is used the pump power can be changed by changing the pump drive rpm by using the affinity laws [Matousek, 1999; Stepanoff, 1965],

$$\frac{Q_{m,(rpm\ pump)_1}}{Q_{m,(rpm\ pump)_2}} = \frac{(rpm\ pump)_1}{(rpm\ pump)_2}; \frac{H_{man,(rpm\ pump)_1}}{H_{man,(rpm\ pump)_2}} = \left(\frac{(rpm\ pump)_1}{(rpm\ pump)_2} \right)^2;$$

[Equation 5.1]

$$\text{and } \frac{N_{pump,(rpm\ pump)_1}}{N_{pump,(rpm\ pump)_2}} = \left(\frac{(rpm\ pump)_1}{(rpm\ pump)_2} \right)^3$$

where, $H_{man,(rpm\ pump)_1}$ is the pump manometric head at $(rpm\ pump)_1$ [m],

$H_{man,(rpm\ pump)_2}$ is the pump manometric head at $(rpm\ pump)_2$ [m], $N_{pump,(rpm\ pump)_1}$

is the pump power at $(rpm\ pump)_1$ [kW], $N_{pump,(rpm\ pump)_2}$ is the pump power at

$(rpm\ pump)_2$ [kW], $Q_{m,(rpm\ pump)_1}$ is the volumetric flow rate of mixture at $(rpm\ pump)_1$

[m³/sec] and $Q_{m,(rpm\ pump)_2}$ is the volumetric flow rate of mixture at $(rpm\ pump)_2$ [m³/sec].

The solid flow rate at the delivery end of the pipeline system is the main design criteria for any centrifugal dredge pump-pipeline system. Based on two- phase flow theories developed by previous researchers [Durand and Condolios, 1952; Führböter, 1961; Grace, 1986; Jufin and Lopatin, 1966; Matousek, 1999, 1997; Newitt et al., 1955; Van den Berg, 1998; Wilson, 1976, 1970; Wilson, 1992-96], parametric models were developed for the designed centrifugal dredge pump-pipeline configuration to predict the pipeline losses and hence the pump power required in order to achieve a desired solid flow rate. The limiting values of the nominal pipeline velocities

for different flow conditions within the pipeline system and material transported were also investigated in order to prevent pipeline blockage.

5.3 Delivered Solid Rate

The delivered solid flow rate (Q_{solid}) [m³/sec] is dependent on the 1) mean mixture velocity (v_m) [m/sec], and 2) delivered volumetric concentration of the solids (C_{vd}) [-].

The relationship between the mixture flow rate (Q_m) [m³/sec] and the solid flow rate (Q_{solid}) [m³/sec] is given [Matousek, 1999],

$$Q_{solid} = Q_m C_{vd} = A_{pipe} v_m C_{vd} \quad \text{[Equation 5.2]}$$

where, A_{pipe} is the cross sectional area of the pipeline [m²]. The volumetric concentration (C_v) [-] determines the fraction of the mixture volume that is occupied by solids. The delivered volumetric concentration gives the fraction of solids delivered from a slurry pipeline. The relationship between delivered volumetric concentration (C_{vd}) [-] and the in-situ volumetric concentration (C_{vdsi}) [-] is given [Matousek, 1999],

$$C_{vdsi} = \frac{C_{vd}}{1 - n_{soil}} \quad \text{[Equation 5.3]}$$

where, n_{soil} is the porosity of soil [-].

The delivered solid flow rate (Q_{solid}) [m³/sec] is usually specified as the design criteria for a particular dredger or is a user-defined quantity based on the requirements of a specific project.

The mean mixture velocity (v_m) [m/sec] of the pipeline was thus estimated as a function of the

delivered solid flow rate (Q_{solid}) [m^3/sec]. The mean mixture velocity (v_m) [m/sec] determines the chances of pipeline blockage due to settling of solid particles. The frictional loss in the pipeline is also a function of the mean mixture velocity (v_m) [m/sec].

The mean mixture velocity (v_m) [m/sec] is dependent on the total energy imparted by the pump to the fluid (either water or mixture). The mean velocity while pumping water can be predicted by a steady state analysis provided the pumping conditions remain constant and a balanced torque exists between the pump drive and the pump. It becomes difficult to predict the mean mixture velocity for dredging practices, since the mixture conditions and the solid properties continuously change within the pipelines. This also results in the change in flow and energy conditions of the pump-pipeline system. A steady state condition can only be assumed if the mixture conditions, solid properties, pumping conditions and pipeline configurations remain constant with time. The steady-state assumption was used in developing the parametric model for the designed centrifugal dredge pump-pipeline configuration.

The design, operational, environmental and soil data considered for the estimation of the mean mixture velocity (v_m) [m/sec] are shown in Table 5.1.

The value of the maximum delivered concentration (C_{vd}) attained by a cutter suction dredger with a submersible pump is 0.18, while the maximum delivered in-situ concentration (C_{vdsi}) attained by the same dredger is 0.30 [Matousek, 1999]. The transport factor for fine to medium sand for high (C_{vd}) varies between 0.9 to 1.00, while that for low (C_{vd}) varies from 0.8 to 1.0

[Matousek, 1999]. If $(C_{vd}) < 0.075$, then the delivered volumetric concentration is denoted as low, otherwise it is considered as high.

Table 5.1 Operational, environmental and soil data for prediction of nominal transport velocity

Design data	
1. Pipeline diameter [m]	D_{pipe}
2. Required solid discharge rate [m ³ /sec]	Q_{solid}
Operational data	
3. Depth of operation [m]	h_w
4. Elevation of discharge [m]	h_{del}
5. Maximum average attainable concentration by a particular type of dredger [-]	(C_{vd})
6. Volumetric concentration [-]	(C_v)
7. Transport factor for various solids and solids concentration [-]	C_{vd}/C_v
Environmental data	
8. Ambient temperature [°C]	T
9. Density of water at 0° C [kg/m ³]	$\rho_{f0} = 999.7$
10. Vapor pressure of water at a particular temperature [kPa]	p_v
Soil data	
11. Type of soil (soil classification)	-
12. Particle size distribution	-
13. Density of dry solid [kg/m ³]	ρ_{soil}
14. Density of in-situ solid [kg/m ³]	ρ_{si}
15. Porosity of soil [-]	n_{soil}

In order to estimate the mean mixture velocity (v_m) [m/sec], a ‘transport factor’ $\left(\frac{C_{vd}}{C_v}\right)$ was chosen. The delivered volumetric concentration (C_{vd}) [-] was estimated from the assumed volumetric concentration (C_v) [-] and the transport factor. The delivered in-situ volumetric concentration (C_{vdsi}) [-] was estimated using Equation 6.3. The calculated delivered in-situ volumetric concentration (C_{vdsi_calc}) [-] was compared with the maximum value for a cutter

suction dredger with a submerged pump. Reiteration was done to obtain the desired value of delivered volumetric concentration (C_{vd}) [-], for which the calculated delivered in-situ volumetric concentration (C_{vdsi_calc}) [-] was equal to the maximum value of delivered in-situ volumetric concentration (C_{vdsi_del}) [-] for a cutter suction dredger with submerged pump. The mixture flow rate (Q_m) [m^3/sec] and hence the mean mixture velocity were estimated from the required value of the solid flow rate (Q_{solid}) [m^3/sec] and the reiterated value of the delivered volumetric concentration (C_{vd}) [-]. In practice, the volumetric concentration along any point on the pipeline section (C_v) [-] is measured by density meters. The measured volumetric concentration along any point on the pipeline section is used for calculating the mixture density. The delivered volumetric concentration (C_{vd}) [-] and the delivered in-situ volumetric concentration (C_{vdsi}) [-] are used to estimate the delivered production or in-situ solid production. The flow rate of solids transported through a dredging pipeline is termed 'production' in the dredging practice.

5.4 Pipeline Blockage

The upper limit of the mean mixture velocity in a pipeline (v_m) [m/sec] is determined by the occurrence of cavitation in the dredge pump, resulting in a considerable reduction of production and damage of the dredge pump. Cavitation is less of an issue at a depth since the hydrostatic pressure suppresses cavitation. The lower limit of the mean mixture velocity in a pipeline (v_m) [m/sec] is determined by the formation of stationary bed in the pipeline and hence pipeline blockage.

The flow pattern in a dredging pipeline, the settling velocity of the solid particles transported, the depositional limit velocity or critical velocity of the mixture and the mean mixture velocity determines the chances of pipeline blockage. The various types of flow patterns observed in dredging pipelines are discussed in details by [Matousek, 1999, 1997]. The flow pattern can be 1) 'fully stratified', where all solid particles occupy a granular bed that is either stationary or slides over the bottom of the pipeline, 2) 'fully suspended', where all solid particles are suspended within a stream of carrying liquid, and 3) 'partially stratified', where the mixture flow exhibits a considerable concentration gradient across the pipeline cross section indicating an accumulation of a portion of solids near the bottom of a pipeline and a non-uniform distribution of the rest of solids across the rest of the pipeline cross sectional area. This flow pattern also known as 'heterogeneous flow' is most common in dredging pipelines.

The flow regime can be either laminar or turbulent within a pipeline, though the latter is most common in dredging pipelines. The settling velocities for solid particles in different regimes were proposed by various researchers. The Stokes equation, Rittinger equation, Budryck equation can be used in estimating the settling velocities of solid particles [Matousek, 1999] for various flow regimes. The Grace method [Grace, 1986] can also be used to determine the settling velocity of solid particles. The nominal transport velocity in the pipeline should be higher than the settling velocities of the respective solids.

The mixture velocity in the pipeline is however most important in determining the chances of pipeline blockage. The mean mixture velocity and the deposition limit velocity (also known as critical velocity) are two parameters used to determine the lower limit of the centrifugal dredge pump-pipeline operation.

The mean velocity in a pipeline (v_m) [m/sec] is obtained from the volumetric flow rate (Q_m) [m^3 /sec] of a matter passing through a pipeline cross section of the area (A_{pipe}) [m^2].

The deposition limit velocity (v_{dl}) [m/sec] is the mixture velocity in the pipeline at which the particles in the bed formed in the pipeline stops sliding over a pipeline wall and forms a stationary deposit leading to pipeline blockage. Empirical models are available to predict the deposition limit velocity [Durand and Condolios, 1952; Führböter, 1961; Jufin and Lopatin, 1966; Van den Berg, 1998]. Semi-empirical model for heterogeneous flow in slurry pipelines is also available [Wilson, 1992-96]. A physical modeling approach has also been used by researchers to predict the deposition limit velocity [Newitt et al., 1955; Wilson, 1976, 1970]. Matousek [1997, 1999] discussed the merits and demerits of all the different models.

In this thesis the model of MTI Holland [Van den Berg, 1998] was used to estimate the deposition limit velocity or critical velocity of mixture flow in a pipeline. This model was developed for the threshold velocity between the ‘fully suspended heterogeneous flow’ regime and the regime of ‘flow with the first particles settling to the bottom’ of a pipeline. This correlation was based on data including those from various dredging pipelines. In practical design aspects, the MTI model thus seems more logical to be used than other empirical models.

The critical velocity according to the MTI model is,

$$v_{dl} = 1.7 \left(5 - \frac{1}{\sqrt{d_{mf}}} \right) \sqrt{D_{pipe}} \left(\frac{C_{vd}}{C_{vd} + 0.1} \right)^{\frac{1}{6}} \sqrt{\frac{S_s - 1}{1.65}} \quad [\text{Equation 5.4}]$$

where, D_{pipe} is the diameter of pipe [m], d_{mf} is the decisive particle diameter [mm] and

$(\rho_{rel_soil}) = \frac{\rho_{soil}}{\rho_f}$ is the relative density of solid [-]. The decisive particle diameter is defined

[Matousek, 1999, 1997], $d_{mf} = \frac{d_{10} + d_{20} + \dots + d_{80} + d_{90}}{9}$, where, d_n is the respective

percentile and gives the particle diameter [mm] for which n percent of (by mass) the particles in

a soil sample are finer. A suitable transport velocity v'_m [m/sec] was estimated from the deposition limit velocity v_{dl} [m/sec] using the relationship [Matousek, 1999, 1997]

$$v'_m = 1.1v_{dl} \quad \text{[Equation 5.5]}$$

5.5 Major Frictional Loss in Horizontal Pipeline

Empirical modeling approach, microscopic modeling approach and macroscopic or physical modeling approach were followed by different researchers in predicting the slurry flow behavior through pipelines. Matousek [1999] gave a detailed review of such works by different workers. An empirical modeling approach was followed by Durand and Condolios [1952], Führböter [1961], Jufin and Lopatin [1966]. A semi empirical approach was followed by the Wilson and GIW model [Clift et al., 1982]. These models predict the frictional head loss in a pipeline and the deposition limit velocity. A physical modeling approach was followed by Newitt et al. [1955], Wilson [1976, 1970]. Each model has its advantages and disadvantages, which are discussed in detail by Matousek [1999].

The mixture flow in the designed pipeline system was assumed to be heterogeneous. The Wilson and GIW model for heterogeneous flow was used for predicting the major frictional loss in the designed pipeline system. The Wilson and GIW model was chosen, since this model can be used

for prediction of friction loss in slurry pipelines of different sizes transporting solids of different sizes at different concentrations. This model is based on the assumption that a power-law relationship exists between the relative solids effect and the mean slurry velocity, which is valid in all slurry flow conditions. The exponent 'M' which is used in this model is assumed to be dependent on the particle size distribution only and hence is easy to compute.

The mean mixture velocity in the pipeline (v_m) [m/sec] was assumed to be constant for the desired production. The density of water at a particular temperature (ρ_{fT}) [kg/m^3] and dynamic viscosity of water at a particular temperature (μ_{fT}) [Pa.s] was assumed constant also. The pipeline diameter (D_{pipe}) [m] was also assumed constant. The Reynolds number (Re) is thus constant and is given,

$$\text{Re} = \frac{v_m D_{pipe} \rho_{fT}}{\mu_{fT}} \quad \text{[Equation 5.6]}$$

When the $\text{Re} > 3000$, the flow of mixture in the pipeline is turbulent.

The density of water (ρ_{fT}) [kg/m^3] at a particular temperature ($T^{\circ}\text{C}$) is given,

$$\rho_{fT} = \left[\rho_{f0} - 0.10512(T-10) - 0.005121(T-10)^2 + 0.00001329(T-10)^3 \right] \quad \text{[Equation 5.7]}$$

The dynamic viscosity of water (μ_{fT}) [Pa.s] at ($T^{\circ}\text{C}$) is given,

$$\mu_{fT} = \left[\frac{0.10}{\left(2.1482 \left((T - 8.345) + \left(8078.4 + (T - 8.435)^2 \right)^{0.5} \right) - 120 \right)} \right] \quad \text{[Equation 5.8]}$$

The Darcy-Weisbach friction factor (λ_f) [-] for the designed pipeline can be assumed constant for a considerable time and is given as [Swami and Jain, 1976],

$$\lambda_f = \frac{0.25}{\left[\log \left(\left(\frac{k}{3.7D_{pipe}} \right) + \left(\frac{5.74}{Re^{0.9}} \right) \right) \right]^2} \quad \text{[Equation 5.9]}$$

where k is the pipeline roughness [m]. This relationship is valid for $5 \cdot 10^3 \leq Re < 10^8$ [Swami and Jain, 1976], which is in the turbulent regime.

The hydraulic gradient for liquid flow (I_f) [-] is given [Matousek, 1999],

$$I_f = \frac{\lambda_f v_m^2}{2D_{pipe}g} \quad \text{[Equation 5.10]}$$

where, g is the acceleration due to gravity [m/sec^2].

The hydraulic gradient for mixture flow in horizontal pipeline (I_m) [-] according to the Wilson and GIW model is given,

$$I_m = I_f + \left[0.22 \left(\frac{v_m}{v_{50}} \right)^{-M} * \left(C_{vd} \left((\rho_{rel_soil} - 1) \right) \right) \right] \quad \text{[Equation 5.11]}$$

where, M is the empirical exponent sensitive to particle size distribution [-], ρ_{rel_soil} is the relative density of solid [-] and v_{50} is the value of mean mixture velocity in the pipeline (v_m) at which one half of solids is suspended in a carrier flow [m/sec] and is given [Wilson and GIW model],

$$v_{50} \approx 3.93(d_{50})^{0.35} \left(\frac{(\rho_{rel_soil})^{-1}}{1.65} \right)^{0.45} \quad [\text{Equation 5.12}]$$

where d_{50} is the mass-median diameter [mm]. The exponent M is given,

$$M = \left[\ln \left(\frac{d_{85}}{d_{50}} \right) \right]^{-1} \quad [\text{Equation 5.13}]$$

The value of M should not exceed 1.7, nor fall below 0.25. In practice d_{50} and d_{85} will vary, but for the calculations performed in this thesis, these were assumed constant. The parameter d_{85} represents the grain size of soil at 85 % passing [mm].

The major head loss in the horizontal pipeline section due to mixture flow ($H_{major_hor_m}$) [m] is given,

$$(H_{major_hor_m}) = I_m * (L_{pipe_hor}) \quad [\text{Equation 5.14}]$$

where, L_{pipe_hor} is the length of the horizontal pipeline section [m].

The pressure drop in the horizontal pipeline section due to mixture flow ($p_{major_hor_m}$) [kPa] is given,

$$(P_{major_hor_m}) = I_m * \rho_{fT} * g * (L_{pipe_hor}) \quad [\text{Equation 5.15}]$$

5.6 Major Frictional Loss in Inclined Pipeline

Empirical and physical models are available for prediction of the major head loss in inclined pipes. Worster and Denny [1955], Gilbert [1960] and Wilson et al. [1997] followed the empirical modeling approach for inclined pipelines. Physical modeling approach was developed by Matousek [1997]. A detailed review of all these modeling approaches for mixture flow in inclined pipelines was given by Matousek [1999, 1997].

The Wilson model for mixture flow in inclined pipes is used in this thesis since this model predicts both the deposition limit velocity and the hydraulic gradient for mixture flow in inclined pipelines as opposed to the other two empirical models.

The discharge pipeline was assumed to be fixed at a particular point either onshore or onboard of the stationary support vessel. The inclination of the pipeline is thus dependent on the movement of the submersible dredger/ miner. The designed vehicle is stationary during the dredging cycle and hence the angle of inclination of the pipelines can be assumed constant for a particular dredging cycle.

The deposition limit velocity for inclined pipelines is given by the Wilson model [Wilson et al., 1997],

$$v_{dl\omega} = v_{dl} + \Delta_D * \sqrt{2g(D_{pipe})((\rho_{rel_soil}) - 1)} \quad [\text{Equation 5.16}]$$

where, v_{dl} is the deposition limit velocity in horizontal pipeline [m/sec], $v_{dl\omega}$ is the deposition limit velocity in inclined pipeline [m/sec] and Δ_D is the Durand deposition parameter, which is

a function of the pipeline inclination [degree]. The values of the Durand deposition parameter are given in Appendix 13.

The suitable transport velocity for mixture flow in inclined pipeline section is [Matousek, 1999, 1997],

$$v_{m\omega} = 1.1v_{dl\omega} \quad [\text{Equation 5.17}]$$

The hydraulic gradient for mixture flow in inclined pipeline ($I_{m\omega}$) [-] according to the Wilson model [Wilson et al., 1997] is given,

$$I_{m\omega} = I_f + (I_m - I_f) \cos \omega^{(1+M\gamma)} \quad [\text{Equation 5.18}]$$

where, the exponent M is given by Equation 6.13; and the power γ has a lower limit of 0.333 for very fine particles and hypothetically an upper limit of unity for very coarse particles. ω is the angle of pipeline inclination, and is considered to have positive value for ascending pipe and negative value for descending pipe.

The major head loss in the inclined pipeline section due to mixture flow ($H_{major_inc_m}$) [m] is given,

$$H_{major_inc_m} = I_{m\omega} L_{pipe_inc} \quad [\text{Equation 5.19}]$$

where, L_{pipe_inc} is the length of the inclined pipeline section [m].

The pressure drop in the inclined pipeline section due to mixture flow is given as [kPa],

$$P_{major_inc_m} = I_{m\omega} \rho f T g L_{pipe_inc} \quad [\text{Equation 5.20}]$$

5.7 Static Head Loss

The head required to pump the mixture from the suction entry to the water level is the static head. This static head is a function of the difference in density between the mixture and the fluid and the distance between the suction entry and the water surface. The static head loss between the suction entry and the water surface ($H_{st_suc_m}$) [m] is given [Matousek, 1999, 1997],

$$H_{st_suc_m} = h_w(\rho_{rel_m} - \rho_{rel_f}) \quad \text{[Equation 5.21]}$$

where h_w is the distance between the suction entry and the water surface [m] (Figure 5.1);

ρ_{rel_f} is the relative density of fluid [-] and ρ_{rel_m} is the relative density of mixture [-].

Similarly, the static head loss due to the discharge elevation ($H_{st_del_m}$) [m] above water surface is given [Matousek, 1999, 1997],

$$H_{st_del_m} = h_{del} * \rho_{rel_m} \quad \text{[Equation 5.22]}$$

The total static head loss $H_{st_total_m}$ [m] is obtained,

$$H_{st_total_m} = H_{st_suc_m} + H_{st_del_m} \quad \text{[Equation 5.23]}$$

The total pressure drop due to the static head loss $p_{st_total_m}$ [m] is given,

$$p_{st_total_m} = H_{st_total_m} * \rho_{fT} * g \quad \text{[Equation 5.24]}$$

5.8 Minor Head Loss

The minor head loss in any pipeline due to mixture flow (H_{minor_m}) [m] is always constant as the number and type of pipe fittings are not changed during an operation. The bending of the

floating pipelines due to waves and currents were neglected for this analysis. The minor head loss for mixture flow in a pipeline is given [Matousek, 1999, 1997],

$$H_{\text{minor}_m} = \sum \xi \frac{v_m^2}{2g} \frac{\rho_m}{\rho_f T} \quad [\text{Equation 5.25}]$$

where, ξ is the minor loss co-efficient [-] and ρ_m is the density of mixture [kg/m^3]. The minor pressure drop due to mixture flow (p_{minor_m}) [kPa] is given [Matousek, 1999, 1997],

$$p_{\text{minor}_m} = \sum \xi \frac{v_m^2}{2} \rho_m \quad [\text{Equation 5.26}]$$

5.9 Entry and Exit Losses

The entry and exit head losses due to mixture flow at the suction bell mouth and the delivery point respectively [H_{entry_m} and H_{exit_m}] [m] for the designed pump-pipeline system are given [Matousek, 1999, 1997],

$$H_{\text{entry}_m} = 3 \frac{(v_{m_pipe_suc})^2}{2g} \quad [\text{Equation 5.27}]$$

$$H_{\text{exit}_m} = \frac{(v_{m_pipe_del})^2}{2g} \quad [\text{Equation 5.28}]$$

where, ($v_{m_pipe_del}$) is the mean mixture velocity in the delivery pipeline [m/sec] and ($v_{m_pipe_suc}$) is the mean mixture velocity in the suction pipeline [m/sec].

The pressure drops due to entry and exit losses (p_{entry_m}) [kPa] and (p_{exit_m}) [kPa] are given,

$$P_{entry_m} = H_{entry_m} * \rho * f * T * g \quad [\text{Equation 5.29}]$$

$$P_{exit_m} = H_{exit_m} \rho f T g \quad [\text{Equation 5.30}]$$

5.10 Predicted Results

This section presents the predicted results for the total head loss for the designed centrifugal dredge pump-pipeline configuration and hence the dredge pump power required. The limiting values of the mean mixture velocity for horizontal and inclined pipelines are also presented.

The required solid discharge rate (Q_{solid}) [m^3/sec] was assumed as $61 \text{ m}^3/\text{hr}$. The diameter of the suction and the discharge pipe was assumed to be same for the calculations. The depth of operation (h_w) was assumed as 50 m, while the elevation of discharge (h_{del}) was considered as 5 m. The volumetric concentration (C_v) was assumed as 0.2, while a transport factor (TF) of 0.9 was considered. An ambient temperature of 25°C was used for all the calculations. Narrow graded sand was chosen as the transporting soil. The representative grain size data for the sand is presented in Appendix 13. The density of dry solid (ρ_{soil}) [kg/m^3], the density of in-situ solid (ρ_{si}) [kg/m^3] and the porosity (n_{soil}) [-] values of different soil types are presented in Appendix 13. For all the calculations the density of dry solid, $\rho_{soil} = 2650 \text{ kg}/\text{m}^3$ and the density of in-situ solid $\rho_{si} = 1950 \text{ kg}/\text{m}^3$ were considered. The total length of the horizontal pipeline sections was assumed as 200 m. The length of the inclined pipeline section under the water was only considered. The length of the inclined pipeline section is dependent on the angle of inclination and the depth of dredging. The length of the inclined pipeline section present under water was calculated as a function of the angle of inclination for the fixed depth of dredging of 50 m.

The delivered volumetric concentration (C_{vd}) [-] calculated was 0.18, which is equal to the maximum value attained by a cutter suction dredger with a submersible pump.

The total head loss estimated for the designed pipeline configuration is a summation of the major, minor, static and entry and exit head losses for the different pipeline sections. The numerical results are presented in Appendix 13, while the final graphical results are presented in this section.

The major head loss for the horizontal pipeline section is dependent of the mean mixture velocity (v_m) [m/sec] and the delivered volumetric concentration (C_{vd}) [-]. Since the delivered volumetric concentration was assumed as constant, the major head loss for the horizontal pipeline section is a function of the mean mixture velocity and hence the diameter of the pipeline (D_{pipe}) [m]. The major head loss for inclined pipeline section for a constant delivered volumetric concentration C_{vd} [-] is a function of the mean mixture velocity (v_m) [m/sec], the pipeline inclination (ω) [degree] and the exponents M and γ . The value of the exponent γ was taken as 0.5. The major head loss for the inclined pipeline section was computed for the different pipeline inclinations. The total major head loss was calculated as a summation of the major head loss for the horizontal pipeline section for a constant delivered volumetric concentration (C_{vd}) [-] and mean mixture velocity (v_m) [m/sec], and the major head loss for the inclined pipeline section for a given inclination and with the same delivered volumetric concentration (C_{vd}) [-] and mean mixture velocity (v_m) [m/sec] as the horizontal pipeline section. The static head loss, the minor head loss and the entry and exit losses were calculated as a function of the dredging

depth and the mean mixture velocity (v_m) [m/sec] and were added to the major head loss to obtain the total head loss for the designed pipeline configuration. The minor loss co-efficient (ξ) = 3 [-] was considered for the calculations.

Total head loss plotted against the diameter of the pipeline for different inclination angles of the inclined pipeline section is shown in Figure 5.3.

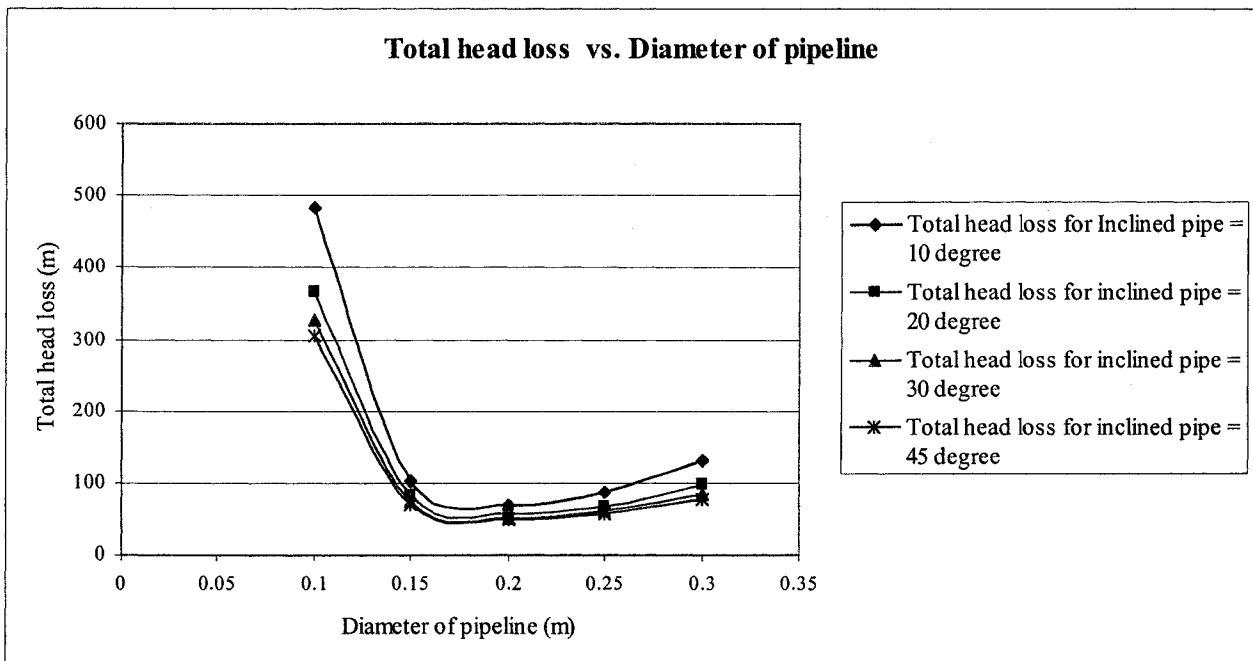


Figure 5.3 Total head loss for designed pipeline configuration ($C_{vd} = 0.18$, $Q_s = 61 \text{ m}^3/\text{hr}$, $h_d = 50 \text{ m}$, Length of horizontal pipeline section = 200 m)

It is observed from Figure 5.3, that at lower pipeline diameters, the total head loss when the inclination of the inclined section is 10 degrees is much higher than the other values. This is not the case with the increase in the pipeline diameter. The length of the inclined pipe section is a function of the angle of inclination of the pipeline section and the depth of dredging. With low angle of inclination, the length of inclined pipe section is much higher. With low pipeline diameter, the mean mixture velocity is also very high. The high values of the mean mixture

velocity and the length of the inclined pipeline section increase the major head loss and hence the total head losses of the designed pipeline system. The hydraulic gradient due to mixture flow in horizontal or inclined pipeline section initially decreases rapidly with increasing pipeline diameter and reaches a minimum value. It then increases with increase in pipeline diameter. As a result of which the parabolic trends are observed in Figure 5.3. From Figure 5.3, it can be concluded that for the designed prototype a pipeline diameter between 0.18 to 0.3 m can be chosen, since the total head loss is much lower for such values. The desired flow rate of mixture through the pipeline and hence the production will decrease with the decrease in the pipeline diameter beyond 0.18m. The change in the total head loss with variation in the inclination of the inclined pipeline section is also lower compared to pipeline diameters < 0.15 m. While designing the pipeline configuration, care must be taken to choose the optimum pipeline diameter and the angle of inclination for the inclined pipeline section, especially if there is a limitation in the pump power available.

The graphical results for the deposition limit velocity, the required transport velocity to avoid pipeline blockage and the mean mixture velocity for different pipeline diameters are presented next. The numerical results are presented in Appendix 13.

It is observed from Figure 5.4 that the deposition limit velocity and the suitable transport velocity for horizontal pipeline section are much lower than the required mean mixture velocity for the desired production at the pipeline delivery point. Hence the chance of pipeline blockage for the chosen soil type is not a concern for the horizontal pipeline section. The mean mixture velocity is the velocity with which the mixture travels in a given pipeline section of a certain diameter. The mean mixture velocity determines the production output. The deposition limit velocity is the mean velocity of mixture in a pipeline section for which the solid particles stop movement and

tend to form a stationary bed in the pipeline section. The transport velocity can be estimated from the deposition limit velocity and gives the minimum required value of the mean mixture velocity in order to avoid pipeline blockage. The mean mixture velocity thus must always be equal to greater than the suitable transport velocity.

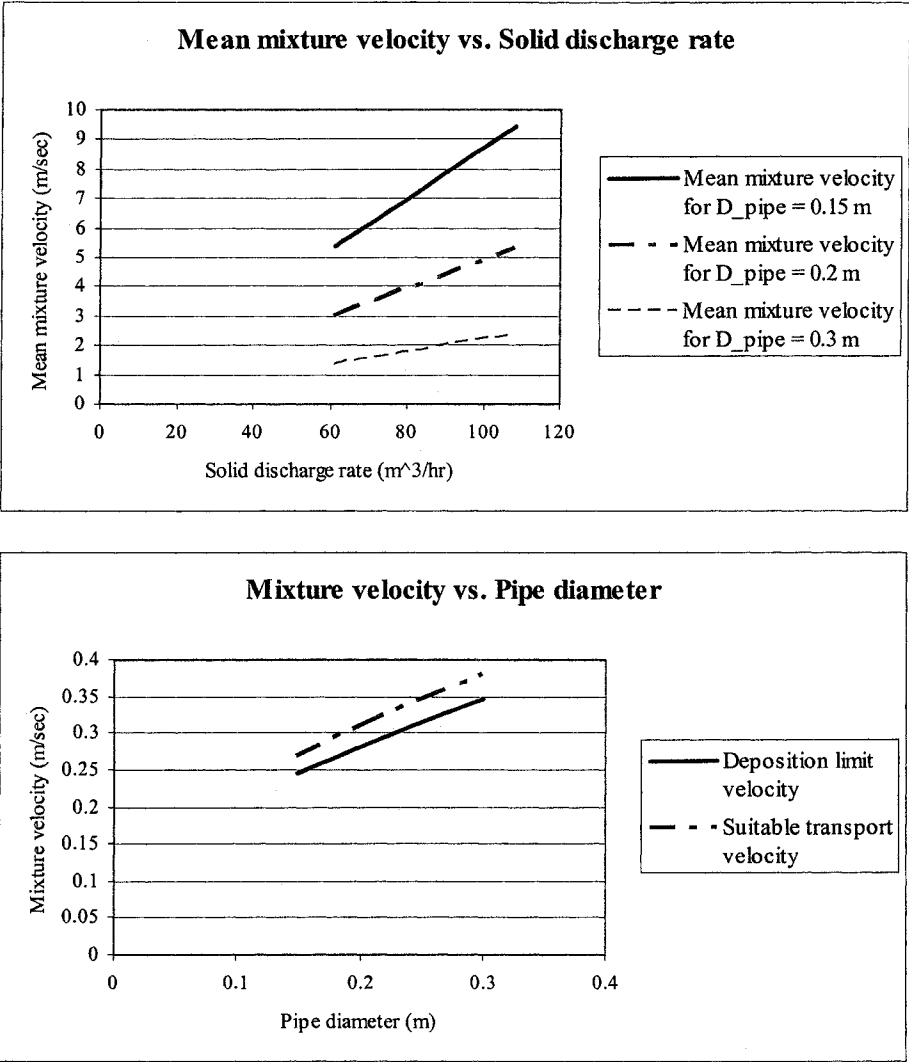


Figure 5.4 Required mixture velocities for horizontal pipeline section

The deposition limit velocity for inclined pipeline section with different inclination angles are graphically presented in Figure 5.5 as a function of the pipeline diameter. The suitable transport velocity and the required mean mixture velocity for inclined pipeline section with different

inclination angles are presented in Figure 5.6. It is observed from Figure 5.6, that the required mean mixture velocity (v_m) [m/sec] approaches the suitable transport velocity for inclined pipeline sections for higher values of pipeline inclinations and pipeline diameter. Attention must be given in choosing the correct pipeline diameter and required mean mixture velocity for higher angles of inclination of inclined pipeline sections.

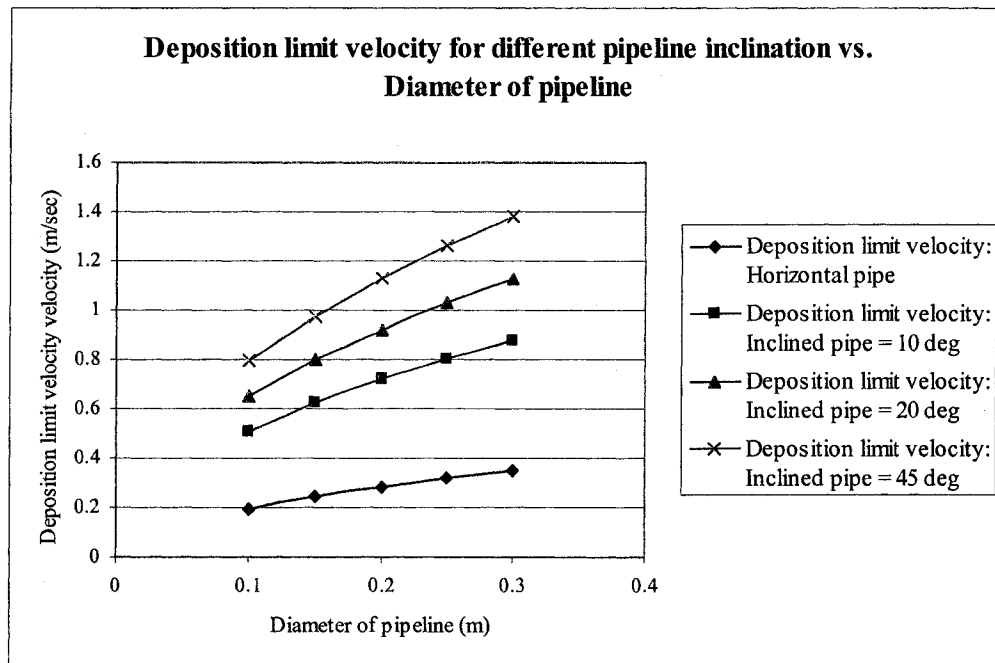


Figure 5.5 Deposition limit velocity for inclined pipeline section

If the pipeline diameter is further increased beyond 0.3 m, the mean mixture velocity will decrease. Depending upon the pipeline inclination, the mean mixture velocity can be lower than the suitable transport velocity. This will increase the chances of pipeline blockage. If the pipeline inclination is increased beyond 45 degrees, the same scenario will take place.

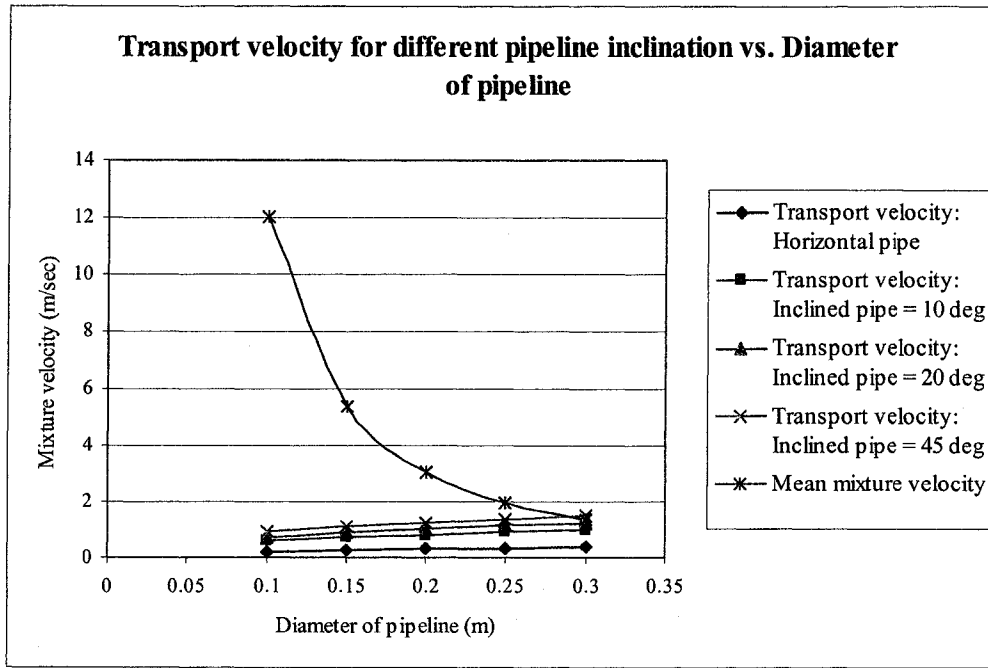


Figure 5.6 Suitable transport velocity and mean mixture velocity for inclined pipeline section with different angles of inclination

The pump power required for the designed pipeline configuration is presented next. The pipeline diameter, the mean mixture velocity and the mixture flow rate at the delivery point are presented in Table 5.2. The pump power required for the values shown in Table 5.2 and the total pressure drop for the designed pipeline system is shown in Figure 5.7.

Table 5.2 Diameter of pipeline, mean mixture velocity and mixture flow rate

Diameter of pipeline (m)	Mean mixture velocity (m/sec)	Mixture flow rate (m ³ /sec)
0.1	12.03	339.97
0.15	5.35	340.18
0.2	3.01	340.25
0.25	1.92	339.12
0.3	1.34	340.82

The pump power required was calculated by using the relationship,

$$N_{pump} = \frac{a_{so_pump} * P_{total_m} * Q_m}{\eta_{pump}} \quad \text{[Equation 5.31]}$$

where, a_{so_pump} is the system operating factor = 1.3 [-] [EEM (P) Ltd. internal report, 1999], p_{total_m} is the total pressure drop in the designed pipeline system [kPa], and η_{pump} is the efficiency of the pump [-] = 60 % [EEM (P) Ltd. internal report, 1999].

There is a rapid drop of required pump power when the pipeline diameter is changed from 0.1 to 0.15 m. This is because of the increase in the head loss due to very high mean mixture velocity. The pump power is a function of the total pressure drop and hence the total head losses in the designed pipeline system. Hence, the same parabolic trend was observed in both Figure 5.3 and 5.7, where the total head loss and the total pump power required were plotted against the pipeline diameter. Since the maximum delivered volumetric concentration was assumed in calculating the pump power required, the pump power shown in Figure 5.7 thus represents the maximum pump power required for the designed pipeline system of the prototype vehicle.

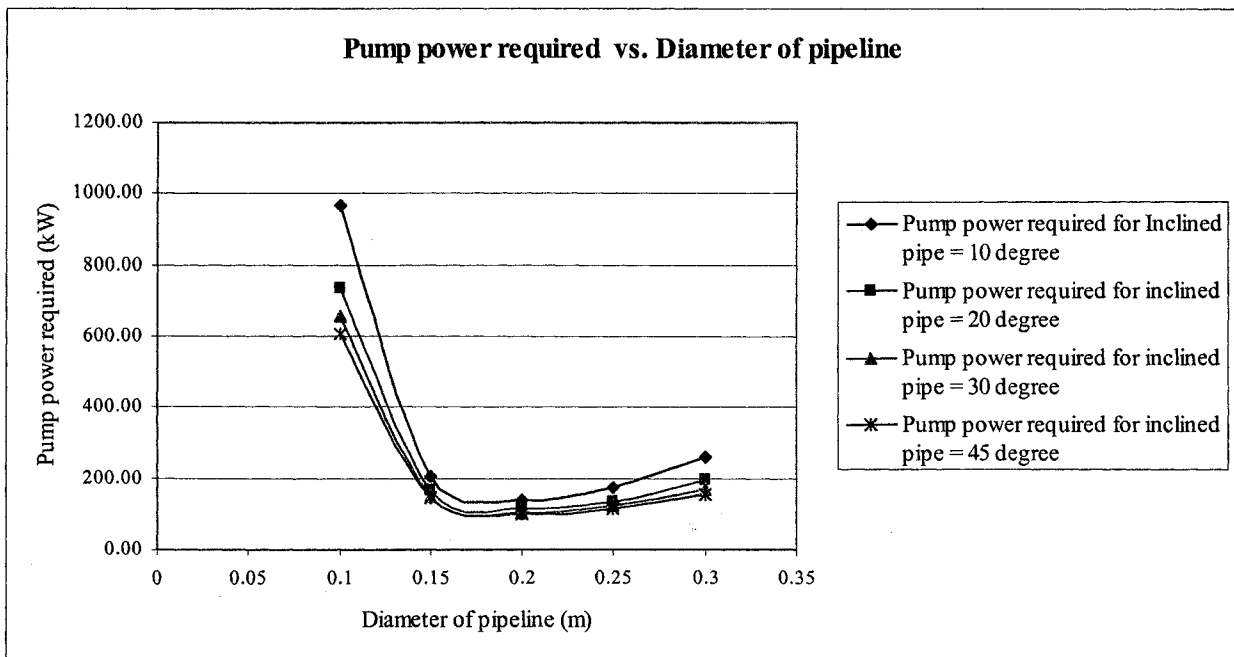


Figure 5.7 Required pump power

5.11 Concluding Remarks

The results predicted for the designed pipeline configuration shows that the suitable pipeline diameter for the designed prototype vehicle is between 0.18 to 0.30m to achieve the desired production output ($61 \text{ m}^3/\text{hr}$) and to avoid pipeline blockage. The assumed production of solids was $61 \text{ m}^3/\text{hr}$ with a delivered volumetric concentration of 18 %, which is the highest volumetric concentration possible for a cutter suction dredger with a submersible pump. The mean mixture velocity varies from 5.35 m/sec to 1.92 m/sec for the suitable pipeline diameter range and assumed solid production rate as mentioned above. The mean mixture velocity for the given pipe line diameter range is far above the deposition limit velocity for transporting narrow graded sand with $d_{50} = 0.42 \text{ mm}$ and $d_{85} = 0.8 \text{ mm}$. The chances of pipeline blockage are thus negligible for the designed pipeline system while transporting narrow graded sand.

It was observed from the total head loss curves for the designed pipeline system that the total head loss depends on the inclination of the inclined pipeline sections. The designed submersible legged dredger/ miner remains stationary in one position while excavating the material. Since the inclination of the inclined pipeline section is dependent on the submersible vehicle movement, the change in pipeline inclination can be a limiting factor for submersible dredgers, which perform locomotion while excavating the underwater material. This is not an issue for the designed submersible legged dredger/ miner, since the vehicle is stationary during the dredging cycle.

The parametric performance evaluation models, for the designed pump-pipeline system, discussed in this chapter, were developed by integrating the works of various researchers on two-phase flow models. These parametric models can be used to evaluate the performance of

different transporting pipeline systems having different diameters, pipeline lengths and pipeline configurations. The mean mixture velocity for the designed pipeline system can be calculated based on the required production of solids. The mean mixture velocity determines the total head loss in the pipeline system and hence the pump power required. The lower limit of the mean mixture velocity can also be determined in order to avoid the chances of pipeline blockage. The pipeline resistance curves i.e. total head loss–mixture flow curves can be obtained from the parametric models discussed in this chapter. The pipeline resistance curves need to be compared with the characteristic curves of centrifugal pumps to choose a suitable centrifugal pump for the proper operation of the designed pump-pipeline system.

CHAPTER 6

SYNCHRONIZATION OF LOCOMOTION AND DREDGING PROCESSES

6.1 Introduction

Complex interrelationships exist between the dynamic processes of excavation, transportation and locomotion of a submersible dredger/ miner. The working environment of a submersible dredger/ miner is a very dynamic environment with active environmental forces (currents and waves) and variations in terrain characteristics. Evaluation of the overall performance of any submersible dredger/ miner requires adequate knowledge about the interrelationships existing between the excavation, transportation and locomotion processes as well as the working environment. This chapter presents the conceptual model, developed to show the complex interrelationships existing between the excavation, transportation and locomotion processes of a submersible walking dredger/ miner by considering the designed vehicle as an example.

6.2 Parameters Influencing Dredging and Locomotion Processes

The parameters influencing the excavation, transportation and locomotion processes were identified and separated into three major groups 1) geometrical parameters, 2) operational parameters, and 3) environmental parameters. These parameters which are interdependent are tabulated in Table 6.1.

Table 6.1 Geometrical, operational and environmental parameters affecting the dredging and locomotion processes

PROCESSES	GEOMETRICAL PARAMETERS	OPERATIONAL PARAMETERS		ENVIRONMENTAL PARAMETERS	
		Kinematics	Kinetics	Fluid	Terrain
Excavation	<ul style="list-style-type: none"> - Cutter geometry - Number and arrangement of blade/pick/ tooth - Blade/ pick/ tooth geometry - Ladder geometry - Distance between the cutters - Shape and dimensions of the suction mouth 	<ul style="list-style-type: none"> - Cutter and ladder trajectory - Cutter rpm - Direction of cutting - Depth of cutting - Swing angle and swing velocity of ladder assembly - Pitching angle and pitching velocity of ladder assembly 	<ul style="list-style-type: none"> - Cutter power 	<ul style="list-style-type: none"> - Waves - Currents - Operating depth 	<ul style="list-style-type: none"> - Slope - Obstacle - Type of material <ul style="list-style-type: none"> a) Non-cohesive soil - Friction angle - Permeability - Porosity - Relative density b) Cohesive soil - Adhesive strength - Cohesive strength - Undrained shear strength
Transportation	<ul style="list-style-type: none"> - Pump design - Pipeline diameter, length and configuration 	<ul style="list-style-type: none"> - Pump rpm 	<ul style="list-style-type: none"> - Pump characteristics <ul style="list-style-type: none"> a) Pump head vs. pump capacity b) Pump power vs. pump capacity c) Pump efficiency vs. pump capacity 		<ul style="list-style-type: none"> - Particle size distribution - Particle shape
Locomotion	<ul style="list-style-type: none"> - Leg design and dimensions - Foot shape and dimensions 	<ul style="list-style-type: none"> - Vehicle velocity - Individual leg velocity - Leg joint parameters 	<ul style="list-style-type: none"> - Locomotion power 		<ul style="list-style-type: none"> - Terrain type <ul style="list-style-type: none"> a) Level b) Undulated - Slope - Obstacle - Bearing capacity of soil - Soil settlement, failure and slip

6.3 Conceptual Model for Performance Evaluation

Two distinct operational cycles were identified for the designed submersible walking dredger/miner which were 1) the dredging cycle and 2) the locomotion cycle.

The dredging cycle is a productive cycle, while the locomotion cycle is a non-productive cycle, when excavation and transportation of soil is not performed. During the locomotion cycle, the centrifugal dredge pump transports water to the surface.

The dredging production is dependent on the sub-processes of loosening, gathering, mixing and transport, as were discussed in Appendix 1. If more soil is loosened than can be gathered, spillage is obvious. When the volume of soil loosened and gathered by the excavation system is higher than the capacity of the transport system, spillage and wastage of energy occurs [Vlasblom, 1999]. If the capacity of the transport system is more than the amount of material generated by the excavation system, a lean mixture will be delivered [Vlasblom, 1999]. In hydraulic dredging, mixing is achieved by the combined action of the excavation system and the suction influence of the centrifugal dredge pump. The mixing process determines the type of flow in a pump-pipeline and hence the production. Synchronization between each of these sub-processes is thus essential to achieve optimum production output at the best efficiency level. Synchronization is possible by physical and mathematical modeling of the interdependency of the dredging sub-processes and hence the operational parameters influencing each of these sub-process (Table 6.1).

The locomotion cycle time of the designed vehicle should be minimized in order to achieve a higher average production during a given period of time. The step sizes of the individual legs and hence the locomotion cycle time of the designed vehicle depends on 1) the geometry and operational parameters of the designed leg linkage, 2) the excavation workspace covered by the excavation system in one setting, 3) the terrain and soil characteristics, and 4) the load incident at each leg and hence the subsequent soil reactions. The load incident at each leg is a function of 1) the vehicle weight, 2) the operation related forces, and 3) the environment related forces. The

subsequent soil reactions depend on 1) the shape and dimensions of the foot, 2) the load incident at each leg, and 3) soil characteristics. Operation related forces include 1) the excavation force, 2) the transportation force, 3) the locomotion force, 4) the umbilical force, and 5) the hydrostatic force. The excavation force includes the cutting force, the frictional force due to soil/ cutting tool interactions and the inertia forces due to swing and lifting/ lowering motions of the ladder assembly. The transportation force consists of the force generated from the dredge pump operation, the impact forces due to sudden pipeline blockage and the vibrations due to change in the density of the mixture. The locomotion force constitutes the drag forces generated due to legs and vehicle body movements, the frictional forces at the foot/ soil interface and the slope negotiation force. Inertial forces and moments together with added mass arise due to linear and angular accelerations of the vehicle, legs and ladder. The relative movements of the umbilical cable and discharge pipeline with respect to the water consist of the umbilical force [Kalske, 1997]. Hydrostatic forces and moments arise from the buoyancy force on the vehicle. The dynamic forces generated due to the operations of the various actuators should also be considered.

Environment related forces include 1) the wave and current forces and 2) the soil reaction forces. Waves and currents only affect the umbilical cable and delivery pipeline in deeper waters, but will also affect the vehicle directly in shallow waters. The soil reaction forces include the normal reaction forces and the frictional forces at the foot/ soil interface. The step sizes of individual leg, the load incident at each leg and the subsequent soil reactions determines the type of gait planning which the designed vehicle can execute in a particular terrain.

The conceptual model showing the interrelationships existing between the excavation, transportation and locomotion processes is shown in Figure 6.1.

From the above discussion it can be seen that the excavation, transportation and locomotion processes of a submersible walking dredger/ miner are highly interdependent and to separate them is impossible.

6.4 Concluding Remarks

The conceptual model developed in this chapter is the basis for designing of controllers for the automation and control of the dredging and locomotion processes of any submersible legged dredger/ miner.

CHAPTER 7

CONCLUSIONS AND RECOMMENDATIONS

7.1 Conclusions and Recommendations

An active legged walking submersible dredger/ miner was designed within the scope of this research. The design was used to manufacture a full scale prototype. The prototype vehicle is shown in Figure 7.1.

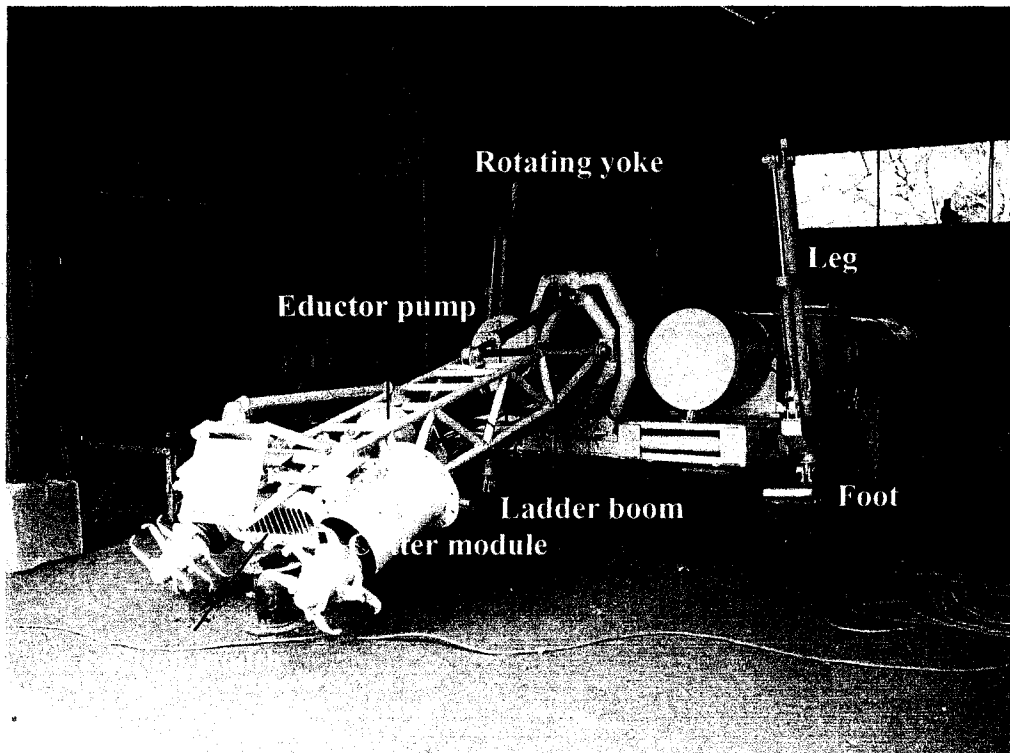


Figure 7.1 Prototype vehicle of 'Golden Tortoise'

Parametric performance models were developed for the designed legged vehicle to evaluate the locomotion, excavation and transportation processes. On-land prototype tests were executed to check the proper functionality of the different systems and also to validate the parametric performance evaluation models for the locomotion process. Comparisons were performed between the designed legged vehicle and tracked vehicle to investigate the advantages and

disadvantages of using an active legged vehicle for underwater dredging/ mining operations. Tracks are commonly used by underwater bottom moving vehicles as the locomotion system. The conclusions of the work are presented here, subdivided according to their main components.

The literature review revealed that surface floating dredgers/ miners have depth limitations and cannot excavate material beyond 150 m. In addition, they also have several operational problems and mobilization issues. Submersible vehicles were found to be a suitable option for deep inland reservoir dredging and offshore dredging and mining purposes. Most of the submersible dredgers available in the marketplace are either tracked vehicles or passive legged vehicles. Tracks are speed effective and easy to control but are not effective in obstacle and slope negotiation. The vehicle body cannot always be kept horizontal with tracked vehicles and hence the excavation tool deviates from the desired trajectory, lowering the production output. Passive legged vehicles are also unable to keep the vehicle body horizontal. This literature review showed the limitations of the existing technology and the absence of suitable technology and led to the configuration of the 'Golden Tortoise'.

Published parametric performance evaluation models were not available for submersible active legged vehicles. A parametric modeling approach is used for off-road wheeled and tracked vehicles, for new design evaluation or performance evaluation under different operating and environmental conditions. Performance evaluation models were not found in the open literature for a twin drum cutter system with a suction mouth in between. Work has been done on the mixture forming processes and prediction of the spillage and hence the excavation production in a crown cutter while excavating hard formations. Empirical specific energy relationships are available for crown cutters in non-cohesive and cohesive soils. The locomotion, excavation and transportation processes of a submersible legged dredger/ miner are interrelated with each other

in a complex fashion. No physical, mathematical or numerical model, which considers these complex interrelationships, was found in the literature. It was decided to develop a conceptual model using the designed submersible active legged dredger/ miner as an example which would show the complex interrelationships existing between the excavation, transportation and locomotion processes. This conceptual model can be used to develop an automatic control system for the designed vehicle.

7.2 Design

Modularity and interchangeability of the different components and equipment are necessary for any good design of a submersible legged dredger/ miner. The change in the operational and environmental parameters can then be easily catered for. The design developed is modular, which helps in easy assembly and transport, with the possibility of interchangeability of the different components and equipment.

The trapezoidal shape of the main body frame proved to be very effective in terms of stability. When the prototype vehicle was resting on its belly and was disturbed from its equilibrium position, the vehicle returned to its initial position within 6 seconds. The trapezoidal shape is also effective for stability issues concerning the soil bearing capacity. The cambered geometry of the main body frame is defined by the camber angle and the camber height. The camber geometry determines the area of contact of the vehicle belly with the soil and thus the ground pressure exerted. The contact area of the vehicle belly with the soil is also dependent on the sinkage of the vehicle belly. This is especially important for very soft cohesive submerged soil. It was found from the designed legged vehicle, that for a fixed camber height and ratio between the length and width of the vehicle, the contact area of the vehicle belly decreases rapidly up to a camber angle of 10 degrees. With further increase in the camber angle, the contact area remains more or less

constant. The numerical values of the contact area varied with different vehicle dimensions and camber height but the same trend was observed for all cases. Thus, when using a trapezoidal main body frame for submerged bottom-moving vehicles, the camber angle should not exceed 10 degrees for safe operation in very soft terrain.

Submersible legged vehicles are slow moving vehicles and thus the drag forces generated by the legs can be neglected while determining the dynamic forces transferred to the foot/ soil interface. The contribution of the ladder assembly in drag generation however cannot be neglected. The ladder assembly is a large structure compared to the legs and usually has a swing velocity ranging from 0.1 to 0.5 m/sec, which is much higher than the forward velocity of the vehicle. The leg drag during swinging is very low. The designed vehicle has an average forward or backward translational velocity of 0.01 m/sec. The force transferred to the foot/ soil interface determines the subsequent soil settlement and failure. The drag forces due to currents, river flows and tidal flows were not considered in this research, since the prototype constructed is suitable for testing and operation in deep inland reservoirs only.

The width of cut for a submersible legged dredger/ miner should always be greater than the width of the vehicle. This is because the legged vehicle performs locomotion in the excavated channel. When the width of cut is lower than the width of the vehicle, difficulties arise in performing locomotion by any submersible legged vehicle. In case of the designed vehicle, the maximum width of cut was 4.7 m, while the width of the vehicle was 2.3 m.

The method of locomotion and the gait plans for any submersible legged dredger/ miner is the most important design criteria. The static stability issues, the stability issues due to soil bearing capacity and the control of the leg actuators must be carefully addressed. A unique method of

locomotion simulating the belly crawling motion of a tortoise or turtle was developed for the designed vehicle, which addressed the above-mentioned issues. Non-periodic gaits are common in natural terrain. Non-periodic gaits are more complex compared to periodic gaits and hence are difficult to control. Periodic gaits were thus developed for both straight line and curvilinear locomotion for the designed active legged vehicle. The designed vehicle has four legs and the four feet are in continuous contact with the ground during the entire locomotion cycle. This together with the simple leg linkage having two degrees of freedom facilitated an easy computation of the leg joint parameters by inverse kinematics and also solved the problems of static stability due to the movement of the vehicle centre of gravity.

The main design principle which should be adopted for any submersible legged dredger/ miner is to simplify the leg linkage design with minimum number of controlling leg joint parameters. Periodic gaits are always easy to control and if possible the 'support phase' and the 'transport phase' of the legs should be kept coincident. When the 'support phase' and the 'transfer phase' of the legs are not coincident, static stability issues and stability issues due to soil bearing capacity should be considered carefully.

The designed vehicle can perform legged locomotion and also belly sliding motion in extremely soft soil. Thus the chances of vehicle capsize are highly reduced for the vehicle.

The ratio between the ground contact area to the power required for excavation and transport was kept high for the designed legged dredger/ miner (0.028) compared to tracked vehicles of similar weight and dimensions (0.022). The average weight to power ratio for the designed legged vehicle (107) was kept lower than existing tracked vehicles (148). The acceptable ground pressure and the length to width ratio of the designed legged vehicle (1.4) were kept lower than a

typical tracked vehicle (1.6). Thus in comparison with tracked vehicles, it is expected that the designed active legged vehicle will be effective with respect to soil bearing capacity, power efficiency and cost effectiveness. These criteria can be used as the basic design criteria for any submersible legged vehicle.

7.3 Locomotion Models

Periodic gait plans were developed for both straight line and curvilinear locomotion on any natural terrain. Experimental validation of the gait plans was performed by full-scale on-land prototype tests. Parametric models were developed for evaluation of the locomotion cycle time, the required soil bearing capacity as a function of the static and dynamic load due to the actuation of the leg hydraulic cylinders and the tractive forces generated during legged locomotion and belly sliding under different slip conditions. Granular and cohesive soils were considered.

Comparisons between the predicted step sizes (where no slip was considered at the foot/soil interface) and the experimental step sizes for forward straight line locomotion showed that the after legs were over predicted by (+)10 % and the forward legs were under predicted by an average value of (-)6 %. The presence of the ladder assembly and the direction of movement will determine the slip or skid action occurring at the foot/ soil interface. The forward legs are dragged during forward straight line locomotion due to the presence of the ladder assembly and hence were found to skid. The after legs on the other hand had a tendency to slip, thereby showing over predicted results. Unlike the forward straight line locomotion, all the four legs were over predicted for backward straight line locomotion. The average deviation percent for the after legs was 38 %, while that for the forward legs was 18.5 %. During backward straight line locomotion, the ladder assembly resists the movements of both the forward and after legs, and

hence they slip. The slip of the after legs is however higher compared to the forward legs. For any legged dredger/ miner performing locomotion in both forward and backward direction, the ladder assembly and the direction of movement will determine the possibility of slip or skid at the foot/ soil interface. In order to have minimum deviation from the desired straight line trajectory, the slip of the four feet should be equal or the swing angles of the legs need to be corrected due to the occurrence of the slip at the feet/ soil interface. The slip at the four feet can be brought close to each other by replacing the manual operation of the electronic switches of the solenoids by automatic control. The corrections for the swing angle of the legs due to the presence of slip at the foot/ soil interface slip factors must be found empirically in different soil types by suitable experiments. Comparisons between these slip factors, which can be kept in a database, should be done during the actual locomotion process and corrections to the leg swing angle can be done based on these values.

Comparisons between predicted step sizes considering the slip at the foot/ soil interface and the experimental step sizes showed that the after portside leg showed a slip of 10 % while the after starboard side leg showed a slip of 10 to 20 % during forward straight line locomotion. During backward straight line locomotion, the after portside leg showed a slip of 20 % while the after starboard side leg showed a slip of 30 %. The amount of slip is dependent on the grouser (teeth or lugs underneath the foot) geometry and the type of soil on which locomotion is performed. The locomotion was performed on dry medium to fine sand. As already emphasized, it is necessary to generate a similar slip percent at all the feet/ soil interfaces during straight line locomotion in order to keep the deviation from the desired straight line path to a minimum. With manual operation of the prototype's electronic switches of the solenoids actuating the directional control valves of the hydraulic cylinders, it was difficult to control the final swing angles of the

legs. Hence different slip percentages were generated. These comparisons, however, give an idea of the magnitude of slip that can be generated at the foot/ soil interfaces of legged dredgers/ miners in relatively dry medium to fine sand. Since the individual foot remains in one position during the entire locomotion cycle, the slip is generated due to shear failure of soil in between the grousers and not due to frictional forces as is common for other legged vehicles.

The deviation from a proposed straight line path and the actual vehicle trajectory during forward straight line locomotion was estimated. The minimum deviation was 28 mm while the maximum deviation was 103 mm. These low deviation values from the proposed straight line trajectory show that the designed leg linkage as well as the proposed method of locomotion is effective for dredging/ mining operations.

A new method of the skid steering principle was developed for turning the legged vehicle through a desired turning angle and turning radius. In the case of tracked vehicles, where skid steering is common, differential thrusts are applied to the outer and inner tracks. The designed vehicle showed that it is possible to turn legged vehicles, with feet fixed to the ground during the entire locomotion cycle by giving differential step sizes to the inner and outer legs. Differential step sizes can be given by unequal step sizes to the outer and inner legs or by keeping the inner legs fixed during the locomotion cycle. The experimental results showed that the turning angle for the designed vehicle was either 1 or 2 degrees during one step, while the turning radii varied from approximately 3.5 to 13 m.

Comparisons between the experimental step sizes for the after portside and after starboard side and the assumed centre of gravity of the vehicle with the predicted step sizes calculated by not considering the slip/ skid at the foot/ soil interface were done for curvilinear locomotion. Smaller

step sizes were given to the inner portside legs, while bigger step sizes were given to the outer starboard side legs. The after portside leg showed deviations ranging from 0 to (-)20 mm. The after starboard side leg showed deviations varying between (+) 40 to (-) 40 mm. Most of the deviations of the assumed centre of gravity of the vehicle were negative and varied from 0 to (-) 40 mm. Negative values suggest that the experimental step size was greater than the predicted step size. The port side leg or the inner leg exhibited skidding during the turning behavior. The starboard side leg on the other hand exhibited both skidding and slipping actions at the foot/ soil interface. Close correspondence between the experimental and predicted values of the turning radii and turning angles were observed when the slip of the outer legs was greater than the slip of the inner legs. The estimated slip for the inner legs varied from 10 to 20 % and that for the outer legs varied between 20 to 30 %.

Due to manual operation of the electronic switches of the solenoids, the prototype vehicle exhibited unusual turning behavior and hence complex slip or skid actions at the foot/ soil interface. Since the inner legs stop swinging earlier than the outer legs, they will always have a tendency to skid. In order to have a more predictable turning behavior, manual operation of the electronic switches needs to be replaced by automatic control. A flow control system in the hydraulic circuits will be required in reducing the skid actions at the inner legs. During turning of legged dredger/ miners where all the feet are kept fixed, the slip of the outer legs will always be higher than the inner legs. Further experimental work needs to be performed to estimate the slip percent at the outer and inner legs during turning in different types of soil. The grouser geometry also needs to be addressed. Such experiments will help to deduce suitable slip factors, which can be used for predicting the turning behavior more accurately and also in the development of controllers for automation of the legged locomotion.

Higher stresses compared to other locomotion trials were generated at the leg swing pin centers during the locomotion trials, when the inner legs were kept fixed and the outer legs were given equal swing angles. The stresses increased further and led to the damage of the grousers of a foot when the vehicle was turned by swinging one leg. From these trials it can be concluded that the best way to turn a legged vehicle by using the principle of skid steering is to give unequal swing angles to the inner and outer legs.

The parametric models developed for predicting the turning behavior of the designed legged vehicle can be used in the evaluation of new designs as well as predicting the vehicle performance under different operating and environmental conditions. The skid steering principle developed for the designed vehicle can be used in designing similar legged vehicles which will perform locomotion by keeping their feet fixed during the locomotion cycle.

The average locomotion cycle time for the designed legged dredger/ miner for straight line and curvilinear locomotion was experimentally measured as 30 seconds. The locomotion cycle is a non-productive cycle and hence should be kept to a minimum. The locomotion cycle time can be decreased by increasing the hydraulic oil flow. This is only necessary in order to achieve a desired average production output over a period of time. The time required to traverse a particular distance is dependent on the step size of the legs as also the locomotion cycle time. If the hydraulic oil flow is controlled in order to achieve the same locomotion cycle time for the different step sizes, the total time required to cover a given distance is only a function of the step size. The step size of the designed legged vehicle is limited by the maximum swing angle possible by both forward and after legs. For the designed vehicle the maximum angle of swing for the forward legs was approximately 25 degrees, while that for the after leg was 50 degrees. This is because of the way the hydraulic cylinders were attached to the main body frame. The

step size is also dependent on the chances of repetitive loading of the soil and the subsequent soil reactions. The optimization of the step size and the chances of repetitive loading and subsequent soil reactions is a subject of further future investigation.

Parametric models were developed to compute the vertical and horizontal forces acting at the foot hinge pin as a function of the static force and the dynamic force due to the operation of the hydraulic cylinders swinging the legs. The swing angle of the leg was changing, while the leg was shifting from its inclined position to a vertical and then back to an inclined position again. The vertical and horizontal forces at the foot hinge pin were thus functions of the swing angle of the leg. The problem was tackled both from a vertical and inclined loading aspect. These parametric models can be used to compute the required soil strength in granular or cohesive soils for any legged vehicle showing either vertical or inclined loading as a function of the leg angle with the vertical.

Bearing capacity is not a problem in granular soils. The bearing capacity requirements for square or circular foot shape for the particular type of leg loading was higher than the rectangular foot shape. In cohesive soil, the bearing capacity requirement for rectangular, square and circular foot shapes is nearly identical up to a vehicle weight of 200 kN for the particular type of leg loading. The bearing capacity requirement in cohesive soil is approximately between 9 to 50 kPa when the weights of the tracked or legged vehicles vary from 30 to 200 kN. With further increase in the vehicle weight, the bearing capacity requirement increases for a rectangular shaped foot for the particular type of leg loading. Thus the choice of rectangular foot for the designed prototype of weight approximately 31 kN is justified.

Comparisons between the prototype legged vehicle with rectangular foot and a tracked vehicle showed that in cohesive soils the bearing capacity requirements for these two types of vehicles are very close up to a vehicle weight of 200 kN. Beyond 200 kN, the dimensions of the rectangular foot of the prototype vehicle needs to be increased.

The horizontal force at the foot hinge pin balances the excavation force and also prevents sliding of the vehicle in the horizontal direction. If necessary this force can be increased by increasing the leg swing angle or by increasing the static force i.e. increasing weight by adding more water to the ballast tanks.

The ratios between the vertical static forces at the foot hinge pin of the forward legs to that of the after legs must also be known for legged vehicles. This ratio determines the differential settlement between the forward and after legs and hence the safety, functionality and reliability of the legged vehicle. The experimentally determined average value of such ratios for the portside legs of the designed legged vehicle was 1.77, while that for the starboard side legs was 1.98. The predicted average value of such ratios was 1.53. No differential settlement was observed between the legs during the execution of the locomotion tests in relatively dry medium to fine sand. Further investigation on cohesive soil must be done in the future to observe the differential settlement effects. The differential settlement also determines the longitudinal and transverse tilt of the vehicle. Symmetrical designs like the 'Golden Tortoise' where pressure vessels of the same dimensions and orientation are attached to both sides of the hull will give lower values of this ratio. The weight distribution on the portside and starboard side of the catamaran hull was also kept similar for the 'Golden Tortoise'.

The parametric models developed for prediction of tractive forces by the foot and the belly during legged locomotion and belly sliding motion respectively show that the shear displacement of the soil is linearly dependent on the step size of the designed legged vehicle. The shear displacement for tracked vehicles is linearly dependent on the distance of the point at which shear displacement is measured from the front of the track. The parametric models developed in this research for the designed legged vehicle can be used to predict the tractive forces generated for different slip percentages for legged vehicles with foot and vertical grousers.

It was observed that in absence of grousers, the foot does not provide sufficient traction to overcome the vehicle weight. The grouser spacing should be greater than the rupture distance for passive soil failure to occur in order to generate sufficient traction by the grousers. The step size of the leg determines the amount of traction generated by the foot in a particular soil. The grouser dimensions and the number of grousers attached to a foot, determine the total tractive force available from the grousers in a particular soil. Thus with increase in the vehicle weight or in the resistance forces (e.g. water drag) the step size of the leg as well as the number of grousers attached to the foot needs to be increased to generate sufficient tractive forces for legged vehicle locomotion.

7.4 Excavation Models

The parametric models developed for the excavation system can be used to evaluate the loosening production, the spillage generated and the excavation power required by a twin drum cutter system with the suction mouth in between. Two different methods were used to evaluate the loosening production, namely the area of integration method and the method of feed. It was observed that the method of feed did not show the variation of loosening production with change in the cutter rpm. The method of integration is thus a better tool in loosening production

estimation for the twin drum cutter system. A mass-damper model was developed to predict the soil lump/ particle trajectory and velocity by considering the gravitational, buoyancy, frictional, drag and current forces acting on the soil lump/ particle. This model can be used to predict the chances of the soil lump/ particle of being picked up by the suction mouth for further transport by the centrifugal dredge pump-pipeline system. This is a basic model and further study needs to be done on this subject to predict the soil lump/ particle trajectory and velocity more accurately.

It was found that for a twin drum cutter system, the trailing cutter performing 'undercutting' should have a lower translatory velocity of the cutter in order to excavate a soil wedge. The leading cutter performing 'overcutting' can have a higher translatory velocity of the cutter in order to form a soil wedge. Since both the leading and trailing cutters should have the same translatory velocity of the cutter, the limiting value for the trailing cutter must be chosen. The number of cutter blades attached in a row (i.e. in the fixing ring) and the ratio between the rotary and translatory velocities of the cutter determines the thickness of the soil wedge formed for the designed drum cutter and also the height of the soil ridge formed on the excavated surface. With increase in the number of blades, thinner soil wedges are formed and the ridge height is also decreased. Thinner soil wedges help in easy mixing. The maximum number of cutter blades, which can be attached to a cutter drum depends on the diameter of the cutter drum. For the designed prototype cutter head, the maximum diameter of the cutter was 300 mm and 3 blades were attached in a row.

Because of the offset of the leading and trailing cutter from the pivot point of the ladder assembly to the main body frame, the translatory velocity of the cutters is a function of the angle which the ladder boom makes with the horizontal. The translatory velocity of cutters is however

almost independent of the angle which the dipper arm makes with the horizontal. This is because the angle only varies between 5 and 10 degrees in the designed excavation system.

The similarity between the virtual cutting edges formed by the pick points of a crown cutter, and that of the blades attached to rows of rings in a drum cutter was deduced in this research. The empirical specific energy relationships for crown cutters were thus used to predict the cutter power required to excavate granular or cohesive material. Such relationships provide an initial estimate only for the designed twin drum cutter system. In the future, actual or model scale tests should be carried out with the designed twin drum cutter system to develop empirical relationships for specific energy requirements.

The maximum step size should never exceed the length of the designed drum cutter.

7.5 Transportation Model

The parametric evaluation models were developed based on two-phase flow theories of previous researchers to predict the delivery production rate and the limiting operating velocities of the designed centrifugal pump-pipeline system. These parametric models can be used to predict the performance of the centrifugal dredge pump-pipeline system of any submersible dredger/ miner.

7.6 Integration of Locomotion and Dredging Processes

The conceptual model developed to show the complex interrelationships existing between the excavation, transportation and locomotion processes must be used for developing overall performance evaluation models for any submersible legged dredger/ miner. The parametric performance models developed for the evaluation of the locomotion, excavation and transportation systems together with this integrated conceptual model can be used in the future to

develop controllers for the designed legged dredger/ miner for the automation of the dredging and locomotion processes.

The main objective of this research work was to develop the design of a suitable active legged submersible dredging or mining platform, which will overcome the limitations of submersible tracked dredgers/ miners and also passive legged dredging vehicles. The mechanical design was found to be very effective through the prototype tests. Other bottom moving vehicles executing tasks other than dredging or mining especially in cohesive soils can also use the principle of locomotion developed in this research. The major modification, which needs to be done with the increase in the depth of operation, is to change the pressure vessels and the hydraulic actuators. The major change, which needs to be done in the future, is the replacement of the manual operation by automatic control. The control task of the vehicle must be distributed in several hierarchical levels. The cutter diameter needs to be increased in order to raise the loosening production.

Reference list

1. Akizono, J., Tanaka, T., Nakagawa, K., Tsuji, T., and Iwasaki, M., 1997, Sea bottom roughness measurement by aquatic walking robot, Proceedings of IEEE, 1997
2. Allmendinger, E.E., (ed.), 1990, *Submersible Vehicle Systems Design*, The Society of Naval Architects and Marine Engineers
3. Amar, F.B., Bidaud, P., Quezdou, F.B., 1993, On modeling and motion planning of planetary vehicles, Int. Conference on Intelligent Robotics System, p 1381-1386
4. Antsaklis, P.J., and Passino, K.M., (ed.), 1993, *An introduction to intelligent and autonomous control*, Kluwer Academic Publishers
5. Apgar, W.J., and Basco, D.R., 1973, An experimental and theoretical study of the flow field surrounding a suction pipe inlet, Center for Dredging Studies Report Number 172, Texas A & M University, TAMU-SG-74-203, Oct., 1973
6. Article in World Dredging & Marine Construction, 1973, Submersible dredge to work on ocean bottom, vol. 9, no. 4, p 13 -14
7. Barker, J.C., 1990, Marine placer development and opportunities in Alaska, *Journal of Mining Engineering*, vol. 42, no.1, p 21-25
8. Bascom, W., 1970, Submersible dredge to work on ocean bottom, World Dredging & Marine Construction, vol.9, no. 4, p 13-14
9. Bekker, M.G., 1956, *Theory of Land Locomotion*, Ann Arbor, MI: University of Michigan Press
10. Boezeman, A.H., Angevaren, C.A., Bos, W.V. D., Vlasblom, W.J., 2000, Structural and dynamic analysis of sub-sea diamond miner MKII, *Terra et Aqua*, no. 81, December, 2000
11. Bonnington, S.T., 1956, Jet pumps, Fourth Conference on Hydromechanics, Ashorne Hill, Leamington, 19-21 April, 1956
12. Burger, den M., W.J., Vlasblom and A.M., Talmon, 1999, Influence of operational parameters on dredge cutter spillage, Proceedings of CEDA Dredging Days 1999, Amsterdam, The Netherlands
13. Caterpillar Handbook
14. Chaziteodorou, G., 1977, *Fundamentals of oceanic mining- a contribution to the extraction and handling of solid mineral resources from the sea*, Ph.D. Thesis, University of Aachen, Belgium

15. Choi, J., Hong, S., Kim, H., 2003, An experimental study on tractive performance of tracked vehicle on cohesive soft soil, Proceedings of the fifth Ocean Mining Symposium, Tsukuba, Japan, September 15-19, ISOPE
16. Coleman, H. W., and Steele, W.G., 1999, *Experimentation and Uncertainty Analysis for Engineers*, John Wiley and Sons
17. Conway, T., 1986, ROV Mantis: A dual purpose underwater vehicle, *IEEE Journal of Oceanic Engineering*, vol. OE-11, no. 3, July, 1986, p 418- 421
18. Cubero, S.N., 2000, A 6-legged hybrid walking and wheeled vehicle, 7 th. International Conference on Mechatronics and Machine Vision in Practice, Obtained from Online Database at <http://mech-eng.curtin.edu.au/HYDROBUG1.pdf>
19. Caurin, G. and Tschichold –Gürman, N., 1994, Development of a robot terrain interaction system for walking machines, Proceedings of IEEE International Conference on Robotics and Automation, p 1013 – 1018, San Diego, CA, USA
20. Clift, R., Wilson, K.C., Addie, G.R, and Carstens, M.R.,1982, A mechanistically- based method for scaling pipeline tests for settling slurries, Proceedings Hydrotransport 8, BHRA, Cranfield, UK, p 91 -101
21. De Beer, E.,1967, Shape factors for shallow foundations, Annales des Travaux Publics de Belgique
22. Deepak, C.R., Shajahan, M.A., Atmanand, M.A., Ravindran, M., Schulte, E., Grebe, H., Schwarz, W., 2003, Underwater mining in shallow waters using flexible riser concept – the first step towards deep sea mining of poly-metallic nodules, International Conference on Coastal and Ocean Technology, 2003
23. Deepak, C.R., Shajahan, M.A., Atmanand, M.A., Annamalai, K., Jeyamani, R., Ravindran, M., Schulte, E., Handschuh, R., Panthel, J., Grebe, H., Schwarz,W., 2001, Development tests on the underwater mining system using flexible riser concept, Proceedings of 4th Ocean Mining Symposium of Int. Society of Offshore and Polar Engineers, 23-27 Sept. 2001, Szczecin , Poland
24. Deepak, C.R., Pugazhaandi, M., Paul, S., Shajahan, M.A., Janakiraman, G., Atmanand, M.A., Annamalai, K., Jeyamani, R., Ravindran, M., 1999, Underwater Sand Mining System for Shallow Waters, Proceedings of Third Ocean Mining Symposium, International Society of Offshore and Polar Engineers, 8- 10 Nov., 1999, Goa, India
25. Denovan, R.C., and Norman, R.V., 1996, Engineering philosophies associated with subsea diamond sampling and mining, Proceedings of Offshore Technology Conference, vol. 1, p 589-609
26. Desa, E., 1999, Opportunities for offshore mineral exploration in the Indian Ocean, Proceedings of the 3rd. ISOPE Ocean Mining Symposium, ISOPE, p 6-13

27. Doebelin, Ernest, O., *Measurement systems: Application and Design*, McGraw Hill, 2002
28. Douglas, C., Montgomery, *Design and Analysis of Experiments*, John Wiley and Sons, 2005
29. "Dredging Research Technical Notes", US Army Engineer Waterways Experiment Station, Technical Note DRP-2-13, January, 1995
30. Dudek, G. and Jenkin, M., 2000, *Computational principles of mobile robotics*, Cambridge University Press, 2000
31. Durand, R., 1953, Basic relationships of the transportation of solids in the pipes-experimental research, Proc. Minnesota International Hydraulics Convention, Minneapolis, Minnesota, p 89-103
32. EEM internal report, 1999
33. Endo, G., and Hirose, S., 2000, Study on Roller-Walker (multi-mode steering control and self contained locomotion), Proceedings of International Conference on Robotics and Automation, San Francisco, 2000
34. Führböter (1961): Read review from Matousek, 1999
35. Gee-Clough, D., 1991, Soil-vehicle interaction, *Journal of Terramechanics*, vol. 28, no. 4, p 289- 296
36. Gerhart, G., Laughery, S., Goetz, R., 2000, Off road vehicle locomotion using Bekker's model, Proceedings of SPIE – The International Society for Optical Engineering, vol. 4024, p 127-136
37. Gilbert, R., 1960, Transport hydraulique et refoulement des mixtures en conduits, *Annales des Ponts et Chausees*, : Read review in English from Matousek, 1999
38. Grace, J.R., 1986, Contacting models and behavior classification of gas-solid and other two-phase suspensions, *Canadian Journal of Chemical Engineers*, no. 64, p 353 - 63
39. Greiner, H., Sheckman, A., Chikyung, W., Elsley, R., Beith, P. 1996, Autonomous legged underwater vehicles for near land warfare, Proceedings of the IEEE Symposium on Autonomous Underwater Vehicle Technology, p 41-48
40. Halme, A., Leppänen, I., Salmi, S., Ylönen, S., 2000, Hybrid locomotion of a wheel-legged machine, CLAWAR 2000, Madrid, 2000
41. Halme, A., Leppänen, I., Salmi, S., 1999, Development of WorkPartner- robot- design of actuating and motion control system, CLAWAR'99, Portsmouth 1999
42. Handschuh R., Grebe, H., Panthel, J., Schulte, E., Wenzlawski, B., Schwarz, W., M.A., Atmanand, Jeyamani, R., Shajahan, M., Deepak, R., Ravindran, M.,, 2001, Innovative Deep

Ocean Mining Concept based on Flexible Riser and Self-propelled Mining Machines, Proceedings of 4th Ocean Mining Symposium of Int. Society of Offshore and Polar Engineers, 23-27 Sept. 2001, Szczecin, Poland

43. Hansen, B., 1965, Design criteria, safety factors and settlement limits, Proceedings Duke university, April 5/6, p 9-13
44. Herbich, J.B., 2000, *Handbook of dredging engineering*, McGraw Hill Inc.
45. Herbich, J.B., 1992, *Handbook of dredging engineering*, McGraw Hill Inc.
46. Hill, J.C.C., 1983, Dredging aids deepwater oil and gas operations, *Petroleum Engineer International*, vol. 55, no.4, p 16-28
47. Hong, S., and Choi, J., 2001, Experimental study on grouser shape effects on trafficability of extremely soft seabed, Proceedings of the fourth Ocean Mining Symposium, ISOPE
48. Hoerner, S.F., *Fluid Dynamic Drag*, Bricktown, N.J., 1965
49. Jonge, L.D., Vlasblom, W.J., Bos, W. van de, Boezeman, A.H., 2001, Modeling and testing of Sub Sea Diamond Mining Machine, CEDA Dredging Days 2001, November, Amsterdam, The Netherlands
50. Juffin and Lopatin, 1966: in Dutch: Review read from Matousek, 1999
51. Kalske, S., 1997, *Motion simulation of underwater vehicles*, Technical Research Centre of Finland, VTT publications, p138
52. Kim, H.W., Hong, S., and Choi, J., 2003, Comparative study on tracked vehicle dynamics on soft soil: Single body vs. Multi body dynamics, Proceedings of the fifth Ocean Mining Symposium, Tsukuba, Japan, September 15 – 19, 2003, International Society of Offshore and Polar Engineers
53. Koblick, M., 1984, *Living and working in the sea*, Van Nostrand Reinhold Company, 1984
54. Kuo, C., 1994, Realizing engineering potential in ocean wealth generation, Proceedings of the Institution of Mechanical Engineers, Part E: *Journal of Process Mechanical Engineering*, vol.208, no. E2, p 107 –122
55. Lagnemma, K., and Dubowsky, S., 2002, Terrain estimation for high-speed rough-terrain autonomous vehicle navigation, Proc. of SPIE- The International Society for Optical Engineering, vol. 4715, p 256- 266
56. Lee T.H., Lee, C.S., and Jung, J, 2003; Prediction of the motion of tracked vehicle on soft soil using krigging metamodel, Proceedings of the fifth Ocean Mining Symposium, Tsukuba, Japan, September 15 – 19, 2003, International Society of Offshore and Polar Engineers

57. Leppänen, I., et al., 1998, Workpartner – Helsinki University of Technology-Autonomous new hybrid walking machine, CLAWAR '98, Brussels, 1998
58. Leussen, W.V., and Nieuwenhuis, J.D., Soil mechanics aspects of dredging, *Journal of Geotechnique*, 34, no. 3, p 359-381
59. Liddle, D., TROJAN: Remotely operated vehicle, *IEEE Journal of Oceanic Engineering*, vol. OE-11, no. 3, July, 1986, p 364-372
60. Lunne T., 1985, Interpretation of cone penetrometer data for offshore sands. *Norges Geotekniske institut Bulletin* no. 156 Oslo
61. Mangkusubroto, K., 1995, Indonesia's ocean resource developments, Proceedings of 1st ISOPE Ocean Mining Symposium, p 229-233
62. Matousek, V., 1999, *Hydraulic transport as one of the dredging processes*, Collediktaat: Baggerprocessen 2, Delft Technical University
63. Matousek, V., 1997, *Flow mechanism of sand water mixtures in pipelines*, Ph.D. thesis, Delft University Press
64. Miedema, S.A. 1999, Considerations on the limits of dredging process, Proc. WEDA 19th Technical conference and 31st Texas A & M Dredging Seminar, Louisville, Kentucky, p 233 - 254
65. Miedema, S.A. 1995, Production estimation based on cutting theories for cutting water saturated sand, Proc. WODCON XIV, Nov. 1995, Amsterdam, The Netherlands
66. Miedema, S.A., 1994, On the snow-plough effect when cutting water saturated sand with inclined straight blades, ASCE Proc. Dredging 94, Orlando, Florida, USA, November
67. Miedema, S.A., 1992, New developments of cutting theories with respect to dredging, the cutting of clay, Proc. WODCON XIII, Bombay, India
68. Miedema, S.A. 1989b, On the cutting forces in saturated sand of a seagoing cutter suction dredger, *Terra et Aqua*, no. 41, December, 1989, Elseviers Scientific Publishers
69. Miedema, S.A. 1989a, On the cutting forces in saturated sand of a seagoing cutter suction dredge, WODCON XII, Orlando, Florida, USA, April 1989, Published also in *Terra et Aqua*, no. 41, December 1989, Elseviers Scientific Publishers
70. Miedema, S.A. 1987, *Calculation of the cutting forces when cutting water saturated sand- Basic theory and applications for 3-D blade movements and periodically varying velocities for in dredging commonly used excavating means*, Ph.D. thesis, Delft University of Technology, Sept. 15, 1987
71. Miedema, S.A., 1984, The cutting of densely compacted sand under water, *Terra et Aqua*, No. 28, October, 1984, p 4-10

72. Moon, J.W., Kim, K.H., Lee, K.Y., 1997, Korean deep sea bed mining exploration, *Journal of Sea Technology*, vol. 38, no. 12, p 29-35
73. Muro, T. 1988, Grouser effect on tractive performance of a bulldozer running on a super weak marine sediment, Proc. of the 2nd Asia-Pacific Conference of the ISTVS, Bangkok, Thailand, Dec 6-10, 1988, p 355-366
74. Nagy, P.V., Whittaker, W.L., and Desa, S., 1992, A walking prescription for statically stable walkers based on walker/ terrain interaction, Proc. of International Conference on Robotics and Automation
75. Nakamaru, E., Kondo, T., Teramoto, A., The design and operation of a dredging robot system, Proceedings of the XIII th World Dredging Congress, 7- 10 th April, 1992, Bombay, India, p 846-868
76. Narewski, M. et al., 2002, Application of Autonomous Remotely Operated Vehicle for Exploration of Polymetallic nodules, Online Database at http://www.underwater.pg.gda.pl/publikacje/application_of_AUV.pdf
77. Newitt, D.M., Richardson, J.F., Abbott, M., and Turtle, R.B., 1955, Hydraulic conveying of solids in horizontal pipes, *Trans. Inst. Chem. Eng.*, 33, p 93-113
78. Nomoto, M., and Hattori, M., A deep ROV “DOLPHIN 3K”: Design and performance analysis, *IEEE Journal of Oceanic Engineering*, vol. OE-11, no. 3, July, 1986, p 373 – 391
79. Norton, R.L., 1999, *Design of Machinery*, 2nd. Ed. McGraw-Hill International Editions
80. Nuttall Jr., C.J., 1971, Traction limits for tracked vehicles crawling the sea bottom, *Journal of Engineering for Industry*, May, 1971, p 717-730
81. PIANC, 1972: *Classification of dredging soils*
82. PIANC, 1984 “Classification of Soils and Rocks to be Dredged”, Report of a Working Group of the Permanent Technical Committee II, Supplement to Bulletin No. 47, Permanent International Association of Navigation Congresses (Also published in *Terra et Aqua*, No. 30, November, 1985)
83. Ports and Dredging 2003, no. 159, Assignment of the world’s largest deep dredging installation, IHC Holland, p 22-23
84. Reece, A.R., Principles of Soil- Vehicle mechanics, Proceedings Institution of Mechanical Engineers, vol. 180, part 2A, 1965 - 1966
85. Report: Paragon International to EEM (P) Ltd., 1994
86. Richardson, M.J., (ed. Richardson, S.), 2002, *The dynamics of dredging*, Placer Management Corporation, Irvine, California, USA, 2002

87. Ross, C.T.F., 1990, *Pressure Vessels under External Pressure Statics and Dynamics*, Elsevier Applied Sciences, 1990
88. Sasaki, S., Yamada, T., Miyata, E., 1991, Articulated tracked vehicle with four degrees of freedom, *Journal of Terramechanics*, vol. 28, no. 2-3, p 189-1999
89. Schlichting, H, 1979, *Boundary layer theory*, McGraw Hill, 7 ed.
90. Schulte, E., Grebe, H., Handschuh, R., Schwarz, W., 2003, Assessment of trafficability of deep sea floor with a self propelled mining machine, International Conference on Coastal and Ocean Technology, 2003
91. Schulte, E., Handschuh, R., Schwarz, W., 2003, Transferability of Soil mechanical parameters to traction potential calculation of a tracked vehicle, Proceedings of the fifth Ocean Mining Symposium, Tsukuba, Japan, September 15-19, ISOPE
92. Scott, S.D., 2001, Deep Ocean Mining, Geoscience Canada, vol. 28, p 87 -96
93. Stepanoff, A.J., 1965, *Pumps and blowers, Two phase flow: Selected advanced topics*, J.Wiley & Sons. Inc.
94. Swamee, P. K. and Jain; A. K., 1976, Explicit equations for Pipe Flow Problems, *Journal of Hydraulic Divn.*, Proceedings ASCE, May 1976, p 657 – 664
95. Teferra. A.,1975, F.B.G. Aachen, Beziehungen zwischen Reibungswinkel und Sondierwiderstanden
96. Terzaghi, K., and Peck, R.B., 1968, *Soil mechanics in engineering practice*, John Wiley & Sons
97. Tsuji, M. and Takaharu, O., 1995, Development of self movable type submersible dredging robot, Robot, Report no. 105, Jul 1995, p 33-37
98. Tuper, E., 2000, *Introduction to Naval Architecture*, third edition – revised print, Butterworth Heinemann, p 86 and 92
99. Turnage, G.W., 1978, A synopsis of tire design and operational considerations aimed at increasing in- soil tire drawbar performance, Proceedings of the 6 th International Conference of the International Society for Terrain – Vehicle Systems, vol. II
100. Unified Soil Classification System, US Army Corps of Engineers, Technical Memorandum No. 3-357, Washington DC, April, 1960
101. Van den Berg, C.H., 1998, *Pipelines as Transportation Systems*, European Mining Course Proceedings, MTI, Holland
102. Van der Steen, 1999-2000, Offshore mining system development

103. Van der Steen, A., 1989, An engineering strategy for reservoir clearance, Summary paper, ESCAP Workshop, New Delhi, 16-20 Oct., 1989
104. Van Os, A.G. and Van Leussen, W., 1987, Basic research on cutting forces in saturated sand, *Journal of Geotechnical Engineering*, Vol. 113, no. 12, Dec. 1987
105. Van Os, A.G., 1977, Behavior of soil when excavated underwater, International Course Modern Dredging, June, 1977, The Hague, The Netherlands
106. Verheul, O., Vercrujisse, P.M., and Miedema, S.A., 2004, The development of a concept for accurate and efficient dredging at great water depths, in Proceedings of XVII WODCON, Hamburg, Germany
107. Vesic, A., 1970, Bearing capacity of shallow foundations
108. Vlasblom, W.J., 2000, Deep dredging techniques
109. Vlasblom, W.J., 1999, *Designing dredging equipment: Part 4: Cutter Dredgers*, Lecture notes, Department of Transport Technology, Delft University of Technology, 1999
110. Weber, M., 1982, Vertical hydraulic conveying of solids by airlift, *Journal of pipelines*, vol.3, p 137-152
111. Wettergreen, D., 1995, *Robotic walking in natural terrain- Gait planning and behavior-based control for statically-stable walking robots*, Ph.D. thesis, The Robotics Institute, Carnegie Mellon University, Pittsburg, 1995
112. Williams, G.L. and Visser, K.G., 1997, The Punaise: A remotely operated submerged dredging system. *Terra et Aqua*, no. 69, December 1997
113. Wilson, K.C. et al. (1997), *Slurry transport using centrifugal pumps*, Blackie Academic & Professional: Review read from Matousek, 1999
114. Wilson, K.C., 1996, Heterogeneous slurries, Chapter 4 .0 of the Proceedings Hydrotransport Seminar. Back to basics- With the Experts, BHRG, Cranfield, UK: Review read from Matousek, 1999
115. Wilson, K.C., 1986, Effect of solids concentration on deposit velocity, *Journal of Pipelines*, 5, p 251 – 257
116. Wilson, K.C., 1979, Deposition limit nomograms for particles of various densities in pipeline flow, Proceedings of Hydrotransport 6, BHRA, Cranfield, UK, p 1-12
117. Wilson, K.C., 1976, A unified physically based analysis of solid-liquid pipeline flow, Proceedings of Hydrotransport 4, BHRA, Cranfield, UK, p 1-6: Review read from Matousek, 1999

118. Worster, R.C. and Denny, D.F. , 1955, Hydraulic transport of solid materials in pipelines, Proceedings Inst. Mech. Engineers., (London), 169, p 563-586: Review read from Matousek, 1999
119. Witting, J.H., Ayers, J., Korav, S., 2000, Development of a biomimetic underwater ambulatory robot: Advantages of matching biomimetic control architecture with biomimetic actuators, Proceedings of SPIE- The International Society for Optical Engineering, v 4196, 2000, p 54-61
120. Wong, J.Y., 1993, *Theory of Ground Vehicles*, 2nd. Ed. , John Wiley & Sons, Inc. 1993
121. Wong, J.Y., Data processing methodology in the characterization of the mechanical properties of terrain, 1980, *Journal of Terramechanics*, vol. 17, no.1
122. Wong, J.Y., and Preston – Thomas, J., On the characterization of the shear stress – displacement relationship of terrain, 1983, *Journal of Terramechanics*, vol. 20, no.1
123. Wong, J.Y., Garber, M., Radforth, J.R., and Dowell, J.T., 1979, Characterization of the mechanical properties of Muskeg with special reference to vehicle mobility, *Journal of Terramechanics*, vol. 16, no. 4
124. Yatsuk, E.P., et al., 1971, *Rotary soil working machines: Construction, calculation and design*, Amerind Publishing Co. Pvt. Ltd.
125. Zhaung, J., Wang, Z., and Liu, J., 1990, Study on the dynamic characteristics of wheeled vehicles on sand, ASME, Applied Mechanics division, AMD, vol. 108, Transportation systems 1990, p 211-217

Webpages:

Web page 1.1: <http://www.ocean-resources.com/issues/article.asp?ID=363&MagID=17>;
Accessed on 18.09.2006

Webpage 1.2: <http://www.smdhydrovision.com/> : Accessed on 18.09.2006

Webpage 1.3: <http://www.dutchseacable.com/> : Accessed 18.09.2006

Webpage 1.4: <http://www.iscpc.org/information/dive.htm> : Accessed 18.09.2006

Webpage 1.5: <http://www.clawar.com/> : Accessed 18.09.2006

Webpage 1.6: <http://www.leggedrobots.ceti.pl/> : Accessed 18.09.2006

Webpage 1.7: <http://www.kimura.is.uec.ac.jp/faculties/legged-robots.html#quadruped>
Accessed 18.09.2006

APPENDIX 1

SOIL BEHAVIOR - BASIC SOIL PARAMETERS DETERMINING PRODUCTION AND MOBILITY IN GRANULAR AND COHESIVE MATERIAL

1.0 Introduction

The classification and description of the soil and rock present in the work area is necessary prior to the evaluation of the excavation and locomotion processes. British Standard (BS) and American Society for Testing and Materials (ASTM) Standard are commonly used for the classification and description of the soil and rock. The PIANC system: 'Classification of Soils and Rock to be Dredged' [1984] is commonly used by the dredging industry for the classification of the soils and rocks for excavation purposes. The soil classifications used for the description of the soil terms in this thesis are presented in section 6.0.

In order to evaluate the excavation and the locomotion processes, the characteristics of the soil data are evaluated from two principally different viewpoints 1) excavation i.e. destruction of the soil by means of the excavation system and 2) stability i.e. prevention of the failure of the soil due to bearing pressures.

2.0 Vehicle Stability due to Soil Bearing Pressures

Problems may occur with the deployment and operation of a submersible legged dredger/ miner because of the limited bearing capacity of the soil resulting in excessive 'sinkage' at the foot/ soil interface. The theories of elasticity and plastic equilibrium as well as the shallow foundation theories can be applied to determine the required bearing capacity of soil for a legged vehicle. The foot of any legged vehicle can be assumed to be rigid footing. When the vertical load applied by the foot to the soil is light, the soil beneath the foot may be in a state of elastic

equilibrium. When the load is increased to a certain level, the soil beneath the foot will pass into a state of plastic flow, resulting in an abrupt increase in the sinkage at the foot/ soil interface. The load (Q_o) [kN] per unit contact area ($A_{contact}$) [m^2] that causes failure is defined as the ‘bearing capacity’ of the soil. The bearing capacity (q_o) [kPa] can be assessed by applying the Buismann–Terzaghi equation [Terzaghi, 1943].

$$q_o = c * N_c + h_{surcharge} * \gamma_{soil} * N_q + \frac{1}{2} * \gamma_{soil} * B_{foot} * N_\gamma \quad [\text{Equation 1}]$$

where, B_{foot} is the width of the foot [m], c is the soil cohesion [kPa], $h_{surcharge}$ is the depth of surcharge [m], N_c, N_q, N_γ are dimensionless ‘bearing capacity factors’ for a long rectangle, and γ_{soil} is the specific weight of the soil [kN/m^3]. The first term represents the influence of the soil cohesion, the second the influence of any surcharge that may be present and the third the effect of the weight of the soil that would be involved in the foundation failure. In case of a legged vehicle the second term due to surcharge can be neglected. The bearing capacity factors are defined,

$$N_q = e^{\pi \tan \phi_{soil}} * \tan^2 \left(\frac{\pi}{4} + \frac{\phi_{soil}}{2} \right)$$

$$N_c = (N_q - 1) * \cot \phi_{soil} \quad [\text{Equation 2}]$$

$$N_\gamma \approx 2 * (N_q + 1) * \tan \phi_{soil}$$

where, ϕ_{soil} is the angle of internal friction of the soil [degree].

For different shape of the foot (Equation 1) is modified as [De Beer, 1967; Vesic, 1970],

$$q_o = c * N_c * \zeta_c + h_{surcharge} * \gamma_{soil} * N_q * \zeta_q + \frac{1}{2} * \gamma_{soil} * B_{foot} * N_\gamma * \zeta_\gamma \quad [\text{Equation 3}]$$

where, $\zeta_c, \zeta_q, \zeta_\gamma$ are dimensionless parameters called 'shape factors'. Shape factors also depend on the angle of internal friction of the soil (ϕ_{soil}) [degree] as well as on functions of the geometrical form of the support. The commonly used shape factors are tabulated in Table 1. The length of the foot is denoted as L_{foot} [m].

Table 1 Shape factors

Shape of base	ζ_c [-]	ζ_q [-]	ζ_γ [-]
Strip	1.00	1.00	1.00
Rectangle	$1 + \left(\frac{B_{foot}}{L_{foot}} \right) \left(\frac{N_q}{N_c} \right)$	$1 + \left(\frac{B_{foot}}{L_{foot}} \right) \tan(\phi_{soil})$	$1 - 0.4 * \left(\frac{B_{foot}}{L_{foot}} \right)$
Circle / Square	$1 + \left(\frac{N_q}{N_c} \right)$	$1 + \tan(\phi_{soil})$	0.60

Vesic [1970] gave the numerical values of the dimensionless bearing capacity factors for different values of the angle of internal friction of the soil (ϕ_{soil}) [degree]. Thus for cohesive soils like saturated clays, the angle of internal friction of the soil (ϕ_{soil}) and the bearing capacity factor, N_γ are zero [-], while the bearing capacity factor, $N_q = 1$ [-] and $N_c = 5.14$ [-]. The bearing capacity equation becomes,

$$q_o = c * 5.14 * \zeta_c \quad \text{[Equation 4]}$$

These calculations are based on non-dynamic loading and as such a safety factor of at least 1.5 [Hansen, 1965] should be considered. The required soil strength for cohesive soils for a given weight of the designed vehicle is thus,

$$c = \frac{Q_o}{5.14 * A_{contact} * \zeta_c} \quad \text{[Equation 5]}$$

where, $A_{contact}$ is the contact area [m²].

In weaker soils, the subsea weight of the vehicle can be reduced by using air tanks or fixed buoyancy blocks.

The vehicle stability in granular material usually does not create a problem. For the worst condition when $c = 0$ kPa and $h_{surcharge} = 0$ m, the bearing capacity equation becomes,

$$q_o = \frac{1}{2} * \gamma_{soil} * B_{foot} * N_{\gamma} * \zeta_{\gamma} \quad \text{[Equation 6]}$$

The sinkage of the machine due to soil deformation is a source of loss of power and traction and may lead to stalling.

3.0 Shear stress–Shear Displacement Relationships

When a torque is applied to the tire or sprocket of a track, shearing action is initiated on the vehicle running gear–terrain interface (Figure 1). To predict the tractive performance and the associated slip of the vehicle running gear, the shear stress–shear displacement relationships of the terrain are required.

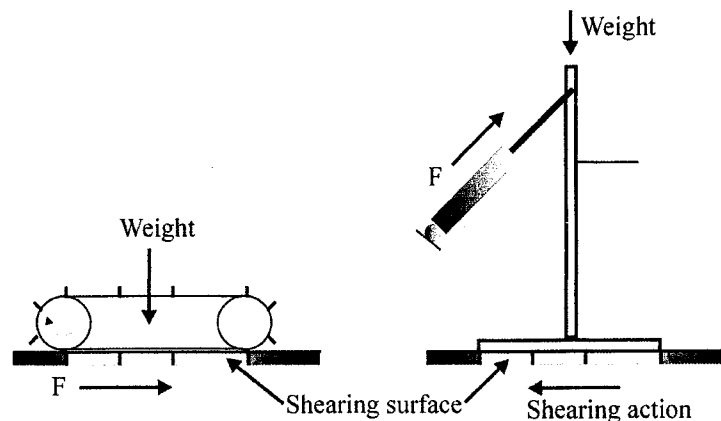


Figure 1 Shear stress at the vehicle running gear-terrain interface (Left Track, Right Leg with foot)

Unlike tracks or wheels, legs are only in contact with the terrain during the ‘support phase’. Thus shearing action is generated during the support phase of the legs, when a torque is applied by the drive. The intermittent traction generated by the legs in ‘support phase’ should be adequate enough to overcome the total external motion resistances (including soil resistances and water drag) of a submersible legged vehicle. Accurate knowledge about the shear stress–shear displacement characteristics of the terrain is thus also necessary for a legged vehicle.

Based on a considerable amount of field data from on-land terrains, three types of shear stress–shear displacement relationships are commonly observed in the literature, which are 1) for loose sand, saturated clay, dry fresh snow and most of the disturbed soils, 2) for organic terrains, and 3) for compact sand, silt and loam and frozen snow [Reece, 1965; Wong, 1993; Wong and Preston–Thomas, 1983]. The shear stress–shear displacement relationships for the first category of terrain are discussed briefly next, since it is more appropriate for the terrain types of the chosen inland working areas for the designed vehicle. The shear stress–shear displacement relationship exhibits a simple exponential form for loose sand, saturated clay and most disturbed soils (Figure 2).

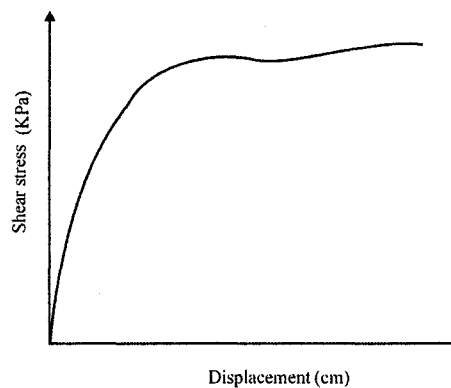


Figure 2 Schematic of shear stress-shear displacement relationship for loose sand, saturated clay and most disturbed soils

The shear stress initially increases rapidly with an increase in the shear displacement and then approaches a constant value with a further increase in shear displacement. This type of shear stress–shear displacement relationship is described by an exponential function as proposed by Janosi and Hanamoto [Wong, 1993].

$$\tau = \tau_{\max} \left(1 - e^{-\frac{j}{K}} \right) \quad \text{[Equation 7]}$$

$$\tau_{\max} = \left(c + p_{soil_normal} * \tan(\phi_{soil}) \right) \quad \text{[Equation 8]}$$

where, c is the soil cohesion [kPa], j is the shear displacement [cm], K is the shear deformation modulus [cm], ϕ_{soil} angle of internal friction of the soil [degree], τ is the shear stress [kPa], and τ_{\max} is the maximum shear stress [kPa]. The shear deformation modulus (K) is considered as a measure of the magnitude of the shear displacement required to develop the maximum shear stress. Based on experimental data [Reece, 1965; Wong, 1993] the value of K varies between 1 cm for firm sandy terrain to 2.5 cm for loose sand and approximately 0.6 cm for clay at maximum compaction. K is also a function of the normal pressure applied to the soil (p_{soil_normal}) [kPa].

The characteristics of soft cohesive soil show highly non-linear properties [Hong and Choi, 2001]. Kim et al. [2003] used the equation proposed by Baladi and Rohani [1978] [Wong, 1993] for the maximum shear stress to study the dynamics of tracked vehicle on soft soil. Lee et al. [2003] developed a sampling technique and a krigging (a regression technique used in geostatistics to approximate or interpolate data) metamodel to predict the motion of a tracked vehicle traveling on soft soil especially for sub sea terrains. For soft ground, the interactions

among track, road wheels and soil become so complicated that the basic theory on pressure-sinkage and shear-traction force is limited in its application. This metamodel was used to predict the vertical sinkage as well as the slip of the track. Acceptable accuracy of the model was achieved. Schulte et al. [2003] used a bentonite-water mixture, which has been shown to be an acceptable deep sea soil substitute, as the material composition and the main characteristics are similar (thixotropy, relation between maximum shear stress and residual shear stress) for measuring the shear stresses using three different devices namely a vane tester, a shear ring and a track segment. Schulte et al. [2003] developed a bentonite-shear displacement-function (BSD-function) to describe the shear stress-shear displacement relationships for bentonite-water mixture.

In this thesis, the Janosi and Hanamoto equation for shear stress-shear displacement (Equation 7 and 8) was used to predict the tractive performance of the designed legged vehicle.

4.0 Soil Parameters Determining Excavation Performance

The soil parameters determining the excavation performance of a submersible dredger/ miner are shown in Figure 3.

The representative values of the soil mechanical parameters shown in Figure 3 are presented in section 7.0.

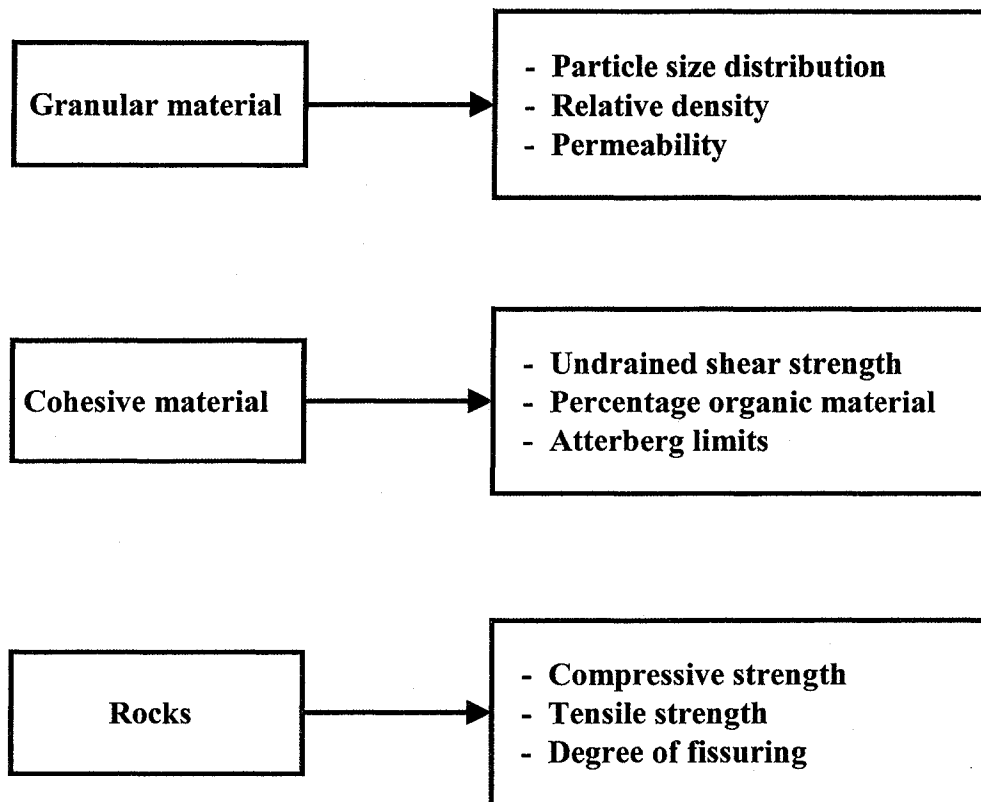


Figure 3 Soil properties determining production

5.0 Soil Behavior during Excavation

To determine the performance of the submersible dredger/ miner it is essential to ascertain which independent soil parameters affect the different dredging processes. The dredging sub-processes taking place cannot always be clearly distinguished, but for evaluation purposes it is useful to identify them. These include 1) loosening i.e. breaking up of the soil or rock to pieces sufficiently small to be picked up by the suction, 2) gathering i.e. bringing the loosened material to a point where mixing and/or transport starts, 3) mixing i.e. mixing of the loosened material with water, and 4) transport i.e. transporting of the loosened material from the seabed to the surface. During these processes the soil is dynamically loaded up to failure to produce a

pumpable mixture. The soil mechanics involved are different from those described in the section 2, which concerned the bearing capacity of soil and prevention of failure and not its destruction.

5.1 Phenomena during Excavation of Granular Material

A shear stress is exerted when the soil is excavated using jets or mechanical cutters. At increasing shear strain loose sand has the tendency to decrease in volume and denser packing of grains will result. When cutting dense sand the opposite phenomena occurs i.e. the packing becomes looser. This phenomenon is called dilatation (Figure 4). If dense sand is saturated with water, and due to the flow resistance in the soil, the change of pore volume cannot be compensated quickly enough by an equal change in water volume, a hydrostatic under-pressure (negative pore pressure) occurs. Hence the effective stresses will increase accordingly until the vapor pressure of water is reached and cavitation occurs, limiting the pore pressure.

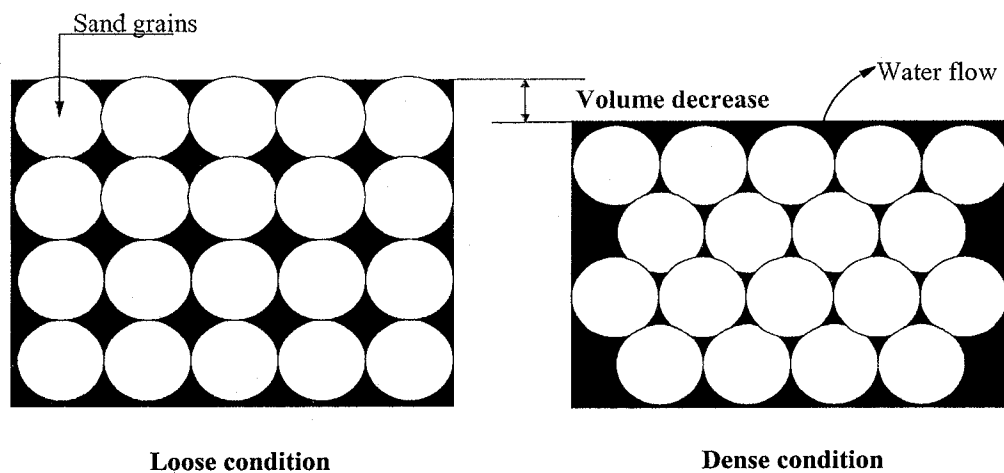


Figure 4 Excavation of loose sand

As described above, the flow of water through the sand forms a major aspect of the excavation process (jetting or mechanical cutting). As a consequence, the permeability of the soil is an

important parameter. The permeability determines if and how pore pressures can build up and disperse, thus influencing the cutting forces, jet productions and the stability of the grain skeleton (Figure 5).

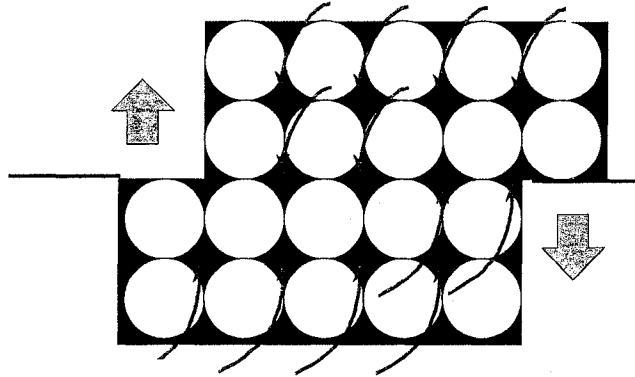


Figure 5 Dilatation of granular material

Usually no direct measurements of permeability of the soil are made during a soil survey. However different correlations are used to estimate the permeability values [Terzaghi, 1943]. Relative density of soil, which is another important soil parameter to determine excavation production, is related to the pore volume of the soil. It is extremely difficult to determine the in-situ pore volume of soil. Teferra [1975] correlated the cone resistance to the relative density.

5.2 Cohesive Material

Generally it can be stated that the process of cutting cohesive material consists of the pushing upwards of a wedge of soil, squeezed between a soil to soil and a soil to metal surface (Coulomb theory). Clay is normally saturated with all the spaces between the particles filled with water. When it is loaded rapidly, part of the load is carried by the water resulting in the strength of the clay being independent of the load, i.e. it behaves as if it is frictionless. This in contrast to sand

which, being very permeable, does not generally share the load with the internal water, hence its strength depends on the load, i.e. it is frictional. If clay is loaded very slowly, the water can be squeezed out and frictional behavior may develop. This may happen, for example, with a rate of loading imposed by a construction of a building. At the loading rates applied during submerged soil excavation, clays can be considered as frictionless. As a consequence the main determining parameter covering the loosening process is the undrained shear strength of the material (S_u) [kPa]. Other parameters such as the Atterberg limits are of lesser importance, however, they give a better insight in the general behavior of the clay after excavation, thus in the mixing and transport processes.

It must be noted that in the stronger clays the discontinuity of the material (fissures) will reduce the excavation forces by providing weaker planes of failure. The stronger the clay gets, the more it has a large scale structure which a water jet or mechanical cutter can exploit. It must be realized that the clay lumps thus produced are no longer determined by the cutting action, because failure mostly occurs along the fissures before the cutting action, hence large slabs of clay can be dislodged.

6.0 Soil Classification Based on Grain Size

Three of the systems most commonly used in the dredging operations are shown in Table 1. The Wentworth system [1922] is one of the earliest systems and is used by nearly all scientists and engineers, except geotechnical engineers [US Army Engineer Waterways Experiment Station, January, 1995]. The USCS [Unified Soil Classification System, April, 1960] is used by the US Army Corps of Engineers and virtually by all US trained geotechnical engineers [US Army Engineer Waterways Experiment Station, January, 1995]. The PIANC definitions [PIANC, 1984]

are based on European geotechnical practice and by utilizing the British definitions [US Army Engineer Waterways Experiment Station, January, 1995].

Table 2 Grain size classification of soils

Group name	Screen opening (mm), based on US standard sieve size Defining upper limit of group		
	Wentworth	USCS	PIANC
Boulder	-	-	-
Cobble	256	300	200
Coarse gravel	64	75	60
Medium gravel	16	-	20
Fine gravel	8	19	6
Coarse sand	2	4.760	2
Medium sand	0.500	2.000	0.600
Fine sand	0.250	0.425	0.200
Coarse silt	0.063	0.074	0.060
Medium silt	0.031		0.020
Fine silt	0.016		0.006
Clay	0.004	0.002	0.002

In this thesis, the PIANC system: 'Classification of Soils and Rock to be Dredged' [1984] is used.

This divides the soil in three categories,

Sand Less than 25 % of the material is finer than 0.06 mm and the percentage of material with a diameter smaller than 0.02 mm is lower than 5 %.

Clay The particle size distribution is not in accordance with the requirements stated above for sands, the plasticity index is greater than 10 % and the undrained shear strength is less than 125 kPa.

Rock The compressive strength of the material is greater than 3.5 MPa.

7.0 Shear Strength of Granular and Cohesive Soils

The in-situ shear strength is measured by in-situ tests or by laboratory tests of undisturbed samples. The shear strength of granular, cohesionless materials (sand and gravel) is directly

related to the relative density [US Army Engineer Waterways Experiment Station, January, 1995]. It is normally estimated by the Standard Penetration Test (SPT) and is expressed in compactness terms based on relative density. This is shown in Table 2, both in US and European Standard Geotechnical practices [US Army Engineer Waterways Experiment Station, January, 1995]. Other field methods like Cone Penetration Test (CPT) are also used, but they can be correlated with the SPT values.

Table 3 Compactness of sands based on Standard Penetration Test

Compactness term	Relative density (%)	SPT N-value Blows/ 30 cm
Very loose	0 - 15	0 - 4
Loose	15 - 35	4 - 10
Medium (firm)	35 - 65	10 - 30
Dense	65 - 85	30 - 50
Very dense	85 - 100	Over 50

The in-situ shear strength of cohesive soils (clay) is defined by the unconfined compressive strength of an undisturbed sample. Field strength test methods like vane shear tests are sometimes used to find the unconfined compressive strength. The unconfined compressive strength values for different consistency of cohesive soils are defined in Table 3. There is a difference between the USCS [HQUSACE, 1960] and the European based PIANC [1984] definitions for consistency definitions of cohesive soils.

Table 4 Consistency of cohesive soils

Consistency term	Unconfined compressive strength		
	USCS [HQUSACE, 1960]		PIANC [1984]
	Tons/ sq ft	kPa	kPa
Fluid ¹	< 0	< 0	< 0
Very soft	0 - 0.25	0 - 25	0 - 40
Soft	0.25 - 0.5	25 - 50	40 - 80
Medium (firm)	0.5 - 1.00	50 - 100	80 - 150
Stiff	1.00 - 2.00	100 - 200	150 - 300
Very stiff	2.00 - 4.00	200 - 400	-
Hard	> 4.00	> 400	> 300

¹ The fluid consistency occurs when a cylindrical test specimen of cohesive soil will not stand unconfined under its own weight, and thus may be considered to have a negative unconfined compressive strength.

8.0 Concluding Remarks

The bearing capacity and the shear stress-shear displacement models discussed in this Appendix were used in the evaluation of the mobility performance of the designed submersible active legged vehicle. The soil properties affecting the excavation were used in developing the parametric performance evaluation models for the excavation process. It must however be stressed, that when estimating the mobility performance of any submersible legged dredger/miner, general predictions regarding the performance of the unit are extremely difficult due to the variation in the make up of the in-situ submersible soil strata either in deep inland reservoirs or shelf areas.

APPENDIX 2

DRAG CALCULATIONS

This Appendix presents the drag calculations for the leg and the cutter modules of the designed submersible legged vehicle.

1.0 Drag Calculations for the Leg

The following assumptions were made for the calculations:

1. The leg and the guide tube through which the leg passes are hollow cylinders.
2. For drag calculations the leg and the cylindrical guide tube were considered as a single cylinder, with diameter equal to the leg tube.
3. The square guide tube of the leg was also considered as a cylindrical body, with a diameter equal to the side of the square cross section.

The following constants were used for the drag calculations of the leg of the designed vehicle (Table 1).

Table 1 Constants used for drag calculation of leg

Constants	Symbol	Value used
ρ_{f_fresh}	Density of fresh water [kg/ m ³]	1000
ρ_{f_sea}	Density of sea water [kg/ m ³]	1020
ν_{fresh}	Viscosity of fresh water at 30 °C [m ² /sec]	0.801*10 ⁻⁶
ν_{sea}	Viscosity of sea water [m ² /sec]	1.19*10 ⁻⁶
C_{d_fa}	Drag co-efficient of submerged cylinder based on projected area [-]	1.2

The design data of the leg is given in Table 2.

Table 2 Design data for leg

Leg part	Length (m)	Diameter (m)
1. Leg tube	1.88	0.0889
2. Square guide tube	0.7	0.04
3. Hydraulic cylinder (lift)	0.9	0.08

The drag calculated for the four legs using a $C_{d_fa} = 1.2$ based on projected area, is given in Table 3. The drags of the different components of the leg were calculated separately and then added to obtain the total drag for one leg. The total drag for one leg was multiplied by four to obtain the total drag generated by the four legs, provided each leg has the same linear velocity.

Table 3 Drag of four legs in fresh and sea water, based on a $C_d = 1.2$ (Projected area)

Velocity of leg (m/sec)	Drag in fresh water (Projected area) (N)	Drag in sea water (Projected area) (N)
0.035	0.785	0.801
0.03	0.577	0.589
0.025	0.401	0.409
0.02	0.256	0.262
0.015	0.144	0.147
0.01	0.064	0.065

Hoerner's expressions were used to estimate the drag based on projected area and wetted surface area. The results for the four legs are shown in Table 4 and 5.

Table 4 Drag of four legs in fresh and sea water, based on Hoerner's expression (Projected area)

Velocity of leg (m/sec)	Drag in fresh water (Projected area) (N)	Drag in sea water (Projected area) (N)
0.035	0.320	0.369
0.03	0.247	0.285
0.025	0.181	0.210
0.02	0.125	0.145
0.015	0.077	0.090
0.01	0.040	0.047

Table 5 Drag of four legs in fresh and sea water based on Hoerner's expression (Wetted surface area)

Velocity of leg (m/sec)	Drag in fresh water (Wetted surface area) (N)	Drag in sea water (Wetted surface area) (N)
0.035	0.01969	0.0227
0.03	0.015154	0.0175
0.025	0.011134	0.0129
0.02	0.007652	0.0089
0.015	0.004737	0.0056
0.01	0.00243	0.0029

2.0 Drag Calculations for the Cutter Module

The following assumptions were made for the calculations:

1. The drag calculations were based on C_d values from literature.
2. The C_d value for small domes based on profile area was used for drag calculation of the cutter.
3. The wetted surface area of the cutter was estimated by assuming the cutter as a right circular cone.

The design data of the cutter module is given in Table 6.

Table 6 Design data for cutter module

Cutter part	Length (m)	Diameter (m)
1. Cutter	0.3	0.0165 (max.) 0.0600 (min.)
2. Pressure vessel module	0.4	0.3200

The total drag calculated for the two cutters and the two pressure modules using the $C_d(\text{Profile area}) = 0.015$ for the cutter and $C_d_{fa} = 0.12$ for the pressure modules are presented next.

Table 7 Total drag of two cutters in fresh and sea water, based on $C_d = 0.015$ (Profile area)

Swing or Pitching velocity of ladder assembly (m/sec)	Drag in fresh water (Profile) (N)	Drag in sea water (Profile) (N)
0.1	0.0153	0.0156
0.2	0.0612	0.0624
0.3	0.1377	0.1404
0.4	0.2447	0.2496
0.5	0.3824	0.3900

Table 8 Total drag of two pressure modules in fresh and sea water, based on $C_{d_fa} = 0.12$ (Frontal area)

Swing or Pitching velocity of ladder assembly (m/sec)	Drag in fresh water (Frontal area) (N)	Drag in sea water (Frontal area) (N)
0.1	1.54	1.57
0.2	6.14	6.27
0.3	13.82	14.10
0.4	24.58	25.07
0.5	38.40	39.17

APPENDIX 3

PRESSURE VESSELS CALCULATIONS

This Appendix presents the input parameters used for the pressure vessels calculations for the ballast tank and the hydraulic and electric modules. The formulas used for the calculations are also presented in this Appendix.

Table 1 Input parameters used for pressure vessel calculations

Constants		
Parameter	Symbol	Value
Design depth of operation (m)	h_w	50.00
Density of water at surface(kg/m ³)	$\rho_{f_surface}$	1000.00
Density of water at design depth(kg/m ³)	$\rho_{f_h_w}$	1028.34
Acceleration due to gravity (m/s ²)	g	9.81
Reduction factor for frame size & spacing(-)	β_1	0.80
Constant for area of frame estimation	β_2	0.40
Pressure at design depth (Pa)	ph_w	504400.71
Material properties		
Material density (kg/m ³)	$\rho_{material}$	7850
Modulus of Elasticity (GPa)	E	207.00
Yield strength (MPa)	S_y	185.00
Poisson's Ratio(-)	ν	0.30
Safety factor (-)	SF	3.00
Allowable stress (MPa)	S_a	61.67
Pressure vessel parameters		
Overall length (m)	LOA	1.000
Outer radius (m)	R_O	0.300
Thickness (m)	t	0.00196
Inner radius (m)	R_I	0.298
Mean radius (m)	R_m	0.299
Stiffener characteristics		
Frame spacing (m)	L_f	0.330
Area of frame (m ²) (estimation)	A_f	0.00026
Rectangular stiffener		
Width of flange (m)	b	0.005
Thickness/height of flange (m)	t_f	0.050

The length of the hydraulic and electric modules was 0.95 m and the outer diameter was 0.3 m.

Formulas used [Allmendinger, 1990] are,

- 1) Critical pressure for Unstiffened Cylinder

$$P_{cr} = \left(\frac{t * S_a}{R_m} \right) \quad \text{[Equation 1]}$$

- 2) Critical pressure for Stiffened cylinder

- 2.1) Axisymmetric yielding

$$P_y = \frac{S_y * t / R_m}{1 + H * \left(\frac{0.85 - B}{1 + Beta} \right)}$$

where,

$$B = \frac{b * t}{A_f + b * t}$$

b = width of flange

$$Beta = \left(\frac{11 * N}{\sqrt{50 * t / R_m}} \right) * \left(\frac{t^2}{A_f + b * t} \right)$$

$$N = \frac{\cosh(Theta) - \cos(Theta)}{\sinh(Theta) + \sin(Theta)}$$

$$Theta = 10 * \left[12 * (1 - new^2) \right]^{1/4} * \left(\frac{L_f}{2 * R_m} \right) * \left(\frac{50 * t}{R_m} \right)^{1/2}$$

$$H \approx \frac{3 * \sinh\left(\frac{Theta}{2}\right) \cos\left(\frac{Theta}{2}\right) + \cosh\left(\frac{Theta}{2}\right) \sin\left(\frac{Theta}{2}\right)}{\sinh(Theta) + \sin(Theta)} \quad \text{[Equation 2]}$$

2.2) Lobar buckling

$$P_b = \frac{2.42 * E}{(1 - n e w^2)^{\frac{3}{4}}} * \frac{\left(\frac{t}{2 * R_m}\right)^{\frac{5}{2}}}{\left(\frac{L_f}{2 * R_m} - 0.45 * \left(\frac{t}{2 * R_m}\right)^{\frac{1}{2}}\right)} \quad \text{[Equation 3]}$$

2.3) General instability

$$P_{cr} = \frac{E * t}{R_m} * \left[\frac{m^4}{\left(n^2 + \frac{m^2}{2} - 1\right) * (n^2 + m^2)^2} \right] + \frac{(n^2 - 1) * EI}{R^3 * L_f}$$

where,

$$m = \frac{\pi * R_m}{L} \quad \text{[Equation 4]}$$

L= Bulkhead or deep frame spacing

I_{xx}= Moment of inertia of shell-stiffener combination about its center of gravity, using one frame spacing as the effective length of the shell; the x-axis is parallel to the longitudinal axis of the cylinder

n = mode number

APPENDIX 4

DATA USED FOR COMPARISONS BETWEEN CATERPILLAR TRACKED VEHICLES AND DESIGNED LEGGED VEHICLE

This Appendix presents the data of Caterpillar tracked vehicles [Caterpillar Handbook] and the relevant data of the prototype of 'Golden Tortoise', which were used for the comparisons between the tracked vehicles and the 'Golden Tortoise'.

Table 1 Data on 'Caterpillar' tracked vehicles [Caterpillar Handbook]

Make	Model	Flywheel power (kW)	Operating weight (kg)	Track width (m)	Track length (m)	Track Gauge (m)	Contact Area (m ²)	Overall Length (m)	Overall Width (m)	Ground Pressure (kPa)
Caterpillar	D3B	48	6545	0.356	1.82	1.42	1.29	2.75	1.79	50
Caterpillar	D4E	56	8820	0.457	1.83	1.52	1.67	3.20	1.85	51
Caterpillar	D5B	78	11700	0.508	2.21	1.88	2.24	3.63	2.36	51

Table 2 Data on prototype vehicle of 'Golden Tortoise'

Make	Model	Total power ⁹ (kW)	Operating weight (kg)	Foot width (m)	Foot Gauge (m)	Foot length (m)	Contact Area (m ²)	Overall Length ¹⁰ (m)	Overall Width (m)	Ground Pressure (kPa)
EEM	GT01	30	3200	0.300	2.6	0.7	0.84	3.30	2.3	37

Table 3 Length-to-width ratio of 'Caterpillar' tracked vehicles and designed legged vehicle

Make	Model	Length to Width Ratio
Caterpillar	D3B	1.54
Caterpillar	D4E	1.73
Caterpillar	D5B	1.54
EEM	GT01	1.4

⁹ Includes dredge pump, eductor pump power and cutter power

¹⁰ Without ladder

APPENDIX 5

EXPERIMENTAL SET UP, MEASURING TECHNIQUES AND MEASURING INSTRUMENTS FOR THE PROTOTYPE TESTS

This Appendix describes the vehicle operation during the full scale on land prototype tests. The experimental set up, the measuring techniques and the measuring instruments for the different types of prototype tests are described in this Appendix.

1.0 Vehicle Operation

The prototype vehicle was remotely operated on land from a small console by one operator. The main power supply came from a 440 V AC-50 Hz cycle main supply line. Remote switches mounted on the console were used to operate the electric induction motors driving the hydraulic pumps of the designed hydraulic circuits. Electronic switches were mounted on the console for the operation of the solenoids of the directional control valves actuating the hydraulic cylinders and hydraulic motors. The remote switches as well as the electronic switches were operated manually by one person from a distance. A battery and a charger were used to supply the 12 V DC to the solenoids operating the directional control valves.

2.0 Measured Parameters and Measuring Techniques

2.1 Hydraulic Oil Pressure

The hydraulic line pressure was measured with pressure gages, which was fixed to the pressure line of the manifold block to which the solenoid operated directional control valves were attached (Figure 1).

2.2 Time for Cylinder Operation

The time required by the different hydraulic cylinders to expand or retract was measured for the hydraulic circuit tests and the gait planning tests. Stop watches were used to measure the time.

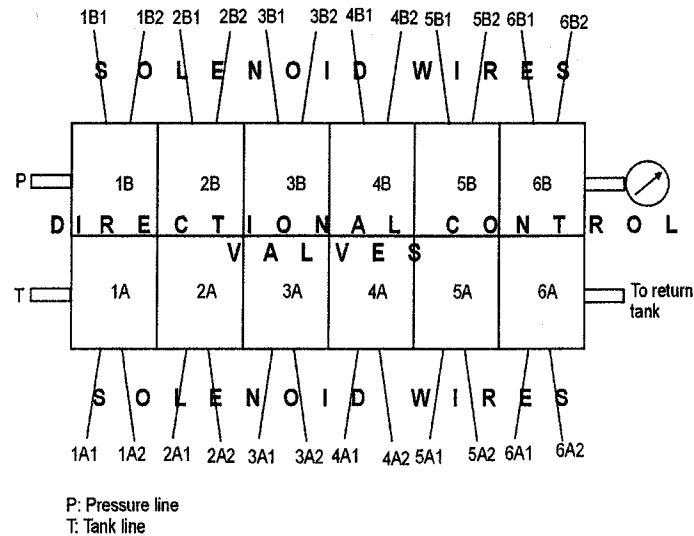


Figure 1 Solenoid actuated directional control valves placed on a manifold controlling the hydraulic actuators

2.3 Leg and Ladder Angles



Figure 2 Angular potentiometer and Inclinometer

Linear angular potentiometer fitted to a data acquisition card (ADAM-4017) and inclinometers were used to measure the swing angles of the leg and the ladder swing and pitch angles (Figure

2). Continuous recording of the angular changes of the legs and the ladder assembly was not necessary for the prototype tests. Hence it was easy to use the inclinometers (Figure 2).

2.4 Step Sizes of the Vehicle

To measure the step size markers were installed at the four corners of the vehicle before the commencement of the locomotion cycle (Figure 3).



Figure 3 Step size measurement techniques during gait planning tests

These markers were considered as origins and all the subsequent measurements were taken from these pegs. As the vehicle moved from the initial position (referred as Position 1) to the next position, markers were again installed (corresponding to Position 2). This procedure was repeated for all the different n-positions of the vehicle. The distance between the marker_1 and marker_n was measured with measuring tape and ruler. This measurement gave the step sizes attained by the designed vehicle. To obtain the vehicle trajectory the distance between marker_(n-1) and marker_n were measured together with the distance between marker_1 and marker_n. These measurements also gave the deviations of the vehicle from the desired trajectory during

straight line locomotion. The vehicle trajectory was plotted on an AutoCAD drawing, from which the step size of the assumed centre of gravity of the vehicle, the turning radius and the turning angle were measured.

2.5 Load Incident at each Leg

A hydraulic load cell and a mechanical load cell were designed to measure the load incident at each leg. The design of the hydraulic load cell considered the principle of transducing the force to a fluid pressure and then measuring the pressure with a pressure gage [Doebelin, 2002; pg 392]. Thus different rubber tubes were filled with water and the water pressure was measured with a pressure gage (Figure 4). The foot was removed and the hydraulic load cell was attached in its place.

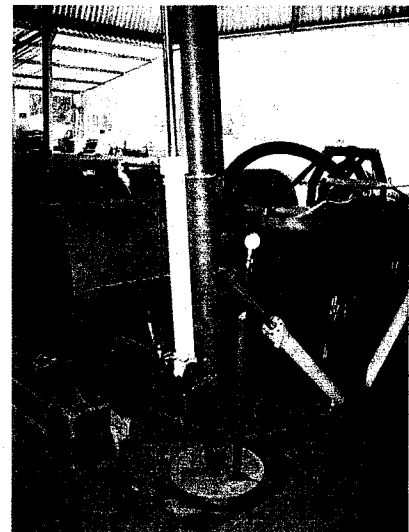
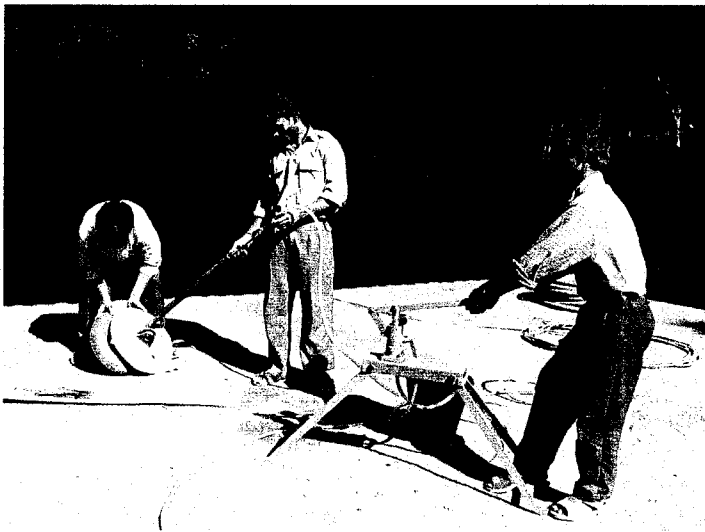


Figure 4 Hydraulic load cell (Left Filling with water, Right Load cell attached to the leg)

A mechanical ring load cell was designed and manufactured, with a 4 strain gage full Wheatstone bridge circuit. This mechanical ring load cell was attached to the Data Acquisition

card (ADAM- 4017) and a laptop computer for obtaining the readings. The system is shown in Figure 5.

The calibration curves for the hydraulic load cells used are given in Figure 6 and Figure 7.

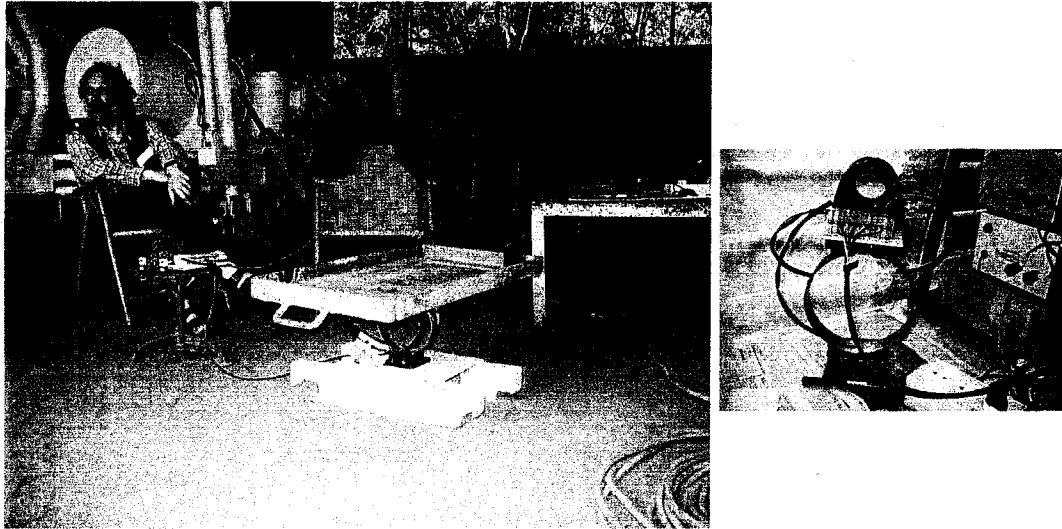


Figure 5 Mechanical ring load cell

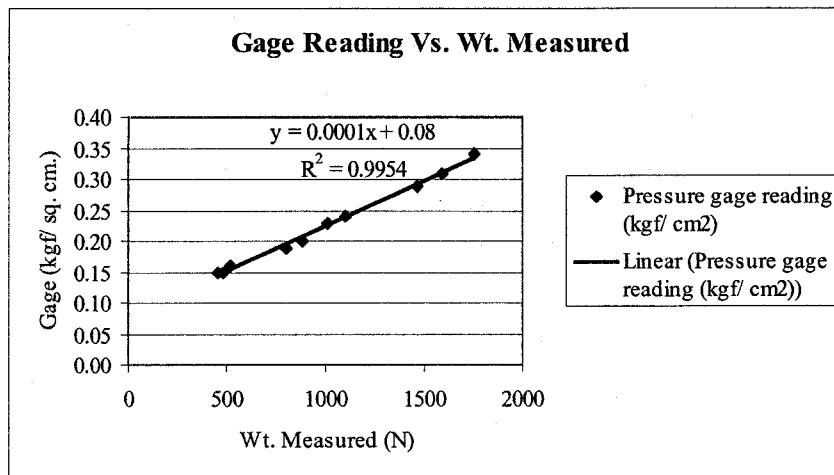


Figure 6 Calibration curve for Hydraulic Load Cell 1

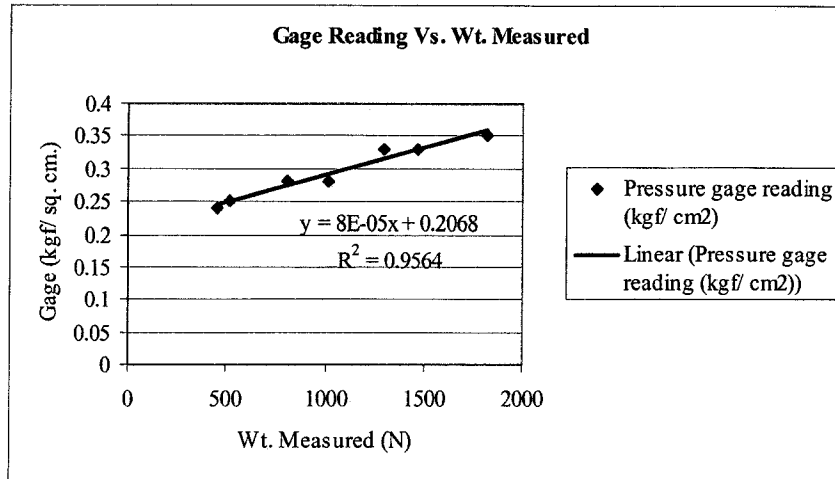


Figure 7 Calibration curve for Hydraulic Load Cell 2

APPENDIX 6

TEST MATRICES, EXPERIMENTAL AND PREDICTED DATA FOR STRAIGHT LINE LOCOMOTION

Simultaneous lifting/ lowering operations of the four legs were necessary for the straight line locomotion on flat terrain. During actual operation it became difficult to manually operate the four electronic switches for the solenoids of the directional control valves actuating the hydraulic cylinders simultaneously. The theoretical locomotion cycle as described in the chapter 2, was thus divided into further smaller steps, so that in all the steps except one, only two switches were operated simultaneously. The steps followed for the forward straight line locomotion on flat terrain are shown in Table 1. When the leg swings in the direction towards the AFT of the vehicle, the swing angle is designated as a (+) angle. When the leg swings towards the FWD direction of the vehicle, the swing angle is designated as a (-) angle. The ladder assembly was kept with zero swing angle and lifted a bit above the ground for all the straight line locomotion tests on flat terrain.

Table 1 Steps for forward straight line locomotion on flat terrain

Steps	Time measured
1. Vehicle on its belly; legs lifted	-
2. FWD legs brought to vertical position (swing angle = 0°)	t_1
3. AFT legs brought to vertical position (swing angle = 0°)	t_1
4. Swing FWD legs by γ_{leg_intl}	t_2
5. Swing AFT legs by γ_{leg_intl}	t_2
6. Lowering of FWD legs and lifting the vehicle off the ground	t_3
7. Lowering of AFT legs and lifting the vehicle off the ground	t_3
8. Swing all legs together by $-\gamma_{leg_fnl}$	t_4
9. Measure $-\gamma_{leg_fnl}$	-
10. Lift AFT legs and lower the vehicle body	t_5
11. Lift FWD legs and lower the vehicle body	t_5
12. Vehicle on its belly and measure the step size for PS and SBS	-

The test matrix used for the forward and backward straight line locomotion on level and flat terrain is presented in Table 2.

Table 2 Test matrix for forward and backward straight line locomotion on flat terrain

Factors	Responses
1. Hydraulic oil pressure: 70 kPa	1. Final angle of swing of legs 2. Step sizes measured at PS_AFT and SBS_AFT corners 3. Vehicle trajectory 4. Time required to move the legs during each step in a locomotion cycle

The experimental data for forward straight line locomotion is shown below.

Table 3 Data for forward straight line locomotion, Leg PS_AFT, 18.11.2004

Parameters	Position 1	Position 2	Position 3	Position 4	Position 5	Average
Initial angle of swing [degree]	20	25	10	20	25	20
Final angle of swing [degree]	22	27	11	18	21	19.6
Total angle of swing [degree]	42	52	21	38	46	39.6
Experimental step size [mm]	220	310	110	230	270	228
Theoretical step size [mm]	260.97	324.19	125.98	234.09	288.89	246.82
Deviation [mm]	40.97	14.19	15.98	4.09	18.89	18.82
Deviation [%]	18.62	4.58	14.52	1.78	7.00	9.30

Table 4 Data for forward straight line locomotion, Leg PS_FWD, 18.11.2004

Parameters	Position 1	Position 2	Position 3	Position 4	Position 5	Average
Initial angle of swing [degree]	20	25	10	20	25	20.00
Final angle of swing [degree]	20	26	10	20	25	20.40
Total angle of swing [degree]	40	51	20	40	50	40.40
Experimental step size [mm]	220	310	110	230	270	228.00
Theoretical step size [mm]	247.36	331.59	119.84	247.36	316.91	252.61
Deviation [mm]	27.36	21.59	9.84	17.36	46.91	24.61
Deviation [%]	12.44	6.96	8.95	7.55	17.37	10.65

Table 5 Data for forward straight line locomotion, Leg SBS_AFT, 18.11.2004

Parameters	Position 1	Position 2	Position 3	Position 4	Position 5	Average
Initial angle of swing [degree]	20	25	10	20	25	20.00
Final angle of swing [degree]	18	26	10	15	15	16.40
Total angle of swing [degree]	38	51	20	35	40	36.40
Experimental step size [mm]	250	320	100	230	270	234.00
Theoretical step size [mm]	234.09	309.74	119.84	214.74	249.51	225.58
Deviation [mm]	-15.91	-10.26	19.84	-15.26	-20.49	-8.42
Deviation [%]	-6.36	-3.20	19.84	-6.64	-7.59	-0.79

Table 6 Data for forward straight line locomotion, Leg SBS_FWD, 18.11.2004

Parameters	Position 1	Position 2	Position 3	Position 4	Position 5	Average
Initial angle of swing [degree]	20	25	10	20	25	20.00
Final angle of swing [degree]	21	24	11	21	24	20.50
Total angle of swing [degree]	41	49	21	41	49	40.50
Experimental step size [mm]	250	320	100	230	270	230.00
Theoretical step size [mm]	254.12	324.19	125.98	254.12	309.74	253.51
Deviation [mm]	4.12	4.19	25.98	24.12	39.74	23.51
Deviation [%]	1.65	1.31	25.98	10.49	14.72	13.12

Table 7 Data for forward straight line locomotion, Leg PS_AFT, 27.12.2004

Parameters	Pos.1	Pos.2	Pos.3	Pos.4	Pos.5	Pos.6	Pos.7	Pos.8	Pos.9	Average
Initial angle of swing [degree]	10	10	10	20	20	25	25	25	10	17.22
Final angle of swing [degree]	28	15	29	19	20	22	19	27	17	21.78
Total angle of swing [degree]	38	25	39	39	40	47	44	52	27	39.00
Experimental step size [mm]	228	122	195	215	240	300	280	300	145	225.00
Theoretical step size [mm]	240.59	150.97	248.27	240.69	247.36	295.74	275.46	331.59	163.81	243.83
Deviation [mm]	12.59	28.97	53.27	25.69	7.36	-4.26	-4.54	31.59	18.81	18.83
Deviation [%]	5.52	23.75	27.32	11.95	3.07	-1.42	-1.62	10.53	12.97	10.23

Table 8 Data for forward straight line locomotion, Leg PS_FWD, 27.12.2004

Parameters	Pos.1	Pos.2	Pos.3	Pos.4	Pos.5	Pos.6	Pos.7	Pos.8	Pos.9	Average
Initial angle of swing [degree]	10	10	10	20	20	25	25	25	10	17.22
Final angle of swing [degree]	21	13	15	14	15	22	18	20	15	17.00
Total angle of swing [degree]	31	23	25	34	35	47	43	45	25	34.22
Experimental step size [mm]	228	122	195	215	240	300	280	300	145	225.00
Theoretical step size [mm]	190.36	138.37	150.97	208.41	214.74	295.74	268.87	282.13	150.97	211.17
Deviation [mm]	-37.64	16.37	-44.03	-6.59	-25.26	-4.26	-11.13	-17.87	5.97	-13.83
Deviation [%]	-16.51	13.42	-22.58	-3.07	-10.53	-1.42	-3.98	-5.96	4.12	-5.17

Table 9 Data for forward straight line locomotion, Leg SBS_AFT, 27.12.2004

Parameters	Pos.1	Pos.2	Pos.3	Pos.4	Pos.5	Pos.6	Pos.7	Pos.8	Pos.9	Average
Initial angle of swing [degree]	10	10	10	20	20	25	25	25	10	17.22
Final angle of swing [degree]	12	15	30	30	29	31	30	24	16	24.11
Total angle of swing [degree]	22	25	40	50	49	56	55	49	26	41.33
Experimental step size [mm]	230	155	195	230	230	315	365	290	145	239.44
Theoretical step size [mm]	132.15	150.97	256.10	319.86	312.03	362.62	354.63	309.74	157.36	261.72
Deviation [mm]	-97.85	-4.03	61.10	89.86	82.03	47.62	-10.37	19.74	12.36	22.27
Deviation [%]	-42.54	-2.60	31.33	39.07	35.67	15.12	-2.84	6.81	8.53	9.84

Table 10 Data for forward straight line locomotion, Leg SBS_FWD, 27.12.2004

Parameters	Pos.1	Pos.2	Pos.3	Pos.4	Pos.5	Pos.6	Pos.7	Pos.8	Pos.9	Average
Initial angle of swing [degree]	10	10	10	20	20	25	25	25	10	17.22
Final angle of swing [degree]	Error	15	21	15	15	22	30	15	13	18.25
Total angle of swing [degree]	Error	25	31	35	35	47	55	40	23	36.38
Experimental step size [mm]	Error	155	195	230	230	315	365	290	145	239.44
Theoretical step size [mm]	Error	150.97	190.36	214.74	214.74	295.74	354.63	249.51	138.37	226.13
Deviation [mm]	Error	-4.03	-4.64	-15.26	-15.26	-19.26	-10.37	-40.49	-6.63	-14.49
Deviation [%]	Error	-2.60	-2.38	-6.64	-6.64	-6.11	-2.84	-13.96	-4.57	-5.72

The test set up used for forward straight line locomotion tests was also followed during the backward straight line locomotion tests. The steps followed during the locomotion cycle were the same as the forward motion (Table 1), with the exception of (-) ve swing angles of the legs in steps 4 and 5 and (+) ve swing angle of the legs in steps 8 and 9. The test matrix for backward straight line locomotion was the same as the forward straight line locomotion (Table 2).

The experimental data for the backward straight line locomotion are presented next.

Table 11 Data for backward straight line locomotion, Leg PS_AFT, 27.12.2004

Parameters	Position 1	Position 2	Position 3	Position 4	Position 5	Position 5	Average
Initial angle of swing [degree]	10	10	20	20	25	25	18.33
Final angle of swing [degree]	15	19	25	24	23	27	22.17
Total angle of swing [degree]	25	29	45	44	48	52	40.50
Experimental step size [mm]	125	135	220	220	210	240	191.67
Theoretical step size [mm]	150.97	176.93	282.13	274.97	302.69	331.59	253.22
Deviation [mm]	25.97	41.93	62.13	54.97	92.69	91.59	61.55
Deviation [%]	20.78	31.06	28.24	24.99	44.14	38.16	31.23

Table 12 Data for backward straight line locomotion, Leg PS_FWD, 27.12.2004

Parameters	Position 1	Position 2	Position 3	Position 4	Position 5	Position 6	Average
Initial angle of swing [degree]	10	10	20	20	25	25	18.33
Final angle of swing [degree]	12	14	20	20	23	15	17.33
Total angle of swing [degree]	22	24	40	40	48	40	35.67
Experimental step size [mm]	125	135	220	220	210	240	191.67
Theoretical step size [mm]	132.15	144.65	247.36	247.36	302.69	249.51	220.62
Deviation [mm]	7.15	9.65	27.36	27.36	92.69	9.51	28.95
Deviation [%]	5.72	7.15	12.44	12.44	44.14	3.96	14.31

Table 13 Data for backward straight line locomotion, Leg SBS_AFT, 27.12.2004

Parameters	Position 1	Position 2	Position 3	Position 4	Position 5	Position 6	Average
Initial angle of swing [degree]	10	10	20	20	25	25	18.33
Final angle of swing [degree]	16	19	27	17	45	28	25.33
Total angle of swing [degree]	26	29	47	37	70	53	43.67
Experimental step size [mm]	100	120	220	220	280	215	192.50
Theoretical step size [mm]	157.36	176.93	296.82	227.57	498.18	339.13	282.67
Deviation [mm]	57.36	56.93	76.82	7.57	218.18	124.13	90.17
Deviation [%]	57.36	47.44	34.92	3.44	77.92	57.73	46.47

Table 14 Data for backward straight line locomotion, Leg SBS_FWD, 27.12.2004

Parameters	Position 1	Position 2	Position 3	Position 4	Position 5	Position 6	Average
Initial angle of swing [degree]	10	10	20	20	25	25	18.33
Final angle of swing [degree]	13	16	18	24	25	17	18.83
Total angle of swing [degree]	23	26	38	44	50	42	37.17
Experimental step size [mm]	100	120	220	220	280	215	192.50
Theoretical step size [mm]	138.37	157.36	234.09	274.97	316.91	262.35	230.68
Deviation [mm]	38.37	37.36	14.09	54.97	36.91	47.35	38.18
Deviation [%]	38.37	31.13	6.41	24.99	13.18	22.02	22.68

The predicted step size results for forward and backward straight line locomotion are presented below.

Table 15 Predicted step sizes with slip for forward straight line locomotion, PS_AFT

Slip (%)	Position1 (mm)	Position2 (mm)	Position3 (mm)	Position4 (mm)	Position5 (mm)	Position6 (mm)	Position7 (mm)	Position8 (mm)	Position9 (mm)
0.1	217.84	136.83	224.69	220.85	227.21	273.68	253.76	308.87	148.53
0.2	193.63	121.63	199.73	196.31	201.96	243.27	225.56	274.55	132.02
0.3	169.43	106.42	174.76	171.77	176.72	212.86	197.37	240.23	115.52
0.4	145.22	91.22	149.79	147.23	151.47	182.45	169.17	205.91	99.02
0.5	121.02	76.02	124.83	122.69	126.23	152.04	140.98	171.59	82.51
0.6	96.82	60.81	99.86	98.15	100.98	121.64	112.78	137.27	66.01
0.7	72.61	45.61	74.90	73.62	75.74	91.23	84.59	102.96	49.51

Table 16 Predicted step sizes with slip for forward straight line locomotion, SBS_AFT

Slip (%)	Position1 (mm)	Position2 (mm)	Position3 (mm)	Position4 (mm)	Position5 (mm)	Position6 (mm)	Position7 (mm)	Position8 (mm)	Position9 (mm)
0.1	119.65	136.83	231.66	296.08	288.67	339.24	331.43	287.43	142.65
0.2	106.36	121.63	205.92	263.18	256.60	301.55	294.61	255.49	126.80
0.3	93.06	106.42	180.18	230.28	224.52	263.85	257.78	223.56	110.95
0.4	79.77	91.22	154.44	197.38	192.45	226.16	220.95	191.62	95.10
0.5	66.47	76.02	128.70	164.49	160.37	188.47	184.13	159.68	79.25
0.6	53.18	60.81	102.96	131.59	128.30	150.77	147.30	127.75	63.40
0.7	39.88	45.61	77.22	98.69	96.22	113.08	110.48	95.81	47.55

Table 17 Predicted step sizes with slip for backward straight line locomotion, PS_AFT

Slip (%)	Position1 (mm)	Position2 (mm)	Position3 (mm)	Position4 (mm)	Position5 (mm)	Position6 (mm)
0.1	136.83	160.45	260.31	253.50	280.51	308.87
0.2	121.63	142.62	231.39	225.34	249.34	274.55
0.3	106.42	124.79	202.47	197.17	218.17	240.23
0.4	91.22	106.97	173.54	169.00	187.00	205.91
0.5	76.02	89.14	144.62	140.83	155.84	171.59
0.6	60.81	71.31	115.69	112.67	124.67	137.27
0.7	45.61	53.48	86.77	84.50	93.50	102.96

Table 18 Predicted step sizes with slip for backward straight line locomotion, SBS_AFT

Slip (%)	Position1 (mm)	Position2 (mm)	Position3 (mm)	Position4 (mm)	Position5 (mm)	Position6 (mm)
0.1	136.83	160.45	274.26	208.34	470.24	316.25
0.2	121.63	142.62	243.78	185.20	417.99	281.11
0.3	106.42	124.79	213.31	162.05	365.74	245.97
0.4	91.22	106.97	182.84	138.90	313.49	210.84
0.5	76.02	89.14	152.36	115.75	261.24	175.70
0.6	60.81	71.31	121.89	92.60	208.99	140.56
0.7	45.61	53.48	91.42	69.45	156.75	105.42

Predicted results for allowable level difference and/ or submergence and slip at the foot/ soil interface are given below.

Table 19 Constants used for prediction of allowable level difference and/ or submergence and slip

Constants	mm
1. Perpendicular distance between leg swing pin centre and foot pin centre	340
2. Stroke of hydraulic lift cylinder	300
3. Stroke of hydraulic swing cylinder	300
4. Distance between FWD and AFT foot pin centre	2200
5. Distance between PS and SBS foot pin centre	2360

The allowable level difference between FWD and AFT legs were calculated below. It was assumed that the AFT legs were at ground level with zero submergence.

Table 20 Allowable level difference and/ or submergence for FWD and AFT legs

$\gamma_{leg_intl} = \gamma_{leg_fnl}$ (AFT legs)	Level difference	$\gamma_{leg_intl} = \gamma_{leg_fnl}$ (FWD legs)	Vehicle tilt	Ratio swing angle, AFT to FWD legs
(degree)	(mm)	(degree)	(degree)	(-)
5	50	4.36	1.30	1.15
10	50	8.74	1.30	1.14
15	50	13.15	1.30	1.14
20	50	17.60	1.30	1.14
30	50	26.72	1.30	1.12
5	100	3.87	2.60	1.29
10	100	7.76	2.60	1.29
15	100	11.70	2.60	1.28
20	100	15.71	2.60	1.27
30	100	24.04	2.60	1.25
5	200	3.15	5.19	1.59
10	200	6.34	5.19	1.58
15	200	9.58	5.19	1.57
20	200	12.91	5.19	1.55
30	200	19.98	5.19	1.50
5	300	2.66	7.77	1.88
10	300	5.35	7.77	1.87
15	300	8.10	7.77	1.85
20	300	10.94	7.77	1.83
30	300	17.05	7.77	1.76

The allowable level difference between PS and SBS legs were calculated below. It was assumed that the PS legs were at ground level with zero submergence.

Table 21 Allowable level difference and/ or submergence for FWD and AFT legs

$\gamma_{leg_intl} = \gamma_{leg_fnl}$ (AFT legs)	Level difference	$\gamma_{leg_intl} = \gamma_{leg_fnl}$ (FWD legs)	Vehicle tilt	Ratio swing angle, AFT to FWD legs
(degree)	(mm)	(degree)	(degree)	(-)
5	50	4.36	1.21	1.15
10	50	8.74	1.21	1.14
15	50	13.15	1.21	1.14
20	50	17.60	1.21	1.14
30	50	26.72	1.21	1.12
5	100	3.87	2.43	1.29
10	100	7.76	2.43	1.29
15	100	11.70	2.43	1.28
20	100	15.71	2.43	1.27
30	100	24.04	2.43	1.25
5	200	3.15	4.84	1.59
10	200	6.34	4.84	1.58
15	200	9.58	4.84	1.57
20	200	12.91	4.84	1.55
30	200	19.98	4.84	1.50
5	300	2.66	7.24	1.88
10	300	5.35	7.24	1.87
15	300	8.10	7.24	1.85
20	300	10.94	7.24	1.83
30	300	17.05	7.24	1.76

APPENDIX 7

TEST MATRICES, EXPERIMENTAL AND PREDICTED DATA FOR CURVILINEAR LOCOMOTION

The steps followed for the two different sets of curvilinear tests performed are given in Table 1 and Table 2.

Table 1 Steps for curvilinear locomotion on flat terrain with inner legs fixed

Steps	Time measured
1. Vehicle on its belly; legs lifted	-
2. FWD legs brought to vertical position (swing angle = 0°)	t_1
3. AFT legs brought to vertical position (swing angle = 0°)	t_1
4. Swing inner legs by $\theta = 0^\circ$	t_2
5. Swing outer legs by φ	t_2
6. Lowering of FWD legs and lifting the vehicle off the ground	t_3
7. Lowering of AFT legs and lifting the vehicle off the ground	t_3
8. Swing all legs together and stop when outer legs reaches $-\varphi$, inner legs with 0°	t_4
9. Measure $-\theta$ and $-\varphi$ for all legs	-
10. Lift AFT legs and lower the vehicle body	t_5
11. Lift FWD legs and lower the vehicle body	t_5
12. Vehicle on its belly and measure the step size for PS and SBS	-

Table 2 Steps for curvilinear locomotion on flat terrain with unequal swing angles

Steps	Time measured
1. Vehicle on its belly; legs lifted	-
2. FWD legs brought to vertical position (swing angle = 0°)	t_1
3. AFT legs brought to vertical position (swing angle = 0°)	t_1
4. Swing inner legs by θ	t_2
5. Swing outer legs by φ ($\varphi > \theta$)	t_2
6. Lowering of FWD legs and lifting the vehicle off the ground	t_3
7. Lowering of AFT legs and lifting the vehicle off the ground	t_3
8. Swing all legs together but stop inner legs a bit earlier than outer legs	t_4
9. Measure $-\theta$ and $-\varphi$ for all legs	-
10. Lift AFT legs and lower the vehicle body	t_5
11. Lift FWD legs and lower the vehicle body	t_5
12. Vehicle on its belly and measure the step size for PS and SBS	-

The test matrices for the curvilinear locomotion on flat terrain are shown in Table 3 and Table 4.

Table 3 Test matrix for curvilinear locomotion with inner legs fixed

Factors	Responses
1. Hydraulic oil pressure: 70 kPa	1. Final angle of swing of legs
2. Initial angle of swing of legs: Inner legs: $\theta = 0^\circ$ Outer legs: $\varphi = 5^\circ, 10^\circ, 15^\circ, 20^\circ$	2. Step sizes measured at PS_AFT and SBS_AFT corners 3. Vehicle trajectory 4. Time required to move the legs

Table 4 Test matrix for curvilinear locomotion with unequal swing angles

Factors	Responses
1. Hydraulic oil pressure: 70 kPa	1. Final angle of swing of legs
2. Initial angle of swing of legs:	2. Step sizes measured at PS_AFT and SBS_AFT corners
Inner legs: $\theta = 5^\circ$	3. Vehicle trajectory
Outer legs: $\varphi = 10^\circ$	4. Time required to move the legs
Inner legs: $\theta = 10^\circ$	
Outer legs: $\varphi = 15^\circ$	
Inner legs: $\theta = 10^\circ$	
Outer legs: $\varphi = 20^\circ$	
Inner legs: $\theta = 5^\circ$	
Outer legs: $\varphi = 15^\circ$	

The experimental data measuring the initial angle, final angle and experimental step size are tabulated below. The experimental data giving the distances measured between marker_1 and marker_n as well as that between marker_(n-1) and marker_n are presented below. The centre of gravity of the designed vehicle was assumed at the mid point of the main body frame, because of the symmetry of the designed vehicle. The different positions of the vehicle during a particular set of curvilinear locomotion test were plotted on an AutoCAD drawing. The experimental step size of the assumed centre of gravity of the vehicle as well as the experimental turning radii and the turning angles for the PS_AFT corner, SBS_AFT corner and the assumed centre of gravity of the vehicle were measured from the AutoCAD drawing. It was assumed that the step sizes, turning radii and turning angles for the PS_AFT corner and the SBS_AFT corner were equal to those for the respective legs.

Table 5 Data for curvilinear locomotion with inner legs fixed for PS_AFT

Parameter	Pos 1	Pos 2	Pos 3	Pos 4	Pos 5	Pos 6	Pos 7	Pos 8	Pos 9	Pos 10	Pos 11	Pos 12
Initial angle	0	0	0	0	0	0	0	0	0	0	0	0
Final angle	0	0	0	-2	0	0	0	0	0	0	0	0
Experimental step size	80	65	45	55	85	70	110	130	90	100	100	100

Table 6 Data for curvilinear locomotion with inner legs fixed for PS_FWD

Parameter	Pos 1	Pos 2	Pos 3	Pos 4	Pos 5	Pos 6	Pos 7	Pos 8	Pos 9	Pos 10	Pos 11	Pos 12
Initial angle	0	0	0	0	0	0	0	0	0	0	0	0
Final angle	0	0	0	0	0	0	0	0	0	0	0	0
Experimental step size	80	20	60	35	25	20	35	40	40	25	30	40

Table 7 Data for curvilinear locomotion with inner legs fixed for SBS_AFT

Parameter	Pos 1	Pos 2	Pos 3	Pos 4	Pos 5	Pos 6	Pos 7	Pos 8	Pos 9	Pos 10	Pos 11	Pos 12
Initial angle	5	5	5	10	10	10	15	15	15	20	20	20
Final angle	-10	-12	-10	-9	-12	-10	-17	-17	-16	-10	-17	-19
Experimental step size	90	65	95	115	120	105	160	160	130	170	110	200

Table 8 Data for curvilinear locomotion with inner legs fixed for SBS_FWD

Parameter	Pos 1	Pos 2	Pos 3	Pos 4	Pos 5	Pos 6	Pos 7	Pos 8	Pos 9	Pos 10	Pos 11	Pos 12
Initial angle	5	5	5	10	10	10	15	15	15	20	20	20
Final angle	-10	-8	-5	-5	-7	-4	-7	-10	-2	-3	-2	-2
Experimental step size	65	100	65	80	85	85	150	120	105	115	100	140

Table 9 Distances between different markers for curvilinear locomotion with inner legs fixed

PS AFT		SBS AFT	
Distances between two markers	(mm)	Distances between two markers	(mm)
1_2	80	1_2	90
1_3	145	1_3	155
2_3	65	2_3	80
1_4	190	1_4	250
3_4	45	3_4	90
1_5	245	1_5	365
4_5	55	4_5	115
1_6	330	1_6	485
5_6	90	5_6	125
1_7	400	1_7	590
6_7	70	6_7	110
1_8	570	1_8	750
7_8	110	7_8	160
1_9	640	1_9	910
8_9	125	8_9	165
1_10	730	1_10	1040
9_10	90	9_10	135
1_11	830	1_11	1210
10_11	100	10_11	170
1_12	930	1_12	1320
11_12	100	11_12	115
1_13	1030	1_13	1520
12_13	100	12_13	200
PS FWD		SBS FWD	
Distances between two markers	(mm)	Distances between two markers	(mm)
1_2	80	1_2	65
1_3	100	1_3	165
2_3	50	2_3	100
1_4	160	1_4	230
3_4	65	3_4	70
1_5	195	1_5	310
4_5	40	4_5	80
1_6	220	1_6	395
5_6	30	5_6	85
1_7	240	1_7	480
6_7	25	6_7	80
1_8	275	1_8	630
7_8	40	7_8	150
1_9	315	1_9	750
8_9	40	8_9	125
1_10	355	1_10	855
9_10	40	9_10	110
1_11	380	1_11	970
10_11	30	10_11	120
1_12	410	1_12	1070
11_12	40	11_12	110
1_13	450	1_13	1210
12_13	35	12_13	140

Table 10 Data for curvilinear locomotion with unequal angles for PS_AFT

Parameter	Pos 1	Pos 2	Pos 3	Pos 4	Pos 5	Pos 6	Pos 7	Pos 8	Pos 9	Pos 10	Pos 11	Pos 12	Av.
Initial angle (deg)	5	5	5	10	10	10	10	10	10	5	5	5	7.50
Final angle (deg)	16	12	11	18	16	15	11	12	19	9	12	14	13.75
Total angle (deg)	21	17	16	28	26	25	21	22	29	14	17	19	21.25
Experimental step size (mm)	175	160	140	180	170	180	170	155	325	95	145	135	169.17

Table 11 Data for curvilinear locomotion with unequal angles for PS_FWD

Parameter	Pos 1	Pos 2	Pos 3	Pos 4	Pos 5	Pos 6	Pos 7	Pos 8	Pos 9	Pos 10	Pos 11	Pos 12	Av.
Initial angle	5	5	5	10	10	10	10	10	10	5	5	5	7.50
Final angle	16	12	10	14	11	10	11	9	9	5	11	9	10.58
Total angle	21	17	15	24	21	20	21	19	19	10	16	14	18.08
Experimental step size	165	140	110	180	148	162	135	150	140	90	120	110	137.50

Table 12 Data for curvilinear locomotion with unequal angles for SBS_AFT

Parameter	Pos 1	Pos 2	Pos 3	Pos 4	Pos 5	Pos 6	Pos 7	Pos 8	Pos 9	Pos 10	Pos 11	Pos 12	Av.
Initial angle	10	10	10	15	15	15	20	20	20	15	15	15	15.00
Final angle	29	25	26	30	25	26	24	22	24	16	20	30	24.75
Total angle	39	35	36	45	40	41	44	42	44	31	35	45	39.75
Experimental step size	235	220	200	235	215	265	225	215	220	150	190	195	213.75

Table 13 Data for curvilinear locomotion with unequal angles for SBS_FWD

Parameter	Pos 1	Pos 2	Pos 3	Pos 4	Pos 5	Pos 6	Pos 7	Pos 8	Pos 9	Pos 10	Pos 11	Pos 12	Av.
Initial angle	10	10	10	15	15	15	20	20	20	15	15	15	15.00
Final angle	23	21	18	20	19	20	16	13	13	7	15	15	16.67
Total angle	33	31	28	35	34	35	36	33	33	22	30	30	31.67
Experimental step size	230	180	185	210	250	220	225	195	205	150	170	180	200.00

Table 14 Distances between different markers for curvilinear locomotion with unequal angles

PS_AFT		SBS_AFT	
Distances between two markers	(mm)	Distances between two markers	(mm)
1_2	175	1_2	235
1_3	335	1_3	455
2_3	165	2_3	225
1_4	475	1_4	655
3_4	140	3_4	200
1_5	655	1_5	890
4_5	185	4_5	240
1_6	825	1_6	1105
5_6	175	5_6	210
1_7	1005	1_7	1370
6_7	180	6_7	265
1_8	1175	1_8	1595
7_8	180	7_8	230
1_9	1330	1_9	1810
8_9	160	8_9	220
1_10	1500	1_10	2030
9_10	175	9_10	220
1_11	1595	1_11	2180
10_11	100	10_11	150
1_12	1740	1_12	2370
11_12	150	11_12	190
1_13	1875	1_13	2565
12_13	135	12_13	200

The turning angle, turning radius and heading angles for the PS_AFT, SBS_AFT and assumed machine CG are given below. Negative heading angle means vehicle turned towards SBS.

Table 15 Turning angle, Radius of turning and Heading angle for curvilinear locomotion with unequal angle (measured from AutoCAD drawing)

PS AFT			
Point	Turning angle (degree)	Radius of turning (m)	Heading angle (degree)
1 2	No reading	No reading	0
2 3	2	6,113	20
3 4	2	3,467	10
4 5	1	13,166	25
5 6	1	11,018	29
6 7	2	4,952	17
7 8	1	8,162	38
8 9	2	5,880	36
9 10	1	8,532	37
10 11	1	4,331	43
11 12	1	7,723	40
12 13	1	7,418	26
SBS AFT			
1 2			-1
2 3	2	8412	15
3 4	2	6026	8
4 5	1	15416	21
5 6	1	13222	25
6 7	2	7290	14
7 8	1	9840	31
8 9	2	8086	29
9 10	1	10725	32
10 11	1	6497	32
11 12	1	10342	35
12 13	1	9753	21
Machine CG			
1 2			14
2 3	2	8410	29
3 4	2	5251	22
4 5	1	14871	32
5 6	1	12818	34
6 7	2	6555	30
7 8	1	10018	43
8 9	2	7723	43
9 10	1	10352	42
10 11	1	6242	51
11 12	1	10007	47
12 13	1	8981	38

Table 16 Initial, final and average headings for curvilinear locomotion with unequal angles (measured from AutoCAD drawing)

Headings	PS AFT	SBS AFT	Machine CG
Initial heading (degree)	0	0	0
Final heading (degree)	26	21	35
Average heading (degree)	27	22	35

APPENDIX 8

LOCOMOTION CYCLE TIME

1.0 Parametric Model for Estimation of Locomotion Cycle Time

1.1 Preparatory Cycle

This cycle starts with the vehicle resting on its belly, while the four vertical legs touch the ground. The legs are lifted from this position for ground clearance and then swinging and lowering action of the legs follow.

The relationship between the lift velocity of the leg lifting cylinder (cylinder rod expanding) ($v_{lhc_leg_e}$) [m/sec], the lift distance (L_{l_pc}) [m] and the lifting time (t_1) [sec] is given in Equation 1(Figure 1).

$$L_{l_pc} = \int_{t_1}^{t_0} (v_{lhc_leg_e}) * t_1 \quad \text{[Equation 1]}$$

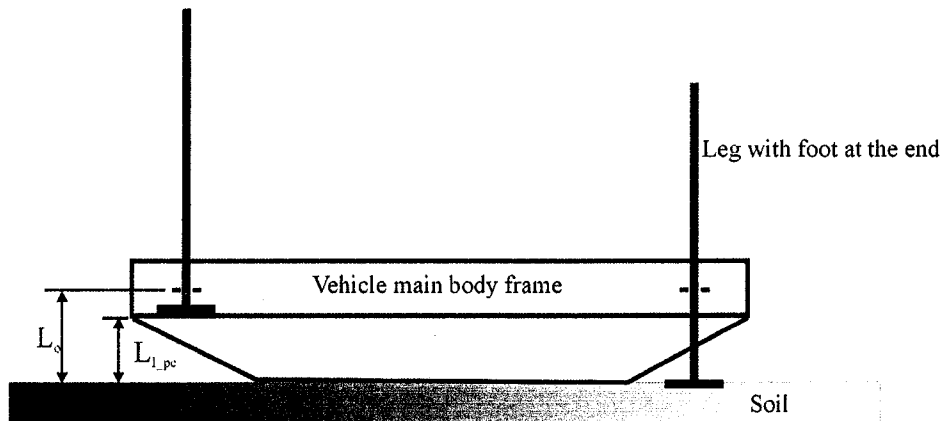


Figure 1 Definition of L_o and L_{l_pc}

The choice of a lifting distance (L_{l_pc}) of 0.2 m is reasonable for leg clearance. The perpendicular distance between the leg swing pin centre and the foot pin centre (L_o) was assumed to be equal to 340 mm.

The analysis of the linear velocity of the leg swing cylinder is shown in Figure 2.

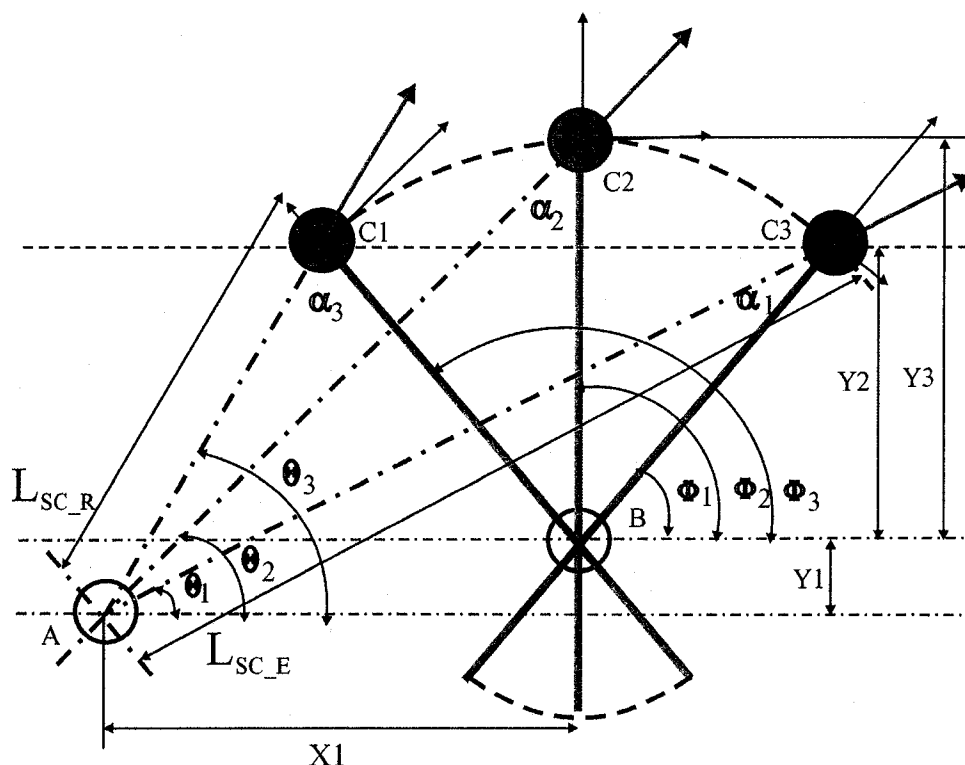


Figure 2 Analyses of leg swing cylinder linear velocity

- A Point of leg swing cylinder attachment with the main body frame
- B Point of leg pin attachment with the main body frame
- C_i Point of swing cylinder attachment with the leg, $i= 1, 2 \dots n$, denoting different leg swing positions

If the linear velocity of the swing cylinder is v_{shc_leg} [m/sec], then the tangential component is

$v_{shc_leg} * \sin \alpha_i$ [m/sec] and the normal component is $v_{shc_leg} * \cos \alpha_i$ [m/sec], where α_i is the

angle between the swing cylinder axis and the leg longitudinal axis at different leg positions [degree]. The normal component is responsible for the swinging of the leg. The angle α_i is a function of the angles θ_i and ϕ_i [degrees]. The relationship between θ_i and ϕ_i and α_i are given next.

$$\begin{aligned}\sin \theta_1 &= \frac{(Y_1 + Y_2)}{L_{SC_E}} \\ \sin \theta_2 &= \frac{(Y_3 + Y_2)}{L_{SC}} \\ \sin \theta_3 &= \frac{(Y_1 + Y_2)}{L_{SC_R}}\end{aligned}\quad \text{[Equation 2]}$$

Also,

$$\begin{aligned}\sin \phi_1 &= \left(\frac{Y_2}{L_{SCP_LP}} \right) \\ \sin \phi_2 &= \left(\frac{Y_3}{L_{SCP_LP}} \right) \\ \sin(180^\circ - \phi_3) &= \left(\frac{Y_2}{L_{SCP_LP}} \right)\end{aligned}\quad \text{[Equation 3]}$$

L_{SC_E} Length of swing cylinder rod in full expansion position [m]

L_{SC_R} Length of swing cylinder rod in full retracted position [m]

L_{SCP_LP} Length between swing cylinder pin attached to main body frame and leg pin attached to main body frame [m]

Again,

$$\alpha_1 + \theta_1 + (180^\circ - \phi_1) = 180^\circ \quad \text{[Equation 4]}$$

$$\alpha_2 + \theta_2 + (180^\circ - \phi_2) = 180^\circ \quad [\text{Equation 5}]$$

$$\alpha_3 + \theta_3 + (180^\circ - \phi_3) = 180^\circ \quad [\text{Equation 6}]$$

α_1, α_2 and α_3 are the angles between the swing cylinder axis and the longitudinal axis of the leg in different positions.

The swing angle of the leg is denoted as a positive angle when the leg is rotating to the AFT of the vehicle and is denoted as a negative angle when the leg is rotating to the FWD direction of the vehicle. In order to swing the legs by a given positive angle the AFT swing cylinders are expanding, while the FWD swing cylinders are retracting. The swing radius for each leg is given by the distance between the swing cylinder rod pin centre and the leg swing pin centre, L_{SCP_LP} [m].

If the leg swings through an angle of (+) $\gamma_{leg_intl_pc}$ [degrees], then the swinging time for the AFT cylinders is,

$$t_2 = \left(\frac{\gamma_{leg_intl_pc}}{\Omega_{shc_e}} \right) \quad [\text{Equation 7}]$$

and that for the FWD cylinders is

$$t_2 = \left(\frac{\gamma_{leg_intl_pc}}{\Omega_{shc_r}} \right) \quad [\text{Equation 8}]$$

where, Ω_{shc_e} is the angular velocity of the AFT cylinders [rad/sec] and Ω_{shc_r} is the angular velocity of the FWD cylinders [rad/sec].

The total length of the leg extended during the lowering cycle is (Figure 3),

$$L_{lo_pc_total} = L_{l_pc} + L_{lo_pc} \quad \text{[Equation 9]}$$

where, $L_{lo_pc} = L_e - L_o$ [m] and $L_e = \frac{L_o}{\cos(\gamma_{leg_intl})}$ [m]

Thus,

$$L_{lo_pc_total} = L_{l_pc} + L_o \left(\frac{1}{\cos(\gamma_{leg_intl})} - 1 \right) \quad \text{[Equation 10]}$$

The time required to lower the leg during the preparatory cycle is,

$$t_3 = \left(\frac{L_{lo_pc_total}}{(v_{lhc_leg_r})} \right) \quad \text{[Equation 11]}$$

where $(v_{lhc_leg_r})$ is the linear velocity of leg lifting/lowering cylinder during cylinder retraction [m/sec].

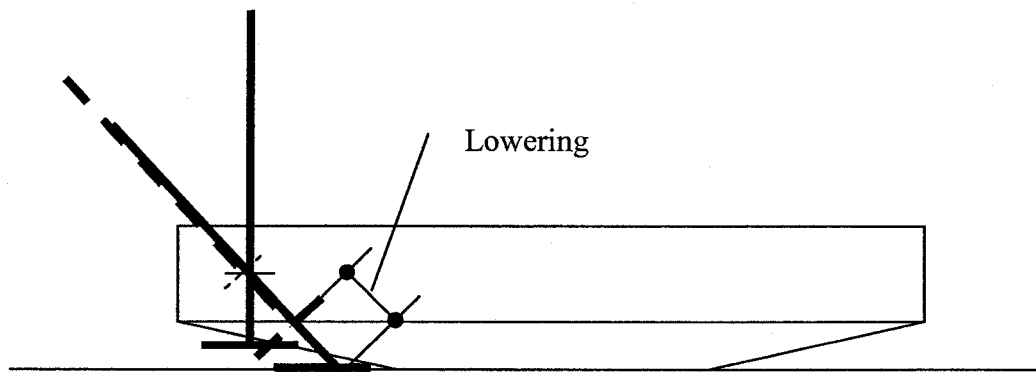


Figure 3 Lowering of leg during preparatory cycle

1.2 Motion Cycle

The legs will swing through an angle of $(\gamma_{leg_intl} + \gamma_{leg_fnl})$ [degrees] during the motion cycle, where γ_{leg_intl} is the initial angle of leg swing [degrees] and γ_{leg_fnl} is the final angle of leg swing [degrees]. The motion cycle will commence once the dredging cycle is completed. The dredging cycle time is denoted by (t_D) [sec].

The time required by the AFT cylinders is,

$$t_4 = \frac{(\gamma_{leg_intl} + \gamma_{leg_fnl})}{\Omega_{shc_r}} \quad \text{[Equation 12]}$$

and the time required by the FWD cylinders is,

$$t_4 = \frac{(\gamma_{leg_intl} + \gamma_{leg_fnl})}{\Omega_{shc_e}} \quad \text{[Equation 13]}$$

where, Ω_{shc_e} is the angular velocity of the AFT cylinders [rad/sec] and Ω_{shc_r} is the angular velocity of the FWD cylinders [rad/sec].

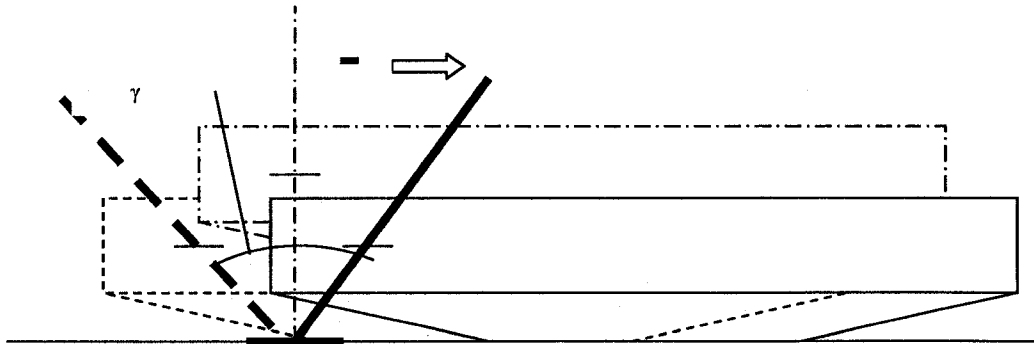


Figure 4 Motion cycle

1.3 Idle Cycle

During the idle cycle lifting, swinging and lowering actions of the legs will be executed, while no dredging or mining activities will be carried out.

The total lifting length during the idle cycle is (Figure 5),

$$L_{l_ic_total} = L_{lo_pc} + L_{l_ic} = L_o \left(\frac{1}{\cos(\gamma_{leg_intl})} - 1 \right) + L_{l_ic} \quad \text{[Equation 14]}$$

where, L_{l_ic} is the lifting distance during the idle cycle [m].

The lifting time during idle cycle is,

$$t_5 = \frac{L_{l_ic_total}}{v_{hc_leg_e}} \quad \text{[Equation 15]}$$

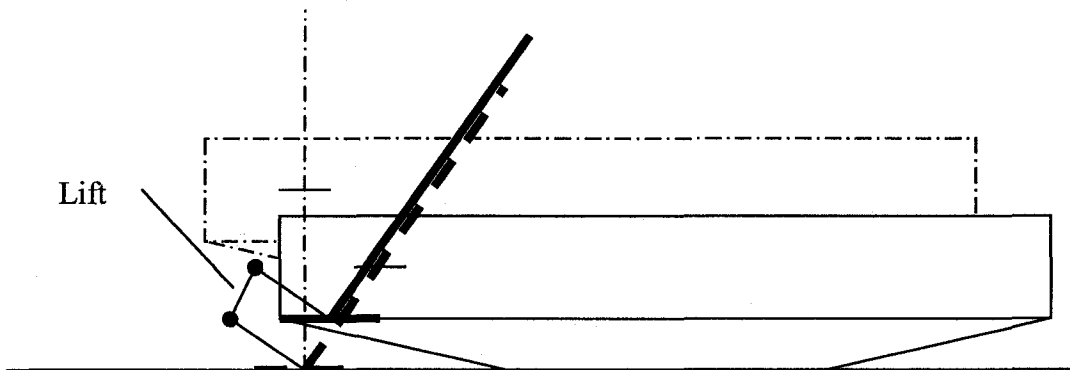


Figure 5 Lifting of legs during idle cycle

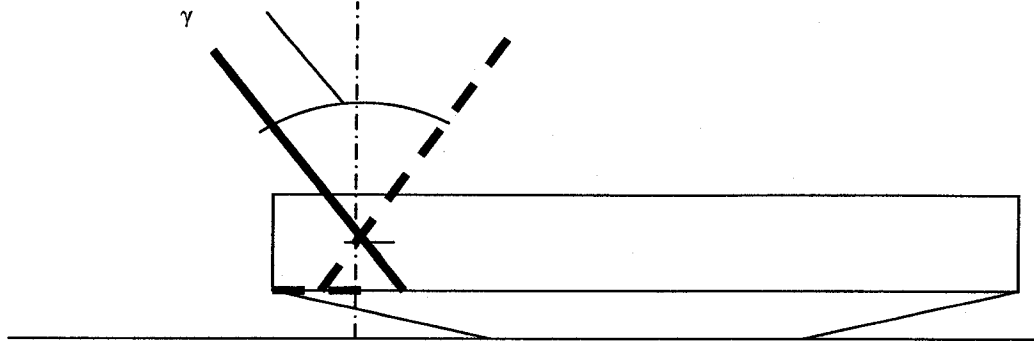


Figure 6 Swinging during idle cycle

The legs will also swing through an angle of $(\gamma_{leg_intl} + \gamma_{leg_fnl})$ [degrees] during the idle cycle, where γ_{leg_intl} is the initial angle of leg swing [degrees] and γ_{leg_fnl} is the final angle of leg swing [degrees]. The time required denoted by t_6 [sec] is equal to t_4 [sec].

The leg will be lowered by L_{l_ic} i.e. the lifting distance during the idle cycle [m]. The time required to lower the leg is,

$$t_7 = \frac{L_{l_ic}}{v_{lhc_leg_r}} \quad \text{[Equation 16]}$$

The total locomotion cycle time is given as,

$$t_{cycle} = \sum_{i=1}^7 t_i \quad \text{[Equation 17]}$$

Dredging or mining operations may start while the idle cycle is still continuing, thereby increasing the effective dredging time.

1.4 Finishing Cycle

After the dredging cycle is finished for one particular setting, the 'motion cycle' and the 'idle cycle' will be repeated till the work space is covered. When dredging in a given workspace is finished, the finishing cycle may be adopted to bring the legs in the same position and orientation as the preparatory cycle, where the required time will be the same.

This parametric model can be used to predict the locomotion cycle time and hence the average production of the designed vehicle as discussed in chapter 7.

The locomotion cycle time for the different types of gait plans are presented next.

Table 1 Locomotion cycle time for forward straight line, PS_AFT, 27.12.2004

Cycle No. (-)	t_1 (sec)	t_2 (sec)	t_3 (sec)	t_4 (sec)	t_5 (sec)	Total cycle time (sec)	γ_i (deg)	γ_f (deg)	Total swing angle (deg)
1	6.63	2.37	7	9	5	30.00	10	-28	38
2	3.60	2.40	5	6	5	22.00	10	-15	25
3	5.21	1.79	4	7	3	21.00	10	-29	39
4	4.38	4.62	5	9	4	27.00	20	-19	39
5	4.50	4.50	5	9	5	28.00	20	-20	40
6	4.21	4.79	6	9	5	29.00	25	-22	47
7	3.89	5.11	7	9	6	31.00	25	-19	44
8	5.19	4.81	6	10	5	31.00	25	-27	52
9	3.78	2.22	3	6	4	19.00	10	-17	27
Average	4.60	3.62	5.33	8.22	4.67	26.44	17.22	-21.78	39.00

Table 2 Locomotion cycle time for forward straight line, PS_FWD, 27.12.2004

Cycle No. (-)	t_1 (sec)	t_2 (sec)	t_3 (sec)	t_4 (sec)	t_5 (sec)	Total cycle time (sec)	γ_i (deg)	γ_f (deg)	Total swing angle (deg)
1	6.10	2.90	5	9	5	28.00	10	-21	31
2	3.39	2.61	6	6	5	23.00	10	-13	23
3	4.20	2.80	5	7	4	23.00	10	-15	25
4	3.71	5.29	7	9	5	30.00	20	-14	34
5	3.86	5.14	6	9	5	29.00	20	-15	35
6	4.21	4.79	6	9	5	29.00	25	-22	47
7	3.77	5.23	5	9	6	29.00	25	-18	43
8	4.44	5.56	6	10	6	32.00	25	-20	45
9	3.60	2.40	4	6	5	21.00	10	-15	25
Average	4.14	4.08	5.56	8.22	5.11	27.11	17.22	-17.00	34.22

Table 3 Locomotion cycle time for forward straight line, SBS_AFT, 27.12.2004

Cycle No. (-)	t_1 (sec)	t_2 (sec)	t_3 (sec)	t_4 (sec)	t_5 (sec)	Total cycle time (sec)	γ_i (deg)	γ_f (deg)	Total swing angle (deg)
1	6.00	5.00	6.4	11	5	33.40	10	-12	22
2	3.60	2.40	5.1	6	4.6	21.70	10	-15	25
3	4.73	1.58	3.8	6.3	2.6	19.00	10	-30	40
4	5.34	3.56	4.5	8.9	3.9	26.20	20	-30	50
5	4.85	3.35	4.5	8.2	4	24.90	20	-29	49
6	4.98	4.02	5.9	9	4.8	28.70	25	-31	56
7	4.80	4.00	6.5	8.8	5.4	29.50	25	-30	55
8	4.51	4.69	5.6	9.2	4.6	28.60	25	-24	49
9	3.14	1.96	3.3	5.1	3.3	16.80	10	-16	26
Average	4.66	3.40	5.07	8.06	4.24	25.42	17.22	-24.11	41.33

Table 4 Locomotion cycle time for forward straight line, SBS_FWD, 27.12.2004

Cycle No. (-)	t_1 (sec)	t_2 (sec)	t_3 (sec)	t_4 (sec)	t_5 (sec)	Total cycle time (sec)	γ_i (deg)	γ_f (deg)	Total swing angle (deg)
1	6.93	4.07	5	11	5	32.00	10	-17	27
2	3.60	2.40	5.8	6	4.5	22.30	10	-15	25
3	4.27	2.03	5.3	6.3	3.2	21.10	10	-21	31
4	3.81	5.09	6.1	8.9	4.3	28.20	20	-15	35
5	3.51	4.69	5.85	8.2	4.4	26.65	20	-15	35
6	4.21	4.79	5.7	9	4.9	28.60	25	-22	47
7	4.80	4.00	5.5	8.8	5.2	28.30	25	-30	55
8	3.45	5.75	5.7	9.2	5.3	29.40	25	-15	40
9	2.88	2.22	4	5.1	3.8	18.00	10	-13	23
Average	4.16	3.89	5.44	8.06	4.51	26.06	17.22	-18.11	35.33

Table 5 Locomotion cycle time for backward straight line, PS_AFT, 27.12.2004

Cycle No. (-)	t_1 (sec)	t_2 (sec)	t_3 (sec)	t_4 (sec)	t_5 (sec)	Total cycle time (sec)	γ_i (deg)	γ_f (deg)	Total swing angle (deg)
1	2.40	1.60	4	4	6	18.00	-10	15	25
2	3.28	1.72	3	5	5	18.00	-10	19	29
3	4.44	3.56	3	8	5	24.00	-20	25	45
4	4.36	3.64	4	8	4	24.00	-20	24	44
5	3.83	4.17	4	8	5	25.00	-25	23	48
6	4.67	4.33	4	9	5	27.00	-25	27	52
Average	3.83	3.17	3.67	7.00	5.00	22.67	-18.33	22.17	40.50

Table 6 Locomotion cycle time for backward straight line, PS_FWD, 27.12.2004

Cycle No. (-)	t_1 (sec)	t_2 (sec)	t_3 (sec)	t_4 (sec)	t_5 (sec)	Total cycle time (sec)	γ_i (deg)	γ_f (deg)	Total swing angle (deg)
1	2.18	1.82	7	4	5	20.00	-10	12	22
2	2.92	2.08	6	5	5	21.00	-10	14	24
3	4.00	4.00	8	8	5	29.00	-20	20	40
4	4.00	4.00	7	8	5	28.00	-20	20	40
5	3.83	4.17	7	8	4	27.00	-25	23	48
6	3.38	5.63	7	9	5	30.00	-25	15	40
Average	3.38	3.62	7.00	7.00	4.83	25.83	-18.33	17.33	35.67

Table 7 Locomotion cycle time for backward straight line, SBS_AFT, 27.12.2004

Cycle No. (-)	t_1 (sec)	t_2 (sec)	t_3 (sec)	t_4 (sec)	t_5 (sec)	Total cycle time (sec)	γ_i (deg)	γ_f (deg)	Total swing angle (deg)
1	2.58	1.62	3.3	4.2	5	16.70	-10	16	26
2	3.21	1.69	2.9	4.9	4	16.70	-10	19	29
3	4.60	3.40	3.2	8	4.2	23.40	-20	27	47
4	3.63	4.27	3.4	7.9	4.2	23.40	-20	17	37
5	5.01	2.79	3.6	7.8	4.7	23.90	-25	45	70
6	4.91	4.39	3.6	9.3	4.2	26.40	-25	28	53
Average	3.99	3.03	3.33	7.02	4.38	21.75	-18.33	25.33	43.67

Table 8 Locomotion cycle time for backward straight line, SBS_FWD, 27.12.2004

Cycle No. (-)	t_1 (sec)	t_2 (sec)	t_3 (sec)	t_4 (sec)	t_5 (sec)	Total cycle time (sec)	γ_i (deg)	γ_f (deg)	Total swing angle (deg)
1	2.37	1.83	5.9	4.2	4.7	19.00	-10	13	23
2	3.02	1.88	5.3	4.9	4.4	19.50	-10	16	26
3	3.79	4.21	7.3	8	4.4	27.70	-20	18	38
4	4.31	3.59	6.2	7.9	4.4	26.40	-20	24	44
5	3.90	3.90	5.8	7.8	4.2	25.60	-25	25	50
6	3.76	5.54	6.3	9.3	4.3	29.20	-25	17	42
Average	3.53	3.49	6.13	7.02	4.40	24.57	-18.33	18.83	37.17

Table 9 Locomotion cycle time for curvilinear locomotion with inner angles fixed, PS_AFT

Cycle No. (-)	t_1 (sec)	t_2 (sec)	t_3 (sec)	t_4 (sec)	t_5 (sec)	Total cycle time (sec)	γ_i (deg)	γ_f (deg)	Total swing angle (deg)
1	-	-	4	5	5	14.00	0	0	0
2	-	-	5	5	5	15.00	0	0	0
3	-	-	4	4	4	12.00	0	0	0
4	-	-	4	4	4	12.00	0	-2	-2
5	-	-	4	4	3	11.00	0	0	0
6	-	-	4	4	4	12.00	0	0	0
7	-	-	4	6	3	13.00	0	0	0
8	-	-	3	6	4	13.00	0	0	0
9	-	-	4	6	4	14.00	0	0	0
10	-	-	3	10	4	17.00	0	0	0
11	-	-	4	7	4	15.00	0	0	0
12	-	-	3	7	4	14.00	0	0	0
Average	-	-	3.83	5.67	4.00	13.50	0.00	-0.17	-0.17

Table 10 Locomotion cycle time for curvilinear locomotion with inner angles fixed, PS_FWD

Cycle No. (-)	t_1 (sec)	t_2 (sec)	t_3 (sec)	t_4 (sec)	t_5 (sec)	Total cycle time (sec)	γ_i (deg)	γ_f (deg)	Total swing angle (deg)
1	-	-	6	5	5	16.00	0	0	0
2	-	-	6	5	6	17.00	0	0	0
3	-	-	5	4	5	14.00	0	0	0
4	-	-	5	4	5	14.00	0	0	0
5	-	-	5	4	5	14.00	0	0	0
6	-	-	5	4	5	14.00	0	0	0
7	-	-	5	6	5	16.00	0	0	0
8	-	-	4	6	5	15.00	0	0	0
9	-	-	5	6	5	16.00	0	0	0
10	-	-	5	8	5	18.00	0	0	0
11	-	-	4	7	5	16.00	0	0	0
12	-	-	4	7	5	16.00	0	0	0
Average	-	-	4.92	5.50	5.08	15.50	0.00	0.00	0.00

Table 11 Locomotion cycle time for curvilinear locomotion with inner angles fixed, SBS_AFT

Cycle No. (-)	t_1 (sec)	t_2 (sec)	t_3 (sec)	t_4 (sec)	t_5 (sec)	Total cycle time (sec)	γ_i (deg)	γ_f (deg)	Total swing angle (deg)
1	3.33	1.67	4.1	5	5	19.10	5	-10	15
2	3.53	1.47	4.1	5	4.6	18.70	5	-12	17
3	2.67	1.33	3.2	4	3.6	14.80	5	-10	15
4	2.08	2.32	3.2	4.4	3.4	15.40	10	-9	19
5	2.35	1.95	3	4.3	3.5	15.10	10	-12	22
6	2.00	2.00	3	4	3.5	14.50	10	-10	20
7	3.19	2.81	3.2	6	3.2	18.40	15	-17	32
8	3.24	2.86	2.9	6.1	3.3	18.40	15	-17	32
9	3.10	2.90	2.9	6	3.6	18.50	15	-16	31
10	3.33	6.67	3	10	3.7	26.70	20	-10	30
11	3.22	3.78	3.1	7	3.5	20.60	20	-17	37
12	3.41	3.59	2.9	7	3.9	20.80	20	-19	39
Average	2.95	2.78	3.22	5.73	3.73	18.42	12.50	-13.25	25.75

**Table 12 Locomotion cycle time for curvilinear locomotion with inner angles fixed,
SBS_FWD**

Cycle No. (-)	t_1 (sec)	t_2 (sec)	t_3 (sec)	t_4 (sec)	t_5 (sec)	Total cycle time (sec)	γ_i (deg)	γ_f (deg)	Total swing angle (deg)
1	3.33	1.67	5.6	5	4.5	20.10	5	-10	15
2	3.08	1.92	5.6	5	5.1	20.70	5	-8	13
3	2.00	2.00	5.1	4	4.5	17.60	5	-5	10
4	1.47	2.93	4.6	4.4	3.9	17.30	10	-5	15
5	1.77	2.53	4.4	4.3	4	17.00	10	-7	17
6	1.14	2.86	4.2	4	4.5	16.70	10	-4	14
7	1.91	4.09	4	6	4.1	20.10	15	-7	22
8	2.40	3.60	4.1	6	4.3	20.40	15	-10	25
9	0.62	4.68	3.8	5.3	4.5	18.90	15	-2	17
10	1.30	8.70	4.4	10	7	31.40	20	-3	23
11	0.64	6.36	4.4	7	4.5	22.90	20	-2	22
12	0.64	6.36	4	7	4.5	22.50	20	-2	22
Average	1.69	3.97	4.52	5.67	4.62	20.47	12.50	-5.42	17.92

2.0 Uncertainty Analyses for Gait Planning Tests

The assumptions used for the uncertainty analyses for the gait planning tests are,

1. For length and angular measurements an uncertainty of half of the smallest scale division is used
2. Scales and tapes used to measure linear distances had an instrumental precision of 1 mm
3. Inclinator used to measure angles had an instrumental precision of 1 degree
4. Standard deviations together with confidence limits at a given confidence interval were calculated
5. The distance between leg swing pin centre and foot hinge pin centre (L_o) is constant

Uncertainty analyses has been done based on standard uncertainty analyses methods [Coleman and Steele, 1999].

Table 13 Constants used for the uncertainty analyses

Parameter	Unit	Value
Precision for scale and tape	mm	1
Error assumed for scale	mm	0.5
L _o	mm	340
L _o High	mm	340.5
L _o Mid	mm	340
L _o Low	mm	339.5
Precision for inclinometer	degree	1
Error assumed for inclinometer	degree	0.5

Table 14 Uncertainty analyses for calculated step size of PS_AFT leg during forward straight line locomotion (t value used at 95 % confidence level = 1.81 and number of samples used = 11)

Leg Swing Angle (degree)	Δ Leg Swing Angle High (radians)	Δ Leg Swing Angle Mid (radians)	Δ Leg Swing Angle Low (radians)	Step size High (mm)	Step size Mid (mm)	Step size Low (mm)	Mean (mm)	Standard Deviation (mm)	Confidence Limit (mm)
21	0.069	0.069	0.069	23.810	23.775	23.740	16.806	17.595	10.07
25	0.034	0.034	0.034	11.890	11.873	11.855			
27	0.191	0.191	0.191	66.186	66.089	65.992			
38	0.017	0.017	0.017	5.943	5.934	5.925			
39	0.017	0.017	0.017	5.943	5.934	5.925			
40	0.034	0.034	0.034	11.890	11.873	11.855			
42	0.034	0.034	0.034	11.890	11.873	11.855			
44	0.034	0.034	0.034	11.890	11.873	11.855			
46	0.017	0.017	0.017	5.943	5.934	5.925			
47	0.069	0.069	0.069	23.810	23.775	23.740			
51	0.017	0.017	0.017	5.943	5.934	5.925			

Table 15 Uncertainty analyses for experimental step size of PS_AFT leg during forward straight line locomotion (t value used at 95 % confidence level = 1.77 and number of samples used = 14)

Step size (mm)	Mean (mm)	Standard Deviation (mm)	Confidence Limit (mm)
110	226.4286	65.15628	31.98585
122			
145			
195			
215			
220			
228			
230			
245			
270			
280			
300			
300			
310			

Table 16 Uncertainty analyses for calculated step size of PS_FWD leg during forward straight line locomotion (t value used at 95 % confidence level = 1.81 and number of samples used = 11)

Leg Swing Angle (degree)	Δ Leg Swing Angle High (radians)	Δ Leg Swing Angle Mid (radians)	Δ Leg Swing Angle Low (radians)	Step size High (mm)	Step size Mid (mm)	Step size Low (mm)	Mean (mm)	Standard Deviation (mm)	Confidence Limit (mm)
20	0.052	0.052	0.052	17.845	17.819	17.792	17.289	8.618	4.933
23	0.034	0.034	0.034	11.891	11.873	11.856			
25	0.104	0.104	0.104	35.788	35.735	35.683			
31	0.052	0.052	0.052	17.845	17.819	17.792			
34	0.017	0.017	0.017	5.943	5.935	5.926			
35	0.087	0.087	0.087	29.790	29.746	29.702			
40	0.052	0.052	0.052	17.845	17.819	17.792			
43	0.034	0.034	0.034	11.891	11.873	11.856			
45	0.034	0.034	0.034	11.891	11.873	11.856			
47	0.052	0.052	0.052	17.845	17.819	17.792			
50	0.034	0.034	0.034	11.891	11.873	11.856			

Table 17 Uncertainty analyses for calculated step size of SBS_AFT leg during forward straight line locomotion (t value used at 95 % confidence level = 1.83 and number of samples used = 10)

Leg Swing Angle (degree)	Δ Leg Swing Angle High (radians)	Δ Leg Swing Angle Mid (radians)	Δ Leg Swing Angle Low (radians)	Step size High (mm)	Step size Mid (mm)	Step size Low (mm)	Mean (mm)	Standard Deviation (mm)	Confidence Limit (mm)
20	0.034	0.034	0.034	11.890	11.873	11.855	21.463	18.560	11.321
22	0.052	0.052	0.052	17.844	17.818	17.792			
25	0.017	0.017	0.017	5.943	5.934	5.925			
26	0.157	0.157	0.157	53.929	53.850	53.771			
35	0.052	0.052	0.052	17.844	17.818	17.792			
38	0.034	0.034	0.034	11.890	11.873	11.855			
40	0.157	0.157	0.157	53.929	53.850	53.771			
49	0.017	0.017	0.017	5.943	5.934	5.925			
50	0.087	0.087	0.087	29.789	29.746	29.702			
55	0.017	0.017	0.017	5.943	5.934	5.925			

Table 18 Uncertainty analyses for experimental step size of SBS_AFT leg during forward straight line locomotion (t value used at 95 % confidence level = 1.77 and number of samples used = 14)

Step size (mm)	Mean (mm)	Standard Deviation (mm)	Confidence Limit (mm)
100	237.5	73.03	35.85
145			
155			
195			
230			
230			
230			
230			
250			
270			
290			
315			
320			
365			

Table 19 Uncertainty analyses for calculated step size of SBS_FWD leg during forward straight line locomotion (t value used at 95 % confidence level = 1.83 and number of samples used = 10)

Leg Swing Angle (degree)	Δ Leg Swing Angle High (radians)	Δ Leg Swing Angle Mid (radians)	Δ Leg Swing Angle Low (radians)	Step size High (mm)	Step size Mid (mm)	Step size Low (mm)	Mean (mm)	Standard Deviation (mm)	Confidence Limit (mm)
21	0.034	0.034	0.034	11.890	11.873	11.855	20.219	10.955	6.682
23	0.034	0.034	0.034	11.890	11.873	11.855			
25	0.104	0.104	0.104	35.787	35.735	35.682			
31	0.069	0.069	0.069	23.810	23.775	23.740			
35	0.087	0.087	0.087	29.789	29.746	29.702			
40	0.0174	0.0174	0.0174	5.943	5.934	5.925			
41	0.104	0.104	0.104	35.787	35.735	35.682			
47	0.034	0.034	0.034	11.890	11.873	11.855			
49	0.034	0.034	0.034	11.890	11.873	11.855			
51	0.069	0.069	0.069	23.810	23.775	23.740			

Table 20 Uncertainty analyses for calculated step size of PS_AFT leg during backward straight line locomotion (t value used at 95 % confidence level = 2.13 and number of samples used = 5)

Leg Swing Angle (degree)	Δ Leg Swing Angle High (radians)	Δ Leg Swing Angle Mid (radians)	Δ Leg Swing Angle Low (radians)	Step size High (mm)	Step size Mid (mm)	Step size Low (mm)	Mean (mm)	Standard Deviation (mm)	Confidence Limit (mm)
25	0.069	0.069	0.069	23.810	23.775	23.740	32.481	33.570	35.752
29	0.261	0.261	0.261	91.236	91.102	90.968			
44	0.017	0.017	0.017	5.943	5.934	5.925			
45	0.052	0.052	0.052	17.844	17.818	17.792			
48	0.069	0.069	0.069	23.810	23.775	23.740			
52									

Table 21 Uncertainty analyses for experimental step size of PS_AFT leg during backward straight line locomotion (t value used at 95 % confidence level = 2.02 and number of samples used = 6)

Step size (mm)	Mean (mm)	Standard Deviation (mm)	Confidence Limit (mm)
125	191.666	48.853	44.132
135			
220			
220			
210			
240			

Table 22 Uncertainty analyses for calculated step size of PS_FWD leg during backward straight line locomotion (t value used at 95 % confidence level = 2.92 and number of samples used = 3)

Leg Swing Angle (degree)	Δ Leg Swing Angle High (radians)	Δ Leg Swing Angle Mid (radians)	Δ Leg Swing Angle Low (radians)	Step size High (mm)	Step size Mid (mm)	Step size Low (mm)	Mean (mm)	Standard Deviation (mm)	Confidence Limit (mm)
22	0.034	0.034	0.034	11.891	11.873	11.856	52.383	42.9951	88.7742189
24	0.279	0.279	0.279	97.637	97.493	97.350			
40	0.139	0.139	0.139	47.854	47.784	47.714			

Table 23 Uncertainty analyses for calculated step size of SBS_AFT leg during backward straight line locomotion (t value used at 95 % confidence level = 2.13 and number of samples used = 5)

Leg Swing Angle (degree)	Δ Leg Swing Angle High (radians)	Δ Leg Swing Angle Mid (radians)	Δ Leg Swing Angle Low (radians)	Step size High (mm)	Step size Mid (mm)	Step size Low (mm)	Mean (mm)	Standard Deviation (mm)	Confidence Limit (mm)
26	0.052	0.052	0.052	17.844	17.818	17.792	53.047	32.430	34.538
29	0.139	0.139	0.139	47.854	47.783	47.713			
37	0.174	0.174	0.174	60.039	59.951	59.863			
47	0.104	0.104	0.104	35.787	35.735	35.682			
53	0.296	0.296	0.296	104.101	103.948	103.795			

Table 24 Uncertainty analyses for experimental step size of SBS_AFT leg during backward straight line locomotion (t value used at 95 % confidence level = 1.77 and number of samples used = 6)

Step size (mm)	Mean (mm)	Standard Deviation (mm)	Confidence Limit (mm)
100	175.833	51.712	40.933
145			
155			
195			
230			
230			

Table 25 Uncertainty analyses for calculated step size of SBS_FWD leg during backward straight line locomotion (t value used at 95 % confidence level = 2.13 and number of samples used = 5)

Leg Swing Angle (degree)	Δ Leg Swing Angle High (radians)	Δ Leg Swing Angle Mid (radians)	Δ Leg Swing Angle Low (radians)	Step size High (mm)	Step size Mid (mm)	Step size Low (mm)	Mean (mm)	Standard Deviation (mm)	Confidence Limit (mm)
23	0.052	0.052	0.052	17.844	17.818	17.792	32.294	24.025	25.587
26	0.209	0.209	0.209	72.375	72.269	72.162			
38	0.069	0.069	0.069	23.810	23.775	23.740			
42	0.034	0.034	0.034	11.890	11.873	11.855			
44	0.104	0.104	0.104	35.787	35.735	35.682			

Table 26 Uncertainty analyses for experimental turning radius of assumed vehicle centre of gravity during curvilinear locomotion with unequal leg swing angles (t value used at 95 % confidence level = 1.81 and number of samples used = 11)

Turning Radius (mm)	Mean (mm)	Standard Deviation (mm)	Confidence Limit (mm)
5251	9211.636	2868.165	1641.658
6242			
6555			
7723			
8410			
8981			
10007			
10118			
10352			
12818			
14871			

Table 27 Uncertainty analyses for experimental turning angle of assumed vehicle centre of gravity during curvilinear locomotion with unequal leg swing angles (t value used at 95 % confidence level = 1.81 and number of samples used = 11)

Turning Angle (degree)	Mean (degree)	Standard Deviation (degree)	Confidence Limit (degree)
1	1.363	0.504	0.288
1			
1			
1			
1			
1			
1			
1			
1			
2			
2			
2			
2			

APPENDIX 9

STATIC LOAD INCIDENT AT LEG

The experimental and predicted results for the static load incident at each leg are presented in this Appendix.

Table 1 Experimental normal load at foot/ soil interface for PS_FWD leg with Load Cell 1

Leg swing angle (degree)	Pressure gage reading (kg/ cm ²)	Load incident at each leg (kN)
0	1.2	11.2
10	0.9	8.2
20	0.8	7.2
-10	1.1	10.2
-20	0.92	8.4

Table 2 Experimental normal load at foot/ soil interface for PS_AFT leg with Load Cell 1

Leg swing angle (degree)	Pressure gage reading (kg/ cm ²)	Load incident at each leg (kN)
0	0.72	6.40
10	0.6	5.20
20	0.5	4.20
-10	0.58	5.00
-20	0.55	4.70

Table 3 Experimental normal load at foot/ soil interface for SBS_FWD leg with Load Cell 2

Leg swing angle (degree)	Pressure gage reading (kg/ cm ²)	Load incident at each leg (kN)
0	1.3	13.67
10	1.2	12.42
20	0.8	7.42
-10	1.2	12.42
-20	0.92	8.92

Table 4 Experimental normal load at foot/ soil interface for SBS_AFT leg with Load Cell 1

Leg swing angle (degree)	Pressure gage reading (kg/ cm ²)	Load incident at each leg (kN)
0	0.8	7.20
10	0.58	5.00
20	0.62	5.40
-10	0.55	4.70
-20	0.68	6.00

Table 5 Predicted normal load at foot/ soil interface

Leg swing angle (degree)	Load incident at AFT leg (kN)	Load incident at FWD leg (kN)
0	6.32	9.38
10	6.04	9.095
20	5.245	8.28
-10	6.04	9.095
-20	5.245	8.28

Table 6 Ratio of normal load at FWD to normal load at AFT foot/ soil interface

Ratio: FWD and AFT:PS Experiment (-)	Ratio: FWD and AFT:PS Experiment (-)	Ratio: FWD and AFT: Predicted (-)
1.75	1.90	1.48
1.58	2.48	1.51
1.71	1.37	1.58
2.04	2.64	1.51
1.79	1.49	1.58

APPENDIX 10

POSITION ANALYSIS OF LEG LINKAGE AND DYNAMIC LOAD INCIDENT AT LEG

This Appendix presents the theory behind the position analyses of the four bar mechanism formed by the designed leg linkage and the hydraulic cylinder swinging the leg. The calculated values of the angles between the different linkages at different positions, the vertical and horizontal components of the dynamic loads acting at the foot pin, the total load (static and dynamic) acting at the foot/ soil interface are given in this Appendix. The required bearing capacities of the soil for a rectangular, square and circular foot are also presented in this Appendix.

1.0 Position Analysis of Leg Linkage

The leg linkage and the swing cylinder is a four bar mechanism as shown in Figure 1. The lengths of the different linkages are denoted by the small letters.

The position analyses for the four bar mechanism gives [Norton, 1999],

$$ae^{j\theta_2} + be^{j\theta_2} - ce^{j\theta_4} - de^{j\theta_1} \quad [\text{Equation 1}]$$

$$a(\cos \theta_2 + j \sin \theta_2) + b(\cos \theta_2 + j \sin \theta_2) - c(\cos \theta_4 + j \sin \theta_4) + d(\cos 0 + j \sin 0) = 0 \quad [\text{Equation 2}]$$

$$\cos \theta_4 = \left(\frac{a^2 + b^2 - c^2 - d^2 + 2ab}{2cd} \right) \quad [\text{Equation 3}]$$

$$\theta_4 = \cos^{-1} \left(\frac{a^2 + b^2 - c^2 - d^2 + 2ab}{2cd} \right)$$

$$\cos \theta_2 = \left(\frac{a^2 + b^2 - c^2 + d^2 + 2ab}{2*(a+b)*d} \right) \quad [\text{Equation 4}]$$

where, a is the length of the swing cylinder of the leg [mm], b is the displacement of the hydraulic cylinder rod [mm], c is the distance between the rod pin centre of the swing cylinder and the swing pin centre of the leg [mm], d is the distance between the swing cylinder pin centre and the swing pin centre of the leg [mm].

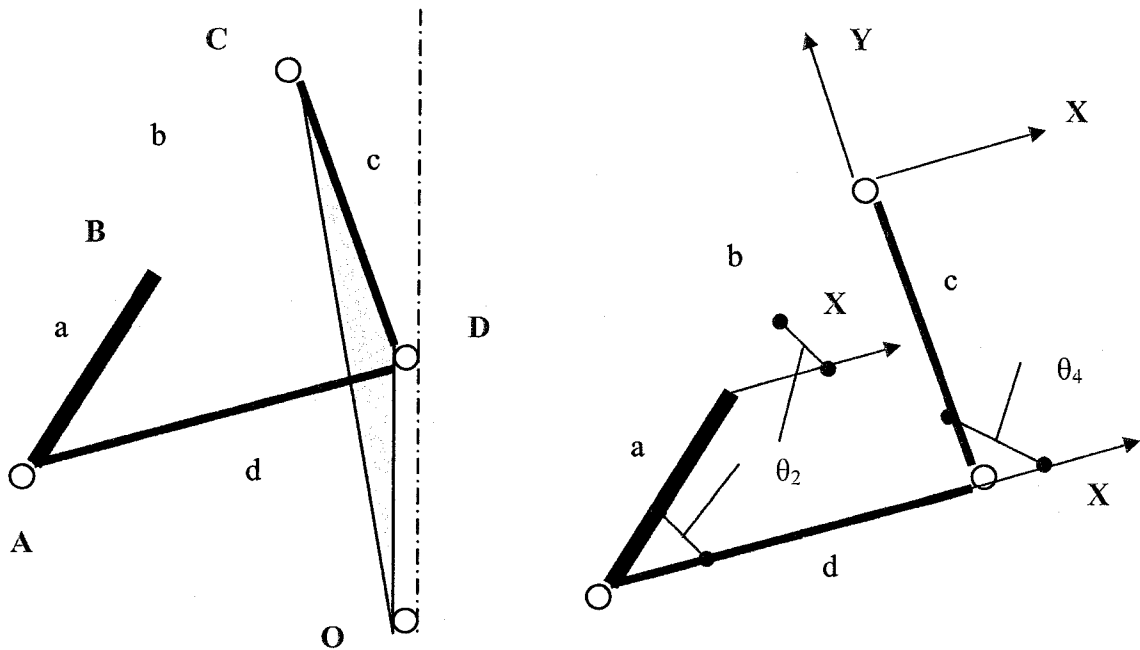


Figure 1 Position analyses for the designed leg linkage

The force generated by the hydraulic oil pressure along the cylinder axis was assumed constant since the hydraulic oil pressure was kept constant. The force along the cylinder rod axis however varies since the cylinder rod velocity first accelerates from zero to a constant velocity of $v_{shc_leg} = \frac{db}{dt}$ [m/sec] and then decelerates to zero again. The magnitude of this force thus changes during the accelerating and decelerating phase, and is controlled by the solenoids of the directional control valves. The force along the swing cylinder rod was resolved into a normal component acting perpendicular to the link 'c' and a tangential component acting along the link

'c' (Figure 3.54). The angle between the links 'b' and 'c' denoted by $(\lambda = \theta_4 - \theta_2)$ [degrees] is varying with time during the swinging action of the leg (Figure 3.54). The magnitudes of the normal and tangential components thus also vary with time.

The angle β_0 is a function of θ_4 and θ_5 [Figure 3.53 and Figure 2] and is expressed,

$$\beta_0 = \theta_4 - \left(\frac{\pi}{2} + \theta_5\right) \quad \text{[Equation 5]}$$

The machine geometry for the determination of the angle β_0 is shown in Figure 2.

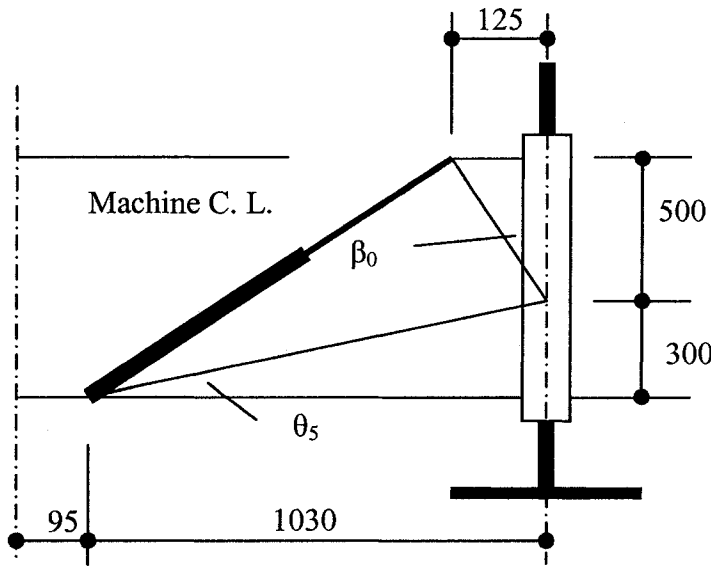


Figure 2 Machine geometry for determination of angle, β_0

From the machine geometry of the prototype vehicle 'Golden Tortoise', it was found that

$$\theta_5 = 16.24^\circ = 0.283 \text{ radians .}$$

The constants used for the estimation of the dynamic loads at the foot/soil interface due to the swing cylinder operation of the legs are presented below. The results from the position analyses are also given.

Table 1 Constants for estimation of the dynamic load at foot/ soil interface

Constants	Value
1. Hydraulic oil pressure [kPa]	100
2. Diameter of swing cylinder [m]	0.0620
3. Diameter of cylinder rod [m]	0.0350
4. Area of swing cylinder [m ²]	0.003
5. Area of cylinder rod [m ²]	0.0010
6. Loss factor [-]	1.0000
7. Cylinder force (expansion) [kN]	0.301754
8. Cylinder force (retraction) [kN]	0.2055915
9. Link length a [mm]	960
10. Link length c [mm]	515
11. Link length d [mm]	1073
12. theta ₅ [degree]	16.24

Table 2 Position analyses for leg linkage

Displacement of cylinder rod (mm)	Angle θ_4 (degree)	Angle θ_2 (degree)	Angle β_0 (degree)
0	116.61	28.66	42.89
10	115.49	28.64	41.78
20	114.38	28.60	40.66
30	113.26	28.55	39.55
40	112.14	28.49	38.43
50	111.02	28.42	37.31
60	109.90	28.34	36.18
70	108.77	28.26	35.06
80	107.64	28.16	33.93
90	106.51	28.05	32.79
100	105.37	27.94	31.66
110	104.23	27.81	30.51
120	103.08	27.68	29.37
130	101.93	27.53	28.22
140	100.77	27.38	27.06
150	99.61	27.22	25.89
160	98.44	27.05	24.72
170	97.26	26.88	23.55
180	96.07	26.69	22.36
190	94.88	26.50	21.17
200	93.68	26.30	19.97
210	92.47	26.09	18.76
220	91.25	25.87	17.54
230	90.02	25.64	16.31
240	88.78	25.41	15.07
250	87.53	25.16	13.82
260	86.27	24.91	12.56
270	85.00	24.65	11.28
280	83.71	24.38	10.00
290	82.41	24.10	8.70
300	81.10	23.82	7.38

Table 3 Vertical force at foot/ soil interface during cylinder expansion

Swing angle = 0°	Swing angle = 10°	Swing angle = 20°	Swing angle = 30°
7.936	7.816	7.458	6.874
12.342	12.155	11.598	10.690
16.848	16.592	15.833	14.593
21.449	21.123	20.157	18.578
26.140	25.743	24.565	22.641
30.915	30.446	29.053	26.777
35.769	35.227	33.614	30.982
40.698	40.080	38.246	35.251
45.694	45.001	42.941	39.579
50.755	49.984	47.697	43.961
55.873	55.025	52.507	48.395
61.044	60.118	57.366	52.874
66.263	65.257	62.271	57.394
71.524	70.439	67.215	61.951
76.822	75.657	72.194	66.540
82.152	80.905	77.203	71.157
87.507	86.179	82.235	75.795
92.883	91.473	87.287	80.451
98.273	96.782	92.353	85.120
103.672	102.098	97.426	89.796
109.073	107.418	102.502	94.475
114.471	112.733	107.574	99.150
119.858	118.039	112.637	103.816
125.229	123.328	117.684	108.468
130.576	128.594	122.709	113.100
135.893	133.831	127.706	117.705
141.172	139.030	132.667	122.277
146.406	144.184	137.585	126.811
151.586	149.286	142.454	131.298
156.705	154.327	147.264	135.732
161.754	159.299	152.009	140.105

Table 4 Vertical force at foot/ soil interface during cylinder retraction

Swing angle = 0°	Swing angle = 10°	Swing angle = 20°	Swing angle = 30°
5.407	5.325	5.081	4.683
8.409	8.281	7.902	7.283
11.479	11.305	10.787	9.942
14.614	14.392	13.733	12.658
17.810	17.539	16.737	15.426
21.063	20.743	19.794	18.244
24.370	24.001	22.902	21.109
27.728	27.307	26.058	24.017
31.133	30.660	29.257	26.966
34.580	34.055	32.497	29.952
38.067	37.490	35.774	32.972
41.591	40.960	39.085	36.024
45.147	44.461	42.427	39.104
48.731	47.991	45.795	42.209
52.341	51.546	49.187	45.335
55.972	55.122	52.600	48.481
59.621	58.716	56.029	51.641
63.283	62.323	59.471	54.813
66.956	65.939	62.922	57.994
70.634	69.562	66.378	61.180
74.314	73.186	69.837	64.368
77.991	76.808	73.293	67.553
81.662	80.422	76.742	70.732
85.321	84.026	80.181	73.902
88.964	87.614	83.605	77.057
92.587	91.182	87.009	80.195
96.184	94.724	90.389	83.310
99.750	98.236	93.740	86.399
103.279	101.712	97.057	89.456
106.767	105.146	100.334	92.477
110.207	108.534	103.567	95.456

Table 5 Horizontal force at foot/ soil interface during cylinder expansion

Swing angle = 0°	Swing angle = 10°	Swing angle = 20°	Swing angle = 30°
0	1.280	2.520	3.685
0	1.914	3.769	5.511
0	2.512	4.947	7.233
0	3.074	6.054	8.851
0	3.599	7.090	10.365
0	4.089	8.053	11.773
0	4.541	8.944	13.076
0	4.957	9.763	14.272
0	5.335	10.508	15.362
0	5.676	11.179	16.344
0	5.979	11.777	17.217
0	6.245	12.299	17.981
0	6.472	12.747	18.635
0	6.660	13.119	19.179
0	6.810	13.414	19.611
0	6.921	13.633	19.930
0	6.993	13.774	20.136
0	7.025	13.836	20.227
0	7.016	13.820	20.203
0	6.967	13.723	20.063
0	6.878	13.547	19.805
0	6.747	13.289	19.428
0	6.574	12.949	18.930
0	6.359	12.526	18.312
0	6.102	12.019	17.571
0	5.802	11.428	16.707
0	5.458	10.751	15.717
0	5.070	9.987	14.600
0	4.638	9.135	13.355
0	4.161	8.195	11.980
0	3.637	7.164	10.474

Table 6 Horizontal force at foot/ soil interface during cylinder retraction

Swing angle = 0°	Swing angle = 10°	Swing angle = 20°	Swing angle = 30°
0	0.872	1.717	2.510
0	1.304	2.568	3.754
0	1.711	3.371	4.928
0	2.094	4.125	6.030
0	2.452	4.830	7.062
0	2.786	5.487	8.021
0	3.094	6.094	8.909
0	3.377	6.651	9.724
0	3.635	7.159	10.466
0	3.867	7.617	11.135
0	4.074	8.024	11.730
0	4.255	8.380	12.251
0	4.409	8.685	12.697
0	4.538	8.938	13.067
0	4.640	9.139	13.361
0	4.716	9.288	13.579
0	4.764	9.384	13.719
0	4.786	9.427	13.781
0	4.780	9.416	13.765
0	4.747	9.350	13.669
0	4.686	9.230	13.493
0	4.597	9.054	13.236
0	4.479	8.822	12.898
0	4.333	8.534	12.476
0	4.158	8.189	11.972
0	3.953	7.786	11.383
0	3.719	7.325	10.708
0	3.455	6.804	9.947
0	3.160	6.224	9.099
0	2.835	5.583	8.162
0	2.478	4.881	7.136

The total vertical and horizontal forces at the foot/ soil interface for the SBS_FWD leg is shown below. The measured values of the static load for the SBS_FWD leg were the highest and hence the static load values of this leg were considered.

Table 7 Total force at foot/ soil interface during cylinder expansion

Displacement of cylinder rod (mm)	Total force (kN) Cylinder expanding, Swing angle = 0°	Total force (kN) Cylinder expanding, Swing angle = 10°	Total force (kN) Cylinder expanding, Swing angle = 20°
0	13.68	12.43	8.927
10	13.68	12.43	8.932
20	13.69	12.44	8.936
30	13.69	12.44	8.940
40	13.70	12.45	8.945
50	13.70	12.45	8.949
60	13.71	12.46	8.954
70	13.71	12.46	8.958
80	13.72	12.47	8.963
90	13.72	12.47	8.968
100	13.73	12.48	8.973
110	13.73	12.48	8.977
120	13.74	12.49	8.982
130	13.74	12.49	8.987
140	13.75	12.50	8.992
150	13.75	12.50	8.997
160	13.76	12.51	9.002
170	13.76	12.51	9.007
180	13.77	12.52	9.012
190	13.77	12.52	9.017
200	13.78	12.53	9.023
210	13.78	12.53	9.028
220	13.79	12.54	9.033
230	13.80	12.54	9.038
240	13.80	12.55	9.043
250	13.81	12.55	9.048
260	13.81	12.56	9.053
270	13.82	12.56	9.058
280	13.82	12.57	9.062
290	13.83	12.57	9.067
300	13.83	12.58	9.072

Table 8 Total force at foot/ soil interface during cylinder retraction

Displacement of cylinder rod (mm)	Total force (kN) Cylinder retracting, Swing angle = 0°	Total force (kN) Cylinder retracting, Swing angle = 10°	Total force (kN) Cylinder retracting, Swing angle = 20°
0	13.68	12.43	7.43
10	13.68	12.43	7.43
20	13.68	12.43	7.43
30	13.68	12.43	7.43
40	13.69	12.44	7.44
50	13.69	12.44	7.44
60	13.69	12.44	7.44
70	13.70	12.45	7.45
80	13.70	12.45	7.45
90	13.70	12.45	7.45
100	13.71	12.46	7.46
110	13.71	12.46	7.46
120	13.72	12.46	7.46
130	13.72	12.47	7.47
140	13.72	12.47	7.47
150	13.73	12.48	7.47
160	13.73	12.48	7.48
170	13.73	12.48	7.48
180	13.74	12.49	7.48
190	13.74	12.49	7.49
200	13.74	12.49	7.49
210	13.75	12.50	7.49
220	13.75	12.50	7.50
230	13.76	12.50	7.50
240	13.76	12.51	7.50
250	13.76	12.51	7.51
260	13.77	12.51	7.51
270	13.77	12.52	7.51
280	13.77	12.52	7.52
290	13.78	12.53	7.52
300	13.78	12.53	7.52

Table 9 Constants for calculation of bearing capacity for different shape of foot

Constants for the calculations	Unit	Value
1. Length of foot for rectangular foot	[m]	0.7
2. Width of foot for rectangular foot	[m]	0.3
3. Length of foot for square foot	[m]	0.45
4. Diameter of circular foot	[m]	0.51

Table 10 Bearing capacity of rectangular foot with vertical leg in granular soil

Cohesion (kPa)	Bearing capacity (kPa)	Bearing capacity* Factor of Safety (kPa)	Allowable vehicle weight (kN)
2	128.41	192.62	107.86
3	173.83	260.75	146.02
4	219.26	328.89	184.18
5	264.68	397.02	222.33
6	310.00	465.00	260.40
7	355.53	533.30	298.65
8	400.95	601.43	336.80
9	446.38	669.57	374.96
10	491.80	737.70	413.11

Table 11 Bearing capacity of square foot with vertical leg in granular soil

Cohesion (kPa)	Bearing capacity (kPa)	Bearing capacity* Factor of Safety (kPa)	Allowable vehicle weight (kN)
2	158.14	237.21	128.09
3	216.81	325.22	175.62
4	275.48	413.22	223.14
5	334.15	501.23	270.66
6	392.82	589.23	318.18
7	451.49	677.24	365.71
8	510.16	765.24	413.23
9	568.83	853.25	460.75
10	627.5	941.25	508.28

Table 12 Bearing capacity of circular foot with vertical leg in granular soil

Cohesion (kPa)	Bearing capacity (kPa)	Bearing capacity* Factor of Safety (kPa)	Allowable vehicle weight (kN)
2	163.58	245.37	133.60
3	222.25	333.38	181.51
4	280.92	421.38	229.43
5	339.59	509.39	277.35
6	398.26	597.39	325.26
7	456.93	685.40	373.18
8	515.6	773.40	421.10
9	574.27	861.41	469.01
10	632.94	949.41	516.93

Table 13 Soil strength of rectangular foot with vertical leg in cohesive soil

Vehicle weight (kN)	Undrained shear strength (kPa)
30	9.62
60	19.24
90	28.86
120	38.48
150	48.10
180	57.72
210	67.34
240	76.96
270	86.58
300	96.20
330	105.82
360	115.44
390	125.06
420	134.68
450	144.30
480	153.93
510	163.55
540	173.17
570	182.79
600	192.41
630	202.03
660	211.65
690	221.27
720	230.89
750	240.51
780	250.13
810	259.75

Table 14 Soil strength of square foot with vertical leg in cohesive soil

Vehicle weight (kN)	Undrained shear strength (kPa)
30	9.05
60	18.10
90	27.14
120	36.19
150	45.24
180	54.29
210	63.34
240	72.39
270	81.43
300	90.48
330	99.53
360	108.58
390	117.63
420	126.67
450	135.72
480	144.77
510	153.82
540	162.87
570	171.91
600	180.96
630	190.01
660	199.06
690	208.11
720	217.16
750	226.20
780	235.25
810	244.30

Table 15 Soil strength of circular foot with vertical leg in cohesive soil

Vehicle weight (kN)	Undrained shear strength (kPa)
30	8.97
60	17.95
90	26.92
120	35.90
150	44.87
180	53.84
210	62.82
240	71.79
270	80.76
300	89.74
330	98.71
360	107.69
390	116.66
420	125.63
450	134.61
480	143.58
510	152.55
540	161.53
570	170.50
600	179.48
630	188.45
660	197.42
690	206.40
720	215.37
750	224.34
780	233.32
810	242.29

Table 16 Soil strength of tracked vehicle in cohesive soil

Vehicle weight (kN)	Undrained shear strength (kPa)
30	7.64
60	15.27
90	22.91
120	30.55
150	38.18
180	45.82
210	53.46
240	61.09
270	68.73
300	76.37
330	84.01
360	91.64
390	99.28
420	106.92
450	114.55
480	122.19
510	129.83
540	137.46
570	145.10
600	152.74
630	160.37
660	168.01
690	175.65
720	183.28
750	190.92
780	198.56
810	206.20

APPENDIX 11

TRACTIVE FORCE FOR DESIGNED VEHICLE AND TRACKED VEHICLE

This Appendix presents the calculated data for the tractive forces available for the designed vehicle and a tracked vehicle of similar dimensions and weight under different slip percentages at the vehicle running gears – soil interfaces.

Table 1 Constants used for calculations of tractive force of ‘Caterpillar’ tracked vehicle D3B in granular soil

Design parameters	Units	Value
1. Length of track	[m]	1.82
2. Width of track	[m]	0.31
3. Constant, K	[cm]	5.00
4. Cohesion	[kPa]	1.00
5. Angle of friction of soil	[degree]	19.70
6. Weight of tracked vehicle	[kN]	65.00
7. Maximum tractive effort	[kN]	24.38

Table 2 Tractive force vs. slip for ‘Caterpillar’ tracked vehicle D3B in granular soil

Slip (%)	5	10	20	30	40	50	60	70	80
Tractive effort (kN)	13.16	17.86	21.04	22.15	22.71	23.04	23.27	23.43	23.55

Table 3 Constants used for calculations of tractive force developed by grousers of foot of the designed legged vehicle in cohesive soil

Design parameters	Units	Value
1. Width of grouser	[m]	0.30
2. Height of grouser	[m]	0.04
3. Length of foot	[m]	0.70
4. Width of foot	[m]	0.30
5. Number of grousers	[-]	8.00
6. Minimum vertical load at foot	[kN]	8.00
7. Specific weight of soil	[kN/m ³]	15.70
8. Cohesion of soil	[kPa]	20.00
9. Friction angle of soil	[degree]	6.00
10. Surcharge of soil	[kPa]	38.10
11. Flow value	[-]	1.23
12. Tractive force per grouser	[kN]	1.10
13. Total tractive force by all grousers	[kN]	8.81

Table 4 Constants used for calculations of tractive force developed by foot of the designed legged vehicle in granular soil

Design parameters	Units	Value
1. Length of foot	[m]	0.70
2. Width of foot	[m]	0.30
3. Maximum vertical load	[kN]	8.00
4. Cohesion of soil	[kPa]	1.00
5. Constant, K	[cm]	5.00
6. Angle of friction of soil	[degree]	19.70
7. Number of legs	[-]	4.00
8. Maximum tractive effort	[kN]	3.07

Table 5 Tractive force vs. slip for Golden Tortoise with step size = 100 mm in granular soil

Slip (%)	5	10	20	30	40	50	60	70	80
Tractive force for one leg (kN)	0.15	0.29	0.54	0.76	0.96	1.13	1.28	1.42	1.54
Total tractive force (kN)	0.59	1.15	2.16	3.05	3.83	4.52	5.14	5.68	6.16

Table 6 Tractive force vs. slip for Golden Tortoise with step size = 300 mm in granular soil

Slip (%)	5	10	20	30	40	50	60	70	80
Tractive force for one leg (kN)	0.42	0.76	1.28	1.65	1.91	2.10	2.24	2.35	2.44
Total tractive force (kN)	1.67	3.05	5.14	6.59	7.64	8.40	8.97	9.41	9.76

Table 7 Constants used for calculations of tractive force developed by belly of the designed legged vehicle in cohesive soil

Design parameters	Units	Value
1. Length of belly	[m]	2
2. Width of belly	[m]	2.3
3. Weight of vehicle	[kN]	31
4. Cohesion of soil	[kPa]	100
5. Constant, K	[cm]	5
6. Angle of friction of soil	[degree]	3
7. Maximum tractive effort	[kN]	461.62

APPENDIX 12

RELATIONSHIP BETWEEN SWING VELOCITY OF CUTTER AND TRANSLATORY VELOCITY OF HYDRAULIC CYLINDER

The relationship between the swing velocity of the cutter and the translatory velocity of the hydraulic cylinder swinging the ladder assembly is presented in this Appendix. This relationship was utilized in determining the volume of soil dislodged by the designed cutter.

The effective distance between the cutter and the swing centre of the ladder assembly (L_e) [m] was given as (Figure1),

$$L_e = L_{boom} * \cos(\alpha) + L_{dipper} * \cos(\beta)$$
$$L_e = \sqrt{(L_{boom} * \cos(\alpha) + L_{dipper} * \cos(\beta))^2 + (L_1)^2}$$
[Equation 1]

The translatory velocity of the cutter (v_{swing_cutter}) [m/sec] was deduced,

$$v_{swing_cutter} = L_e * \omega_{ladder}$$
[Equation 2]

The relationship between the angular velocity (ω_{ladder}) [rad/sec] and the swing velocity of the ladder assembly (v_{swing_ladder}) [m/sec] was deduced,

$$v_{shc_ladder_tangential} = L_2 * \omega_{ladder} = v_{swing_ladder}$$
[Equation 3]

The cylinder rod translatory velocity was obtained as (Figure 2),

$$v_{shc_ladder} = v_{swing_ladder} * \cos(\alpha_{swing} + \gamma_{ladder})$$
[Equation 4]

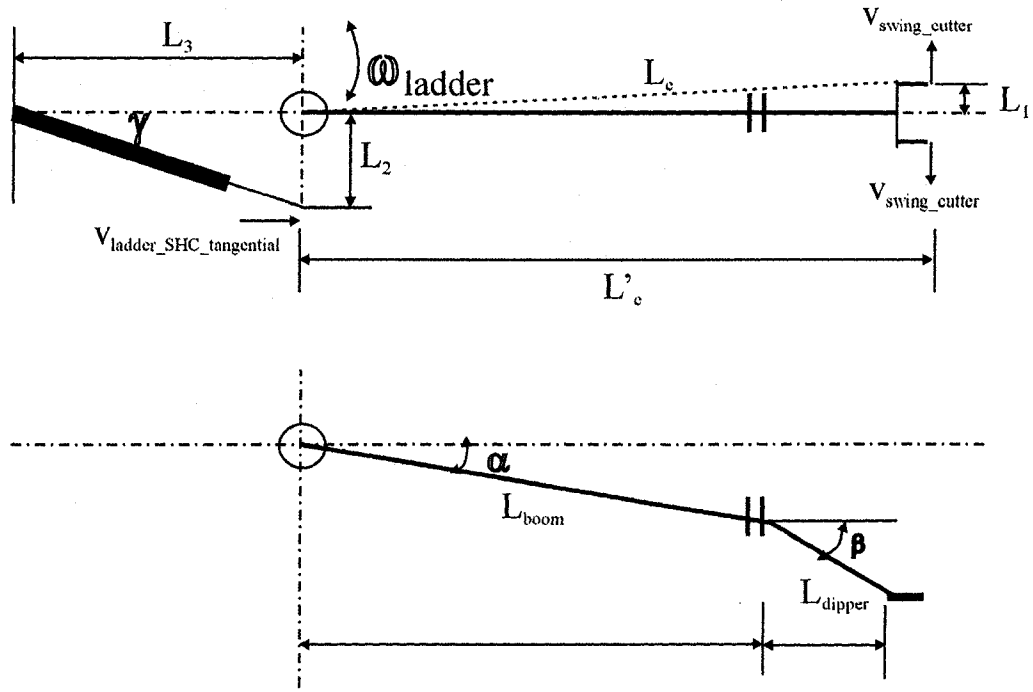


Figure 1 Swing geometry (Top Plan view, Bottom Elevation)

The hydraulic oil flow rate was calculated,

$$v_{shc_ladder} = \frac{Q_{shc_ladder}}{A_{hc}} \quad \text{[Equation 5]}$$

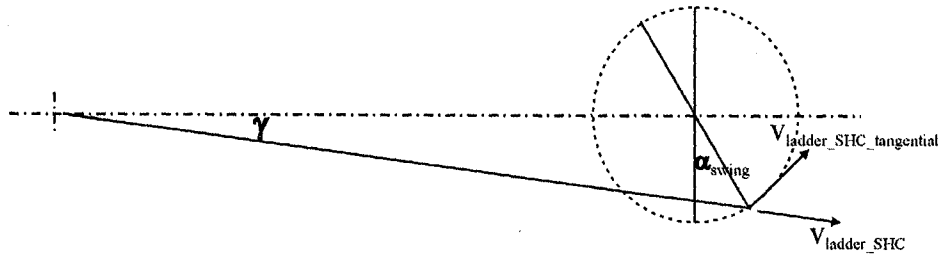


Figure 2 Swing geometry (cont.)

The constant and the variables chosen for the simulations are tabulated in Table 1.

Table 1 Constants and variables for evaluation of the loosening production

Constants			
Factors	Symbol	Value	
1. Diameter of hydraulic cylinder for ladder swing [m]	D_{shc_ladder}	0.043	
2. Linear distance between central axis of ladder and central axis of cutter drum [m]	L_1	0.49	
3. Linear distance between the pivot point of the ladder assembly and the point of swing cylinder attachment on the rotating yoke [m]	L_2	0.23	
4. Length of the boom [m]	L_{boom}	2.25	
5. Length of the dipper [m]	L_{dipper}	1.1	
6. Radius of the cutter drum measured from cutter blade tip to centre line of drum [m]	R_{cutter}	0.29	
7. Width of blade [m]	B_{blade}	0.07	
Variables			
Factors	Symbol	Value	
		Maxm.	Min.
8. Hydraulic oil flow into the hydraulic cylinder for ladder swing [m ³ /sec]	Q_{shc_ladder}	0.0002	0.00005
9. Cutter rpm [-]	rpm_{cutter}	90	50
10. Number of cutter blades in a row [-]	z_{blade}	2	4
11. Angle which the boom makes with the horizontal [degree]	α	30	5
12. Half angle of swing of the ladder [degree]	α_{swing}	30	5
13. Angle which the dipper makes with the horizontal [degree]	β	10	5
14. Angle between ladder swing cylinder and the central axis of the vehicle [degree]	γ_{ladder}	10	5
15. Depth of cut [m]	h_{cut}	0.3	0.1

Table 2 Ladder assembly and cutter swing velocities

Q_{shc_ladder}	v_{shc_ladder}	α_{swing}	v_{swing_ladder}	α	β	γ_{ladder}	v_{swing_cutter}
[m ³ /sec]	[m/sec]	[degree]	[m/sec]	[degree]	[degree]	[degree]	[m/sec]
Low hydraulic oil flow and Low swing angle of ladder							
0.00005	0.0344	5	0.035	30	10	5	0.467
0.00005	0.0344	5	0.035	30	5	5	0.469
0.00005	0.0344	5	0.036	30	10	10	0.476
0.00005	0.0344	5	0.036	30	5	10	0.478
0.00005	0.0344	5	0.035	5	10	5	0.511
0.00005	0.0344	5	0.035	5	5	5	0.513
0.00005	0.0344	5	0.036	5	10	10	0.521
0.00005	0.0344	5	0.036	5	5	10	0.523
Low hydraulic oil flow and High swing angle of ladder							
0.00005	0.0344	30	0.042	30	10	5	0.562
0.00005	0.0344	30	0.042	30	5	5	0.564
0.00005	0.0344	30	0.045	30	10	10	0.600
0.00005	0.0344	30	0.045	30	5	10	0.603
0.00005	0.0344	30	0.042	5	10	5	0.614
0.00005	0.0344	30	0.042	5	5	5	0.617
0.00005	0.0344	30	0.045	5	10	10	0.657
0.00005	0.0344	30	0.045	5	5	10	0.659
High hydraulic oil flow and Low swing angle of ladder							
0.0002	0.1378	5	0.1399	30	10	5	1.869
0.0002	0.1378	5	0.1399	30	5	5	1.876
0.0002	0.1378	5	0.1426	30	10	10	1.905
0.0002	0.1378	5	0.1426	30	5	10	1.913
0.0002	0.1378	5	0.1399	5	10	5	2.044
0.0002	0.1378	5	0.1399	5	5	5	2.052
0.0002	0.1378	5	0.1426	5	10	10	2.084
0.0002	0.1378	5	0.1426	5	5	10	2.092
High hydraulic oil flow and High swing angle of ladder							
0.0002	0.1378	30	0.1682	30	10	5	2.246
0.0002	0.1378	30	0.1682	30	5	5	2.255
0.0002	0.1378	30	0.1798	30	10	10	2.401
0.0002	0.1378	30	0.1798	30	5	10	2.411
0.0002	0.1378	30	0.1682	5	10	5	2.457
0.0002	0.1378	30	0.1682	5	5	5	2.466
0.0002	0.1378	30	0.1798	5	10	10	2.628
0.0002	0.1378	30	0.1798	5	5	10	2.637

Table 3 Loosening production for one cutter with depth of cut = 0.1 m during ‘overcutting’

Cutter rpm	v_{swing_cutter} (m/sec)	x_{min} (m)	x_{max} (m)	y_{min} (m)	y_{max} (m)	Area of soil wedge (m ²)	Loosening production for one cutter (m ³ /sec)
50	0.6	0.30	0.54	0.19	0.276	0.0421	0.0221
60	0.6	0.2874	0.4875	0.19	0.280	0.0330	0.0208
70	0.6	0.2776	0.4492	0.19	0.281	0.0261	0.0192
80	0.6	0.2703	0.4240	0.19	0.283	0.0214	0.0180
90	0.6	0.2646	0.3980	0.19	0.282	0.0175	0.0165

Table 4 Loosening production for one cutter with depth of cut = 0.2 m during ‘overcutting’

Cutter rpm	v_{swing_cutter} (m/sec)	x_{min} (m)	x_{max} (m)	y_{min} (m)	y_{max} (m)	Area of soil wedge (m ²)	Loosening production for one cutter (m ³ /sec)
50	0.6	0.3119	0.5520	0.09	0.276	0.0910	0.0478
60	0.6	0.3058	0.5060	0.09	0.280	0.0731	0.0460
70	0.6	0.3015	0.4731	0.09	0.281	0.0601	0.0442
80	0.6	0.2983	0.4484	0.09	0.283	0.0511	0.0429
90	0.6	0.2958	0.4292	0.09	0.282	0.0437	0.0413

Table 5 Constants used for prediction of trajectory and velocity of soil lump/ particle

Symbol	Description	Value
π	A constant	3.14 [-]
g	Acceleration due to gravity	9.81 [m/sec ²]
C_d	Drag co-efficient for soil lump/ particle	0.2 [-]
R_{cutter}	Radius of cutter	0.29 [m]
ρ_{soil}	Density of soil	2650 [kg/m ³]
ρ_{f0}	Density of water at 0 ° C	999.7 [kg/m ³]
v_{cur}	Velocity of current	2 [m/sec]
v_{swing_cutter}	Swing velocity of cutter	0.6 [m/sec]
v_{swing_ladder}	Swing velocity of ladder assembly	0.045 [m/sec]
α_{cur}	Angle which the current vector makes with horizontal	20 [degree]
ψ	Angle between tangential velocity of cutter and the horizontal	20 [degree]
μ_{soil_blade}	Co-efficient of friction between soil and blade	0.3 [-]
x_0	Initial condition of position of the soil lump/ particle from the arbitrary reference frame	
v_0	Initial condition of velocity of the soil lump/ particle when ejected into water by cutters	

The forces and constants calculated for evaluating the soil lump/ particle trajectory and velocity are presented below. The values for the leading cutter are denoted by the subscript l , while the values for the trailing cutter are denoted by subscript t . C_1, C_2, C_3 and C_4 denote the co-efficient constants for the differential equations of motions for the soil lump/ particle as presented in section 4.3.2.

Table 6 Forces and constants for prediction of soil lump/ particle trajectory and velocity with diameter of soil particle = 0.002 m

rpm_l	rpm_t	m_s	F_g	F_b	F_{fl}	F_{ft}	F_{dl}	F_{dt}	F_c	C_{ll}	C_{lt}	C_2	C_{3l}	C_{3t}	C_{4l}	C_{4t}
90	50	1.1095e-005	1.0884e-004	4.0333e-005	1.9713e-005	1.9910e-005	0.0034	0.0013	0.0012	4.9879e-004	3.7080e-004	0.0514	1.8908e-005	1.9287e-005	0.0016	0.0012
70	50	1.1095e-005	1.0884e-004	4.0333e-005	1.9792e-005	1.9910e-005	.0022	0.0013	0.0012	4.3479e-004	3.7080e-004	0.0514	1.9061e-005	1.9287e-005	0.0014	0.0012
50	90	1.1095e-005	1.0884e-004	4.0333e-005	1.9910e-005	1.9713e-005	0.0013	0.0034	0.0012	3.7080e-004	4.9879e-004	0.0514	1.9287e-005	1.8908e-005	0.0012	0.0016
50	70	1.1095e-005	1.0884e-004	4.0333e-005	1.9910e-005	1.9792e-005	0.0013	0.0022	0.0012	3.7080e-004	4.3479e-004	0.0514	1.9287e-005	1.9061e-005	0.0012	0.0014
70	70	1.1095e-005	1.0884e-004	4.0333e-005	1.9792e-005	1.9792e-005	0.0022	0.0022	0.0012	4.3479e-004	4.3479e-004	0.0514	1.9061e-005	1.9061e-005	0.0014	0.0014

Table 7 Forces and constants for prediction of soil lump/ particle trajectory and velocity with diameter of soil particle = 0.02 m

rpm_l	rpm_t	m_s	F_g	F_b	F_{fl}	F_{ft}	F_{dl}	F_{dt}	F_c	C_{ll}	C_{lt}	C_2	C_{3l}	C_{3t}	C_{4l}	C_{4t}
90	50	0.0111	0.1088	0.0403	0.0197	0.0199	0.3362	0.1349	0.1233	0.0499	0.0371	5.1380	0.0189	0.0193	0.1556	0.1204
70	50	0.0111	0.1088	0.0403	0.0198	0.0199	0.2242	0.1349	0.1233	0.0435	0.0371	5.1380	0.0191	0.0193	0.1380	0.1204
50	90	0.0111	0.1088	0.0403	0.0199	0.0197	0.1349	0.3362	0.1233	0.0371	0.0499	5.1380	0.0193	0.0189	0.1204	0.1556
50	70	0.0111	0.1088	0.0403	0.0199	0.0198	0.1349	0.2242	0.1233	0.0371	0.0435	5.1380	0.0193	0.0191	0.1204	0.1380
70	70	0.0111	0.1088	0.0403	0.0198	0.0198	0.2242	0.2242	0.1233	0.0435	0.0435	5.1380	0.0191	0.0191	0.1380	0.1380

APPENDIX 13

RELEVANT DATA FOR ESTIMATION OF HEAD LOSS OF DESIGNED PIPELINE SYSTEM

The relevant data used for the performance evaluation of the designed pump-pipeline system (Chapter 5) are presented in this Appendix.

Table 1 Vapor pressure of water at different temperatures [Matousek, 1999]

Temperature [°C]	p_v , Vapour pressure [Pa]
0	0.61×10^3
5	0.87×10^3
10	1.23×10^3
15	1.70×10^3
20	2.34×10^3
25	3.17×10^3
30	4.24×10^3

Table 2 Typical values of density and porosity of various soils [Matousek, 1999]

Soil type	Density of solids [kg/m ³]	Density of in situ soil [kg/m ³]	Porosity [-]
Silt	2650	1100- 1400	80 - 90
Loose clay	2650	1400 -1600	60 - 80
Packed clay	2650	1800 - 2000	35 - 50
Sand with clay	2650	1800 - 2000	40 - 50
Sand	2650	1900 - 2000	35 - 45
Coarse sand with gravel	2650	2050 - 2200	28 - 36
Clay boulders	2650	2320	20

Table 3 Characteristic particle sizes for medium sand samples [Matousek, 1999]

Particle size	Narrow- graded sand
d_{50}	0.42
d_{85}	0.8
d_{15}	0.36
d_s (mean diameter)	0.38
d_{mf} (decisive diameter)	0.42

Table 4 Angle of inclination (ω) of pipeline vs. Durand deposition parameter (ΔD)
[Wilson et al., 1997]

Angle of Inclination (ω^0)	Durand Deposition Parameter (ΔD)
-10	-0.16
0	0.00
10	0.17
20	0.25
30	0.35
40	0.35
45	0.33
50	0.30

Table 5 Minor loss co-efficient for bends [Matousek, 1999]

r/D	ξ [-] for Bend angle [0]					
	15 0	22.5 0	30 0	45 0	60 0	90 0
1.5	0.03	0.050	0.085	0.13	0.17	0.20
2.0	0.03	0.045	0.060	0.09	0.12	0.13
3.0	0.03	0.045	0.055	0.08	0.10	0.13
5.0	0.03	0.045	0.050	0.07	0.08	0.11
10.0	0.03	0.045	0.050	0.07	0.07	0.11

Table 6 Minor loss co-efficient for Knee [Matousek, 1999]

SI	α , Knee angle [0]	ξ [-]
1	30 0	0.15
2	45 0	0.30

Table 7 Minor loss co-efficient for Gate valve [Matousek, 1999]

SI	ξ [-]
1	0.1

Table 8 Minor loss co-efficient for ball valve [Matousek, 1999]

SI	ξ [-]
1	0.2 to 0.3

The results from the calculations are presented next.

Table 9 Mean mixture velocity vs. pipe diameter for horizontal pipeline

Pipe diameter (m)	Mean mixture velocity (m/sec)
0.1	12.03
0.15	5.35
0.2	3.01
0.25	1.92
0.3	1.34

Table 10 Data for pipeline diameter = 0.15 m for horizontal pipeline

Solid discharge rate (m ³ /sec)	Solid discharge rate(m ³ /hr)	Mean mixture velocity (m/sec)	Mixture flow rate(m ³ /hr)
0.017	61.2	5.35	324
0.02	72	6.29	396
0.03	108	9.44	612

Table 11 Data for pipeline diameter = 0.20 m for horizontal pipeline

Solid discharge rate (m ³ /sec)	Solid discharge rate(m ³ /hr)	Mean mixture velocity (m/sec)	Mixture flow rate(m ³ /hr)
0.017	61.2	3.01	324
0.02	72	3.54	396
0.03	108	5.31	612

Table 12 Data for pipeline diameter = 0.30 m for horizontal pipeline

Solid discharge rate (m ³ /sec)	Solid discharge rate(m ³ /hr)	Mean mixture velocity (m/sec)	Mixture flow rate(m ³ /hr)
0.017	61.2	1.34	324
0.02	72	1.57	396
0.03	108	2.36	612

Table 13 Deposition limit and transport velocity for horizontal pipeline

Pipe diameter (m)	Deposition limit velocity (m/sec)	Suitable transport velocity (m/sec)
0.15	0.244	0.269
0.2	0.282	0.31
0.25	0.316	0.347
0.3	0.346	0.38

The total head loss and pump power required data for the designed pump pipeline system for various inclination of the inclined pipeline section are presented below. The solid flow rate chosen was 0.017 m³/ sec = 61 m³/ hr, and the delivered volumetric concentration chosen was 0.18 for all the calculations. The depth of operation was 50 m and the elevation of discharge was

5 m. The system operation factor for the pump pipeline system was considered as 1.3, while the pump efficiency was taken as 60 %.

Table 14 Data for inclination of inclined pipeline section = 10 degree

Pipeline diameter (m)	Mean mixture velocity (m/sec)	Total head loss (m)	Total pressure drop (kPa)	Mixture flow rate (m ³ /hr)	Power required (kW)
0.1	12.03	481.98	4713.96	339.97	964.52
0.15	5.35	101.38	991.57	340.18	203.01
0.2	3.01	68.974	674.68	340.25	138.16
0.25	1.92	87.465	855.459	339.12	174.60
0.3	1.34	129.384	1265.543	340.82	259.59

Table 15 Data for inclination of inclined pipeline section = 20 degree

Pipeline diameter (m)	Mean mixture velocity (m/sec)	Total head loss (m)	Total pressure drop (kPa)	Mixture flow rate (m ³ /hr)	Power required (kW)
0.1	12.03	365.03	3570.16	339.97	730.49
0.15	5.35	81.24	794.6	340.18	162.68
0.2	3.01	55.604	543.9	340.25	111.38
0.25	1.92	67.495	660.079	339.12	134.72
0.3	1.34	96.074	939.753	340.82	192.76

Table 16 Data for inclination of inclined pipeline section = 30 degree

Pipeline diameter (m)	Mean mixture velocity (m/sec)	Total head loss (m)	Total pressure drop (kPa)	Mixture flow rate (m ³ /hr)	Power required (kW)
0.1	12.03	326.89	3197.1	339.97	654.16
0.15	5.35	74.56	729.22	340.18	149.30
0.2	3.01	50.954	498.36	340.25	102.05
0.25	1.92	60.385	590.589	339.12	120.54
0.3	1.34	84.174	823.323	340.82	168.88

Table 17 Data for inclination of inclined pipeline section = 45 degree

Pipeline diameter (m)	Mean mixture velocity (m/sec)	Total head loss (m)	Total pressure drop (kPa)	Mixture flow rate (m ³ /hr)	Power required (kW)
0.1	12.03	302.66	2960.16	339.97	605.68
0.15	5.35	70.18	686.43	340.18	140.54
0.2	3.01	47.664	466.23	340.25	95.47
0.25	1.92	55.215	539.999	339.12	110.21
0.3	1.34	75.444	738.003	340.82	151.38

The deposition limit velocity and the suitable transport velocity for the horizontal and inclined pipeline sections are presented next.

Table 18 Data for inclination of inclined pipeline section = 10 degree

Pipeline diameter (m)	Mean mixture velocity (m/sec)	Deposition limit velocity: Horizontal pipe (m/sec)	Suitable transport velocity: Horizontal pipe (m/sec)	Deposition limit velocity: Inclined pipe (m/sec)	Suitable transport velocity: Inclined pipe (m/sec)
0.1	12.03	0.19	0.22	0.506	0.557
0.15	5.35	0.245	0.269	0.62	0.682
0.2	3.01	0.2823	0.31	0.716	0.787
0.25	1.92	0.315	0.347	0.8	0.88
0.3	1.34	0.346	0.38	0.877	0.964

Table 19 Data for inclination of inclined pipeline section = 20 degree

Pipeline diameter (m)	Mean mixture velocity (m/sec)	Deposition limit velocity: Horizontal pipe (m/sec)	Suitable transport velocity: Horizontal pipe (m/sec)	Deposition limit velocity: Inclined pipe (m/sec)	Suitable transport velocity: Inclined pipe (m/sec)
0.1	12.03	0.19	0.22	0.65	0.716
0.15	5.35	0.245	0.269	0.797	0.876
0.2	3.01	0.2823	0.31	0.92	1.012
0.25	1.92	0.315	0.347	1.029	1.131
0.3	1.34	0.346	0.38	1.127	1.239

Table 20 Data for inclination of inclined pipeline section = 45 degree

Pipeline diameter (m)	Mean mixture velocity (m/sec)	Deposition limit velocity: Horizontal pipe (m/sec)	Suitable transport velocity: Horizontal pipe (m/sec)	Deposition limit velocity: Inclined pipe (m/sec)	Suitable transport velocity: Inclined pipe (m/sec)
0.1	12.03	0.19	0.22	0.795	0.874
0.15	5.35	0.245	0.269	0.97	1.07
0.2	3.01	0.2823	0.31	1.124	1.236
0.25	1.92	0.315	0.347	1.257	1.382
0.3	1.34	0.346	0.38	1.377	1.514

